

**SOLUTION H₂S CHEMISTRY OF Pd-BIS(DIPHENYLPHOSPHINO)METHANE
(DPM) COMPLEXES; CATALYTIC CONVERSION OF H₂S TO H₂**

By

TERRANCE YU HUNG WONG

B.Sc., The University of British Columbia, 1990

**A THESIS SUBMITTED IN PARTIAL FULFILLMENT OF
THE REQUIREMENTS FOR THE DEGREE OF
DOCTOR OF PHILOSOPHY**

in

**THE FACULTY OF GRADUATE STUDIES
(Department of Chemistry)**

**We accept this thesis as conforming
to the required standard**

THE UNIVERSITY OF BRITISH COLUMBIA

June 1996

© Terrance Yu Hung Wong, 1996

In presenting this thesis in partial fulfilment of the requirements for an advanced degree at the University of British Columbia, I agree that the Library shall make it freely available for reference and study. I further agree that permission for extensive copying of this thesis for scholarly purposes may be granted by the head of my department or by his or her representatives. It is understood that copying or publication of this thesis for financial gain shall not be allowed without my written permission.

Department of CHEMISTRY

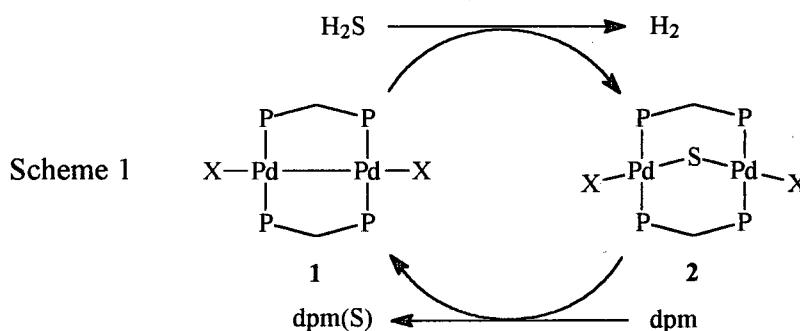
The University of British Columbia
Vancouver, Canada

Date SEPT 4, 1996

ABSTRACT

This thesis describes studies on the interaction of H_2S with mono- and dinuclear Pd - dpm (bis(diphenylphosphino)methane) complexes with the ultimate goal being to catalyze the conversion of H_2S to H_2 and elemental sulfur (S_8).

Solution kinetic and mechanistic studies were performed on the abstraction of sulfur from $\text{Pd}_2\text{X}_2(\mu\text{-S})(\mu\text{-dpm})_2$ [$\text{X} = \text{Cl}$ (**2a**), Br (**2b**), I (**2c**)] using dpm to give, respectively, $\text{Pd}_2\text{X}_2(\text{dpm})_2$ [$\text{X} = \text{Cl}$ (**1a**), Br (**1b**), I (**1c**)] and $\text{dpm}(\text{S})$ (process **2** \rightarrow **1**):

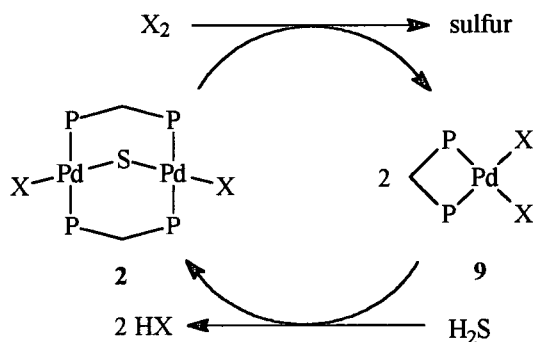


The reaction is first-order in both **2** and dpm with the reactivity trend in CHCl_3 being $\text{X} = \text{Cl} > \text{Br} > \text{I}$. The activation parameters for the chloride system are $\Delta H^\ddagger = 41 \pm 3 \text{ kJ mol}^{-1}$ and $\Delta S^\ddagger = -127 \pm 10 \text{ J K}^{-1} \text{ mol}^{-1}$, and for the bromide, $\Delta H^\ddagger = 38 \pm 1 \text{ kJ mol}^{-1}$ and $\Delta S^\ddagger = -144 \pm 4 \text{ J K}^{-1} \text{ mol}^{-1}$, showing that the entropy term is dominant in governing reactivity. No intermediates were seen in low temperature NMR studies. **2b** and **1b** undergo rapid diphosphine ligand exchange with dpm-d_2 ; with **2b**, prior to any S-abstraction, $\text{Pd}_2\text{Br}_2(\mu\text{-S})(\text{dpm})(\text{dpm-d}_2)$ and $\text{Pd}_2\text{Br}_2(\mu\text{-S})(\text{dpm-d}_2)_2$ are present, while $\text{Pd}_2\text{Br}_2(\text{dpm})(\text{dpm-d}_2)$ and $\text{Pd}_2\text{Br}_2(\text{dpm-d}_2)_2$ are formed, as well as **1b** and $\text{dpm}(\text{S})\text{-d}_2$, in the abstraction reaction of **2b** with dpm-d_2 . The distribution of products is close to statistical based on the stoichiometries of the reactants. Reaction of **2b** with 1,1'-bis(diphenylphosphino)ethane (dpmMe) proceeds in an analogous way generating **1b**,

$\text{Pd}_2\text{Br}_2(\text{dpm})(\text{dpmMe})$, $\text{Pd}_2\text{Br}_2(\text{dpmMe})_2$, and the monosulfides $\text{dpm}(\text{S})$ and $\text{dpmMe}(\text{S})$. **1b** undergoes slow diphosphine ligand exchange, and **2b** undergoes no ligand exchange, with dpmMe prior to S-abstraction. The findings are rationalized in terms of intermediates and transition states that include formulations with three equivalent diphosphines. No sulfur abstraction occurs on treating **2b** with PPh_3 , PPh_2Me , or $\text{Ph}_2\text{P}(\text{CH}_2)_3\text{PPh}_2$. Some studies were carried out on the catalyzed reaction $\text{H}_2\text{S} + \text{dpm} \rightarrow \text{H}_2 + \text{dpm}(\text{S})$, which is the first reported, homogeneously catalyzed conversion of H_2S to H_2 .

The removal of the bridged S atom from **2** using halogens (process **2** \rightarrow **9**) was investigated, and kinetic and mechanistic studies on the $X = \text{I}$ system in CHCl_3 reveal that the reaction proceeds via oxidative addition of I_2 to give $\text{Pd}_2\text{I}_4(\text{dpm})_2$ (**10c**), which then undergoes unimolecular decomposition to give $\text{PdI}_2(\text{dpm})$ (**9c**); the sulfur is recovered in its elemental form (forward reaction - Scheme 2). The oxidative addition reaction is in the stopped-flow time regime, and is first-order in both **2c** and I_2 ; the activation parameters are $\Delta H^\ddagger = 32 \pm 1 \text{ kJ mol}^{-1}$ and $\Delta S^\ddagger = -91 \pm 3 \text{ J K}^{-1} \text{ mol}^{-1}$. The decomposition of **10c** is slower and is simply first-order in **10c**; the activation parameters are $\Delta H^\ddagger = 80 \pm 1 \text{ kJ mol}^{-1}$ and $\Delta S^\ddagger = -26 \pm 3 \text{ J K}^{-1} \text{ mol}^{-1}$. Depending on reaction conditions, the by-product $\text{PdI}_2(\text{dpm}(\text{S}))$ (**11c**) also forms via reaction of **9c** with an S_n species where $n < 8$; **11c** and the chloro analogue were synthesized by other routes and were characterized by X-ray analyses which reveal the envelope configuration of the five-membered $\overline{\text{Pd-PPh}_2\text{CH}_2\text{P}(\text{S})\text{Ph}_2}$ chelate ring.

Scheme 2



The dinucleation reaction ($9 \rightarrow 2$) (Scheme 2) was studied in DMSO and on alumina in $CHCl_3$, and proceeds rapidly to form **2** and HX. In DMSO, the reaction is established as an equilibrium; however, a side-product, probably $Pd(SH)_2(dpm)$, also forms. In $CHCl_3$, the $9 \rightarrow 2$ reaction proceeds completely in the presence of an alumina catalyst which functions to activate the H_2S prior to the dinucleation process; **2** is thought to form via the coupling of the undetected, intermediate $PdX(SH)(dpm)$. With important catalytic implications seen for the $X = I$ system, some photodecomposition studies of HI in the presence of alumina were performed; formation of I_2 occurs, while the concomitantly formed H atoms react with $CHCl_3$ to generate CH_2X_2 species where $X = Cl$ and/or I.

TABLE OF CONTENTS

Abstract	ii
List of Tables	xii
List of Figures	xiv
List of Non-standard/Less Common Abbreviations	xxiii
Numerical Key to Palladium Complexes	xxvi
Acknowledgements	xxvii
1 INTRODUCTION	1
1.1 Properties, occurrences, and uses of H ₂ S	2
1.2 Recovery of both H ₂ and elemental sulfur from H ₂ S	6
1.2.1 Thermodecomposition of H ₂ S	7
1.2.2 Photodecomposition of H ₂ S	12
1.2.3 Electrochemical decomposition of H ₂ S	18
1.2.4 Plasmachemical decomposition of H ₂ S	22
1.2.5 Radiolytic decomposition of H ₂ S	23
1.3 Homogeneous catalytic conversion of H ₂ S to H ₂	24
1.4 Transition metal - H ₂ S chemistry	28
1.5 The chemistry of transition metal - dpm complexes	33
1.6 Statement of the problem	36
1.7 References for Chapter 1	37
2 GENERAL EXPERIMENTAL PROCEDURES	46

2.1	Materials	47
2.1.1	Dibenzylideneacetone (dba)	50
2.1.2	1,1'-bis(diphenylphosphino)ethane (dpmMe)	50
2.1.3	Triphenylphosphine sulfide (Ph ₃ PS)	51
2.1.4	Bis(diphenylphosphino)methane monosulfide (dpm(S))	51
2.1.5	<i>Trans</i> -dichlorobis(benzonitrile)palladium(II) (PdCl ₂ (PhCN) ₂)	52
2.1.6	Tris(dibenzylideneacetone)dipalladium(0)-chloroform solvate (Pd ₂ (dba) ₃ •CHCl ₃)	52
2.1.7	Dichlorobis-μ-[bis(diphenylphosphino)methane]dipalladium(I) (Pd ₂ Cl ₂ (dpm) ₂)	53
2.1.8	Dibromobis-μ-[bis(diphenylphosphino)methane]dipalladium(I) (Pd ₂ Br ₂ (dpm) ₂)	53
2.1.9	Diiodobis-μ-[bis(diphenylphosphino)methane]dipalladium(I) dichloromethane solvate (Pd ₂ I ₂ (dpm) ₂ •CH ₂ Cl ₂)	54
2.1.10	Dichloro-μ-sulfidobis-μ-[bis(diphenylphosphino)methane]dipalladium(II) (Pd ₂ Cl ₂ (μ-S)(dpm) ₂)	54
2.1.11	Dibromo-μ-sulfidobis-μ-[bis(diphenylphosphino)methane]dipalladium(II) (Pd ₂ Br ₂ (μ-S)(dpm) ₂)	55
2.1.12	Diiodo-μ-sulfidobis-μ-[bis(diphenylphosphino)methane]dipalladium(II) (Pd ₂ I ₂ (μ-S)(dpm) ₂)	55
2.1.13	Dichloro[bis(diphenylphosphino)methane]palladium(II) (PdCl ₂ (dpm))	56
2.1.14	Dibromo[bis(diphenylphosphino)methane]palladium(II) (PdBr ₂ (dpm))	56
2.1.15	Diiodo[bis(diphenylphosphino)methane]palladium(II) (PdI ₂ (dpm))	57
2.1.16	Dichloro-μ-sulfoxobis-μ-[bis(diphenylphosphino)methane]dipalladium(II) (Pd ₂ Cl ₂ (μ-SO)(dpm) ₂)	57
2.1.17	Diiodo-μ-sulfoxobis-μ-[bis(diphenylphosphino)methane]dipalladium(II) (Pd ₂ I ₂ (μ-SO)(dpm) ₂)	58

2.1.18	Dimercapto- μ -sulfidobis- μ -[bis(diphenylphosphino)methane]dipalladium(II) (Pd ₂ (SH) ₂ (μ -S)(dpm) ₂)	58
2.2	Instrumentation	59
2.2.1	Nuclear magnetic resonance spectroscopy	59
2.2.2	Electronic absorption spectroscopy	60
2.2.3	Stopped-flow electronic absorption spectroscopy	60
2.2.4	Thin-layered chromatography	60
2.2.5	Gas chromatography	61
2.2.6	Photochemistry	61
2.2.7	Electron spin resonance spectroscopy	62
2.2.8	Elemental, mass, and X-ray crystallographic and photoelectron analyses	62
2.3	Treatment of kinetic data	62
2.4	References for Chapter 2	65
3	KINETIC AND MECHANISTIC ASPECTS OF SULFUR ABSTRACTION FROM Pd ₂ X ₂ (μ -S)(dpm) ₂ USING dpm OR dpmMe and CATALYTIC CONVERSION OF H ₂ S TO H ₂	67
3.1	Introduction	68
3.2	Results	69
3.3	Discussion	98
3.4	Experimental section	123
3.4.1	Preparation of dpm-d ₂	123
3.4.2	Preparation of dpm(S)-d ₂	124
3.4.3	Preparation of dpmMe(S)	124

3.4.4	Preparation of $\text{dpm}(\text{S})_2$, $\text{dpe}(\text{S})$, $\text{dpe}(\text{S})_2$, $\text{dpp}(\text{S})$, and $\text{dpp}(\text{S})_2$	125
3.4.5	Preparation of H_2S	126
3.4.6	Preparation of $\text{Pd}_2\text{Br}_2(\text{dpm-d}_2)_2 \cdot 2\text{H}_2\text{O}$ (4b)	126
3.4.7	Preparation of $\text{Pd}_2\text{Br}_2(\mu\text{-S})(\text{dpm-d}_2)_2$ (8b)	128
3.4.8	Kinetic measurements	128
3.4.9	Mechanistic studies	129
3.4.10	Catalytic conversion of H_2S	131
3.5	References for Chapter 3	133
4	KINETIC AND MECHANISTIC ASPECTS OF SULFUR ABSTRACTION FROM $\text{Pd}_2\text{X}_2(\mu\text{-S})(\text{dpm})_2$ USING HALOGENS	135
4.1	Introduction	136
4.2	Results	140
4.3	Discussion	165
4.4	Experimental section	181
4.4.1	Preparation of $\text{PdCl}_2(\text{dpm}(\text{S}))$ (11a)	181
4.4.2	Preparation of $\text{PdBr}_2(\text{dpm}(\text{S}))$ (11b)	182
4.4.3	Preparation of $\text{PdI}_2(\text{dpm}(\text{S}))$ (11c)	182
4.4.4	Preparation of $\text{PdCl}_2(\text{dpm}(\text{S})_2)$	183
4.4.5	Kinetic studies	183
4.4.6	Mechanistic studies	184
4.4.7	X-ray crystallographic analysis of $\text{PdI}_2(\text{dpm}(\text{S})) \cdot 0.5\text{CH}_2\text{Cl}_2$	188
4.5	References for Chapter 4	189

5	PRELIMINARY STUDIES ON THE REACTION OF PdX ₂ (dpm) WITH H ₂ S IN DIMETHYLSULFOXIDE; FORMATION OF Pd ₂ X ₂ (μ-S)(dpm) ₂	194
5.1	Introduction	195
5.2	Results	196
5.3	Discussion	220
5.4	Experimental section	229
5.4.1	Preparation of gaseous HI	229
5.4.2	Reaction of PdX ₂ (dpm) (9) with H ₂ S	229
5.4.3	Reaction of PdX ₂ (dpm) (9) with elemental sulfur	231
5.4.4	Reaction of Pd ₂ I ₂ (μ-S)(dpm) ₂ (2c) with I ₂	231
5.4.5	Reaction of Pd ₂ X ₂ (μ-S)(dpm) ₂ (2) with HX	231
5.4.6	Reaction of Pd ₂ (SH) ₂ (μ-S)(dpm) ₂ with I ₂	232
5.4.7	Reaction of PdX ₂ (dpm) (9) with NaSH	233
5.4.8	Photodecomposition studies of HI, HBr, and H ₂ S	233
5.5	References for Chapter 5	234
6	REACTION OF PdX ₂ (dpm) WITH H ₂ S IN THE PRESENCE OF ALUMINA; CATALYZED FORMATION OF Pd ₂ X ₂ (μ-S)(dpm) ₂	236
6.1	Introduction	237
6.2	Results	239
6.3	Discussion	257
6.4	Experimental section	268

6.4.1	NMR spectroscopic studies	268
6.4.2	Surface studies	270
6.4.3	Synthetic-scale studies	271
6.4.4	Photodecomposition of HI	273
6.5	References for Chapter 6	274
7	MISCELLANEOUS REACTIONS	276
7.1	Reaction of $\text{Pd}_2\text{X}_2(\mu\text{-S})(\text{dpm})_2$ with alkyl halides	277
7.2	Reaction of $\text{PdX}_2(\text{dpm})$ (9) with H_2S in the presence of silica gel or aluminosilicate; catalyzed formation of $\text{Pd}_2\text{X}_2(\mu\text{-S})(\text{dpm})_2$ (2)	281
7.3	Reaction of $\text{Pd}_2\text{X}_2(\mu\text{-S})(\text{dpm})_2$ (2) with CO	282
7.4	References for Chapter 7	285
8	GENERAL CONCLUSIONS AND RECOMMENDATIONS FOR FUTURE STUDIES	286
	APPENDIX	291
	Appendix I - Free energy of decomposition of H_2S , ΔG_d	292
	Appendix II - Kinetic data from the study of the reaction: $\text{Pd}_2\text{X}_2(\mu\text{-S})(\text{dpm})_2 + \text{dpm}$	294
	Appendix III - Computer program to simulate the outcome of the reaction between $\text{Pd}_2\text{Br}_2(\mu\text{-S})(\text{dpm})_2$ and n mole equivalent dpm-d_2	295
	Appendix IV - Determination of the concentration of H_2S in chloroform	299
	Appendix V - Kinetic data from the study of the reaction: $\text{Pd}_2\text{I}_2(\mu\text{-S})(\text{dpm})_2 + \text{I}_2$	301
	Appendix VI - X-ray crystal structure data for $\text{PdI}_2(\text{dpm}(\text{S})) \cdot 0.5\text{CH}_2\text{Cl}_2$	302

Appendix VII - Synthesis and characterization of $[\text{Pd}(\text{dpm}(\text{S}))_2]\text{Cl}_2 \cdot 0.5 \text{CH}_2\text{Cl}_2$,
trans-bis- η -P,S-(bis(diphenylphosphino)methane monosulfide)palladium(II) chloride
0.5 CH_2Cl_2 solvate

311

LIST OF TABLES

2.1	Some materials used and their sources.	48
2.2	Palladium complexes used and their respective reference(s) for synthetic procedures.	49
3.1	NMR data for the dinuclear palladium complexes, diphosphines, and the diphosphine monosulfides.	70
3.2	Temperature dependence for the bimolecular rate constant of the reaction of $\text{Pd}_2\text{Cl}_2(\mu\text{-S})(\text{dpm})_2$ (2a) (k_{Cl}) and $\text{Pd}_2\text{Br}_2(\mu\text{-S})(\text{dpm})_2$ (2b) (k_{Br}) with dpm in CHCl_3 .	75
3.3	Conditions used in the study of the catalysis of reaction 3.1.3 at R.T. using $\text{Pd}_2\text{Br}_2(\text{dpm})_2$ (1b) or $\text{Pd}_2\text{Br}_2(\mu\text{-S})(\text{dpm})_2$ (2b).	93
4.1	NMR data for the palladium complexes.	141
4.2	Temperature dependence for the bimolecular (k_{I}) and unimolecular (k_{D}) rate constants for the formation and decomposition of the intermediate, $\text{Pd}_2\text{I}_4(\text{dpm})_2$ (10c), respectively, in CDCl_3 .	150
4.3	Reaction of $\text{Pd}_2\text{X}_2(\mu\text{-S})(\text{dpm})_2$ (2) with X_2 under various conditions; yield of by-product $\text{PdX}_2(\text{dpm}(\text{S}))$ (11).	155
4.4	Activation parameters for some halogenation studies of dinuclear metal complexes and unsaturated systems.	169
4.5	Polarity (Q) of selected solvents at 25 °C (measured by $(\epsilon-1)/(2\epsilon+1)$ where ϵ is the dielectric constant).	169
5.1	NMR data for complexes and other compounds discussed in Chapter 5.	197
5.2	Results from studies on the reaction of $\text{PdX}_2(\text{dpm})$ (9a , 1.8×10^{-2} M; 9b , 1.5×10^{-2} M; 9c , 1.3×10^{-2} M) with H_2S at R.T. in DMSO-d_6 ; 1 = $\text{Pd}_2\text{X}_2(\text{dpm})_2$, 2 = $\text{Pd}_2\text{X}_2(\mu\text{-S})(\text{dpm})_2$, 11 = $\text{PdX}_2(\text{dpm}(\text{S}))$, Y = probably $\text{Pd}(\text{SH})_2(\text{dpm})$.	199
5.3	Results from studies on the reaction of $\text{PdX}_2(\text{dpm})$ (9a , 3.6×10^{-2} M; 9b , 3.0×10^{-2} M; 9c , 2.7×10^{-2} M) with 1 mole equivalent of elemental sulfur in DMSO-d_6 .	206
5.4	Results from studies on the reaction of $\text{Pd}_2\text{X}_2(\mu\text{-S})(\text{dpm})_2$ (2a , 1.8×10^{-2} M; 2b , 1.7×10^{-2} M; 2c , 1.5×10^{-2} M) with $\text{HX}(\text{g})$.	208

5.5	Results from photodecomposition studies of HI, HBr, and H ₂ S.	216
6.1	Summary of the content make-up in Expts. 1 - 18; 9a = PdCl ₂ (dpm).	240
I.1	Absolute free energies values, G, for H ₂ S, H ₂ , S ₂ (g), S ₈ (g), and S ₈ (s,l), and free energy of decomposition for H ₂ S, ΔG _d (H ₂ S), in the temperature range 298 to 1800 K.	293
IV.1	Dependence of the vapour pressure of CHCl ₃ on temperature in the range T = 215.15 to 334.45 K.	299
VI.1	Atomic coordinates of PdI ₂ (dpm(S))•0.5CH ₂ Cl ₂ (11c).	306
VI.2	Bond lengths (Å) in the complex PdI ₂ (dpm(S))•0.5CH ₂ Cl ₂ (11c).	308
VI.3	Bond angles (°) in the complex PdI ₂ (dpm(S))•0.5CH ₂ Cl ₂ (11c).	309
VII.1	Atomic coordinates of [Pd(dpm(S)) ₂]Cl ₂ •0.5CH ₂ Cl ₂ .	317
VII.2	Bond lengths (Å) of [Pd(dpm(S)) ₂]Cl ₂ •0.5CH ₂ Cl ₂ .	319
VII.3	Bond angles (°) of [Pd(dpm(S)) ₂]Cl ₂ •0.5CH ₂ Cl ₂ .	320
VII.4	C-H•••Cl interactions in the complex [Pd(dpm(S)) ₂]Cl ₂ •0.5CH ₂ Cl ₂ .	322

LIST OF FIGURES

- 3.1a Visible absorption spectral changes (350 - 550 nm region) as a function of time for a CHCl_3 solution of $\text{Pd}_2\text{Br}_2(\mu\text{-S})(\mu\text{-dpm})_2$ (**2b**) (6.52×10^{-5} M) on addition of dpm (1.96×10^{-2} M) at 25 °C. 72
- 3.1b A rate-plot analyzed for a pseudo-first-order dependence on **2b**; A_t and A_∞ represent the absorption at 428 nm at times t and ∞ , respectively. 72
- 3.2a The dependence of the pseudo-first-order rate constants, k_{obs} , on $[\text{dpm}]$ at **[2b]** = 6.52×10^{-5} M, in CHCl_3 . 74
- 3.2b Eyring plot of the temperature dependence of the bimolecular rate constant, k_{Br} . 74
- 3.3a The dependence of the pseudo-first-order rate constants, k_{obs} , on $[\text{dpm}]$ at **[2a]** = 6.52×10^{-5} M, in CHCl_3 at 30 °C. 76
- 3.3b Eyring plot of the temperature dependence of the bimolecular rate constant, k_{Cl} . 76
- 3.4 The ^1H NMR (300 MHz) spectrum of the isolated Pd products from the reaction of **2b** with dpm-d_2 at a 1:1 mole ratio in CD_2Cl_2 at R.T. 80
- 3.5 The $^{31}\text{P}\{^1\text{H}\}$ NMR (121 MHz) spectrum of the isolated Pd products from the reaction of **2b** with dpm-d_2 at a 1:1 mole ratio in CD_2Cl_2 at R.T. 81
- 3.6 The ^1H NMR (300 MHz) spectrum of the isolated phosphine monosulfide products from the reaction of **2b** with dpm-d_2 at a 1:1 mole ratio in CD_2Cl_2 at R.T. 82
- 3.7 The $^{31}\text{P}\{^1\text{H}\}$ NMR (121 MHz) spectrum of the isolated phosphine monosulfide products from the reaction of **2b** with dpm-d_2 at a 1:1 mole ratio in CD_2Cl_2 at R.T. 83
- 3.8 The $^{31}\text{P}\{^1\text{H}\}$ NMR spectrum (121 MHz) of the completed *in situ* reaction between **2b** and dpm-d_2 (1:5 mole ratio) in CDCl_3 at R.T. (72 h); X = unknown. 84

3.9	The ^1H NMR (300 MHz) spectrum of the completed <i>in situ</i> reaction between 2b and dpm-d ₂ (1:5 mole ratio) in CDCl_3 at R.T. (72 h).	85
3.10	The ^1H NMR spectrum (300 MHz) of the isolated Pd products from the reaction 2b and dpmMe (1:1 mole ratio) in CD_2Cl_2 at R.T.	87
3.11	The $^{31}\text{P}\{^1\text{H}\}$ NMR (121 MHz) spectrum of 2b on addition of 1 mole equivalent of dpm-d ₂ ; the spectrum was recorded at R.T. immediately after sample preparation in CDCl_3 .	89
3.12	The ^1H NMR spectrum (300 MHz) recorded at R.T. in CDCl_3 of 1b on addition of 1 mole equivalent of dpmMe (72 h).	90
3.13	The $^{31}\text{P}\{^1\text{H}\}$ NMR spectrum (121 MHz) recorded at R.T. in CDCl_3 of 1b on addition of 1 mole equivalent of dpmMe (72 h).	91
3.14	The UV-vis spectrum of the isolated catalytically inactive species (in CHCl_3).	94
3.15	The ^1H NMR spectrum (300 MHz) recorded at R.T. in CDCl_3 of the isolated catalytically inactive species.	95
3.16	The $^{31}\text{P}\{^1\text{H}\}$ NMR spectrum (121 MHz) recorded at R.T. in CDCl_3 of the isolated catalytically inactive species.	96
3.17	The UV-vis spectrum obtained from studies of the catalyzed dpm + H_2S reaction using 1b in CHCl_3 after 24 h (Expt. 2).	97
3.18	The ^1H NMR spectrum (300 MHz) recorded at R.T. in CDCl_3 of 2b on addition of 1 mole equivalent of dpe (72 h).	105
3.19	The $^{31}\text{P}\{^1\text{H}\}$ NMR spectrum (121 MHz) recorded at R.T. in CDCl_3 of 2b on addition of 1 mole equivalent of dpe (72 h).	106
3.20	The ^1H (300 MHz) and $^{31}\text{P}\{^1\text{H}\}$ (121 MHz) NMR spectra recorded at R.T. in CDCl_3 of 2b on addition of 1 mole equivalent of dpp (72 h) (species W).	107

- 3.21 The ^1H NMR spectrum (300 MHz) recorded at R.T. in CDCl_3 of species **W** on addition of 3 mole equivalent of dpp (72 h). 109
- 3.22 The $^{31}\text{P}\{^1\text{H}\}$ NMR spectrum (121 MHz) recorded at R.T. in CDCl_3 of species **W** on addition of 3 mole equivalent of dpp (72 h). 110
- 3.23 The ^1H (300 MHz) and $^{31}\text{P}\{^1\text{H}\}$ (121 MHz) NMR spectra recorded at R.T. in CDCl_3 of **2b** on addition of 1 mole equivalent of dpm(S) (72 h) (species **Y**). 115
- 3.24 Mass spectrum (FAB, matrix = thioglycerol + CHCl_3) obtained of species **Y**. 116
- 3.25 The UV-vis spectra of species isolated from reactions of $\text{Pd}_2\text{X}_2(\mu\text{-S})(\text{dpm})_2$ (**2**) with 1 mole equivalent of dpm(S) in CHCl_3 ($\text{X} = \text{Cl}$ (species **X**), Br (species **Y**), I (species **Z**)). 117
- 3.26 Mass spectrum (FAB, matrix = thioglycerol + CHCl_3) of the catalytically inactive species **VII** with the region from 1400 to 1650 m/z expanded. 122
- 3.27 Schematic diagram showing experimental setup for preparation of H_2S from reaction of CaS with aq. HCl . 127
- 4.1 Preliminary ^1H (300 MHz) and $^{31}\text{P}\{^1\text{H}\}$ (121 MHz) NMR study of the reaction of $\text{Pd}_2\text{I}_2(\mu\text{-S})(\text{dpm})_2$ (**2c**, 1.6×10^{-2} M) with 1 mole equivalent I_2 in CDCl_3 at R.T.; **9c** = $\text{PdI}_2(\text{dpm})$, **10c** = $\text{Pd}_2\text{I}_4(\text{dpm})_2$, **11c** = $\text{PdI}_2(\text{dpm}(\text{S}))$. 143
- 4.2 Mass spectrum (electron impact) of the yellow precipitate isolated from the synthetic-scale reaction of $\text{Pd}_2\text{I}_2(\mu\text{-S})(\text{dpm})_2$ (**2c**) with I_2 in CHCl_3 at R.T. 145
- 4.3 Visible absorption spectral changes (320 - 650 nm region) as a function of time ($\Delta T = 120$ s) for a CHCl_3 solution of $\text{Pd}_2\text{I}_2(\mu\text{-S})(\text{dpm})_2$ (**2c**, 9.4×10^{-5} M) on addition of I_2 (3.8×10^{-4}) at 25 °C. Inset: a rate-plot analyzed for a first-order dependence on $\text{Pd}_2\text{I}_4(\text{dpm})_2$ (**10c**); A_t and A_∞ represent the absorption at 396 nm at times t and ∞ , respectively. 146

- 4.4 Electronic absorption spectra of S_8 (conc. = 1.25×10^{-3} M; λ , nm (ϵ , $M^{-1} \text{ cm}^{-1}$) = 244 (828), 266 (910)) and I_2 (conc. = 3.94×10^{-4} M; λ , nm (ϵ , $M^{-1} \text{ cm}^{-1}$) = 512 (879) in CHCl_3 at R.T. 148
- 4.5 The dependence of the first-order rate constant, k_{obs} , on $[I_2]$ for the decomposition of the intermediate $\text{Pd}_2\text{I}_4(\text{dpm})_2$ (**10c**) (formed from reaction with 9.4×10^{-5} M $\text{Pd}_2\text{I}_2(\mu\text{-S})(\text{dpm})_2$ (**2c**)) in CHCl_3 at 25 °C. 149
- 4.6 Eyring plot of the temperature dependence for the unimolecular rate constants, k_D , for the decomposition of $\text{Pd}_2\text{I}_4(\text{dpm})_2$ (**10c**). 149
- 4.7 Absorption spectral changes at $\lambda = 510$ nm as a function of time for the formation of $\text{Pd}_2\text{I}_4(\text{dpm})_2$ (**10c**) in CHCl_3 at 25 °C from reaction of $\text{Pd}_2\text{I}_2(\mu\text{-S})(\text{dpm})_2$ (**2c**) (9.9×10^{-5} M) with I_2 (4.9×10^{-4} M). 151
- 4.8 Rate-plot analyzed for a pseudo-first-order dependence on $\text{Pd}_2\text{I}_2(\mu\text{-S})(\text{dpm})_2$ (**2c**) (initial conc. = 9.9×10^{-5} M) during reaction with I_2 (initial conc. = 4.9×10^{-4} M) in CHCl_3 at 25 °C to form the intermediate $\text{Pd}_2\text{I}_4(\text{dpm})_2$ (**10c**); A_t and A_∞ represent the absorption at 510 nm at times t and ∞ , respectively. 151
- 4.9 The dependence of the pseudo-first-order rate constants, k_{obs} , for the formation of $\text{Pd}_2\text{I}_4(\text{dpm})_2$ (**10c**) on $[I_2]$ from reaction with $\text{Pd}_2\text{I}_2(\mu\text{-S})(\text{dpm})_2$ (**2c**, 9.9×10^{-5} M) in CHCl_3 . 153
- 4.10 Eyring plot of the temperature dependence for the bimolecular rate constants, k_1 , for the formation of $\text{Pd}_2\text{I}_4(\text{dpm})_2$ (**10c**) from reaction of $\text{Pd}_2\text{I}_2(\mu\text{-S})(\text{dpm})_2$ (**2c**) with I_2 in CHCl_3 . 153

- 4.11 ORTEP drawing and stereoview of $\text{PdI}_2(\text{dpm}(\text{S}))$ (**11c**). Hydrogen atoms are omitted. 159
- 4.12 ORTEP and PLUTO drawings of $\text{PdCl}_2(\text{dpm}(\text{S}))$ (**11a**). Hydrogen atoms are omitted. 160
- 4.13 ^1H (300 MHz) and $^{31}\text{P}\{^1\text{H}\}$ NMR spectra of the "completed" reaction of $\text{Pd}_2\text{Br}_2(\mu\text{-S})(\text{dpm})_2$ (**2b**) with 1 mole equivalent of Br_2 in CDCl_3 at R.T.; **9b** = $\text{PdBr}_2(\text{dpm})$, **11b** = $\text{PdBr}_2(\text{dpm}(\text{S}))$. 162
- 4.14a Visible absorption spectral changes (320-600 nm region) as a function of time for a CH_3CN solution of $\text{Pd}_2\text{I}_2(\mu\text{-S})(\text{dpm})_2$ (**2c**) (9.4×10^{-5} M) on addition of I_2 (9.4×10^{-5} M) at 23.5 °C; **9c** = $\text{PdI}_2(\text{dpm})$. 164
- 4.14b A rate-plot analyzed for an approximate second-order dependence on $\text{Pd}_2\text{I}_4(\text{dpm})_2$ (**10c**); A_t and A_∞ represent the absorption at 360 nm at times t and ∞ , respectively. 164
- 5.1 Representative ^1H (200 MHz) and $^{31}\text{P}\{^1\text{H}\}$ (81 MHz) NMR spectra showing results from the immediate reaction at R.T. in DMSO-d_6 of $\text{PdI}_2(\text{dpm})$ (**9c**, 1.3×10^{-2} M) with 0.5 mole equivalent H_2S in the absence of light (Schlenk techniques were employed); **1c** = $\text{Pd}_2\text{I}_2(\text{dpm})_2$, **2c** = $\text{Pd}_2\text{I}_2(\mu\text{-S})(\text{dpm})_2$, **Y** = probably $\text{Pd}(\text{SH})_2(\text{dpm})$. 200
- 5.2 Representative ^1H (300 MHz) and $^{31}\text{P}\{^1\text{H}\}$ (121 MHz) NMR spectra showing results from the immediate reaction at R.T. in DMSO-d_6 of $\text{PdBr}_2(\text{dpm})$ (**9b**, 1.5×10^{-2} M) with 0.5 mole equivalent H_2S in the absence of light (Schlenk techniques were employed); **2b** = $\text{Pd}_2\text{Br}_2(\mu\text{-S})(\text{dpm})_2$, **Y** = probably $\text{Pd}(\text{SH})_2(\text{dpm})$. 201

- 5.3 Representative ^1H (300 MHz) and $^{31}\text{P}\{^1\text{H}\}$ (121 MHz) NMR spectra showing results from the immediate reaction at R.T. in DMSO- d_6 of $\text{PdCl}_2(\text{dpm})$ (**9a**, 1.8×10^{-2} M) with 0.5 mole equivalent H_2S in the absence of light (Schlenk techniques were employed); **2a** = $\text{Pd}_2\text{Cl}_2(\mu\text{-S})(\text{dpm})_2$, **Y** = probably $\text{Pd}(\text{SH})_2(\text{dpm})$. 202
- 5.4 Representative ^1H (200 MHz) and $^{31}\text{P}\{^1\text{H}\}$ (81 MHz) NMR spectra showing results from the exposure of the iodide system (reaction of $\text{PdI}_2(\text{dpm})$ (**9c**, 1.3×10^{-2} M) with 0.5 mole equivalent H_2S in the absence of light using Schlenk techniques) to laboratory light for 5 d; **11c** = $\text{PdI}_2(\text{dpm}(\text{S}))$. 204
- 5.5 ^1H (200 MHz) and $^{31}\text{P}\{^1\text{H}\}$ (81 MHz) NMR spectra showing results from the reaction of $\text{Pd}_2\text{Br}_2(\mu\text{-S})(\text{dpm})_2$ (**2b**, 1.7×10^{-2} M) with 2 mole equivalent HCl at R.T. in DMSO- d_6 ; spectra recorded 1 h after sample preparation. 210
- 5.6 ^1H (200 MHz) and $^{31}\text{P}\{^1\text{H}\}$ (81 MHz) NMR spectra showing results from the reaction of $\text{Pd}_2\text{Br}_2(\mu\text{-S})(\text{dpm})_2$ (**2b**, 1.7×10^{-2} M) with 2 mole equivalent HCl at R.T. in DMSO- d_6 ; spectra recorded after exposure of the system to laboratory light for 1 d; **9a** = $\text{PdCl}_2(\text{dpm})$, **9b** = $\text{PdBr}_2(\text{dpm})$, **11a** = $\text{PdCl}_2(\text{dpm}(\text{S}))$, **11b** = $\text{PdBr}_2(\text{dpm}(\text{S}))$. 211
- 5.7 ^1H (300 MHz) and $^{31}\text{P}\{^1\text{H}\}$ (121 MHz) NMR spectra of the completed reaction between $\text{Pd}_2(\text{SH})_2(\mu\text{-S})(\text{dpm})_2$ (1.9×10^{-2} M) and 1 mole equivalent I_2 at R.T. in DMSO- d_6 ; **2c** = $\text{Pd}_2\text{I}_2(\mu\text{-S})(\text{dpm})_2$. 213
- 5.8 $^{31}\text{P}\{^1\text{H}\}$ NMR spectra (121 MHz) showing the partial formation of $\text{Pd}_2\text{X}_2(\mu\text{-S})(\text{dpm})_2$ (**2**) from the reaction of $\text{PdX}_2(\text{dpm})$ (**9**) with 0.5 mole equivalent NaSH at R.T. in DMSO- d_6 ; **Y** = probably $\text{Pd}(\text{SH})_2(\text{dpm})$. 214
- 5.9 Electronic absorption spectrum of I_2 in chloroform from the photodecomposition of $\text{HI}(\text{g})$ (0.040 mmol) (amount of I_2 not quantified). 217

5.10	Electronic absorption spectrum of NaI_3 in DMSO-d_6 (amount of NaI_3 not quantified).	218
5.11	Electronic absorption spectra of an authentic sample of Br_2 in DMSO-d_6 and Br_2 from photodecomposition of HBr (10 μL 8.83 M HBr(aq.) dissolved in 0.5 mL DMSO-d_6 ; 12 h exposure to laboratory light) (amount of Br_2 not quantified).	219
6.1	Representative ^1H NMR spectrum (300 MHz) of samples 1 or 2 containing γ -alumina powder (15 mg) in CDCl_3 with and without the presence of H_2S (110 μL at STP), respectively.	242
6.2	^1H NMR spectra (300 MHz) showing the extent of the reaction at R. T. of $\text{PdCl}_2(\text{dpm})$ (9a) with H_2S in CDCl_3 in the presence of γ -alumina under various experimental conditions; 2a = $\text{Pd}_2\text{Cl}_2(\mu\text{-S})(\text{dpm})_2$.	243
6.3	^1H NMR spectra (300 MHz) showing the progress of the reaction at R. T. of $\text{PdCl}_2(\text{dpm})$ (9a , 8.9×10^{-3} M) with 2.5 mole equivalent H_2S in CDCl_3 in the presence of α -alumina (15 mg); 2a = $\text{Pd}_2\text{Cl}_2(\mu\text{-S})(\text{dpm})_2$.	245
6.4	X-ray photoelectron spectra of γ -alumina: a) experimental; b) literature, taken from ref. 4, pertaining to a surface cleaned by bombardment with Ar.	247
6.5	X-ray photoelectron spectrum (Mg $\text{K}\alpha$, R.T.) of sample 13 consisting of $\text{PdCl}_2(\text{dpm})$ (9a) adsorbed on γ -alumina.	248
6.6	X-ray photoelectron spectra (Mg $\text{K}\alpha$, R.T.) showing the Pd 3d photoelectron signals for samples 13, 15, and 16.	248

- 6.7 X-ray photoelectron spectra (Mg K α , R.T.) showing the Cl 2p and S 2p photoelectron signals of samples 13, 14, 15, and 16. 249
- 6.8 X-ray photoelectron spectra (Mg K α , R.T.) showing the S 2p and Cl 2p photoelectron signals of samples 17 and 18, respectively. 249
- 6.9a Electronic spectrum (250 to 650 nm) of I $_3^-$ (MeOH) isolated from synthetic-scale studies. 253
- 6.9b Electronic spectrum of an authentic sample of I $_3^-$ in MeOH (prepared from I $_2$ + NaI) ($\epsilon_{292} = 2.89 \times 10^4 \text{ M}^{-1} \text{ cm}^{-1}$, $\epsilon_{360} = 1.66 \times 10^4 \text{ M}^{-1} \text{ cm}^{-1}$). 253
- 6.10 Electronic spectrum (250 to 700 nm) of I $_2$ in MeOH ($\epsilon_{292} = 2540 \text{ M}^{-1} \text{ cm}^{-1}$, $\epsilon_{360} = 1380 \text{ M}^{-1} \text{ cm}^{-1}$, $\epsilon_{442} = 930 \text{ M}^{-1} \text{ cm}^{-1}$). 254
- 6.11 ^1H NMR spectrum (300 MHz) showing the results from the photodecomposition of HI(aq.) (~2 μL , 7.58 M) at R.T. in CDCl $_3$ in the presence of α -alumina (15 mg); X = Cl and/or I. 254
- 7.1 ^1H (200 MHz) and $^{31}\text{P}\{^1\text{H}\}$ (81 MHz) NMR spectra showing the progress of the reaction in CDCl $_3$ at R.T. of Pd $_2\text{I}_2(\mu\text{-S})(\text{dpm})_2$ (**2c**, $1.6 \times 10^{-2} \text{ M}$) with a 10-fold excess of MeI after 3 d; **1c** = Pd $_2\text{I}_2(\text{dpm})_2$, **9c** = PdI $_2(\text{dpm})$, **11c** = PdI $_2(\text{dpm}(\text{S}))$. [The spectra of the various Pd species are discussed in Sections 3.2 (**1c** and **2c**) and 4.2 (**9c** and **11c**).] 278
- 7.2 ^1H (200 MHz) and $^{31}\text{P}\{^1\text{H}\}$ (81 MHz) NMR spectra showing the progress of the reaction in CDCl $_3$ at R.T. of Pd $_2\text{I}_2(\mu\text{-S})(\text{dpm})_2$ (**2c**, $1.6 \times 10^{-2} \text{ M}$) with a 10-fold excess of EtI after 5 d; **1c** = Pd $_2\text{I}_2(\text{dpm})_2$, **9c** = PdI $_2(\text{dpm})$, **11c** = PdI $_2(\text{dpm}(\text{S}))$. 279

- 7.3 $^{31}\text{P}\{^1\text{H}\}$ NMR spectrum (81 MHz) recorded for the reaction of $\text{Pd}_2\text{Cl}_2(\mu\text{-S})(\text{dpm})_2$ (**2a**) with 700 psi CO at R.T. in CDCl_3 after 24 h; **1a** = $\text{Pd}_2\text{Cl}_2(\text{dpm})_2$, **9a** = $\text{PdCl}_2(\text{dpm})$, **11a** = $\text{PdCl}_2(\text{dpm}(\text{S}))$, **X** = unknown. [The spectra of the various Pd species are discussed in Sections 3.2 (**1a**) and 4.2 (**9a** and **11a**).] 283
- 7.4 $^{31}\text{P}\{^1\text{H}\}$ NMR spectrum (81 MHz) recorded for the reaction of $\text{Pd}_2\text{I}_2(\mu\text{-S})(\text{dpm})_2$ (**2c**) with 1 atm CO at R.T. in CDCl_3 after 11 d; **1c** = $\text{Pd}_2\text{I}_2(\text{dpm})_2$, **9c** = $\text{PdI}_2(\text{dpm})$, **11c** = $\text{PdI}_2(\text{dpm}(\text{S}))$, **Y**, **Z** = unknown. 283
- I.1 Dependence of the free energy of decomposition of H_2S , $\Delta G_d(\text{H}_2\text{S})$, on temperature in the range 298 to 1800 K. 292
- IV.1 Plot of $\ln(p(\text{CHCl}_3))$ versus $1/T$. 299
- VI.1 Unit cell of the complex $\text{PdI}_2(\text{dpm}(\text{S}))\cdot 0.5\text{CH}_2\text{Cl}_2$. 305
- VII.1 ORTEP drawing of $[\text{Pd}(\text{dpm}(\text{S}))_2]\text{Cl}_2$. Hydrogen atoms are omitted. 314
- VII.2 Stereoview of $[\text{Pd}(\text{dpm}(\text{S}))_2]\text{Cl}_2$. Hydrogen atoms are omitted. 315
- VII.3 Stereoview of the unit cell of $[\text{Pd}(\text{dpm}(\text{S}))_2]\text{Cl}_2$. 315
- VII.4 PLUTO drawing showing $1/2$ of $[\text{Pd}(\text{dpm}(\text{S}))_2]\text{Cl}_2$ with interactions with a dichloromethane solvate molecule. 316

LIST OF NON-STANDARD/LESS COMMON ABBREVIATIONS

A_0, A_t, A_∞	= absorbance at times zero, t, and infinite time
b	= path length (spectroscopy)
BDH	= British Drug Houses Chemicals Ltd.
br	= broad
CIL	= Cambridge Isotope Laboratories
Cp	= cyclopentadienyl
δ	= chemical shift (NMR)
d	= doublet (NMR), or deuterium, or day
dba	= dibenzylideneacetone
DMSO	= dimethylsulfoxide
dpe	= 1,2-bis(diphenylphosphino)ethane
dpe(S)	= 1,2-bis(diphenylphosphino)ethane monosulfide
dpe(S) ₂	= 1,2-bis(diphenylphosphino)ethane disulfide
dpm	= bis(diphenylphosphino)methane
dpm(S)	= bis(diphenylphosphino)methane monosulfide
dpm(S) ₂	= bis(diphenylphosphino)methane disulfide
dpmMe	= 1,1-bis(diphenylphosphino)ethane
dpmMe(S)	= 1,1-bis(diphenylphosphino)ethane monosulfide
dpp	= 1,3-bis(diphenylphosphino)propane
dpp(S)	= 1,3-bis(diphenylphosphino)propane monosulfide
dpp(S) ₂	= 1,3-bis(diphenylphosphino)propane disulfide

dq	= doublet of quartets
dqn	= doublet of quintets
dt	= doublet of triplets
ϵ	= extinction coefficient, or dielectric constant
FAB	= fast atom bombardment (mass spectrometry)
$\Delta G_d(\text{H}_2\text{S})$	= free energy of decomposition of H_2S
GC	= gas chromatography
HDS	= hydrodesulfurization
k	= rate constant
k_B	= Boltzmann's constant ($1.38066 \times 10^{-23} \text{ J K}^{-1}$)
k_{obs}	= observed pseudo-first order rate constant
μ	= bridging, or micro
m	= multiplet (NMR)
M	= metal, or unit of molarity
MCB	= Matheson, Coleman, and Bell
MSD	= Merck, Sharp, and Dohme
m/z	= mass to charge ratio
<i>n</i>	= stoichiometric equivalent
p	= pressure, or pseudo (NMR)
Ph	= phenyl
q	= quartet
qn	= quintet
R	= alkyl or aryl group, or reagent, or gas constant ($8.31442 \text{ J K}^{-1} \text{ mol}^{-1}$)

s	= singlet (NMR), or second
sh	= shoulder
t	= triplet (NMR), or time
T	= temperature
TLC	= thin-layered chromatography
TMS	= tetramethylsilane
V	= volume

NUMERICAL KEY TO PALLADIUM COMPLEXES

1	$\text{Pd}_2\text{X}_2(\text{dpm})_2$	10c	$\text{Pd}_2\text{I}_4(\text{dpm})_2$
1a	$\text{Pd}_2\text{Cl}_2(\text{dpm})_2$	11	$\text{PdX}_2(\text{dpm}(\text{S}))$
1b	$\text{Pd}_2\text{Br}_2(\text{dpm})_2$	11a	$\text{PdCl}_2(\text{dpm}(\text{S}))$
1c	$\text{Pd}_2\text{I}_2(\text{dpm})_2$	11b	$\text{PdBr}_2(\text{dpm}(\text{S}))$
2	$\text{Pd}_2\text{X}_2(\mu\text{-S})(\text{dpm})_2$	11c	$\text{PdI}_2(\text{dpm}(\text{S}))$
2a	$\text{Pd}_2\text{Cl}_2(\mu\text{-S})(\text{dpm})_2$		
2b	$\text{Pd}_2\text{Br}_2(\mu\text{-S})(\text{dpm})_2$		
2c	$\text{Pd}_2\text{I}_2(\mu\text{-S})(\text{dpm})_2$		
3b	$\text{Pd}_2\text{Br}_2(\text{dpm})(\text{dpm-d}_2)$		
4b	$\text{Pd}_2\text{Br}_2(\text{dpm-d}_2)_2$		
5b	$\text{Pd}_2\text{Br}_2(\text{dpm})(\text{dpmMe})$		
6b	$\text{Pd}_2\text{Br}_2(\text{dpmMe})_2$		
7b	$\text{Pd}_2\text{Br}_2(\mu\text{-S})(\text{dpm})(\text{dpm-d}_2)$		
8b	$\text{Pd}_2\text{Br}_2(\mu\text{-S})(\text{dpm-d}_2)_2$		
9	$\text{PdX}_2(\text{dpm})$		
9a	$\text{PdCl}_2(\text{dpm})$		
9b	$\text{PdBr}_2(\text{dpm})$		
9c	$\text{PdI}_2(\text{dpm})$		
10	$\text{Pd}_2\text{X}_4(\text{dpm})_2$		
10a	$\text{Pd}_2\text{Cl}_4(\text{dpm})_2$		
10b	$\text{Pd}_2\text{Br}_4(\text{dpm})_2$		

*With a great sigh of relief, I finally set my pen down knowing full
well that arriving at the end means that I really just begun.*

ACKNOWLEDGMENTS

I would like to thank Professor Brian James for his patience and guidance during my PhD work. I also would like to thank past and present members of the James' group, particularly Mr. Jeffrey Posakony and Mr. Stephen Cheng for their many valuable discussions. The services of the department are greatly appreciated. A big thanks goes to Mr. Kevin Lindstrom for his help in searching the Chemical Abstracts. I am indebted to Dr. Yoshikata Koga for first providing me an opportunity to explore the realm of chemistry -- to Mrs. Koga, thanks for the great dinners you've prepared for the Koga group over the years. I thank my family for their love and support; their emphasis on the importance of education has taught me much. Last but not least, I thank my lovely wife Christina for her unfailing love, and it is to her that I dedicated this thesis.

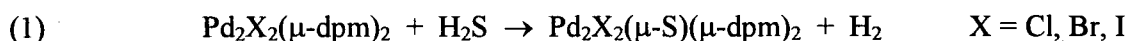
TYHW

CHAPTER 1

Introduction

Chapter 1 Introduction

Some research in this laboratory focuses on the development of homogeneous catalytic systems for the recovery of H₂ from H₂S. In particular, Pd complexes are employed, following the initial discovery (reaction 1)[†] that quantitative sulfur abstraction from H₂S with concomitant H₂ evolution readily occurs in solution under ambient conditions.¹ Detailed aspects of this reaction and its implications are presented in this Introduction, as well as an account of other methods developed for the decomposition of H₂S, following a brief description of the properties, occurrences, and uses of this compound.



1.1 Properties, occurrences, and uses of H₂S^{2,3,4}

The discovery of H₂S is credited to the Swedish chemist, Carl Wilhelm Scheele, who published the first systematic study of the gas in 1777.⁵ Although he named it *Schwefelluft* meaning sulfur air, H₂S was more prosaically and appropriately referred to as *stinkende*; the readily identifiable odor resembling rotten eggs cannot be mistaken by the average person.

Hydrogen sulfide is a colourless gas with melting and boiling points at, respectively, -82.9 and -61.8 °C. It is denser than air, and at ~20 °C, the specific gravity is 1.19 times that of air. Solubility occurs in a variety of polar and non-polar solvents including alcohols, ethers, glycerol, hydrocarbons, water, and amine solutions. In aqueous solution, two acid dissociation constants exist at pK_a ~7 and 12. H₂S is the only thermodynamically stable binary sulfur-hydrogen

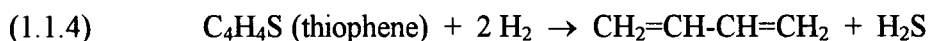
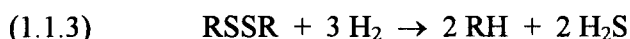
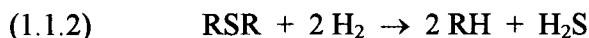
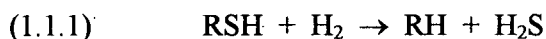
[†] The μ-symbol for the bridging diphosphine ligand(s) will be omitted for convenience throughout the text.

compound occurring in nature; the standard enthalpy and free energy of formations are -20.64 and $-33.02 \text{ kJ mol}^{-1}$, respectively. Above $500 \text{ }^\circ\text{C}$, the equilibrium with its elemental constituents becomes apparent because of kinetic and thermodynamic control, and at temperatures $> 1500 \text{ }^\circ\text{C}$, the decomposition of H_2S even becomes thermodynamically favourable (see Section 1.21 and Appendix I).

The toxicity of H_2S is comparable to that of HCN in terms of rapidity of action and concentration from which death will result. At low concentrations between 0.014 and 140 mg m^{-3} (0.01 and 100 ppm), the characteristic odor is instantly recognized; however, at H_2S concentrations above 210 mg m^{-3} , paralysis of the olfactory apparatus occurs, accompanied by rapid loss of consciousness and subsequent respiratory failure. Often, individuals who are revived following immediate medical attention do not recall ever detecting the noxious odor. Interestingly, H_2S is normally found in the human breath and is probably the cause of halitosis.

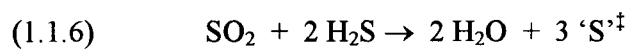
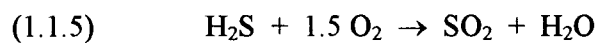
Hydrogen sulfide occurs naturally in coal, natural gas, oil, volcanic gases, sulfur springs and lakes, soil, and to lesser extents swamps and marshes. It results from either the action of steam on mineral sulfides and sulfates at elevated temperatures or the bacteriologic decomposition of mineral sulfates or S-containing organic matter. With the exception of the fossil fuel reserves, these biogenic sources contribute to the natural global sulfur cycle in which an atmosphere concentration of 3 to $30 \text{ } \mu\text{g m}^{-3}$ (2.1 to 21 ppb) H_2S is maintained. In the troposphere, H_2S is oxidized by the ozone present to sulfur oxides which are then taken up by plants and metabolized. The cycle is completed by herbivorous consumption by animals and subsequent bacterial action on these animals (or plants) at death. Apart from natural occurrences, anthropogenic sources of H_2S are becoming increasingly important, and there is cause for concern as consequential hazardous effects on the environment are becoming more pronounced (acid rain, smog, plant deterioration,

and adverse effects on aquatic life). The two main industrial sources are the Kraft wood pulping process⁶ and the hydrodesulfurization⁷ in the refinement of petroleum. In the Kraft process, NaSH is used in the cooking liquor to enhance the strength of the paper produced; H₂S is formed when the spent cooking liquor is evaporated and burned to recover the chemicals. In hydrodesulfurization, petroleum is treated with H₂ over Mo-Co or W-Ni sulfide catalysts to remove the sulfur components normally present including mercaptans, sulfides, disulfides, and sulfur heterocyclics (eqs. 1.1.1 - 1.1.4). This process must be carried out in order to prevent catalyst poisoning during the subsequent cracking and reforming stages; furthermore, sulfur emissions into the air will be reduced when the processed fuels are used. The H₂S, which has to be recovered, is then either recycled, for example, to regenerate NaSH for the Kraft process, or oxidized to elemental sulfur (see below).



Despite the negative qualities, H₂S surprisingly has many industrial uses^{2,3,4} including: (1) the preparation of inorganic and organic compounds; (2) the preparation of extreme pressure lubricants and cutting oils; (3) the purification of hydrochloric and sulfuric acids; (4) the hair removal process in the leather industry; and (5) the production of heavy water.⁸ Most of the recovered H₂S is used in the manufacture of sulfuric acid, more of which is produced than any other chemical.⁹ For convenience of shipping and storage, H₂S is usually oxidized to elemental sulfur, and there exists several technologies, the most important being the Claus process (eqs.

1.1.5, 1.1.6).¹⁰ Essentially, a portion of the H₂S is burned to SO₂, which is then combined with the remaining H₂S in the presence of a catalyst to produce elemental sulfur.



[†] For convenience, 'S' is written for elemental sulfur instead of the correct 1/8 S₈ formulation.

1.2 Recovery of both H₂ and elemental sulfur from H₂S

Decreasing fossil fuel reserves has prompted an intensive search for alternative methods of obtaining energy. The focus is on hydrogen as there is much interest in a hydrogen economy,¹¹ and the lack of an adequate H₂ supply has made the search for possible sources a main research goal. Hydrogen is not only important as an energy source but also as a raw material in many chemical processing industries among which the refining of petroleum is a major consumer. Because H₂ is not found in nature, the current source comes from the steam reforming of CH₄.¹² In view of the great demand for H₂ by both the chemical and energy sectors, researchers are looking to the abundantly available H₂S as a possible source. Because of the inherent toxicity of H₂S, high priority is placed on its removal by the industries that produce it. In the Claus process, the sulfur is recovered but the H₂ value is lost. Much research is devoted to finding and developing methods for decomposing H₂S into its elements, and a process which recovers both H₂ and sulfur could be of considerable worth.

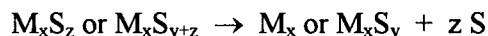
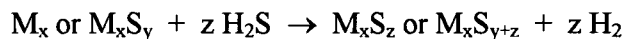
The following subsections outline such methods which can be classified under four main categories: (1) thermodecomposition, (2) photodecomposition, (3) electrochemical decomposition, and (4) plasmachemical decomposition. A fifth category, radiolytic decomposition of H₂S, is included for the sake of completeness but the emphasis in this area is not on recovery purposes. Decompositions of H₂S in homogeneous solution systems with formation of H₂ are described later (see Sections 1.3 and 1.4); no literature can be found concerning recovery of both H₂ and elemental S in solution systems.

1.2.1 Thermodecomposition of H₂S

Hydrogen sulfide can be thermally decomposed at high temperatures into H₂ and S (elemental sulfur). Historically, the first such study was of a fundamental nature reported Taylor and Pickett¹³ in 1927 where high temperatures were achieved by electrically heating a Pt filament. Similar fundamental studies^{14,15,16} have followed, providing a basic understanding of the kinetics and mechanism of the reaction, with Kaloidas and Papayannakos¹⁷ recently proposing a free-radical mechanism. The first industrial approach to the study is documented in 1958 when Massey¹⁸ patented a process for recovering both H₂ and 'S' by decomposing H₂S over glowing W filaments. Few groups have since studied such direct routes¹⁹⁻²³ as the high temperatures required (~1000 °C) make the process uneconomical; however, the use of concentrated solar energy alone or in conjugation with a catalyst (see below) has been reported.²⁴⁻²⁷

In the interest of economics, methods employing lower temperatures are sought after and for this reason catalysis has received increasing attention since Weiner and Leggett²⁸ in 1958 first proposed a two-step process involving Fe, Co, and Ni sulfide catalysts. Development in this thermocatalytic decomposition area, in general, involved transition metal oxides and sulfides. (The introduction of a catalyst, of course, serves only to accelerate the rate at which the equilibrium, $\text{H}_2\text{S} \rightleftharpoons \text{H}_2 + \text{'S'}$, is established; the equilibrium concentrations of each species are unaffected. However, if either or both products are continually removed, higher conversions of H₂S are attained as the reaction is forced to the right.) Optimal temperatures ranged from 400 to 800 °C and two types of catalytic processes are seen. The first type is described as being truly catalytic, the composition of the catalyst being unchanged after the reaction as evidenced by X-ray diffraction measurements. Examples include MoS₂, WS₂, and Cr₂S₃ and studies have shown that their

catalytic activities depend inversely on temperature over this 400 - 800 °C range.²⁹⁻³² Mechanistic studies with MoS₂ have suggested that H₂S decomposes via oxidative addition at an active site on the surface, followed by elimination of H₂ and subsequently 'S'.^{33,34} The second type of catalytic process involves two steps:²⁸



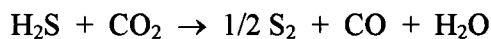
In the first step, H₂S reacts with a metal, M_x, or metal sulfide, M_xS_y, to generate H₂ and a metal sulfide, M_xS_z, or a higher metal sulfide, M_xS_{y+z}. The M_xS_z or M_xS_{y+z} is then thermally decomposed in the second step liberating 'S' and regenerating the metal or lower metal sulfide. The mono- and disulfides of Fe, Co, and Ni are well studied^{12,31,32,35,36} but are not effective catalysts due to the formation of non-stoichiometric forms as a result of varying degrees of sulfidation and/or thermal decomposition.^{12,31} Copper sulfides, Cu₂S, Cu₉S₅, and CuS, are also ineffective for the same reasons.³¹ However, the polysulfides, Co₉S₈³⁶ and Ni₃S₂,³⁶ are effective but require longer desulfurization times at higher temperatures particularly for Ni₃S₂.³⁷ The vanadium sulfide, V₂S₃, was found to be the most effective polysulfide catalyst, and VS³⁸ and VS₄³⁹ were proposed as intermediates. Silver is an effective M_x, with the Ag₂S produced easily de-sulfurized.³⁶ Mixed metal sulfides, Ni-Mo sulfide,^{25b} Co-Mo sulfide,^{25b} Fe₇S₈/MoS₂,⁴⁰ Fe₇S₈/NiS_{1.20},⁴⁰ V₂S₃/Cu₉S₅,³⁸ V₂S₃/Fe₇S₈,³⁸ and V₂S₃/ZnS,³⁸ were examined for cooperative effects and had activity comparable to that of MoS₂. The metal oxides, V₂O₅-MoO₃⁴¹ and Mn nodules,⁴² do catalyze the thermodecomposition of H₂S but the active catalysts are the sulfides formed in the initial sulfidation step. In the case of Mn nodules, which were studied more for their sulfur absorbent properties, the activity was attributed to the high Fe content. Chivers and Lau studied the alkali metal sulfides M₂S (M = Li, Na, and K) and polysulfides M₂S_x (x = 2-4; M = Na and K), and discovered that

Li₂S was the only active species and, within the above two-step scheme, Li₂S₂ was formed.⁴³ The aluminas, α-Al₂O₃ and γ-Al₂O₃, were often used as supports with increased catalytic activity resulting in some cases.³⁰ They themselves were tested in the range 500 - 1000 °C and, whereas α-alumina did not catalyze the decomposition,^{17a} γ-alumina was effective as a physically active medium for H₂S adsorption and subsequent decomposition.⁴⁴ Activation energies for the catalyzed H₂S thermodecomposition range from 14 to 27 kcal mol⁻¹ compared to values of 42 to 50 kcal mol⁻¹ for the uncatalyzed reaction.^{15,17a,25b,30,39} By continuous or intermittent removal of either or both H₂ and 'S', conversions of more than 95% of H₂S have been achieved.³⁰

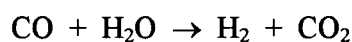
A few different approaches to the thermodecomposition of H₂S have also been explored. Raymont¹⁹ proposed an open loop system where the thermodynamically unfavourable decomposition of H₂S is coupled with the favourable oxidation of CO via a two-step process:



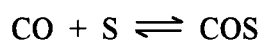
where the SO₂ required is produced in a manner similar to the Claus process. The overall reaction produces H₂, 'S', and CO₂. Alternatively, the COS formed in the first step could be thermally decomposed at high temperatures (*i.e.* 830 °C) giving 'S' and CO, and by rapid cooling the 'S' could be separated from CO which is then recycled back to the first step.^{45,46,47} Towler et al.⁴⁸ and Bowman⁴⁶ extended similar chemistry using CO₂:

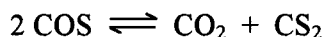


The sulfur is cooled and removed, and the remaining gases undergo the water gas shift reaction:



COS and CS₂ are side-products that invariably form, for example via the following reactions:

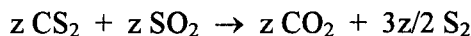
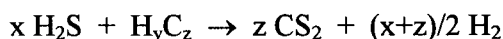




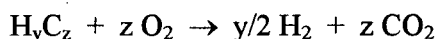
but after separation of sulfur, the residual COS and CS₂ can be reduced at high temperatures via the reaction:



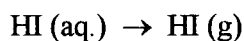
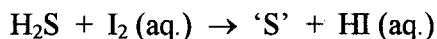
with the resulting CO subjected to the water gas shift reaction.⁴⁶ In the preceding examples of both open and closed loop systems, conversion of H₂S to H₂ and elemental sulfur is greater than when H₂S is heated alone, but the rate-limiting step is still the thermal dissociation of H₂S for which transition metal sulfide catalysts are used particularly MoS₂. Raymont¹⁹ also studied another open loop system based on the oxidation of hydrocarbons,^{49,50} as shown by the following scheme:



The overall reactions produce H₂ from H₂S and hydrocarbons, using the oxidation of the carbon present in hydrocarbons as the driving force:



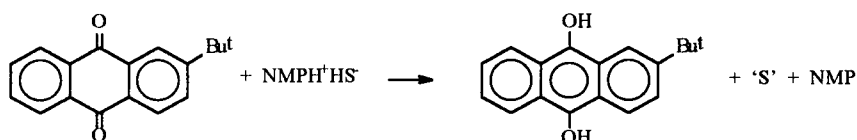
In a different approach, Chen⁵¹ investigated the reaction of H₂S with I₂ in aqueous solution, and found that HI was formed while sulfur precipitated. The elemental 'S' was removed and the aqueous HI solution was treated to obtain anhydrous HI which was decomposed at high temperatures and pressures over a high surface area catalyst.



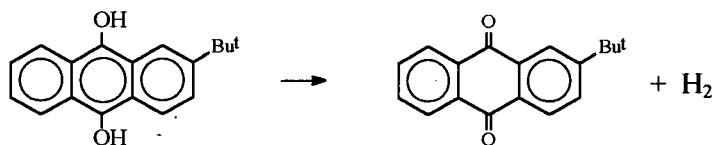
Plummer⁵² studied the interaction of H₂S with quinones, and described a three-step process involving two catalysts with emphasis on the importance of the reaction solvent. He identified N-methyl-2-pyrrolidone (NMP) as an effective polar medium:



H₂S reacts with NMP to form the quaternary ion complex which then reacts with the quinone, t-butyl anthraquinone, to yield sulfur and the corresponding hydroquinone:



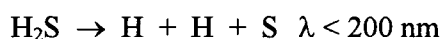
After removal of the sulfur, the hydroquinone is catalytically dehydrogenated over CrO₃ at high temperatures, and H₂ is recovered.



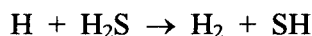
Despite unfavourable thermodynamics, the thermodecomposition of H₂S to H₂ and S can be achieved using open or closed loop systems. Combining the use of catalysts and the intermittent or continuous removal of products, high conversions of nearly 100% are possible.

1.2.2 Photodecomposition of H₂S

The photodissociation of H₂S has been extensively studied at a fundamental level, and references can be traced through Okabe's review.⁵³ By means of flash photolysis, the primary process following absorption of light in the ultraviolet has been shown to be the production of H atoms and S atoms or SH radicals:



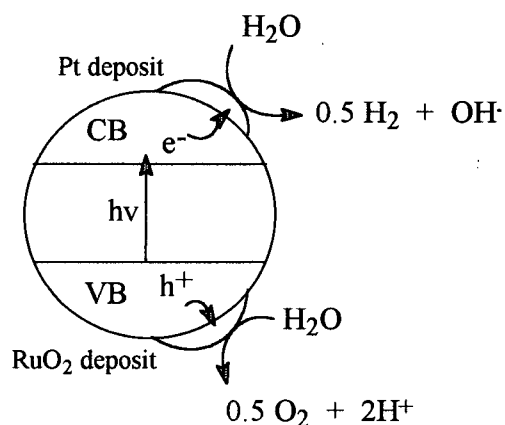
At $\lambda > 200$ nm, the fates of H and SH radicals are as illustrated in the secondary reactions:



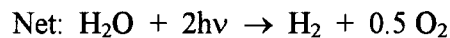
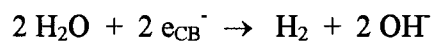
The main final products though are H₂ and elemental sulfur. For industrial application, the use of ultraviolet radiation is not practical because of the energy expenditure; however, work with laser radiation of noble gas halide compounds (low energy consumption) has been reported.⁵⁴ Currently, researchers are seeking to exploit solar energy either as solely a heat source (see Section 1.2.1) or as a cheap and plentiful source of photons. The energy available from visible light, however, is not sufficient to affect dissociation of the H-SH bond, but when certain semiconductor particulates are present, redox processes take place on the surfaces resulting in solar-driven efficient production of H₂ and elemental sulfur.

Research in visible light-induced cleavage of H₂S using semiconductor materials stemmed from investigations of microheterogeneous and colloidal systems that decompose water into H₂ and O₂.^{55,56} Semiconductor materials, such as CdS and TiO₂, possess several attractive properties as light harvesting units: a) high extinction coefficients; b) fast carrier diffusion (migration) to solid-

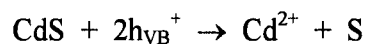
surface interface; and c) suitable positioning of conduction and valence bands.⁵⁷ The band gaps of these materials, in particular, correspond to energy differences coinciding with those of visible light. For instance, CdS has a band gap of 2.4 eV corresponding to an absorption edge of ~520 nm. As such, these materials have been shown to decompose water upon illumination via generation of charge carriers, *i.e.* conduction band electrons, e_{CB}^- , and valence band holes, h_{VB}^+ . Co-deposits of noble metal catalysts, Pt and RuO_2 , prevent recombination of $e_{CB}^- h_{VB}^+$ by facilitating separation through trapping and promotion of these charge carriers in interfacial transfer to acceptor molecules:



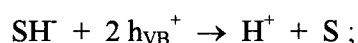
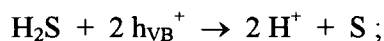
Thus, water is reduced or oxidized by e_{CB}^- or h_{VB}^+ , respectively, to yield H_2 and O_2 , and the net reaction is accomplished by two quanta of light:



In the case of CdS, RuO_2 also serves to prevent photocorrosion, for example, via the following reaction, by effectively scavenging the valence band holes as they form:



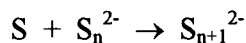
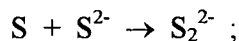
The analogous chemistry has been applied to H₂S using CdS colloidal dispersions.⁵⁷⁻⁷¹ Whereas both Pt and RuO₂ are required to photodecompose water, these noble metals need not be present as photocleavage of H₂S is possible on bare CdS. The rate of hydrogen production (r(H₂)), however, significantly increases when RuO₂ is present, the enhancement being attributed to effective h_{VB}⁺ separation and transfer to the solution. At the solid-solution interface, the holes oxidize H₂S, SH⁻, or S²⁻ depending on the pH:



Higher r(H₂) were seen at higher pH, with a sigmoidal dependence of r(H₂) on pH, the effective S²⁻ concentration being governed by the pK_a.⁵⁸ The oxidation process is envisaged as adsorbed SH⁻ or S²⁻ species scavenging the holes trapped by the noble metal deposit. The presence of Pt proved superfluous as no improvement in H₂ yields was seen. Apparently, adsorbed SH⁻ or S²⁻ induces a cathodic shift in the flat band potential and thereby greatly increasing the driving force for the reduction of H₂O to H₂ making the intervention of Pt unnecessary;⁵⁸ however, recent reports^{70,71} describe platinized CdS to be quite effective, with H₂ yields even higher than those achieved with RuO₂ deposited-CdS. These discrepancies were not addressed although earlier reports⁵⁷ emphasized that the method of preparing semiconductor colloids is crucial and that usage of different salts (*i.e.* Cd(NO₃)₂, Cd(SO₄), and CdCl₂) results in remarkable differences in r(H₂), for example, in the order NO₃⁻ > SO₄²⁻ > Cl⁻. The rationale given ascribed differences to modification of active sites for H₂O reduction and/or increase in the extent of charge separation.

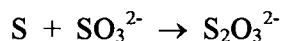
Attempts to improve photocatalytic activity were studied by employing different semiconductors or different metal deposits, or by adding chemical sinks. One problem inherent in

photodecomposing H_2S is the formation of polysulfides, S_n^{2-} , resulting from the reaction of S, once formed from oxidation of SH^- or S^{2-} , with S^{2-} or other S_n^{2-} species:

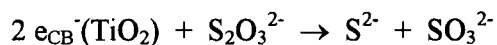


Once the solution is saturated with S_n^{2-} , elemental sulfur begins to precipitate out. Neither S nor polysulfide interferes with the actual redox processes but the polysulfides absorb in the blue-green region of the spectrum (~ 500 nm) and catalytic activity is therefore progressively reduced. If, however, the solution is kept shallow and continuously flowing over an inclined bed of immobilized semiconductor particulates, then reduction in activity is eliminated.^{70,71} A further advantage in this approach is the resultant separation of products (H_2 gas percolates countercurrently); the issue of product separation from solutions containing colloidal dispersions remains to be resolved.⁷¹

Addition of SO_3^{2-} was explored as a chemical sink as it reacts with S to form thiosulfate which is colourless.^{59,60}



A significant increase in $r(\text{H}_2)$ was observed; however, as the concentration ratio of SO_3^{2-} to S^{2-} is increased, a retarding effect is observed because of interference from $\text{S}_2\text{O}_3^{2-}$ competing with SH^- or S^{2-} for active sites.⁶⁰ TiO_2 particles were then found to be capable of efficiently photoreducing thiosulfate back to sulfide and sulfite,⁶³ and illumination by visible light produced $e_{\text{CB}}^- h_{\text{VB}}^+$ pairs that respectively reduce and oxidize $\text{S}_2\text{O}_3^{2-}$ according to the following reactions:



When coupled with CdS/RuO_2 , the system could potentially give higher H_2 yields, but S^{2-} would be catalytically recycled. In actuality, the system performs poorly, giving lower $r(\text{H}_2)$ than with

CdS/RuO₂ alone.⁶⁴ Astonishingly high $r(\text{H}_2)$ were observed, on the other hand, when RuO₂ was deposited on TiO₂ instead of CdS; in fact, the system is superior to that of CdS/RuO₂. The results were attributed to effective charge carrier separation; an inter-particle e_{CB}^- transfer to TiO₂ vectorially displaces the charges and thereby preventing electron-hole recombination. Thereafter, the e^- migrates and is trapped by RuO₂ which subsequently promotes an interfacial transfer to H₂O. Holes remaining on CdS do not transfer to TiO₂, perhaps being inhibited for energetic reasons, but migrate to the surface to oxidize sulfide. Replacement of RuO₂ by Pt on TiO₂ results in suppression of H₂ production, and no catalytic activity is seen when TiO₂/RuO₂ is used alone.⁶⁴ A combination of CdS/RuO₂ + TiO₂/RuO₂ was studied for which 100% photodecomposition of H₂S under direct sunlight irradiation was reported, the method of colloid preparation being emphasized.⁶⁶

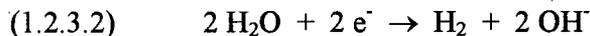
Metal deposits and semiconductor dispersions have been investigated. For example, vanadium sulfide or oxide dispersions loaded with RuO₂ give results comparable to those of the CdS/RuO₂ system.⁶⁷ Furthermore, a mixture of V₂O₅ and V₂S₃ semiconductor dispersions loaded with Pt or RuO₂ give higher H₂ yields due to additional vectorial displacement of charges via inter-particle e^- transfer from V₂O₅ to V₂S₃ (*cf.* the CdS + TiO₂/RuO₂ system). Pt on V₂S₃ facilitates interfacial e^- transfer more efficiently than RuO₂ on TiO₂, a phenomenon yet to be explained.⁶⁹ Substitution of RuO₂ by RuS₂ on CdS dispersions improves photocleavage of H₂S several-fold.⁶⁵ Finally, thin films of CdSe have been studied in the photoelectrolysis of H₂S where CdSe is utilized as a photoanode connected to a Pt cathode by Cu wire.⁶⁸ The chemistry is the same; sulfide is oxidized to elemental S, and H₂ evolves at the cathode. An advantage to this system is that electricity can also be generated.

Of note, an indirect method of photodecomposing H_2S using oxidants such as I_2 has been patented.⁷² Iodine reacts with H_2S in water to form aq. HI and elemental sulfur. After the sulfur is removed, the aq. HI is fed into a photoelectrolyzer, and H_2 and I_2 are produced at the cathode and photoanode, respectively; the I_2 is subsequently recycled. This method parallels those reported earlier where aq. HI is generated, but is either treated to give anhydrous HI which is then thermally decomposed (see Section 1.2.1) or directly electrolyzed (see Section 1.2.3). Alternatively, the HI formed in solution could be directly photodecomposed without prior treatment of any kind (see Chapter 5).

1.2.3 Electrochemical decomposition of H₂S

The electrochemical decomposition of H₂S has been studied as a means of recovering H₂ and elemental sulfur. The methods reported in the literature can be classified into two groups, direct and indirect. Direct conversion is simply accomplished by passage of current through an electrolyte solution containing H₂S. Indirect conversion involves reaction with an oxidant to produce elemental sulfur which is then separated prior to electrochemical treatment of the spent oxidant for regeneration and simultaneous production of H₂. The required electronics are usually determined both experimentally and by application of Nernstian fundamentals, and vary with factors such as temperature, concentration, choice of electrode and electrolyte materials, and usage of ion-selective membranes separating the anodic and cathodic compartments. In general, higher potentials are needed for indirect conversion but anode passivation is avoided as sulfur is not electrochemically produced as in the direct processes; however, the sulfur is usually in a sticky, plastic form requiring further treatment and purification to obtain the crystalline form that is produced in direct conversion methods.

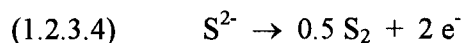
Along with recovery of valuable commodities, direct electrochemical conversion of H₂S has also been explored in the areas of metal refining⁷³ and coal and natural gas processing.⁷⁴ In these processes, electrolysis of H₂S is carried out in basic solvents or solutions or in molten alkali sulfide electrolytes. One problem inherent in the direct method is the rapid passivation of the anode once oxidation takes place to form elemental sulfur.^{75,76} The sulfur coats the electrode and the electrochemical process terminates as the current decreases to zero. To circumvent the problem, basic solvents or solutions are used, most commonly aqueous NaOH.⁷⁷⁻⁸³ The respective anodic and cathodic reactions are as follows:



As previously noted (Section 1.2.2), elemental sulfur in basic media is unstable and reacts with S^{2-} to form soluble polysulfides S_n^{2-} . By forced mechanical convection, anode passivation is minimized and elemental sulfur precipitates from the bulk solution once saturation with polysulfides is reached. Immiscible organic solvents such as toluene have also been employed to extract the sulfur as it forms.⁸⁰ In a different approach, the electrochemical decomposition of H_2S in molten alkali sulfides has been studied as a means to process sour hydrocarbon feeds.^{74,84} High temperatures (600 - 1000 °C) are used to mimick thermal conditions normally encountered in industry. Binary mixtures of M_2S (M = Li, Na, K) are identified as appropriate electrolyte materials in view of the sulfidic nature of H_2S . As a gaseous stream containing H_2S enters the cathodic compartment, reduction occurs and the resultant H_2 is subsequently carried off with the now-sweetened stream:

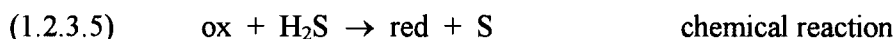


The sulfide produced then migrates through the electrolyte suspended in an inert matrix to the anode, and gaseous S_2 forms via oxidation:

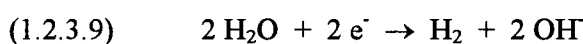
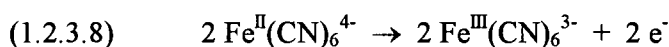
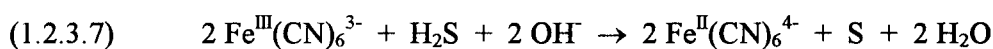


An inert gas such as N_2 is used in the anodic compartment to sweep away the gaseous sulfur for condensation elsewhere. Anode passivation is not an issue here as high temperatures are present.

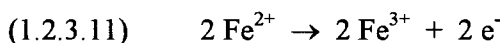
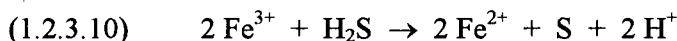
Anode passivation is not seen in indirect electrochemical conversion of H_2S as the sulfur is formed via chemical reaction with an oxidant and is separated prior to electrochemical treatment of the spent oxidant. Reactions 1.2.3.5 and 1.2.3.6 represent the process in general where ox and red are oxidized and reduced species, respectively:



The various oxidants studied can be classified into three groups: (1) Fe(III) compounds; (2) halogens; and (3) quinones. Of the iron(III) compounds investigated, $\text{Fe}^{\text{III}}(\text{CN})_6^{3-}$ complexes were the first to be studied in indirect electrochemical decomposition of H_2S .⁸⁵ The chemical reaction with H_2S is performed in basic aqueous systems (reaction 1.2.3.7). Thereafter, the spent oxidant is regenerated according to reactions 1.2.3.8 and 1.2.3.9 with production of H_2 .

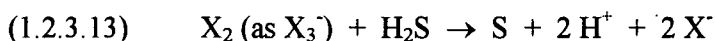


Similarly, $\text{Fe}(\text{III})\text{Cl}_3$ salts have been studied, and in aqueous acidic systems, the reactions are as follows:

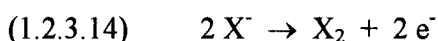


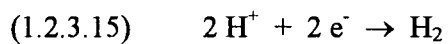
Numerous patents exist for this process,⁸⁶ and successful bench-scale development has been reported.⁸⁷ With halogens, Br_2 and I_2 are typically used, and employed in aqueous acidic conditions such that solubilization occurs forming the corresponding trihalides, Br_3^- and I_3^- .⁸⁸⁻⁹¹

Reaction with H_2S proceeds according to reaction 1.2.3.13 where X = halide:

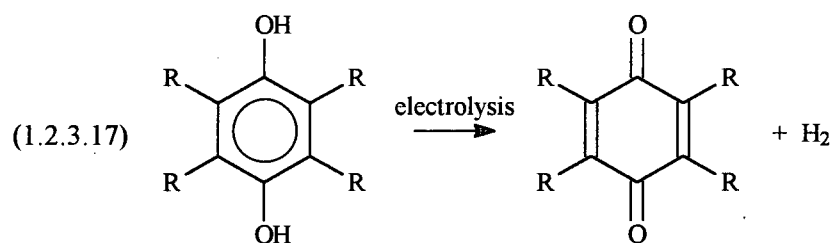
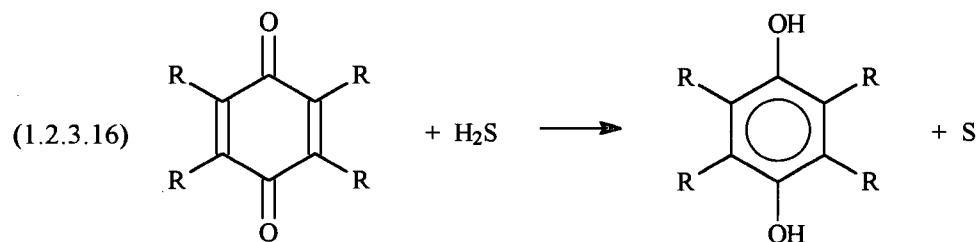


After the precipitated sulfur is removed, the remaining acidic solution is electrolyzed, regenerating X_2 with accompanying H_2 production:



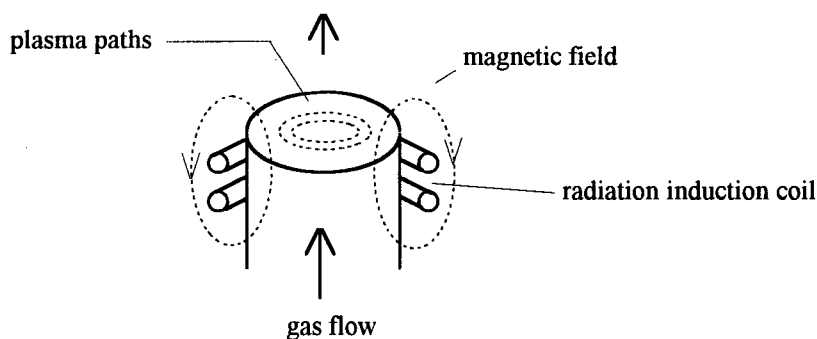


Finally, indirect electrochemical decomposition of H_2S has also been examined using quinones (see also Section 1.2.1), and the process is briefly depicted as follows.⁹²



1.2.4 Plasmachemical decomposition of H₂S

Currently, there is rapid development of a novel technology first introduced in the Soviet Union during the mid-1980s.^{93,94} Plasmachemical decomposition of H₂S into H₂ and elemental sulfur using microwave or radio frequency radiation has been achieved.^{95,96} The process is economically attractive due to low energy expenditures, and the small scale industry level has been reached,⁹⁶ competing successfully with traditional H₂S removal processes such as the Claus method (see Section 1.1). The principle involves the generation of a conducting plasma (cations and electrons) which in the presence of a fluctuating magnetic field, produced by the applied radiation, flows in a closed annular path:



Through cationic or electronic impact, atomization of the entering gas stream occurs and subsequent product formation follows as the stream exits. High temperatures are often present (ohmic heating), and thermodecomposition can also take place. The formed sulfur is removed via condensation, and the remaining H₂ gas is recycled to decompose unconverted H₂S; overall conversion efficiencies in excess of 99% are typically seen.

Plasma decomposition of H₂S by passage through an electrical discharge has also been explored.⁹⁷⁻¹⁰⁰ The methodology is not new,^{101,102,103} and recent resurgence is the result of the

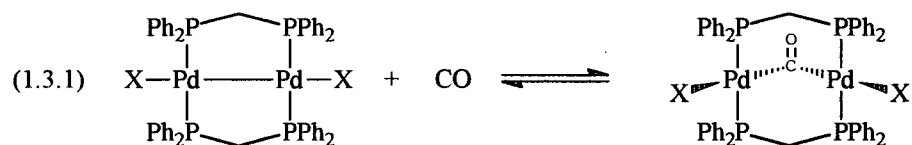
ongoing search for economic as well as ecologically sound ways to process H_2S . As in microwave or radio frequency plasmachemical decomposition, the mechanistic aspects are not well understood, but mechanisms resembling those in photodecomposition have been proposed for both types of technologies (see Section 1.2.2).^{94,98,104}

1.2.5 Radiolytic decomposition of H_2S

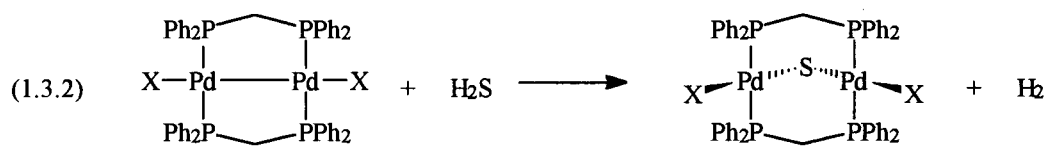
Radiolytic decomposition of H_2S has been investigated^{105,106} but the potential use for recovering H_2 and elemental sulfur is unrealistic because of the radioactive nature of the α -, β -, and γ -particles employed. Particle energies are of the order 10^6 eV (*cf.* HS-H and S-H bond strengths^{107,108} are ~ 360 kJ mol⁻¹ or 3.7 eV per molecule), and a variety of ions, excited molecules, atoms, and free radicals are produced during the primary and secondary processes. The chemistry resembles the radical mechanisms encountered in the photodecomposition of gaseous H_2S . H_2 and elemental sulfur are the main products along with small amounts of sulfanes, H_2S_n .

1.3 Homogeneous catalytic conversion of H₂S to H₂

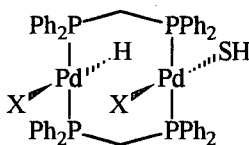
Research in this laboratory on the separation of components in coal gasification streams using coordination compounds¹⁰⁹⁻¹¹² has stimulated an interest in transition metal - H₂S chemistry. The well-known Pd₂X₂(dpm)₂ complexes¹¹³ (X = halide, NCO) show excellent selectivity for CO in the presence of CO₂, N₂, O₂, H₂, C₂H₄, and C₂H₂, with rapid reversible binding observed:



Tests were made for H₂S, an impurity often present in such streams, and resulted in the first homogeneous solution reaction showing a quantitative 1:1 H₂S uptake : H₂ evolution stoichiometry at a metal center:¹

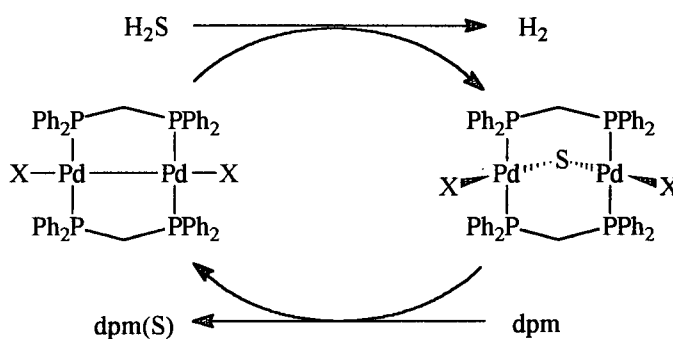


Deuterium labelling studies¹¹⁴ demonstrated that the H₂ evolved came exclusively from H₂S. Related studies showing H₂ generation from homogeneous reactions with H₂S can be found in the literature (see Section 1.4) but involve 'simple' S-abstraction by metal centres. Detailed kinetic and mechanistic investigations^{114,115} revealed that reaction 1.3.2 proceeds via oxidative addition that generates a hydrido(mercapto) intermediate (**I**); H₂ production is then envisaged as deprotonation of SH followed by protonation of the hydride ligand, with concomitant formation of the μ-S species, a so-called 'A-frame' structure.¹¹⁶



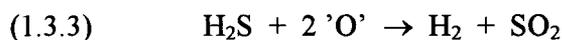
I

Prior adduct formation with H_2S en route to the intermediate, although not detected, was not ruled out;¹¹⁴ indeed, in this respect, a few transition metal - H_2S complexes have been characterized¹¹⁷⁻¹²² including ^1H NMR spectroscopic evidence for the species $\text{Pt}(\text{PPh}_3)_2(\text{SH}_2)$ ¹²⁰ en route to formation of a more stable hydrido(mercapto) complex, as well as recent X-ray crystallographic characterization of $\text{Ru}(\text{SH}_2)(\text{PPh}_3)(\text{'S}_4\text{'})$ ($\text{'S}_4\text{'}$ = tetradentate 2,2'-(ethylenedithio)bis(thiophenolate)dianion)¹²¹ and $\text{Ru}(\text{SH}_2)\text{Cl}_2(\text{P-N})(\text{PR}_3)$ ($\text{P-N} = o$ -diphenylphosphino-*N,N*-dimethylaniline, $\text{R} = p$ -tolyl).¹²² The rate-determining step for reaction 1.3.2 was shown not to be the subsequent conversion of the intermediate I, and the observed reactivity trend $\text{X} = \text{Cl} > \text{Br} > \text{I}$ was rationalized by the reactivity being governed by the off-rates (*i.e.* $\text{I} \rightleftharpoons \text{H}_2\text{S adduct} \rightleftharpoons \text{Pd}_2\text{X}_2(\text{dpm})_2 + \text{H}_2\text{S}$). The same reactivity trend for the CO systems is definitely governed by off-rates.¹¹⁰ Unlike reaction 1.3.1, reaction 1.3.2 was shown to be irreversible even under 10 atm H_2 .^{1,114} A search for a possible kinetic role of the bridging dpm ligands in the forward reaction was complicated by the abstraction of sulfur from the bridged-sulfide complex by added dpm. This observation has led to further kinetic and mechanistic studies (see Chapter 3) and the first reported homogeneous catalytic conversion of H_2S to H_2 ,¹²³ illustrated below:



dpm(S) = bis(diphenylphosphino)methane monosulfide

Alternatively, the sulfur could be eliminated as SO_2 from $\text{Pd}_2\text{X}_2(\mu\text{-S})(\text{dpm})_2$ following oxidation by H_2O_2 and/or *m*-chloroperbenzoic acid to the $\text{Pd}_2\text{X}_2(\mu\text{-SO}_2)(\text{dpm})_2$ ¹¹⁵ species which spontaneously loses SO_2 ,¹²⁴ and the net reaction 1.3.3 could be affected catalytically using the $\text{Pd}_2\text{X}_2(\text{dpm})_2$ complexes.^{1,115}



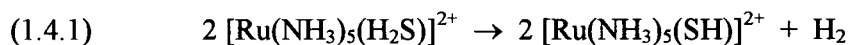
The possibility of immobilizing $\text{Pd}_2\text{X}_2(\text{dpm})_2$ on solid supports,¹¹¹ for instance via the methylene group(s) of the dpm ligand(s), has resulted in the syntheses of several complexes of the types $\text{Pd}_2\text{X}_2(\text{dpm})(\text{dpmMe})$,¹¹¹ *syn*- and *anti*- $\text{Pd}_2\text{X}_2(\text{dpmMe})_2$,^{111,125} and $\text{Pd}_2\text{X}_2(\text{dpmMe})(\text{Ph}_2\text{Ppy})$ ¹¹¹ (dpmMe = 1,1-bis(diphenylphosphino)ethane; Ph_2Ppy = 2-(diphenylphosphino)pyridine). These were tested for reactivity toward CO and/or H_2S : only $\text{Pd}_2\text{X}_2(\text{dpm})(\text{dpmMe})$ and *syn*- $\text{Pd}_2\text{X}_2(\text{dpmMe})_2$, where the Me groups are on the same side with respect to the Pd-C-Pd plane, showed reactivity and this was slow compared to that of $\text{Pd}_2\text{X}_2(\text{dpm})_2$, reflecting steric impositions within the A-frames in accommodating the Me group(s).^{111,125} With H_2S , the corresponding $\mu\text{-S}$ complex and concomitant H_2 formation were observed; kinetics and mechanisms were not studied, but a similar oxidative addition as in reaction 1.3.2 via intermediates akin to I is readily visualized. The incorporation of Ph_2Ppy bridging ligands was a matter of synthetic convenience, and in separate studies a series of $\text{Pd}_2\text{X}_2(\text{PPh}_n\text{py}_{3-n})_2$ ($n \geq 1$)

complexes have been prepared with the goal of imparting solubility in aqueous systems;¹²⁶ the chemistry with H₂S has not been explored yet. Of note, in extending the chemistry of H₂ recovery from hydrides of group 16 elements, the Pd₂X₂(dpm)₂ complexes also react with H₂Se¹²⁷ and H₂O¹²⁷ but the reactions are not clean and side-products, including, as yet, uncharacterized species, are seen. With H₂Se, Pd₂Cl₂(μ-Se)(dpm)₂ is formed along with H₂ but Pd₂(dpm)₂(μ-Se)Cl(SeH) and Pd₂(dpm)₂(μ-Se)(SeH)₂ are also produced due to the greater acidity of H₂Se. With H₂O, the reaction is complex and NMR spectroscopic data reveal numerous unidentified products; however, separate studies showed that Pd₂Cl₂(dpm)₂(μ-O) can be generated at low temperatures, for example by treating Pd₂Cl₂(dpm)₂ with *m*-chloroperbenzoic acid at -50 °C; warming above -50 °C causes decomposition, again to unidentified products. Clearly, these discoveries together with other metal/H₂X (X = Se, O) systems^{128,129} demonstrate that H₂ recovery is not necessarily limited to H₂S systems.

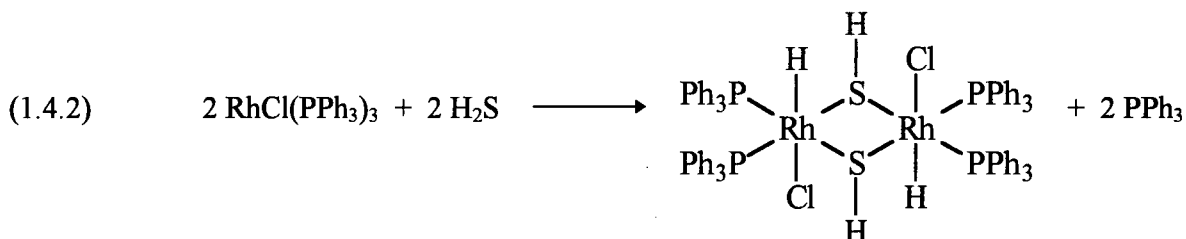
1.4 Transition metal - H₂S chemistry

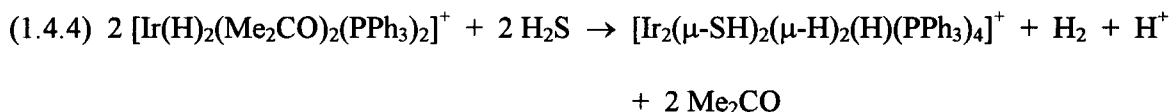
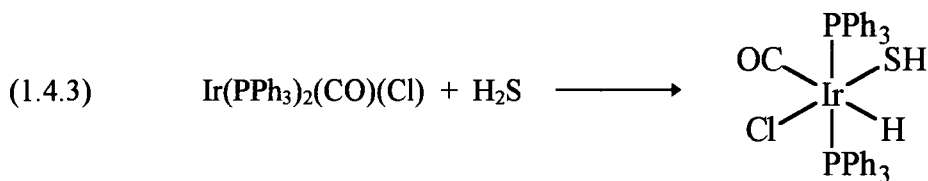
There is considerable interest in transition metal - H₂S chemistry because of its relevance in biological cycles, the formation of ores, the hydrodesulfurization catalytic process, and in the potential use of H₂S as a source of H₂ and organosulfur compounds. Literature dealing with the subject is plentiful and can be traced through recent references.¹³⁰⁻¹³³ In view of this laboratory's efforts to study the recovery of H₂ from H₂S (see Section 1.3), it seems appropriate to review briefly the literature regarding similar chemistry, particularly in homogeneous systems. The area of recovering H₂ from H₂S in heterogeneous systems has been described earlier (see Section 1.2).

Outside of this laboratory's current work with Pd, the interaction of H₂S has been explored mainly with complexes of Ru, Rh, and Ir. Kuehn and Taube first reported¹¹⁷ a system generating H₂ from H₂S and tentatively suggested reaction 1.4.1, but stated that [Ru(NH₃)₅(H₂S)]²⁺ was not obtained in pure state.

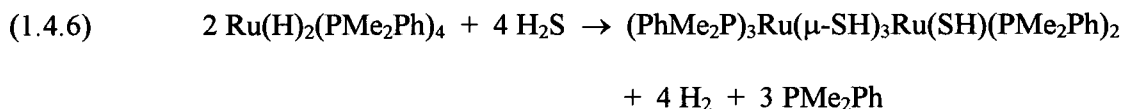
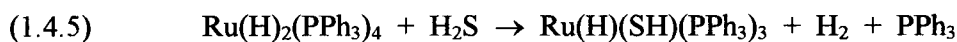


Pignolet's group was the first to initiate solution studies focusing on the recovery of H₂ from H₂S, and examined Rh and Ir phosphine complexes: hydrido(mercapto) species were formed but no H₂ production was seen (reactions 1.4.2 and 1.4.3).¹³⁴ The formation of H₂, however, was observed in later studies using Ir hydrido precursors (reaction 1.4.4).¹³⁵

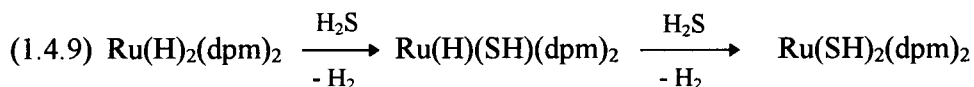
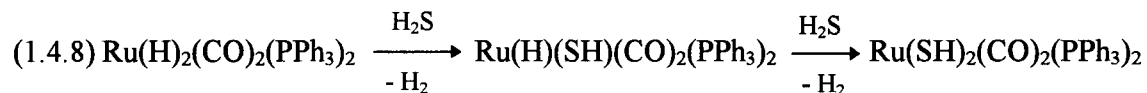
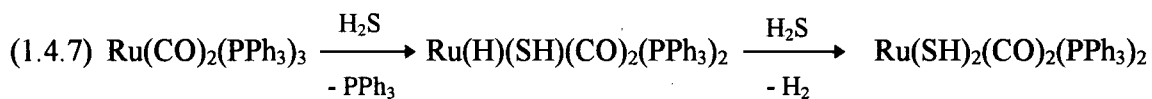




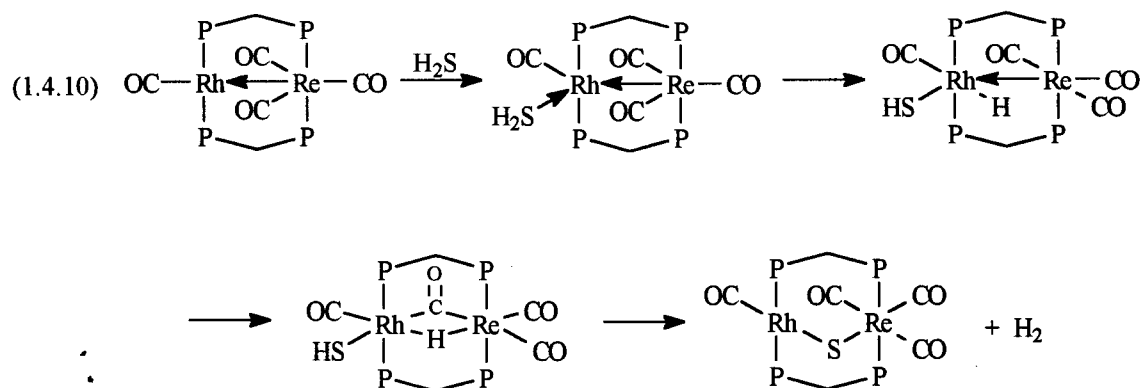
Similarly, Osakada et al. had studied earlier the reaction of H_2S with Ru(II) hydrido complexes (reactions 1.4.5 and 1.4.6).^{136,137} Quantitative evolution of H_2 was reported, but its origin was not addressed.

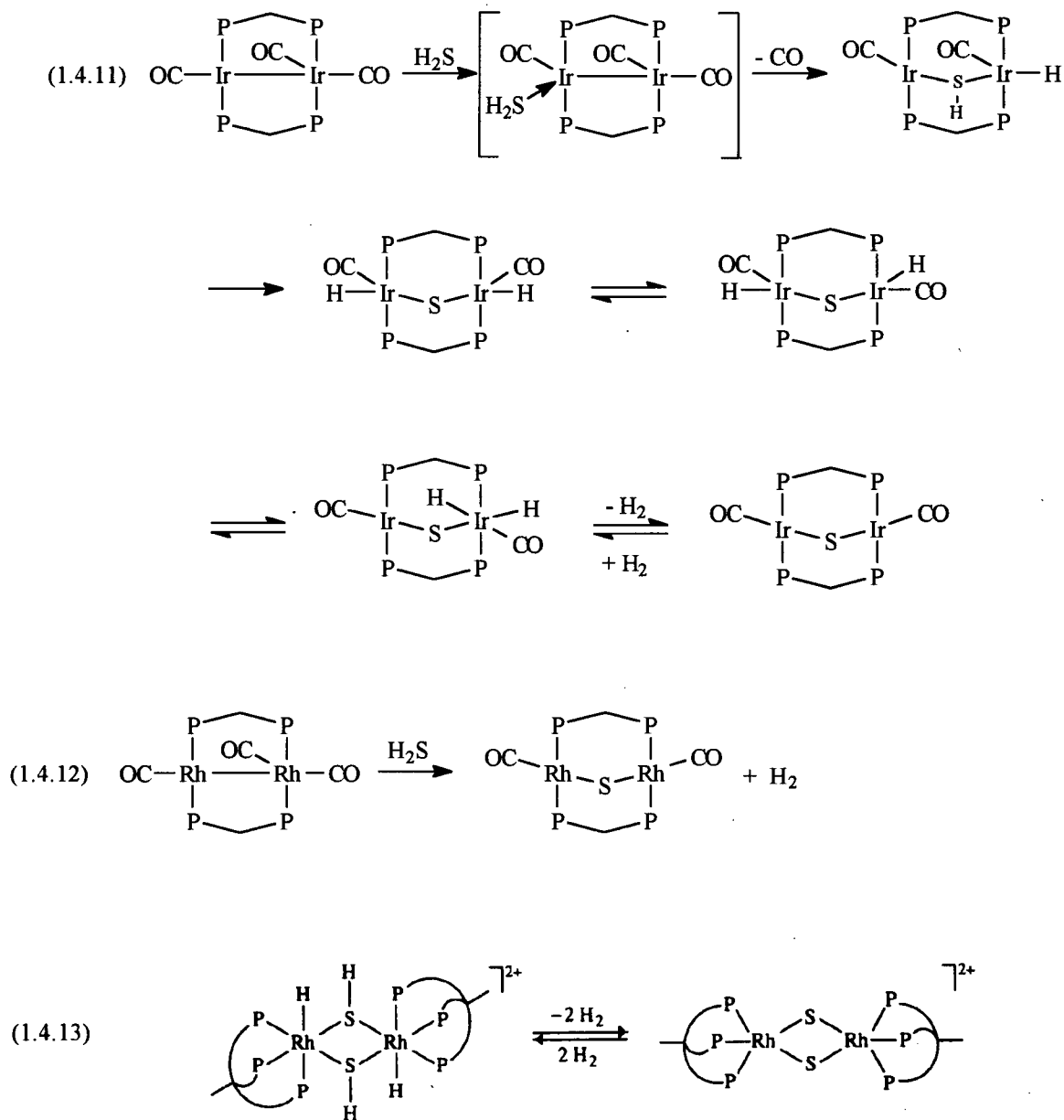


James et al. in their work^{131,138,139} demonstrated oxidative addition of H_2S to Ru(0) complexes, with the resulting Ru(II)-hydrido(mercapto) species reacting with further H_2S to generate H_2 (reaction 1.4.7); other Ru(II)-dihydrides (*cf.* reactions 1.4.5 and 1.4.6) also generated H_2 on reaction with H_2S via an assumed protonation of coordinated hydride (reactions 1.4.8 and 1.4.9). Two mechanisms to account for the formation of H_2 were proposed: (1) following dissociation of H_2S to H^+ and SH^- , protonation of the metal hydride liberates H_2 , and the vacant site thus generated is coordinated by SH^- ; and (2) coordination of H_2S at a vacated site, resulting from the loss of a labile phosphine ligand, followed by protonation of the hydride ligand, elimination of H_2 , and subsequent re-coordination of the phosphine. The possibility of the first mechanism seems remote as H_2S is a very weak acid in THF,¹³⁰ the solvent in which the reactions were studied.

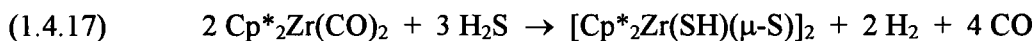
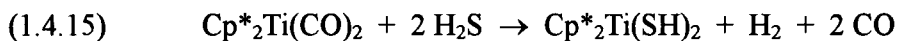


Homo- and hetero-bimetallic complexes of Ir, Rh, and Re have been used by Cowie et al. in reactions with H_2S to ascertain further (*cf.* Section 1.3) the roles of adjacent metals in the activation of S-H bonds (reactions 1.4.10 - 1.4.12).^{130,133} NMR spectroscopy was invaluable in providing evidence for the illustrated intermediates (those not in brackets) that lead to the products. The findings show how two metals in proximity can provide means for double-activation (*i.e.* successive oxidation additions) as in reaction 1.4.11. Reaction 1.4.11 shows reversible H_2 elimination, a phenomenon that has been previously seen by Bianchini et al. within a characterized doubly-bridged mercapto binuclear Rh complex formed from reaction of (triphos)RhCl(C_2H_4) with H_2S (reaction 1.4.13).¹⁴⁰

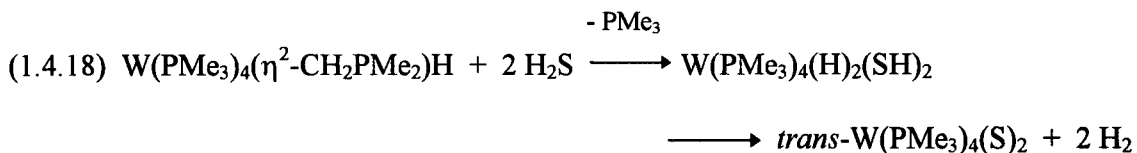




In other studies, Bottomley et al.¹⁴¹ and Howard and Parkin¹⁴² have examined the interactions of H₂S with metallocenes of Ti and Zr (reactions 1.4.14 - 1.4.17). Reaction 1.4.14 is complicated and the stoichiometry has not been unequivocally substantiated.¹⁴⁴ The H₂ is presumably formed via protonation of intermediate hydrides.

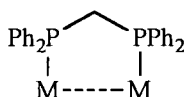


Rabinovich and Parkin have investigated the interaction of H₂S with W phosphine complexes¹⁴³ in attempts to unravel the role the metal plays in hydrodesulfurization,⁷ quantitative evolution of H₂ was observed for reaction 1.4.18, which is the first to demonstrate formation of a terminal sulfide ligand from an H₂S reaction. That facile elimination of H₂ from H₂S occurs to give W(PMe₃)₄(S)₂ is of considerable interest in view of the proposal that hydrogenation of organic substrates during HDS may involve hydrogen transfer from an -SH group.¹⁴⁴



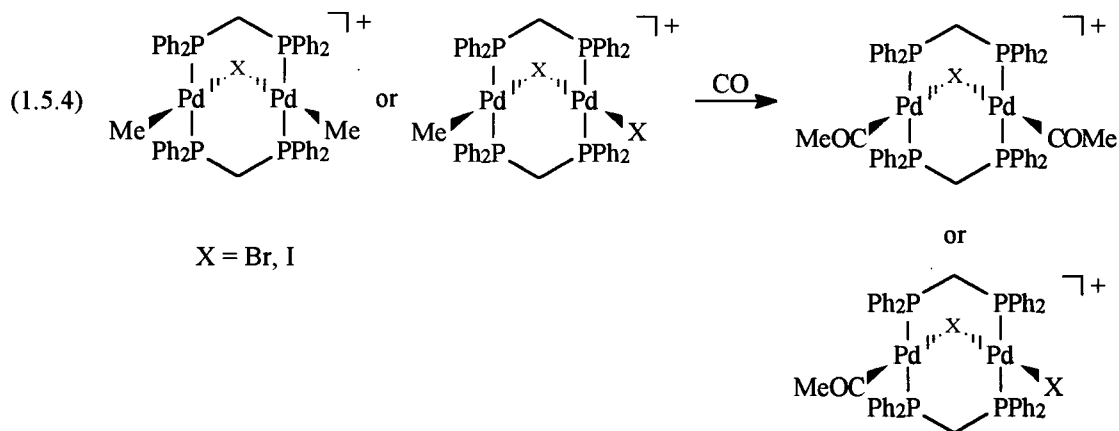
1.5 The chemistry of transition metal - dpm complexes

The expectation that two metal atoms in proximity can lead to reactivity patterns different to those of a single metal has resulted in broad development of the chemistry of binuclear complexes. In this respect, bis(diphenylphosphino)methane serves as a versatile ligand that is able to lock two metals in close vicinity forming closed (metal-metal bonded) or “open” five-membered rings:

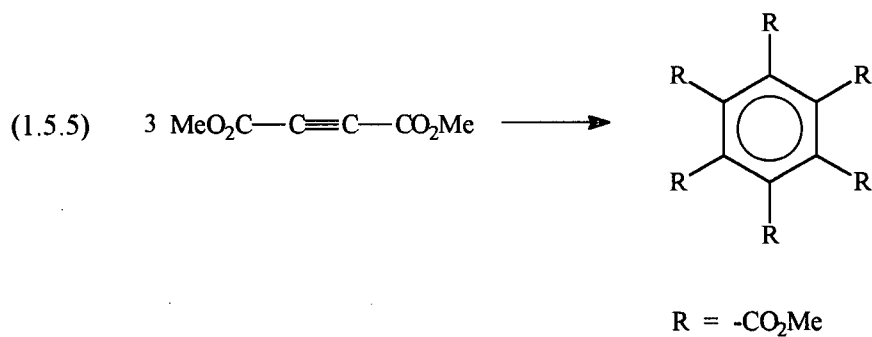


The ligand essentially prevents dissociation of dimer to monomer and can promote bridging by other groups as well as promoting reactions involving formation and cleavage of metal - metal bonds. Since the first dpm-bridged dinuclear complex, $[\text{RhCl}(\text{CO})(\text{dpm})]_2$, was prepared by Mague and Mitchener in 1969,¹⁴⁵ many more have emerged and examples can be found for most of the transition metals. Because of the enormity of the subject, no attempt will be made here to review the chemistry, and the present short discussion is confined to more notable examples of reactivity found with the intensively studied dpm-bridged dinuclear complexes of group 10 elements of which Pd and Pt have drawn the most attention. There are several excellent reviews on transition metal - dpm complexes that include a description of mononuclear as well as heterobimetallic species containing dpm also as a chelating, non-bridging ligand.¹⁴⁶⁻¹⁴⁹

Of note, the dpm-chemistry of Ni is relatively new and little developed. Kubiak's group reported the first dpm-bridged dinickel complex, $[\text{Ni}_2(\mu\text{-CNMe})(\text{CNMe})_3(\mu\text{-dpm})_2]\text{PF}_6$, which is asymmetrical and contains a dative metal-metal bond.¹⁵⁰

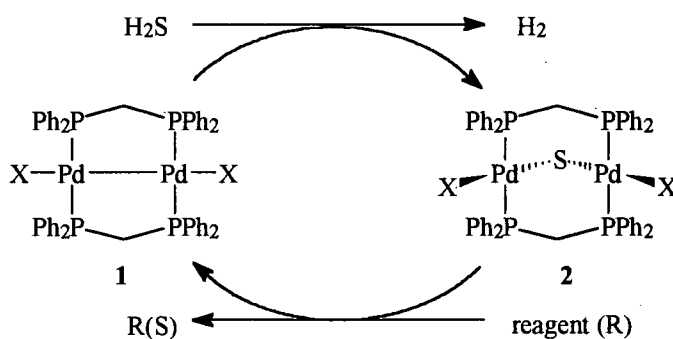


The $\text{Pd}_2\text{X}_2(\mu\text{-dpm})_2$ complexes have been shown to exhibit catalytic activity. For example, the cyclotrimerization of alkynes is catalyzed by $\text{Pd}_2\text{Cl}_2(\mu\text{-dpm})_2$ or $\text{Pd}_2\text{I}_2(\mu\text{-dpm})_2$ (reaction 1.5.5).¹⁵⁹ Preliminary mechanistic studies indicated that the reaction proceeds via a metallocyclic alkene, A-frame intermediate (see above). The second example involves work from this laboratory that demonstrated that the $\text{Pd}_2\text{X}_2(\text{dpm})_2$ complexes catalyze the conversion of H_2S and dpm to H_2 and dpm(S) (see Section 1.3 and Chapter 3).^{123,160}



1.6 Statement of the problem

From the foregoing discussion, it is clear that an interest in transition metal - H₂S chemistry is the impetus for the present thesis work. Further exploration of the sulfur abstraction from Pd₂X₂(μ-S)(dpm)₂ by dpm (process 2 → 1, R = dpm, in the figure below) was conducted (Chapter 3) in order to answer pertinent questions associated with the reaction, such as the role of the bridging dpm ligands, the effect of the auxiliary ligands, the nature of reaction intermediates, and the reasons for the unsuccessful sulfur abstraction by other phosphines (*i.e.* dpe, PPh₃, and PPh₂Me).¹⁶⁰ In addition, further studies concentrated on unearthing other reagents for effective removal of sulfur from 2 to regenerate 1; possible candidates included CO (Chapter 7) as well as the halogens, X₂ (Chapter 4). Chapter 2 outlines general experimental procedures while Chapters 5 and 6 describe the reaction of PdX₂(dpm) with H₂S to generate 2.



1.7 References for Chapter 1

1. Lee, C-L.; Besenyei, G.; James, B.R.; Nelson, D.A.; Lilga, M.A. *J. Chem. Soc., Chem. Commun.* **1985**, 1175.
2. Subcommittee on Hydrogen Sulfide, Committee on Medical and Biologic Effects of Environmental Pollutants, Division of Medical Services, Assembly of Life Sciences, National Research Council in 'Hydrogen Sulfide,' University Park Press, Baltimore, 1979.
3. Canada, Environmental Protection Programs Directorate, Technical Services Branch in 'Hydrogen Sulfide - Technical Services Branch, Environmental Protection Programs Directorate, Environmental Protection Service,' Gov. Doc. No. En48-10/17-1984E, The Service, Ottawa, 1984.
4. Hydrogen Sulfide, vol. 22, p. 114. In H.F. Mark, J.J. Mcketta, Jr., and D.F. Othmer. Kirk-Othmer Encyclopedia of Chemical Technology (3rd ed.), Toronto: John Wiley & Sons, Inc., 1983.
5. Scheele, K.W. *Ann. de Chim.* **1777**, *25*, 233; through ref. 2.
6. Kraft Chemical Pulping, vol. 19, p. 395. In H.F. Mark, J.J. Mcketta, Jr., and D.F. Othmer. Kirk-Othmer Encyclopedia of Chemical Technology (3rd ed.), Toronto: John Wiley & Sons, Inc., 1983.
7. (a) Gates, B.C.; Katzer, J.R.; Schuit, G.C.A. in 'Chemistry of Catalytic Processes,' McGraw-Hill, New York, 1979, ch. 5. (b) Sanchez-Delgado, R.A. *J. Mol. Catalysis* **1994**, *86*, 287.
8. Deuterium and Tritium, vol. 7, p. 544. In H.F. Mark, J.J. Mcketta, Jr., and D.F. Othmer. Kirk-Othmer Encyclopedia of Chemical Technology (3rd ed.) Toronto: John Wiley & Sons, Inc., 1983.
9. *Chem. Eng. News* **1995**, *73*, 38.
10. Sulfur Recovery, vol. 22, p. 267. In H.F. Mark, J.J. Mcketta, Jr., and D.F. Othmer. Kirk-Othmer Encyclopedia of Chemical Technology (3rd ed.) Toronto: John Wiley & Sons, Inc., 1983.
11. Hydrogen Energy Progress-IV; Veziroglu, T.N.; Van Vorst, W.D.; Kelly, J.H., Eds.; Advances in Hydrogen Energy 3; Pergamon Press: Toronto, 1982.
12. Berk, D.; Heidemann, R.A.; Svrcek, W.Y.; Behie, L.A. *Can. J. Chem. Eng.* **1991**, *69*, 944.
13. Taylor, H.A.; Pickett, C.F. *J. Phys. Chem.* **1927**, *31*, 1212.

14. Kingman, F.E.T. *Trans. Faraday Soc.* **1936**, 32, 903.
15. Darwent, B. de B.; Roberts, R. *Proc. Roy. Soc. London, Ser A* **1953**, 216, 344.
16. Raymont, M.E.D. Ph.D. Dissertation, University of Calgary, Alberta, Canada, 1974.
17. (a) Kaloidas, V.E.; Papayannakos, N.G. *Chem. Eng. Sci.* **1989**, 44, 2493. (b) Kaloidas, V.E.; Papayannakos, N.G. *Int. J. Hydrogen Energy* **1987**, 12, 403.
18. Massey, L.G. US Patent 2 984 548 (1958); *Chem. Abstr.* 55, 21510a (1961).
19. Raymont, M.E.D. *Hydrocarbon Processing* **1975**, 139.
20. Bogossian, A. FR Patent 2 238 668 (1975); *Chem. Abstr.* 83, 134380 (1975).
21. Daley, W.D.; Young, R.D. US Patent 4 461 755 (1984); *Chem. Abstr.* 101, 154222 (1984).
22. Hellmer, L.; Keunecke, G.; Pachaly, R.; Leil, R.; Al-Muddarris, G.R.; Stauffer, A.; Vangala, V.R. *Chem. Abstr.* 94, 33047 (1981).
23. Takeda, T. JP Patent 89 270 502 (1989); *Chem. Abstr.* 112, 237702 (1990).
24. Borton, D.N.; Rogers, W.E. *Proc. Intersoc. Energy Convers. Eng. Conf.* **1990**, 4, 315.
25. (a) Salman, O.A.; Bishara, A.; Marafi, A.; Abu-Khalifeh, H.; Al-Sayegh, A. *Adv. Hydrogen Energy* 8 (Hydrogen Energy Prog. 8, vol. 2) **1990**, 539. (b) Bishara, A.; Salman, O.A.; Khraishi, N.; Marafi, A. *Int. J. Hydrogen Energy* **1987**, 12, 679.
26. Kappauf, T.A. *Diss. Abstr. Int. B* **1989**, 50, 651.
27. Fletcher, E.A.; Noring, J.E.; Murray, J.P. *Int. J. Hydrogen Energy* **1984**, 9, 587.
28. Weiner, J.G.; Leggett, C.W. US Patent 2 979 384 (1958); *Chem. Abstr.* 55, 21510d (1961).
29. Kotera, Y.K.; Todo, N.T.; Fukuda, K.N. US Patent 3 962 409 (1976); *Chem. Abstr.* 79, 33200 (1973).
30. Fukuda, K.N.; Dokiya, M.; Kameyama, T.; Kotera, Y. *Ind. Eng. Chem. Fundam.* **1978**, 17, 243.
31. Hirota, K.; Aizawa, K.; Nishizawa, T. *Z. Naturforsch.* **1979**, 34a, 43.
32. Chivers, T.; Hyne, J.B.; Lau, C. *Int. J. Hydrogen Energy* **1980**, 5, 499.
33. Katsumoto, M.; Fueki, K.; Mukaibo, T. *Bull. Chem. Soc. Jpn.* **1973**, 46, 3641.
34. Sugioka, M.; Aomura, K. *Int. J. Hydrogen Energy* **1984**, 11, 891.
35. Knoche, K.F.; Cremer, H.; Steinborn, G.; Schneider, W. *Int. J. Hydrogen Energy* **1977**, 2, 269.

36. Kiuchi, H.; Nakamura, T.; Funaki, K.; Tanaka, T. *Int. J. Hydrogen Energy* **1982**, *7*, 477.
37. Kiuchi, H.; Funaki, K.; Tanaka, T. *Metallurgical Trans. B* **1983**, *14*, 347.
38. Chivers, T.; Lau, C. *Int. J. Hydrogen Energy* **1987**, *12*, 235.
39. Al-Shamma, L.M.; Naman, S.A. *Int. J. Hydrogen Energy* **1987**, *14*, 173.
40. Chivers, T.; Lau, C. *Int. J. Hydrogen Energy* **1987**, *12*, 561.
41. Zhang, Y.; Teng, Y.; Zang, X.; Wang, Z. *Huadong Huagong Xueyuan Xuebao* **1991**, *17*, 586.
42. Yumura, M.; Furimsky, E. *Appl. Catalysis* **1985**, *16*, 157.
43. Chivers, T.; Lau, C. *Int. J. Hydrogen Energy* **1985**, *10*, 21.
44. Bandermann, F.; Harder, K.B. *Int. J. Hydrogen Energy* **1985**, *10*, 21.
45. Dokiya, M.; Fukuda, K.; Yokokawa, H.; Kameyama, T. *Bull. Chem. Soc. Jpn.* **1978**, *51*, 150.
46. Bowman, M.G. US Patent 4 999 178 (1991); *Chem. Abstr.* 115, 117319 (1991).
47. Rendall, W.A.; Moir, M.E.; Szarka, J. GB Patent 2 248 444; *Chem. Abstr.* 117, 51829 (1992).
48. (a) Towler, G.P.; Lynn, S. *Ind. Eng. Chem. Res.* **1993**, *32*, 2800. (b) Towler, G.P.; Lynn, S. *Ind. Eng. Chem. Res.* **1993**, *32*, 2812.
49. Schuman, S.C. US Patent 3 388 971 (1968); *Chem. Abstr.* 69, 44920 (1968).
50. Nixon, I.G. *Chem. Brit.* **1974**, 179.
51. Chen, W.C. US Patent 4 066 739 (1978); *Chem. Abstr.* 88, 107468 (1978).
52. Plummer, M.A. *Hydrocarbon Processing* **1987**, 38.
53. Okabe, H. in 'Photochemistry of Small Molecules,' Wiley-Interscience Publication, Wiley & Sons, Toronto, 1978, ch. 6, p. 204, and references therein.
54. Fujii, T. JP Patent 63 267 420; *Chem. Abstr.* 110, 157677 (1989).
55. Kalyanasundaram, K.; Borgarello, E.; Gratzel, M. *Helv. Chim. Acta* **1981**, *64*, 362.
56. Kalyanasundaram, K.; Borgarello, E.; Duonghong, D.; Gratzel, M. *Angew. Chem. Int. Ed. Engl.* **1981**, *20*, 987.
57. Serpone, N.; Borgarello, E.; Barbeni, M.; Pelizzetti, E. *Inorg. Chim. Acta* **1984**, *90*, 191.
58. Borgarello, E.; Kalyanasundaram, K.; Gratzel, M.; Pelizzetti, E. *Helv. Chim. Acta* **1982**, *65*, 243.

59. Borgarello, E.; Erbs, W.; Gratzel, M. *Nouv. J. Chim.* **1983**, *7*, 195.
60. Thewissen, D.H.M.W.; Tinnemans, A.H.A.; Eeuwhorst-Reinten, M.; Timmer, K.; Mackor, A. *Nouv. J. Chim.* **1983**, *7*, 191.
61. Borgarello, E.; Gratzel, M.; Kalyanasundaram, K.; Pelizzetti, E. *Chemtech.* **1983**, *13*, 118.
62. Gratzel, M. (Ed.) in 'Energy Resources Through Photochemistry and Catalysis,' Academic Press, New York, 1983, ch. 3, p. 95.
63. Borgarello, E.; Desilvestro, J.; Gratzel, M.; Pelizzetti, E. *Helv. Chim. Acta* **1983**, *66*, 1827.
64. Serpone, N.; Borgarello, E.; Gratzel, M. *J. Chem. Soc., Chem. Commun.* **1984**, 342.
65. Thewissen, D.H.M.W.; Van der Zouwen-Assink, E.A.; Timmer, K.; Tinnemans, A.H.A.; Mackor, A. *J. Chem. Soc., Chem. Commun.* **1984**, 941.
66. Barbeni, M.; Pelizzetti, E.; Borgarello, E.; Serpone, N.; Gratzel, M.; Balducci, L.; Visca, M. *Int. J. Hydrogen Energy* **1985**, *10*, 249.
67. Naman, S.A.; Aliwi, S.M.; Al-Emara, K. *Int. J. Hydrogen Energy* **1986**, *11*, 33.
68. Kainthla, R.C.; Bockris, J. O'M. *Int. J. Hydrogen Energy* **1987**, *12*, 23.
69. Naman, S.A.; Al-Emara, K. *Int. J. Hydrogen Energy* **1987**, *12*, 629.
70. Linkous, C.A.; Muradov, N.Z.; Ramser, S.M.; Mingo, T.E.; Zidan, R.A. *Front. Sci. Ser.* **1993**, *7* (New Energy Systems and Conversions), 173.
71. Linkous, C.A.; Mingo, T.E.; Muradov, N.Z. *Int. J. Hydrogen Energy* **1994**, *19*, 203.
72. Osawa, Y.; Murata, S.; Tanaka, K. JP Patent 87 12 601; *Chem. Abstr.* 106, 198662 (1987).
73. Lee, R.; Grove, E. US Patent 2 839 381 (1958); *Chem. Abstr.* 52, 14503f (1958).
74. Lim, H.S.; Winnick, J. *J. Electrochem. Soc.* **1984**, *131*, 562.
75. Farooque, M.; Fahidy, T.Z. *J. Electrochem. Soc.* **1977**, *124*, 1191.
76. Grishaeva, G.A.; Shalepova, N. Ya.; Tret'yak, A.N.; Novikov, G.I. *Vesti Akad. Navak BSSR, Ser. Fiz.-Energ. Navuk* **1982**, *2*, 85; *Chem. Abstr.* 97, 100542 (1982).
77. Bolmer, P.W. US Patent 3 409 520 (1968); *Chem. Abstr.* 70, 39514 (1969).
78. Gregory, T.D.; Feke, D.L.; Angus, J.C.; Brosilow, C.B.; Landau, U. *J. Applied Electrochem.* **1980**,

- 10, 405.
79. Dandapani, B.; Scharifker, B.R.; Bockris, J. O'M. *Proc. Intersoc. Energy Convers. Eng. Conf.* **1986**, *1*, 262.
80. Shih, Y.S.; Lee, J.L. *Ind. Eng. Chem. Process Des. Dev.* **1986**, *25*, 834.
81. Nygren, K.; Atanasoski, R.; Smyrl, W.H.; Fletcher, E.A. *Energy* **1989**, *14*, 323, and references therein.
82. Anani, A.A.; Mao, Z.; White, R.E.; Srinivasan, S.; Appleby, A.J. *J. Electrochem. Soc.* **1990**, *137*, 2703.
83. Mao, Z.; Anani, A.A.; White, R.E.; Srinivasan, S.; Appleby, A.J. *J. Electrochem. Soc.* **1991**, *137*, 1299.
84. Alexander, S.R.; Winnick, J. *AIChE Journal* **1994**, *40*, 613, and references therein.
85. Fischer, F. US Patent 1 891 974 (1932); *Chem. Abstr.* *22*, 4676 (1928).
86. (a) Honna, K.; Noguchi, H.; Iida, H.; Goto, M. JP Patent 94 209 153 (1993); *Chem. Abstr.* *121*, 208919 (1994). (b) Honna, K.; Iida, H. JP Patent 04 238 803 (1992); *Chem. Abstr.* *117*, 236655 (1992). (c) Honna, K.; Iida, H. JP Patent 91 136 661 (1992); *Chem. Abstr.* *118*, 215837 (1993). (d) Honna, K.; Kikuchi, O. JP Patent 90 409 679 (1992); *Chem. Abstr.* *117*, 254356 (1992). (e) Kikuchi, T.; Komori, N.; Iida, H. JP Patent 90 169 709 (1992); *Chem. Abstr.* *116*, 109500 (1992). (f) Noguchi, H.; Isshiki, S. JP Patent 88 160 445 (1990); *Chem. Abstr.* *112*, 121612 (1990). (g) Noguchi, H.; Itsushiki, S. JP Patent 87 216 133 (1989); *Chem. Abstr.* *111*, 136916 (1989). (h) Konishi, T.; Kikuchi, O. JP Patent 86 58 060 (1987); *Chem. Abstr.* *107*, 239271 (1987). (i) Iida, H.; Misune, K. JP Patent 95 228 914 (1987); *Chem. Abstr.* *107*, 224985 (1987). (j) Agency of Industrial Sciences and Technology, Japan JP Patent 82 64 962 (1984); *Chem. Abstr.* *100*, 23986 (1984).
87. Mizuta, S.; Kondo, W.; Fujii, K.; Iida, H.; Isshiki, S.; Noguchi, H.; Kikuchi, T.; Sue, H.; Sakai, K. *Ind. Eng. Chem. Res.* **1991**, *30*, 1601.
88. Keller, H.F. US Patent 3 401 101 (1968); *Chem. Abstr.* *69*, 88621 (1968).
89. Deem, C.K. US Patent 4 220 505 (1981); *Chem. Abstr.* *94*, 32975 (1981).

90. Schuetz, G. Eur. Pat. Appl. EP 168 022; *Chem. Abstr.* 104, 112212 (1986).
91. (a) Kalina, D.W.; Maas, Jr., E.T. *Int. J. Hydrogen Energy* **1985**, *10*, 157. (b) Kalina, D.W.; Maas, Jr., E.T. *Int. J. Hydrogen Energy* **1985**, *10*, 163.
92. Patton, R.A. US Patent 2 819 950 (1958); *Chem. Abstr.* 52, 7636c (1958).
93. Asisov, R.J.; Vakur, A.K.; Gutsol, A.F.; Givotov, V.K.; Krashenninnikov, E.G.; Krotov, M.F.; Rusanov, V.D.; Fridman, A.A.; Sholin, G.V. *Int. J. Hydrogen Energy* **1985**, *10*, 475.
94. Krashenninnikov, E.G.; Rusanov, V.D.; Sanyuk, S.V.; Fridman, A.A. *Sov. Phys. Tech. Phys.* **1986**, *31*, 645.
95. (a) Harkness, J.B.L.; Gorski, A.J.; Daniels, E.J. *Proc. Intersoc. Energy Convers. Eng. Conf.* **1990**, *6*, 197. (b) Harkness, J.B.L.; Gorski, A.J.; Daniels, E.J. US Patent 5 211 923 (1991); *Chem. Abstr.* 119, 75745 (1993).
96. Bagautdinov, A.Z.; Jivotov, V.K.; Eremenko, J.J.; Kalachev, I.A.; Musinov, S.A.; Pampushka, A.M.; Rusanov, V.D.; Zoller, V.A. *Front. Sci. Ser.* **1993**, *7* (New Energy Systems and Conversions), 123.
97. Haas, L.A.; Khalafalla, S.E. US Natl. Tech. Inform. Service, Bureau of Mines, Report of Investigations No. 7780 (1973).
98. Traus, I.; Suhr, H. *Plasma Chem. Plasma Process.* **1992**, *12*, 275.
99. (a) Jorgensen, P.; Czernichowski, A.; Chapelle, J.; Meguernes, K. FR Patent 2 620 436 (1989); *Chem. Abstr.* 111, 107383 (1989). (b) Czernichowski, A.; Jorgensen, P.; Lesueur, H.; Chapelle, J.; Meguernes, K. *Colloq. Phys.* **1990**, (C5, Eur. Congr. Therm. Plasma Processes Mater. Behav. High Temp., 1990), C5-65/C5-71.
100. Khrikulov, V.V.; Ismailov, Kh.I. *Gazov. Prom-st.* **1994**, *4*, 38; *Chem. Abstr.* 122, 221442 (1995).
101. Schwarz, R.; Kunzer, W. *Z. Anorg. Allg. Chem.* **1929**, *183*, 287.
102. Ferrero, P.; Corbaz, J. *Helv. Chim. Acta* **1931**, *14*, 912.
103. Kolokina, L. *J. Phys. Chem. (USSR)* **1935**, *6*, 428.
104. Nicholas, J.E.; Amodio, C.A.; Baker, M.J. *J. Chem. Soc., Faraday Trans. 1* **1979**, *75*, 1868.
105. Boyd, A.W.; Willis, C.; Miller, O.A. *Can. J. Chem.* **1973**, *51*, 1228, and references therein.

106. Forys, M.; Jezierska, K. *Radiochem. Radioanal. Lett.* **1969**, *1*, 237, and references therein.
107. Kerr, J.A. *Chem. Rev.* **1966**, *66*, 465.
108. Ginter, D.S.; Ginter, M.L.; Innes, K.K. *Astrophys. J.* **1964**, *139*, 365.
109. Nelson, D.A.; Hallen, R.T.; Lee, C-L.; James, B.R. in 'Recent Developments in Separation Science,' N. Li and J.M. Calo, Eds., CRC, Cleveland, Ohio, 1986, vol. 9, p. 1.
110. Lee, C-L.; James, B.R.; Nelson, D.A.; Hallen, R.T. *Organometallics* **1984**, *3*, 1360.
111. Lee, C-L.; Yang, Y.P.; Rettig, S.J.; James, B.R.; Nelson, D.A.; Lilga, M.A. *Organometallics* **1986**, *5*, 2220.
112. Lyke, S.E.; Lilga, M.A.; Ozanich, R.M.; Nelson, D.A. *Ind. Eng. Chem. Prod. Res. Dev.* **1986**, *25*, 517.
113. Benner, L.S.; Balch, A.L. *J. Am. Chem. Soc.* **1978**, *100*, 6099.
114. Barnabas, A.F.; Sallin, D.; James, B.R. *Can. J. Chem.* **1989**, *67*, 2009.
115. Besenyi, G.; Lee, C-L.; Gulinski, J.; Rettig, S.J.; James, B.R.; Nelson, D.A.; Lilga, M.A. *Inorg. Chem.* **1987**, *26*, 3622.
116. Kubiak, C.P.; Eisenberg, R. *J. Am. Chem. Soc.* **1977**, *99*, 6129.
117. Kuehn, G.C.; Taube, H. *J. Am. Chem. Soc.* **1976**, *98*, 689.
118. Herberhold, M.; Suss, G. *Angew. Chem. Int. Ed. Engl.* **1976**, *15*, 366; *J. Chem. Res. Synop.* **1977**, 246.
119. Weiss, A.; Plass, R.; Weiss, A. *Z. Anorg. Allg. Chem.* **1956**, *283*, 390.
120. Ugo, R.; LaMonica, G.; Cenini, S.; Segre, A.; Conti, F. *J. Chem. Soc. A* **1971**, 522.
121. Sellman, D.; Lechner, P.; Knoch, F.; Moll, M. *Angew. Chem. Int. Ed. Engl.* **1991**, *30*, 552.
122. Mudalige, D.C. Ph.D. Dissertation, University of British Columbia, Vancouver, 1994.
123. Wong, T.Y.H.; Barnabas, A.F.; Sallin, D.; James, B.R. *Inorg. Chem.* **1995**, *34*, 2278.
124. Balch, A.L.; Benner, L.S.; Olmstead, M.M. *Inorg. Chem.* **1979**, *18*, 2996.
125. Besenyi, G.; Lee, C-L.; Xie, Y.; James, B.R. *Inorg. Chem.* **1991**, *30*, 2446.
126. Xie, Y.; Lee, C-L.; Yang, Y.; Rettig, S.J.; James, B.R. *Can. J. Chem.* **1992**, *70*, 751.

127. Besenyei, G.; Lee, C-L.; James, B.R. *J. Chem. Soc., Chem. Commun.* **1986**, 1750.
128. Bottomley, F.; Chin, T.T.; Egharevba, G.O.; Kane, L.M.; Pataki, D.A.; White, P.S. *Organometallics* **1988**, 7, 1214.
129. Hillhouse, G.L.; Bercaw, J.E. *J. Am. Chem. Soc.* **1984**, 106, 5472.
130. McDonald, R.; Cowie, M. *Inorg. Chem.* **1993**, 32, 1671.
131. Jessop, P.G.; Lee, C-L.; Rastar, G.; James, B.R.; Lock, C.J.L.; Faggiani, R. *Inorg. Chem.* **1992**, 31, 4601.
132. Shih, K-Y.; Fanwick, P.E.; Walton, R.A. *Inorg. Chem.* **1992**, 31, 3663.
133. Antonelli, D.M.; Cowie, M. *Inorg. Chem.* **1990**, 29, 3339.
134. Mueting, A.M.; Boyle, P.D.; Pignolet, L.H. *Inorg. Chem.* **1984**, 23, 44, and references therein.
135. Mueting, A.M.; Boyle, P.D.; Wagner, R.; Pignolet, L.H. *Inorg. Chem.* **1988**, 27, 271.
136. Osakada, K.; Yamamoto, T.; Yamamoto, A. *Inorg. Chim. Acta* **1984**, 90, L5.
137. Osakada, K.; Yamamoto, T.; Yamamoto, A.; Takenaka, A.; Sasada, Y. *Inorg. Chim. Acta* **1985**, 105, L9.
138. Lee, C-L.; Chisholm, J.; James, B.R.; Nelson, D.A.; Lilga, M.A. *Inorg. Chim. Acta* **1986**, 121, L7.
139. a) Jessop, P.G.; Rettig, S.J.; Lee, C-L.; James, B.R. *Inorg. Chem.* **1991**, 30, 4617. b) Jessop, P.G.; Rastar, G.; James, B.R. *Inorg. Chim. Acta*, in press.
140. Bianchini, C.; Mealli, C.; Meli, A.; Sabat, M. *Inorg. Chem.* **1986**, 25, 4618.
141. Bottomley, F.; Drummond, D.F.; Egharevba, G.O.; White, P.S. *Organometallics* **1986**, 5, 1620.
142. Howard, W.A.; Parkin, G. *Organometallics* **1993**, 12, 2363.
143. Rabinovich, D.; Parkin, G. *J. Am. Chem. Soc.* **1991**, 113, 5904.
144. Angelici, R.J. *Acc. Chem. Res.* **1988**, 21, 387.
145. Mague, J.T.; Mitchener, J.P. *Inorg. Chem.* **1969**, 8, 119.
146. Balch, A.L. in 'Catalytic Aspects of Metal Phosphine Complexes,' E.C. Alyea and D.W. Meek, eds., ACS Adv. Chem. Ser., 1982, v. 196, p. 243.
147. Puddephatt, R.J. *Chem. Rev.* **1983**, 99, and references therein.

148. Shaw, B.L. *Proc. Indian Natn. Sci. Acad.* **1986**, 52A, 744.
149. Chaudret, B.; Delavaux, B.; Poilblanc, R. *Coord. Chem. Rev.* **1988**, 86, 191.
150. DeLaet, D.L.; Powell, D.R.; Kubiak, C.P. *Organometallics* **1985**, 4, 954.
151. Brown, M.P.; Puddephatt, R.J.; Rashidi, M.; Seddon, K.R. *J. Chem. Soc., Dalton Trans.* **1977**, 951.
152. Pringle, P.G.; Shaw, B.L. *J. Chem. Soc., Chem. Commun.* **1982**, 81.
153. Olmstead, M.M.; Benner, L.S.; Hope, H.; Balch, A.L. *Inorg. Chim. Acta* **1979**, 32, 193.
154. Brown, M.P.; Franklin, S.J.; Puddephatt, R.J.; Thomson, M.A.; Seddon, K.R. *J. Organomet. Chem.* **1979**, 178, 281.
155. Gossel, M.C.; Moulding, R.P.; Seddon, K.R. *Inorg. Chim. Acta Lett.* **1982**, 64, L275.
156. Weng, W.Z.; James, B.R. To be published.
157. Espinet, P.; Fornies, J.; Fortunato, C.; Hidalgo, G.; Martines, F.; Tomas, M.; Welch, A.J. *J. Organomet. Chem.* **1986**, 317, 105.
158. Lee, C-L.; Hunt, C.T.; Balch, A.L. *Organometallics* **1982**, 1, 824.
159. Lee, C-L.; Hunt, C.T.; Balch, A.L. *Inorg. Chem.* **1981**, 20, 2498.
160. Barnabas, A.F. M.Sc. Dissertation, University of British Columbia, Vancouver, 1989.

CHAPTER 2

General Experimental Procedures

Chapter 2 General Experimental Procedures

A general description of the materials, techniques, and instrumentation used during the course of the thesis work will be presented in this chapter. Detailed information on experiments and synthetic routes to novel compounds can be found in subsequent chapters.

2.1 Materials

Tables 2.1 and 2.2 list the materials and compounds used with reference to commercial sources and/or literature procedures. Commercially available chemicals were pure and were used as received. The synthetic routes for the Pd complexes listed in Table 2.2 are also given; in each case, the spectroscopic data listed agree closely with those given in the literature. Unless otherwise stated, all syntheses were carried out using standard Schlenk techniques and under an inert atmosphere of N₂; purities were assessed by NMR spectroscopy and/or elemental analyses. All non-deuterated solvents were obtained from MCB, BDH, Aldrich, Eastman, Fisher, or Mallinckrodt Chemical Co., and were freshly distilled under N₂ over their respective drying agents prior to use (*i.e.* benzene, diethyl ether, hexanes, THF, and toluene using Na/benzophenone; MeOH and EtOH using Mg/I₂; CH₂Cl₂ and CHCl₃ using CaH₂; and acetone using K₂CO₃). Deuterated solvents (CD₂Cl₂, CDCl₃, CD₃CN, C₆D₆, DMSO-d₆, CH₃OD, and D₂O) were obtained from CIL, Isotec Inc., or MSD Isotopes, and were de-oxygenated or de-gassed and dried (except D₂O) over activated molecular sieves (Fisher, type 4A, grade 514, 8 - 12 mesh). Purified N₂ (U.S.P.), Ar (H.P.), and H₂ (U.S.P.) were obtained from Union Carbide Canada Ltd., H₂S (C.P.)

Table 2.1 Some materials used and their sources.

Chemical	Source
γ -alumina (neutral)	Fisher
aluminum hydroxide (Al(OH) ₃)	Aldrich
aluminum oxide (α -Al ₂ O ₃ , corundum)	Alfa Products
benzonitrile (PhCN)	Aldrich
bis(diphenylphosphino)ethane (dpe)	Strem
1,1'-bis(diphenylphosphino)ethane (dpmMe)	ref. 1
bis(diphenylphosphino)methane (dpm)	Aldrich
bis(diphenylphosphino)methane monosulfide (dpm(S))	ref. 2
bis(diphenylphosphino)propane (dpp)	Strem
bromine (Br ₂)	BDH
calcium sulfide (CaS)	Alfa Products
dibenzylideneacetone (dba)	ref. 3
ethyl iodide (CH ₃ CH ₂ I)	BDH
hydrobromic acid (HBr (48% aq.))	Fisher
hydriodic acid (HI (59% aq.))	Fisher
hydrochloric acid (HCl (37% aq.))	Fisher
iodine (I ₂)	BDH
methyl iodide (CH ₃ I)	Fisher
methyl lithium (MeLi (1.40 M in Et ₂ O))	Aldrich
palladium(II) chloride (PdCl ₂)	Johnson Matthey Ltd.
sodium acetate (NaOAc)	Mallinckrodt
sodium bromide (NaBr)	Anachemia
sodium hydrosulfide (NaSH)	Aldrich
sodium iodide (NaI)	Fisher
sulfur	Aldrich
tetrabutylammonium iodide ((CH ₃ (CH ₂) ₃) ₄ NI)	Eastman
tetrapropylammonium bromide ((CH ₃ (CH ₂) ₂) ₄ NBr)	Kodak
triphenylphosphine (PPh ₃)	Strem

Table 2.2 Palladium complexes used and their respective reference(s) for synthetic procedures.

Compound	Source
<i>trans</i> -Pd(PhCN) ₂ Cl ₂	refs. 4, 5, 6
Pd ₂ (dba) ₃ •CHCl ₃	refs. 4, 7
Pd ₂ Cl ₂ (dpm) ₂ (1a)	refs. 4, 8
Pd ₂ Br ₂ (dpm) ₂ (1b)	refs. 4, 9
Pd ₂ I ₂ (dpm) ₂ •CH ₂ Cl ₂ (1c)	refs. 4, 9
Pd ₂ Cl ₂ (μ-S)(dpm) ₂ (2a)	refs. 4, 10
Pd ₂ Br ₂ (μ-S)(dpm) ₂ (2b)	refs. 4, 10
Pd ₂ I ₂ (μ-S)(dpm) ₂ (2c)	refs. 4, 10
PdCl ₂ (dpm) (9a)	refs. 4, 11, 12
PdBr ₂ (dpm) (9b)	refs. 4, 11
PdI ₂ (dpm) (9c)	-
Pd ₂ Cl ₂ (μ-SO)(dpm) ₂	ref. 10
Pd ₂ I ₂ (μ-SO)(dpm) ₂	-
Pd ₂ (SH) ₂ (μ-S)(dpm) ₂	ref. 10

and anhydrous HCl from Matheson Gas Co., anhydrous HBr from Linde, O₂ (U.S.P.) and CO (C.P.) from Praxair, and COS from Aldrich. All gases were used without further purification.

2.1.1 Dibenzylideneacetone (dba)

The dba ligand was readily available in this laboratory. Synthesis can be done according to a published method.³ Acetone (1.45 g, 25 mmol) is condensed with PhCHO (5.3 g, 50 mmol) in a solution of NaOH in aq. EtOH (90 mL). The resulting yellow product is filtered off, washed with water (2 x 20 mL), and dried *in vacuo*. Recrystallization is done using hot ethyl acetate.

2.1.2 1,1'-Bis(diphenylphosphino)ethane (dpmMe)

The dpmMe ligand was readily available in this laboratory. Synthesis can be done according to a published method.¹ A solution of MeLi (18.4 mL, 28.8 mmol) is added dropwise to Ph₂PH¹³ (5.35 g, 28.7 mmol) dissolved in benzene (50 mL). The resulting yellow solution is stirred for 3 h before 1,1-dichloroethane (1.41 g, 14.3 mmol) is added. The mixture is stirred for another 3 h prior to filtration through Celite. The filtrate is concentrated under vacuum to give a yellow oil; EtOH (300 mL) is added to yield white crystals that are purified by dissolution in 30 mL of CH₂Cl₂ followed by reprecipitation via addition of 100 mL of EtOH.

2.1.3 Triphenylphosphine sulfide (Ph₃PS)

This compound¹⁴ was synthesized as a precursor to dpm(S). PPh₃ (40.0 g, 0.15 mol) and sulfur (5 g, 0.16 mol) were suspended in toluene (70 mL), and the mixture was refluxed for 2 h. The resulting yellow clear solution was filtered through a column (2.5 x 8.0 cm) of neutral alumina to remove the excess sulfur. CH₂Cl₂ (30 mL) was used to elute any product remaining in the column. The colourless filtrate was rotovaped to remove the solvents and the white crystalline product subsequently appeared. Yield: 43.9 g (98%).

2.1.4 Bis(diphenylphosphino)methane monosulfide (dpm(S))

This compound was synthesized according to a published method.² To a stirred suspension of Ph₃PS (20.6 g, 0.0700 mol) in a mixture of THF (110 mL) and Et₂O (85 mL) was added MeLi (50 mL, 1.40 M in Et₂O) over a 30 min period. The resulting red solution was stirred for 1 h before a solution of Ph₂PCl¹⁵ (15.4 g, 0.0700 mol) in Et₂O (70 mL) was slowly added over a 2 h period. The colour slowly changed to yellow with accompanying precipitation of LiCl. After the solution was stirred overnight, the solvents were removed by rotary evaporation. The resulting red-yellow oil was dissolved in CH₂Cl₂ (100 mL), and the solution was washed with distilled H₂O (3 x 100 mL) and dried over MgSO₄. The CH₂Cl₂ was rotovaped off and the resulting viscous yellow oil was dissolved in minimal hot ethanol. The solution was cooled and crystallization of the white product occurred. Yield: 17.1 g (59 %). ¹H NMR (20 °C, CDCl₃): δ 7.0 - 8.0 m (20H, Ph), δ 3.36 dd (2H, CH₂, J_{HH} = 12.6 Hz, J_{PH} = 1.1 Hz). ³¹P{¹H} NMR (20 °C, CDCl₃): δ -28.1, 40.1

AB pattern ($J_{PP} = 75.9$ Hz). Anal. Calcd for $C_{25}H_{22}P_2S$: C, 72.10; H, 5.32. Found: C, 71.89; H, 5.28.

2.1.5 *Trans*-dichlorobis(benzonitrile)palladium(II) ($Pd(PhCN)_2Cl_2$)

This compound was synthesized according to a published method.⁴⁻⁶ $PdCl_2$ (2.0 g, 11.3 mmol) was suspended in benzonitrile (50 mL) and the mixture heated to and kept at 100 °C for 8 h. The greater part of $PdCl_2$ dissolved to give a red solution which was filtered while still warm. The filtrate was poured into hexanes (300 mL) and a light yellow precipitate immediately formed. The yellow product was filtered off, washed with hexanes and dried *in vacuo*. Yield: 4.0 g (92%).

2.1.6 Tris(dibenzylideneacetone)dipalladium(0)-chloroform solvate ($Pd_2(dba)_3 \cdot CHCl_3$)

This compound was synthesized according to a published method.^{4,7} $PdCl_2$ (1.05 g, 5.9 mmol) was added to a hot (~ 50 °C) MeOH solution (150 mL) containing dba (4.6 g, 19.6 mmol) and NaOAc (3.9 g, 47.5 mmol). The mixture was stirred at 40 °C to give a red-purple precipitate. After being cooled to complete precipitation, the mixture was filtered, and the solid was then washed successively with H_2O and acetone and dried *in vacuo*. The precipitate was dissolved in hot $CHCl_3$ (300 mL), and the mixture was filtered to give a deep violet solution. Slow addition of Et_2O (400 mL) afforded deep purple needles which were filtered off, washed with Et_2O , and dried *in vacuo*. Yield: 2.2 g (75%). The crystal structure of this compound has been reported.⁷

2.1.7 Dichlorobis- μ -[bis(diphenylphosphino)methane]dipalladium(I) ($\text{Pd}_2\text{Cl}_2(\text{dpm})_2$)

This compound was synthesized according to a published method.^{4,8} $\text{Pd}(\text{PhCN})_2\text{Cl}_2$ (0.41 g, 1.01 mmol), $\text{Pd}_2(\text{dba})_3\cdot\text{CHCl}_3$ (0.55 g, 0.53 mmol), and dpm (0.82 g, 2.1 mmol) were dissolved in CH_2Cl_2 (50 mL). The mixture was refluxed for 30 min and the resulting red solution was then cooled to R.T. The solution was filtered to remove any insoluble materials, and the filtrate was concentrated under vacuum to ~10 mL. Et_2O (20 mL) was added and a yellow-orange precipitate formed. The product was then filtered off, washed with acetone (2 x 10 mL) to remove any palladium(II) monomer, and dried *in vacuo*. Yield: 1.0 g (90 %). ^1H NMR (20 °C, CDCl_3): δ 7.0 - 8.0 m (40H, Ph), δ 4.17 qn (4H, CH_2 , $J_{\text{PH}} = 4$ Hz). $^{31}\text{P}\{^1\text{H}\}$ NMR (20 °C, CDCl_3): δ -5.5 s.

2.1.8 Dibromobis- μ -[bis(diphenylphosphino)methane]dipalladium(I) ($\text{Pd}_2\text{Br}_2(\text{dpm})_2$)

This compound was synthesized according to a published method.^{4,9} $\text{Pd}_2\text{Cl}_2(\text{dpm})_2$ (0.23 g, 0.22 mmol) was dissolved in CH_2Cl_2 (10 mL), and a solution of NaBr (0.20 g, 2 mmol) in aq. MeOH (10 mL MeOH : 1 mL H_2O) was added. The resulting solution was stirred for 1 h before being filtered and concentrated under vacuum until an orange precipitate was formed. Aqueous MeOH was added to complete the precipitation and the product was filtered off. The product was recrystallized using $\text{CH}_2\text{Cl}_2/\text{aq. MeOH}$ and was dried *in vacuo*. Yield: 0.24 g (97 %). ^1H NMR (20 °C, CDCl_3): δ 7.0 - 8.0 m (40H, Ph), δ 4.26 qn (4H, CH_2 , $J_{\text{PH}} = 4$ Hz). $^{31}\text{P}\{^1\text{H}\}$ NMR (20 °C, CDCl_3): δ -6.15 s. The crystal structure of this compound has been reported.¹⁶

**2.1.9 Diiodobis- μ -[bis(diphenylphosphino)methane]dipalladium(I) dichloromethane solvate
(Pd₂I₂(dpm)₂•CH₂Cl₂)**

This compound was synthesized according to a published method.^{4,9} Pd₂Cl₂(dpm)₂ (0.23 g, 0.22 mmol) was dissolved in CH₂Cl₂ (10 mL) and a solution of NaI (0.15 g, 1 mmol) in aq. MeOH (10 mL) was added. The resulting solution was stirred for 1 h before being filtered and concentrated under vacuum until a purple precipitate was formed. Aqueous MeOH was added to complete the precipitation; the product was filtered off, washed with acetone (2 x 10 mL), and dried *in vacuo*. Yield: 0.26 g (90 %). ¹H NMR (20 °C, CDCl₃): δ 7.0 - 8.0 m (40H, Ph), δ 4.23 qn (4H, CH₂, J_{PH} = 4 Hz). ³¹P{¹H} NMR (20 °C, CDCl₃): δ -11.3 s.

**2.1.10 Dichloro- μ -sulfidobis- μ -[bis(diphenylphosphino)methane]dipalladium(II)
(Pd₂Cl₂(μ -S)(dpm)₂)**

This compound was synthesized according to a published method.^{4,10} Pd₂Cl₂(dpm)₂ (0.50 g, 0.48 mmol) was dissolved in CH₂Cl₂ (50 mL) and H₂S gas was bubbled through the solution for 20 min at R.T. The colour changed from orange-red to brown with accompanying precipitation of a brown solid. Et₂O (50 mL) was slowly added to complete the precipitation; the product was filtered off, washed successively with acetone (2 x 10 mL) and Et₂O (10 mL), and dried *in vacuo*. Yield: 0.50 g (97 %). ¹H NMR (20 °C, CDCl₃): δ 7.0 - 8.0 m (40H, Ph), δ 4.70 d qn (2H, CH, J_{HH} = 13 Hz, J_{PH} = 6 Hz), δ 2.79 d qn (2H, CH, J_{HH} = 13 Hz, J_{PH} = 4 Hz). ³¹P{¹H} NMR (20 °C, CDCl₃): δ 5.5 s. The crystal structure of this compound has been reported.¹⁷

2.1.11 Dibromo- μ -sulfidobis- μ -[bis(diphenylphosphino)methane]dipalladium(II)**(Pd₂Br₂(μ -S)(dpm)₂)**

This compound was synthesized according to a published method.^{4,10} Pd₂Br₂(dpm)₂ (0.50 g, 0.44 mmol) was dissolved in CH₂Cl₂ (50 mL) placed in a Schlenk tube stoppered with a rubber septum. H₂S (50 mL, 1 atm at 25 °C) was injected, and the reaction mixture was allowed to react for 3 h. The colour changed from orange-red to brown with accompanying precipitation of a brown solid. Et₂O (50 mL) was added to complete the precipitation; the solid was filtered off, washed successively with acetone (2 x 10 mL) and Et₂O (10 mL), and dried *in vacuo*. Yield: 0.51 g (98 %). ¹H NMR (20 °C, CDCl₃): δ 7.0 - 8.0 m (40H, Ph), δ 4.83 d qn (2H, CH, J_{HH} = 12.8 Hz, J_{PH} = 7.6 Hz), δ 2.88 d qn (2H, CH, J_{HH} = 12.8 Hz, J_{PH} = 3.2 Hz). ³¹P{¹H} NMR (20 °C, CDCl₃): δ 5.96 s.

2.1.12 Diiodo- μ -sulfidobis- μ -[bis(diphenylphosphino)methane]dipalladium(II)**(Pd₂I₂(μ -S)(dpm)₂)**

This compound was synthesized according to a published method.^{4,10} Pd₂Cl₂(μ -S)(dpm)₂ (0.25 g, 0.23 mmol) was dissolved in CH₂Cl₂ (25 mL) and a solution of NaI (0.30 g, 2 mmol) in aq. MeOH (10 mL) was added. The mixture was stirred for 1 h before being concentrated under vacuum to ~10 mL. Precipitation of a brown solid was completed by addition of MeOH (50 mL). The product was filtered off, washed successively with aq. MeOH (2 x 10 mL) and Et₂O (10 mL), and dried *in vacuo*. Yield: 0.32 g (90%). ¹H NMR (20 °C, CDCl₃): δ 7.0 - 8.0 m (40H, Ph), δ

4.95 d qn (2H, CH, $J_{\text{HH}} = 14$ Hz, $J_{\text{PH}} = 6$ Hz), δ 3.06 d qn (2H, CH, $J_{\text{HH}} = 14$ Hz, $J_{\text{PH}} = 3$ Hz).

$^{31}\text{P}\{^1\text{H}\}$ NMR (20 °C, CDCl_3): δ 6.1 s.

2.1.13 Dichloro[bis(diphenylphosphino)methane]palladium(II) ($\text{PdCl}_2(\text{dpm})$)

This compound was synthesized according to a published method.^{4,11,12} A solution of $\text{Pd}(\text{PhCN})_2\text{Cl}_2$ (0.30 g, 0.77 mmol) in CH_2Cl_2 (10 mL) was added with stirring to a CH_2Cl_2 (10 mL) solution containing dpm (0.30 g, 0.78 mmol). The reaction mixture was stirred for 2 h and concentrated under vacuum to ~10 mL before Et_2O (50 mL) was added to the yellow solution affording a pale yellow solid that was filtered off and reprecipitated twice from $\text{CH}_2\text{Cl}_2/\text{Et}_2\text{O}$. The product was finally washed with Et_2O (2 x 10 mL) and dried *in vacuo*. Yield: 0.39 g (90%). ^1H NMR (20 °C, CDCl_3): δ 7.0 - 8.0 m (20H, Ph), δ 4.21 t (2H, CH_2 , $J_{\text{PH}} = 10.8$ Hz). $^{31}\text{P}\{^1\text{H}\}$ NMR (20 °C, CDCl_3): δ -54.7 s. The crystal structure of this compound has been reported.¹²

2.1.14 Dibromo[bis(diphenylphosphino)methane]palladium(II) ($\text{PdBr}_2(\text{dpm})$)

This compound was synthesized according to a published method.^{4,11} $\text{PdCl}_2(\text{dpm})$ (0.25 g, 0.45 mmol) was dissolved in CH_2Cl_2 (10 mL) and a solution of NaBr (0.20 g, 2 mmol) in aq. MeOH (10 mL) was added. The mixture was stirred for 1 h before being filtered and concentrated under vacuum to ~10 mL. Et_2O (25 mL) was added to complete the precipitation of a yellow solid. The product was filtered off, washed successively with aq. MeOH (2 x 10 mL) and Et_2O (10 mL), and dried *in vacuo*. Yield: 0.26 g (90%). ^1H NMR (20 °C, CDCl_3): δ 7.0 - 8.0 m (20H,

Ph), δ 4.37 t (2H, CH₂, J_{PH} = 10.5 Hz). ³¹P{¹H} NMR (20 °C, CDCl₃): δ -56.2 s. The crystal structure of this compound has been reported.¹⁸

2.1.15 Diiodo[bis(diphenylphosphino)methane]palladium(II) (PdI₂(dpm))

PdCl₂(dpm) (0.10 g, 0.18 mmol) was placed in CH₂Cl₂ (20 mL) and a solution of NaI (0.40 g, 2.7 mmol) in aq. MeOH (10 mL) was added. The resulting orange solution was stirred for 1 h before being reduced in volume under vacuum to ~10 mL. Et₂O (30 mL) was added to precipitate an orange solid that was filtered off, washed successively with aq. MeOH (2 x 10 mL) and Et₂O (10 mL), and dried *in vacuo*. Yield: 0.13 g (97%). ¹H NMR (20 °C, CDCl₃): δ 7.0 - 8.0 m (20H, Ph), δ 4.42 t (2H, CH₂, J_{PH} = 10.0 Hz). ³¹P{¹H} NMR (20 °C, CDCl₃): δ -63.2 s. UV/vis (20 °C, CHCl₃): λ , nm (ϵ , M⁻¹ cm⁻¹): 430 (6455). Anal. Calcd for C₂₅H₂₂I₂P₂Pd: C, 40.33; H, 2.98. Found: C, 40.34; H, 2.97. The crystal structure of this compound has been reported.¹⁹

2.1.16 Dichloro- μ -sulfoxobis- μ -[bis(diphenylphosphino)methane]dipalladium(II) (Pd₂Cl₂(μ -SO)(dpm)₂)

This compound was synthesized according to a published method.¹⁰ Pd₂Cl₂(μ -S)(dpm)₂ (0.30 g, 0.28 mmol) was dissolved in CH₂Cl₂ (40 mL) and a methanolic solution of H₂O₂ (40 mL 30% H₂O₂ in 10 mL MeOH) was added. The mixture was stirred at R.T. for 2 h, after which the orange CH₂Cl₂ layer was removed and concentrated under vacuum to 10 mL. Addition of 50 mL of MeOH precipitated an orange solid that was filtered off, washed with MeOH (2 x 10 mL), and dried *in vacuo*. Yield: 0.28 g (90%). ¹H NMR (20 °C, CDCl₃): δ 7.0 - 8.0 m (40H, Ph), δ 4.78 d t

(1H, CH₂, J_{HH} = 13.5 Hz, J_{PH} = 10.5 Hz), δ 3.89 d t (1H, CH₂, J_{HH} = 13.5 Hz, J_{PH} = 7.5 Hz), δ 2.53 m (1H, CH₂), δ 2.27 m (1H, CH₂). ³¹P{¹H} NMR (20 °C, CDCl₃): δ 20 to -5 AA'BB' pattern. The crystal structure of this compound has been reported.¹⁰

2.1.17 Diiodo-μ-sulfoxobis-μ-[bis(diphenylphosphino)methane]dipalladium(II)

(Pd₂I₂(μ-SO)(dpm)₂)

Pd₂I₂(dpm)₂(μ-S) (0.20 g, 0.16 mmol) was dissolved in CH₂Cl₂ (10 mL) and a methanolic solution of H₂O₂ (30%, 1 mL in 5 mL MeOH) was added. The colour immediately changed from brown to red-brown. The solution was stirred for 1 h before MeOH (25 mL) was added to precipitate a red-brown solid that was filtered off, washed with MeOH (2 x 10 mL), and dried *in vacuo*. Yield: 0.16 g (80%). ¹H NMR (20 °C, CDCl₃): δ 7.0 - 8.0 m (40H, Ph), δ 4.98 d t (1H, CH₂, J_{HH} = 12 Hz, J_{PH} = 13.5 Hz), δ 4.18 d t (1H, CH₂, J_{HH} = 15 Hz, J_{PH} = 9 Hz), δ 2.58 m (1H, CH₂), δ 2.26 m (1H, CH₂). ³¹P{¹H} NMR (20 °C, CDCl₃): δ 19 to -7 AA'BB' pattern. A satisfactory elemental analysis could not be obtained.

2.1.18 Dimercapto-μ-sulfidobis-μ-[bis(diphenylphosphino)methane]dipalladium(II)

(Pd₂(SH)₂(μ-S)(dpm)₂)

This compound was synthesized from a procedure slightly modified from that reported.¹⁰ PdCl₂(dpm) (0.31 g, 0.55 mmol) was suspended in CH₂Cl₂ (10 mL) and a solution of NaSH (0.62 g, 11 mmol) in aq. MeOH (5 mL H₂O : 5 mL MeOH) was added dropwise. The solution became clear within minutes with accompanying colour changed from yellow to red-brown. The solution

was then washed with distilled H₂O (to extract the excess NaSH) until the aqueous layer was at neutral pH. The organic layer was reduced in volume under vacuum to ~5 mL before Et₂O (30 mL) was added to precipitate a brown solid that was filtered off, washed successively with MeOH (3 x 10 mL) and Et₂O (2 x 10 mL), and dried *in vacuo*. Yield: 0.14 g (47 %). ¹H NMR (20 °C, CDCl₃): δ 7.0 - 8.0 m (40H, Ph), δ 4.71 d qn (2H, CH₂, J_{HH} = 13.5 Hz, J_{PH} = 5.7 Hz), δ 3.03 d qn (2H, CH₂, J_{HH} = 13.2 Hz, J_{PH} = 3.0 Hz), δ -1.54 qn (2H, SH, J_{PH} = 5.7 Hz). ³¹P{¹H} NMR (20 °C, CDCl₃): δ 14.8 s.

2.2 Instrumentation

2.2.1 Nuclear magnetic resonance spectroscopy

NMR spectra were recorded on a Bruker AC200E or Varian XL 300 NMR spectrometer using the residual protonated species in the deuterated solvents as internal references for ¹H NMR (7.24 ppm for CDCl₃, 7.18 ppm for C₆D₆, 5.32 ppm for CD₂Cl₂, 2.49 ppm for DMSO-d₆, and 1.93 ppm for CD₃CN; all shifts are relative to TMS) or 85% H₃PO₄ as an external reference for ³¹P{¹H} NMR with the downfield shifts being positive. Samples were prepared in 5 mm NMR tubes fitted with poly(propylene) caps, rubber septa, or poly(tetrafluoroethylene) J. Young valves (Aldrich). Unless otherwise stated, all samples were prepared under 1 atm of N₂. Low temperature NMR studies were performed using the Varian XL 300 NMR spectrometer.

2.2.2 Electronic absorption spectroscopy

UV-vis spectroscopic measurements were performed using 1 cm quartz cells on a Hewlett Packard 8452A diode-array or a Perkin-Elmer 552A spectrophotometer both equipped with a temperature regulating unit. The accompanying UV-vis quantification software (HP 89532A, HP 89532K, and HP 89532Q) for the diode-array instrument was used for both general spectral acquisition and kinetic experiments (see Section 2.3 for treatment of kinetic data).

2.2.3 Stopped-flow electronic absorption spectroscopy

Kinetically fast reactions were monitored by stopped-flow measurements using a path length of 1 cm on the Applied Photophysics Stopped-Flow spectrometer (Model SF.17MV) equipped with a 150 W Xenon arc lamp, temperature regulating unit, and the SF.17MV kinetic software. The temperature regulating unit houses the dual syringe sample inlet system driven by a pneumatic pump. In a typical kinetic setup, the two syringes were filled with the appropriate solutions and thermostated at the appropriate temperature. Data were automatically collected by the computer after manually initiating the pump (see Section 2.3 for treatment of kinetic data).

2.2.4 Thin-layered chromatography

Analytical thin-layered chromatography was carried out using Merck silica gel on plastic sheets (Mesh 60, layer thickness 0.2 mm) with F₂₅₄ fluorescent indicator. Species identification was done by comparison of degrees of retention with those of authentic samples. Qualitative

assessment of the status of a reaction, in general, was made by noting the disappearance of a reactant (usually a phosphine species).

2.2.5 Gas chromatography

Gas chromatographic analyses were performed on a temperature-programmable Hewlett Packard 5890A instrument equipped with a thermal conductivity detector (TCD). Retention times were established using authentic samples. A 10 ft packed molecular sieve column was used for qualitative analysis of H₂ with He as the carrier gas (see Chapter 3). Instrument settings were as follows: oven temp. = 75 °C; injector temp. = 90 °C; detector temp. = 200 °C; and column head pressure = 40 kPa. Retention time: $t_R(\text{H}_2) = 1.65 \text{ min}$ (inverted peak²⁰).

2.2.6 Photochemistry

Photochemical experiments were carried out at R.T. using either an 18 W TLC UV lamp (Mineralight[®], model UVG-11) or a 100 W medium pressure Hg vapour lamp (Ace Glass Inc.). Samples were usually prepared in either a septum-sealed NMR tube or an NMR tube fitted with a PTFE J. Young valve.

2.2.7 Electron spin resonance spectroscopy

ESR spectra were obtained at X-band frequencies using a Bruker ECS-106 spectrometer. Samples were prepared in the frozen-state at liquid N₂ temperatures (-196 °C) in 4 mm ESR tubes (see Chapter 4). Analyses were performed by Dr. F.G. Herring of this department.

2.2.8 Elemental, mass, and X-ray crystallographic and photoelectron spectroscopic analyses

Analyses of these types were performed by the technical staff at this department (elemental analyses by Mr. P. Borda, mass spectroscopy by Dr. G. Eigendorf and his staff, and X-ray crystallography by Dr. S.J. Rettig). XPS (or ESCA) was carried out by Dr. P.C. Wong in Dr. K.A.R. Mitchell's surface science laboratories.

2.3 Treatment of kinetic data

Throughout the course of this thesis work, the kinetics of several reactions were monitored spectrophotometrically, and thus it seems appropriate to discuss briefly the treatment of kinetic data. Either by conventional or stopped-flow spectrophotometry, the solution electronic absorption of a system was measured as a function of time under pseudo-first-order conditions. From these absorbances (A) vs. time (t) measurements, semilog plots of $\ln(A_{\infty} - A_t)$ vs. t were obtained (where A_{∞} and A_t are the absorbances at $t = \infty$ and t, respectively) from which the observed rate constants, k_{obs} , were evaluated from the slopes. The justification of such plots is presented below.

In the reactions studied kinetically, the systems are well-behaved (*i.e.* there is in every case isosbesticity in spectrophotometric measurements and the absence of observable intermediates as determined by variable temperature NMR measurements) and are characteristic of one absorbing species going to another, *e.g.* $X \rightarrow Y$. Firstly, under pseudo-first-order conditions (*i.e.* with the non-absorbing reactant species in excess), the disappearance of X follows a first-order rate decay as expressed by eq. 2.3.1, where $[X]_t$ and $[X]_0$ are the concentrations of X at time = t and 0, respectively.

$$(2.3.1) \quad [X]_t = [X]_0 \exp(-k_{\text{obs}}t)$$

The rate of Y appearing is as described in eq. 2.3.2.

$$(2.3.2) \quad [Y]_t = [X]_0 - [X]_t \exp(-k_{\text{obs}}t)$$

The absorbances according to the Beer-Lambert law at time = t for X and Y are given by

$$(2.3.3) \quad A_t^X = \epsilon_X b [X]_t$$

and

$$(2.3.4) \quad A_t^Y = \epsilon_Y b [Y]_t$$

(where b is the path length and ϵ_X and ϵ_Y are the molar absorptivities of X and Y, respectively),

and the total absorbance of the system is given by

$$(2.3.5) \quad A_t = A_t^X + A_t^Y = \epsilon_X b [X]_t + \epsilon_Y b [Y]_t$$

From eq. 2.3.2, $[Y]_t = [X]_0 - [X]_t$, and hence,

$$(2.3.6) \quad A_t = \epsilon_X b [X]_t + \epsilon_Y b ([X]_0 - [X]_t)$$

When the reaction is complete (*i.e.* at $t = \infty$), the absorbance of the system is given by

$$(2.3.7) \quad A_\infty = A_\infty^Y = \epsilon_Y b [Y]_\infty = \epsilon_Y b [X]_0$$

Subtraction of eq. 2.3.6 from eq. 2.3.7 yields

$$(2.3.8) \quad A_\infty - A_t = \epsilon_Y b [X]_0 - \epsilon_X b [X]_t - \epsilon_Y b ([X]_0 - [X]_t) = (\epsilon_Y b - \epsilon_X b) [X]_t$$

Eq. 2.3.8 states that $A_\infty - A_t$ is proportional to $[X]$ at time = t which justifies the plotting of $\ln(A_\infty - A_t)$ vs. t for a first-order analysis. Furthermore, substitution of eq. 2.3.8 into eq. 2.3.1 gives

$$(2.3.9) \quad (A_\infty - A_t)/(\epsilon_Y b - \epsilon_X b) = (A_0/\epsilon_X b)\exp(-k_{\text{obs}}t)$$

where A_0 is the initial absorbance of the system (*i.e.* that of X at $[X]_0$). Expressed in natural logarithms, eq. 2.3.9 upon rearrangement becomes

$$(2.3.10) \quad \ln(A_\infty - A_t) = \ln[(\epsilon_Y - \epsilon_X)A_0/\epsilon_X] - k_{\text{obs}} t$$

Analyses of the various kinetic data showed excellent correlation between the observed y -intercept and $\ln[(\epsilon_Y - \epsilon_X)A_0/\epsilon_X]$. The kinetic quantification software function-fits the A vs. t data into the general equation

$$(2.3.11) \quad A_t = K_1 \exp(-K_2 t) + K_3$$

where $K_1 = A_0 - A_\infty$ (A_0 is the initial absorbance at $t = 0$), $K_2 = k_{\text{obs}}$, and $K_3 = A_\infty$. It is noted here that both semilog plots and function-fitting were used to obtain observed rate constant values.

The rate constants for the reaction, k , were then evaluated from the k_{obs} values either directly, knowing the concentrations of the non-absorbing species, or from the slopes of k_{obs} vs. [non-absorbing species] plots as

$$(2.3.12) \quad k_{\text{obs}} = k [\text{non-absorbing species}]$$

The k values were obtained at other temperatures, and activation parameters, ΔH^\ddagger and ΔS^\ddagger , were obtained from usual Eyring plots ($\ln k/T$ vs. $1/T$) as

$$(2.3.13) \quad k = k_B T/h \exp(\Delta S^\ddagger/R) \exp(-\Delta H^\ddagger/RT)$$

where k_B is the Boltzmann's constant ($1.38066 \times 10^{-23} \text{ J K}^{-1}$), h = Planck's constant ($6.62618 \times 10^{-34} \text{ J s}$), and R = gas constant ($8.31442 \text{ J K}^{-1} \text{ mol}^{-1}$).

2.4 References for Chapter 2

1. Lee, C-L.; Yang, Y-P.; Rettig, S.J.; James, B.R.; Nelson, D.A.; Lilga, M.A. *Organometallics* **1986**, *5*, 2220.
2. (a) Grim, S.O.; Mitchell, J.D. *Syn. React. Inorg. Metal-Org. Chem.* **1974**, *4*, 221. (b) Grim, S.O.; Walton, E.D. *Inorg. Chem.* **1980**, *19*, 1982.
3. Conard, C.R.; Dolliver, M.A. *Org. Syn., Coll. Vol. 2*, John Wiley, Toronto, p. 167.
4. Barnabas, A.F. M.Sc. Dissertation, University of British Columbia, Vancouver, 1989.
5. Kharasch, M.S.; Seyler, R.C.; Mayo, F.R. *J. Am. Chem. Soc.* **1941**, *63*, 2088.
6. Doyle, J.R.; Slade, P.E.; Jonassen, H.B. *Inorg. Synth.* **1960**, *6*, 216.
7. Ukai, T.; Kawazura, H.; Ishii, Y.; Bonnet, J.; Ibers, J.A. *J. Organomet. Chem.* **1974**, *65*, 253.
8. Balch, A.L.; Benner, L.S. *Inorg. Synth.* **1982**, *21*, 47.
9. Benner, L.S.; Balch, A.L. *J. Am. Chem. Soc.* **1978**, *100*, 6099.
10. Besenyi, G.; Lee, C-L.; Gulinski, J.; Rettig, S.J.; James, B.R.; Nelson, D.A.; Lilga, M.A. *Inorg. Chem.* **1987**, *26*, 3622.
11. Jenkins, J.M.; Verkade, J.G. *Inorg. Synth.* **1968**, *11*, 108.
12. Steffen, W.L.; Palenik, G.J. *Inorg. Chem.* **1976**, *15*, 2432.
13. Bianco, V.D.; Doronzo, S. *Inorg. Synth.* **1976**, *16*, 161.
14. Olah, G.A.; Berrier, A.; Ohannesian, L. *Nouv. J. Chim.* **1986**, *10*, 253.
15. Hideyuki, I.; Yukitaka, U.; Masayuki, U. JP Patent 03 52,894 [91 52,894] (1989); Chem. Abstr. 115, 49982, 1991.
16. Holloway, R.G.; Penfold, B.R. *J. Chem. Soc., Chem. Commun.* **1976**, 485.
17. Balch, A.L. in 'Catalytic Aspects of Metal Phosphine Complexes,' E.C. Alyea and D.W. Meek, eds., ACS Advances in Chemistry Series, 1982, v. 196, p. 243.
18. Peters, K.; Peters, E.-M.; Von Schnering, H.G.; Abicht, H.-P.Z. *Z. Kristallogr.* **1984**, *168*, 149.
19. Davies, J.A.; Pinkerton, A.A.; Syed, R.; Vilmer, M. *J. Chem. Soc., Chem. Commun.* **1988**, 47.

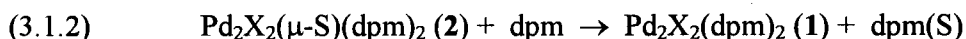
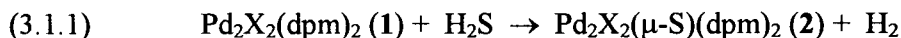
20. Only H₂ has thermal conductivity greater than He. See HP 5890A Gas Chromatograph Reference Manual, Hewlett-Packard Company, 2086, vol. I, p. 11-39. Depending on the concentration, the H₂ peak may appear as positive (low conc.), negative (high conc.), or a split peak (intermediate conc.) when using He as the carrier gas.

CHAPTER 3

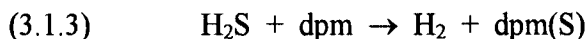
**Kinetic and Mechanistic Aspects of Sulfur Abstraction from $\text{Pd}_2\text{X}_2(\mu\text{-S})(\text{dpm})_2$
Using dpm or dpmMe and Catalytic Conversion of H_2S to H_2 .**

3.1 Introduction

The discovery in this laboratory of the stoichiometric abstraction of sulfur from H₂S using Pd₂X₂(dpm)₂ complexes [X = Cl (**1a**), Br (**1b**), I (**1c**)] (reaction 3.1.1)¹ had prompted subsequent kinetic and mechanistic studies on this reaction.^{2,3} In the course of these investigations, deuterium labelling and low temperature NMR spectroscopic experiments demonstrated that H₂S oxidatively adds across the metal-metal bond to generate hydrido mercapto intermediates. Product formation occurs via deprotonation of the coordinated SH and protonation of the coordinated hydride to give the bridged sulfide complex Pd₂X₂(μ-S)(dpm)₂ [X = Cl (**2a**), Br (**2b**), I (**2c**)] with concomitant H₂ evolution. Attempts to unravel the role of the bridging diphosphine, for example by adding excess dpm, had been thwarted by the unexpected quantitative abstraction of the bridging S atom (reaction 3.1.2), where dpm(S) is the monosulfide.²



It was then of interest to examine closely reaction 3.1.2 via kinetic and mechanistic studies and these are reported in this chapter. Reactions 3.1.1 and 3.1.2 imply a catalytic cycle, the net reaction 3.1.3, and some experiments were also carried out to substantiate the catalysis.



Reaction 3.1.3 appears to be the first reported, homogeneously catalyzed conversion of H₂S to H₂.⁴ Some rationale for the previously studied, unsuccessful sulfur abstraction from **2** by other phosphines (*i.e.* PPh₃, PPh₂Me, Ph₂P(CH₂)₃PPh₂)⁵ is also presented.

3.2 Results

Reaction 3.1.2 and its stoichiometry were readily demonstrated by NMR studies (Table 3.1). Complexes **2a** - **2c** reveal a singlet at δ 5.5 - 6.1 in the $^{31}\text{P}\{^1\text{H}\}$ NMR spectrum at ambient conditions in CH_2Cl_2 for the four equivalent P atoms,³ while the corresponding singlets for **1a** - **1c** are in the δ -5.5 to -11.3 region.^{1,2} The $^{31}\text{P}\{^1\text{H}\}$ NMR spectrum of the monosulfide dpm(S) consists of an AB doublet (δ -28.1, 40.1, J_{PP} 75.9 Hz), the lower field signal being that of the P(V) center.⁶ In the ^1H NMR spectra of **2a** - **2c**, the CH_2 resonances appear as AB doublets with additional coupling to the four P atoms, while in **1a** - **1c** the equivalent CH_2 protons show a characteristic quintet pattern. Table 3.1 summarizes the NMR data measured in the present work for all the Pd complexes and diphosphine compounds; kinetic data can be found in Appendix II.

The rates of the reconversion reaction **2** \rightarrow **1** (eq. 3.1.2) were noticed qualitatively during preliminary kinetic and mechanistic studies, and were found to be dependent on the nature of the auxiliary ligand X and on the concentration of dpm used. The reactivity trend in CHCl_3 observed was $\text{X} = \text{Cl} > \text{Br} > \text{I}$, and, of these, the bromide system was chosen for a detailed, classical spectrophotometric study. Only limited kinetic data for the chloride system and qualitative observations for the iodide system were obtained because of complexities based on the photosensitivity of **1a** and **1c**, respectively.^{2,3,7}

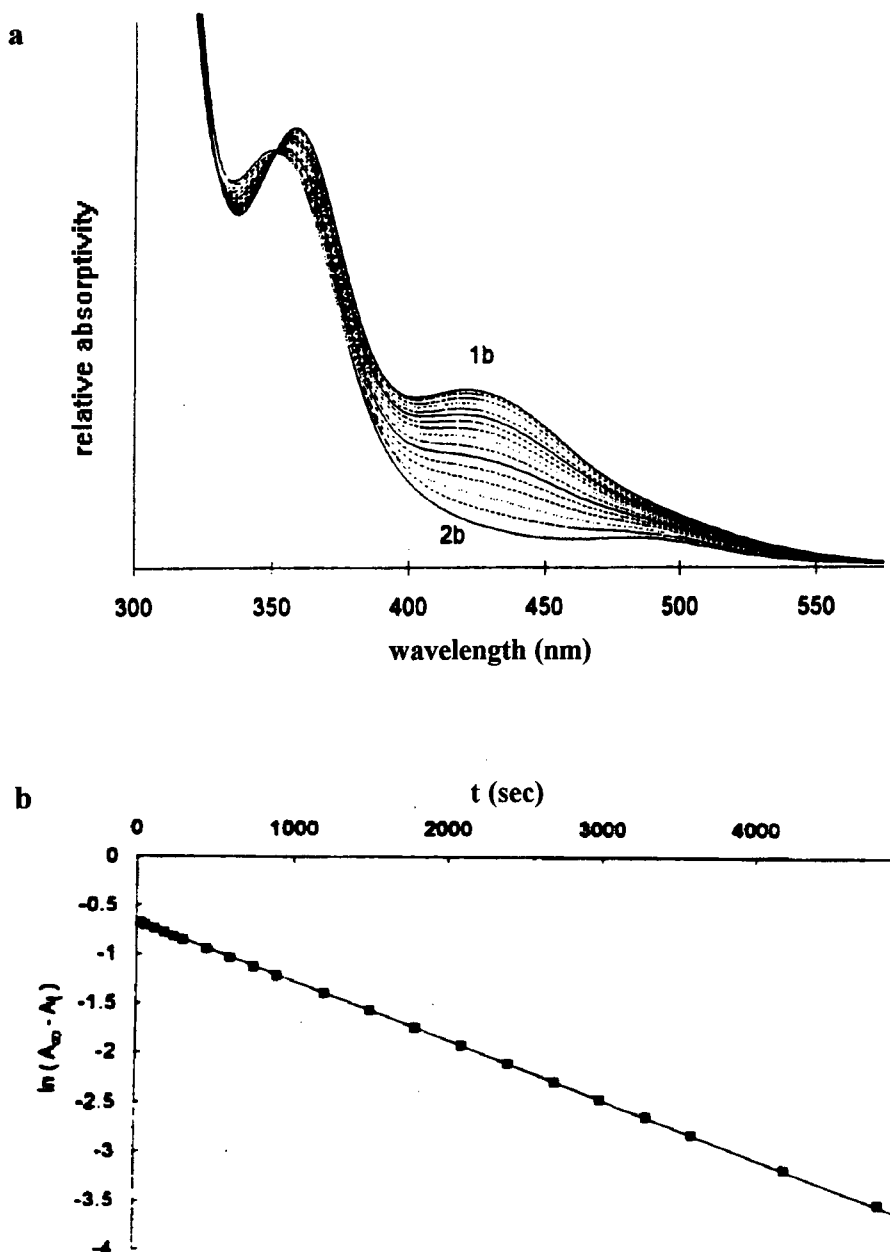
The kinetics of the reconversion reaction (**2** \rightarrow **1**) were studied using solution electronic spectroscopy. Species **2** are brown and have absorption maxima in the 325 - 350 and 470 - 485 nm regions, while the products (**1**) are reddish-orange (Cl and Br), or purple (I), and have two or three absorption maxima in the 340 - 590 nm region.^{2,3} Figure 3.1 shows spectral changes on treating a CHCl_3 solution of the bromide **2b** with dpm at 25 °C; rates for the bromide system are

Table 3.1. NMR Data for the Dinuclear Palladium Complexes, Diphosphines, and the Diphosphine Monosulfides.

Compound ^a	δ (¹ H) ^b	δ (³¹ P) ^c
Pd ₂ Cl ₂ (dpm) ₂ (1a)	4.17 ^d (4.0)	-5.5
Pd ₂ Br ₂ (dpm) ₂ (1b)	4.19 ^d (4.0) 4.24 ^e	-6.15 -5.5 ^e
Pd ₂ I ₂ (dpm) ₂ (1c)	4.23 ^d (4.0)	-11.3
Pd ₂ Cl ₂ (μ -S)(dpm) ₂ (2a)	2.79 ^f (12.6, 3.5) 4.73 (12.6, 6.1)	5.52
Pd ₂ Br ₂ (μ -S)(dpm) ₂ (2b)	2.88 ^f (12.8, 3.2) (2.90 ^e) 4.83 (12.8, 7.6)	5.96 6.14 ^e
Pd ₂ I ₂ (μ -S)(dpm) ₂ (2c)	3.06 ^f (14.0, 3.0) 4.95 (14.0, 6.0)	6.08
Pd ₂ Br ₂ (dpm)(dpm-d ₂) (3b)	4.19 ^g 4.24 ^e	-6.30 ^h -5.7 ^e
Pd ₂ Br ₂ (dpm-d ₂) ₂ (4b)	<i>i</i>	-6.35
Pd ₂ Br ₂ (dpm)(dpmMe) (5b)	4.98 ^{j,e} , 4.55 ^k , 3.72 ^k 1.00 ^k (Me)	<i>l</i>
Pd ₂ Br ₂ (dpmMe) ₂ (6b)	4.98 ^{m,e} 1.00 ^{n,e} (Me)	16.1 ^e
Pd ₂ Br ₂ (μ -S)(dpm)(dpm-d ₂) (7b)	2.88 ^{g,e} , 4.83 ^g	5.95 ^{h,e}
Pd ₂ Br ₂ (μ -S)(dpm-d ₂) ₂ (8b)	<i>i</i>	6.00 ^e
Pd ₂ I ₄ (dpm) ₂	5.14 ^{d,e} (3.6)	-1.52 ^e
dpm	2.81 ^{o,e} (1.6)	-22.5 ^e
dpm-d ₂	<i>i</i>	-23.0 ^e
dpm(S)	3.36 ^p (12.6, 1.1) 3.35 ^e	-28.1, 40.1 (75.9) ^q
dpm(S)-d ₂	<i>i</i>	-28.3, 39.9 (76.4) ^q
dpmMe	3.20 ^r (7.2) 0.99 ^k (Me) (7.5, 10.2)	-6.94
dpmMe(S)	3.64 ^{s,e} 1.16 ^{k,e} (Me) (7.4, 10.2)	-13.4, 51.9 (94.3) ^q

^a The μ -symbol for the bridging diphosphine ligand(s) is omitted for convenience throughout this Table and the text. ^b In CD_2Cl_2 , unless stated otherwise, at 20 °C with respect to TMS; J_{HH} and/or J_{PH} values in Hertz are given in parentheses; signals for CH_2 protons unless indicated otherwise. ^c Singlets in CD_2Cl_2 at 20 °C with respect to 85% H_3PO_4 , downfield being positive. ^d Quintet. ^e In CDCl_3 . ^f Doublets of quintets for each of 2 sets of CH_2 protons. ^g Assumed triplet. ^h 'Tight' AB quartet. ⁱ No CH_2 protons observed. ^j Triplet of quartets. ^k Doublet of triplets. ^l AA'BB' pattern (see Fig. 3.13). ^m Quartet of quintets. ⁿ Doublet of quintets. ^o Triplet. ^p Doublet of doublets. ^q AB pattern, J_{PP} values in Hertz given in parentheses. ^r Quartet. ^s Multiplet.

Fig. 3.1. a) Visible absorption spectral changes (350 - 550 nm region) as a function of time for a CHCl_3 solution of $\text{Pd}_2\text{Br}_2(\mu\text{-S})(\mu\text{-dpm})_2$ (**2b**) (6.52×10^{-5} M) on addition of dpm (1.96×10^{-2} M) at 25°C . b) A rate-plot analyzed for a pseudo-first-order dependence on **2b**; A_t and A_∞ represent the absorption at 428 nm at times t and ∞ , respectively.



followed by observing the increasing absorption at 428 nm as a function of time, and the observed isosbestic point shows a well-behaved system. The pseudo-first-order rate constants, k_{obs} , obtained from the excellently linear semi-log plots (Fig. 3.1b), are strictly first-order in [dpm] (Fig. 3.2) and are independent of the [2b] from $(0.81 - 13.0) \times 10^{-5}$ M. Thus, the rate law takes the simple form

$$\text{Rate} = -\frac{d}{dt}[\mathbf{2b}] = k_{\text{obs}}[\mathbf{2b}] = k_{\text{Br}}[\text{dpm}][\mathbf{2b}] \quad (3.2.1)$$

where k_{Br} is the bimolecular rate constant for the reaction. The temperature dependence data for k_{Br} (Table 3.2) are obtained similarly from the first-order plots at other temperatures (Fig. 3.2a); an Eyring plot of the data from 20 - 35 °C gives an excellent straight line and the activation parameters $\Delta H^\ddagger = 38 \pm 1 \text{ kJ mol}^{-1}$ and $\Delta S^\ddagger = -144 \pm 4 \text{ J K}^{-1} \text{ mol}^{-1}$ (Fig. 3.2b).

The corresponding studies on the faster chloride system were performed, the increasing absorbance being monitored at 416 nm where spectral changes are greatest. Because of the photosensitivity of **1a**, specifically at the later stages of the reaction where isosbesticity is lost, more limited kinetic data were obtained. The reconversion reaction **2a** \rightarrow **1a** was monitored when the solution was kept in the dark, with the optical density being recorded by a sampling rather than a continuous monitoring method. Analysis of the earlier visible spectral changes (~ 2 half-lives), using an A_∞ value from the known absorption spectrum of **1a**, also gives results that are strictly first-order in [dpm] (Fig. 3.3a). The pseudo-first-order rate constant is also found to be independent of the [2a] from $(3.26 - 13.0) \times 10^{-5}$ M. Thus, the rate law for the chloride system also takes the same form as eq. 3.2.1, but with a bimolecular rate constant k_{Cl} . The temperature dependence data for k_{Cl} were obtained at a single [dpm] of 1.96×10^{-2} M, and with [2a] = $6.52 \times$

Fig. 3.2. a) The dependence of the pseudo-first-order rate constants, k_{obs} , on $[\text{dpm}]$ at $[\text{2b}] = 6.52 \times 10^{-5} \text{ M}$, in CHCl_3 . b) Eyring plot of the temperature dependence of the bimolecular rate constant, k_{B} .

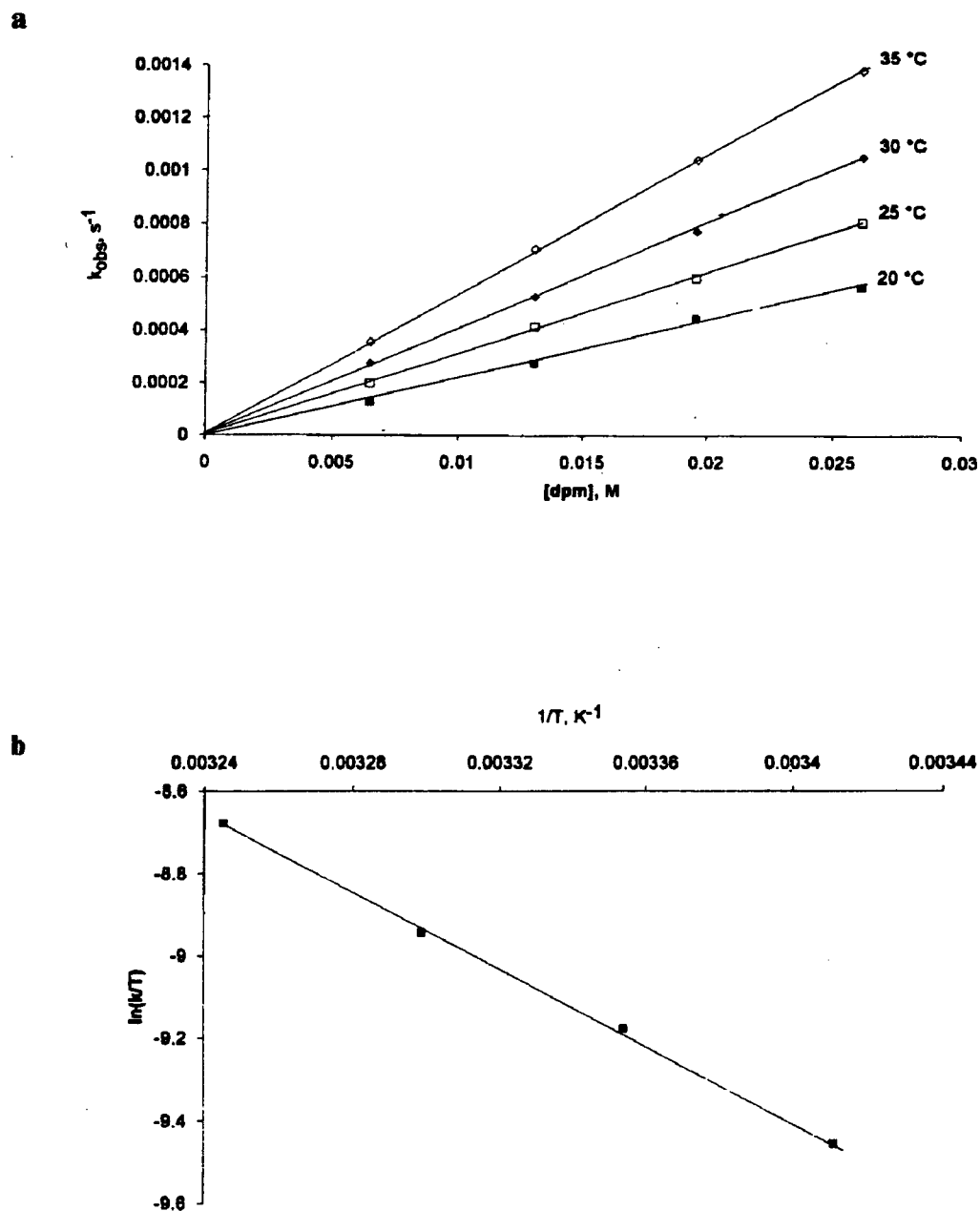
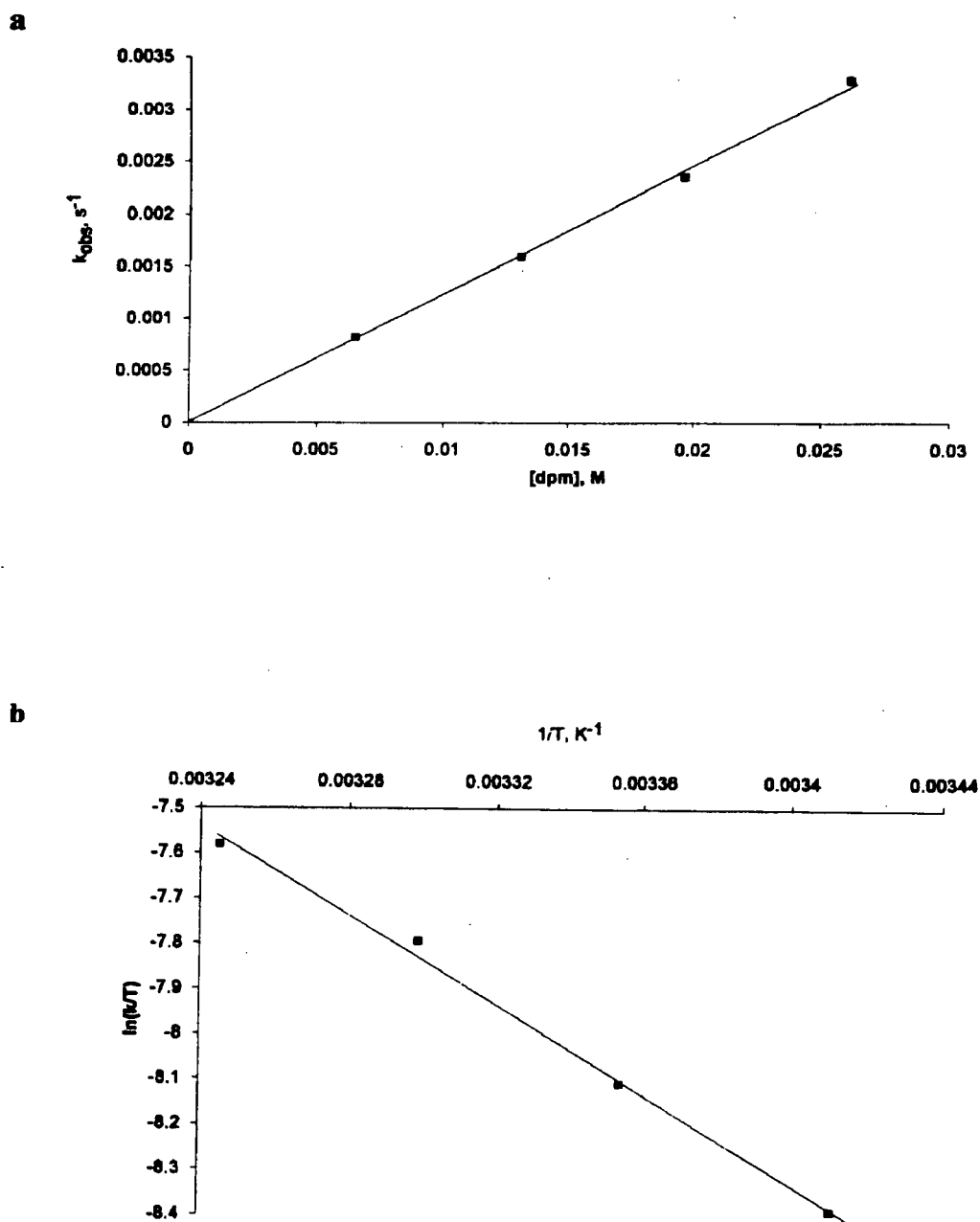


Table 3.2. Temperature dependence for the bimolecular rate constant of the reaction of $\text{Pd}_2\text{Cl}_2(\mu\text{-S})(\text{dpm})_2$ (**2a**) (k_{Cl}) and $\text{Pd}_2\text{Br}_2(\mu\text{-S})(\text{dpm})_2$ (**2b**) (k_{Br}) with dpm in CHCl_3 .

Temp, K	$k_{\text{Cl}}, \text{M}^{-1}\text{s}^{-1}$	$k_{\text{Br}}, \text{M}^{-1}\text{s}^{-1}$
293	0.0667 ^a	0.0229
298	0.0898	0.0308
303	0.125 ^a	0.0396
308	0.157 ^a	0.0524

^a Obtained at a single $[\text{dpm}] = 1.96 \times 10^{-2} \text{ M}$.

Fig. 3.3. a) The dependence of the pseudo-first-order rate constants, k_{obs} , on $[\text{dpm}]$ at $[\text{2a}] = 6.52 \times 10^{-5} \text{ M}$, in CHCl_3 at 30°C . b) Eyring plot of the temperature dependence of the bimolecular rate constant, k_{Cl} .



10^{-5} M (Table 3.2); an Eyring plot is reasonably linear and gives the activation parameters $\Delta H^\ddagger = 41 \pm 3 \text{ kJ mol}^{-1}$ and $\Delta S^\ddagger = -127 \pm 10 \text{ J K}^{-1} \text{ mol}^{-1}$ (Fig. 3.3b).

Only qualitative observations could be made for the iodide system due to its inherent photosensitive nature; the light source (either laboratory light or that of the spectrophotometer) readily induces formation of the monomer $\text{PdI}_2(\text{dpm})^2$ from **1c**, the product of the reconversion reaction. Under the same conditions used to study the other two systems, the iodide reaction is extremely slow, even at higher temperatures (*e.g.* 35°C), but the thermal reaction between **2c** and dpm gives the 'expected' products, **1c** and dpm(S). Again, analysis of the early visible spectral changes, using an A_∞ value from the known absorption spectrum of **1c**, gives $k_{\text{obs}} \sim 7 \times 10^{-5} \text{ s}^{-1}$ at 25°C for a reaction with $[\text{dpm}] = 6.53 \times 10^{-3} \text{ M}$ corresponding to a bimolecular k_1 rate constant of $\sim 1 \times 10^{-2} \text{ M}^{-1} \text{ s}^{-1}$. The limited data show that the rate constant is about three times lower than k_{Br} and about nine times lower than k_{Cl} .

Low temperature NMR studies were performed on all three systems but no intermediates were observed en route to formation of **1** from **2**, even at temperatures as low as -80°C (in CD_2Cl_2). For systems in CDCl_3 , the probe temperature was raised in 20° increments, and new signals were first observed around -40°C in each case and which corresponded to those of the products, **1** and dpm(S). NMR samples in CD_2Cl_2 were made up and sometimes left at -78°C for 72 h before analyses were done in an attempt to allow sufficient time for formation of intermediates; again intermediates were not seen, although some **1** and dpm(S) were observed for both the chloride and bromide systems. For the iodide system, however, no products were formed, this being consistent with the kinetic studies which show the iodide reaction to be much slower. These NMR studies show that the reconversion reaction is kinetically possible at -80°C (at least for the chloride and bromide systems), when dpm is present in a five-fold excess at $\sim 85 \text{ mM}$.

Extrapolation of the k values of Table 3.1 to -78°C gives k_{Cl} and k_{Br} values of 9.4×10^{-6} and $5.4 \times 10^{-6} \text{ M}^{-1} \text{ s}^{-1}$, respectively; use of these values at the noted conditions suggests conversions to **1a** and **1b** of ~ 20 and $\sim 11\%$, respectively, while the observed values are about 25 and 15%. (Note: although no extensive kinetic studies were performed in CH_2Cl_2 , a single experiment at R. T. qualitatively shows that k_{Br} of the reaction in CH_2Cl_2 is approx. twice that in CHCl_3 . The use of 20 and 11% values is conservative, and an upper limit would be 40 and 22% conversion to **1a** and **1b**, respectively.) The kinetics of the reaction **2b** \rightarrow **1b** were also studied in the presence of a bromide salt in order to find a possible kinetic role for an ionic species; addition of a 10- or 100-fold excess of tetrapropylammonium bromide to **2b** during a reaction with dpm at 25°C produced no change in the observed rate constant. Also, in reactions between **2b** and dpm- d_2 , and between $\text{Pd}_2\text{Br}_2(\mu\text{-S})(\text{dpm-d}_2)_2$ (**8b**) and dpm or dpm- d_2 , no kinetic isotope effect was seen in the observed rate constant at 30°C .

During the reaction of **2b** with either deuterated dpm (dpm- d_2) or methylated dpm (dpmMe), the colour changed from the brown of **2b** to reddish, as with dpm itself, and sulfur was again completely abstracted to give diphosphine monosulfides (see below). Complementary *in situ* NMR experiments (even when the phosphines were added in excess) showed that the products formed were the same as those obtained in the larger-scale synthetic experiments.

Although no kinetic measurements were done on the reaction of **2b** with dpmMe, *in situ* NMR experiments indicate that the reaction is some 30 times slower than that of **2b** with dpm (or dpm- d_2).

In the reaction of **2b** with dpm- d_2 at a 1 : 1 mole ratio, the ^1H spectrum of the Pd product(s) reveals the expected, less informative multiplet between δ 7.0 and 8.0 due to the phenyl rings of the phosphine ligands; also seen is the characteristic quintet at δ 4.19 due to the dpm CH_2

protons of the product **1b** (Fig. 3.4). However, the ratio of the integrated areas of the multiplet to the quintet is ~15:1, not the 10:1 expected for the 40 phenyl protons and 4 CH₂ protons of **1b**, and moreover the ³¹P{¹H} NMR spectrum shows not only the singlet of **1b** at δ -6.15 but also a 'tight' AB quartet at δ -6.30 (Fig. 3.5). As discussed below, this quartet is due to the mono-dpm-d₂ substituted complex, Pd₂Br₂(dpm)(dpm-d₂) (**3b**), and this product is formed with **1b** in the ratio of probably about 1:1. The CH₂ resonance of **3b** is assumed to be a triplet that is buried under the δ 4.19 quintet; and indeed the 'quintet' resonances are not of the classical 1:4:6:4:1 intensities because of the presence of the underlying triplet. The ¹H NMR spectrum of the phosphine monosulfide products reveals a doublet of doublets of reduced integration (1:15, relative to that of the phenyl protons) at δ 3.36 (Fig. 3.6), and in the ³¹P{¹H} NMR spectrum, a second set of doublets slightly upfield to those at δ 40.1 and -28.1 that are due to dpm(S) (Fig. 3.7). The second set of signals, as also discussed below, is attributed to the deuterated monosulfide product, dpm(S)-d₂, and which is formed with dpm(S) in the ratio of 1:2. Of interest, in an *in situ* NMR experiment in CDCl₃ where **2b** is reacted with a 5-fold excess of dpm-d₂, the same final products are observed; however, dpm(S)-d₂ is formed in a slightly greater than 1:1 mole ratio to dpm(S), judging from a qualitative analysis of the ³¹P{¹H} NMR spectrum (Fig. 3.8). Although the signals due to the diphosphine monosulfide products are resolved, the signals of the Pd products appear as one broad singlet, as do those of dpm and dpm-d₂; the singlet at δ ~ -6 is thought to result from a mixture of **1b**, **3b**, and the 'di-substituted' Pd₂(dpm-d₂)₂Br₂ (**4b**) resulting from a ligand exchange of **1b** and/or **2b** with dpm-d₂, as discussed later. The ¹H NMR spectrum shows the expected Pd products at δ 4.24, the dpm(S) product at δ 3.35, and the dpm signal at δ 2.81 (Fig. 3.9). Analysis of the CH₂ region signals shows that the ratios of the integrated peak areas of the Pd products (**1b** + **3b** + **4b**) to dpm(S), dpm to dpm(S), and dpm to the Pd products are (to within ±0.3) 2.3, 2.9, and 1.3 to 1,

Fig. 3.4. The ^1H NMR (300 MHz) spectrum of the isolated Pd products from the reaction of **2b** with dpm-d_2 at a 1:1 mole ratio in CD_2Cl_2 at R.T.

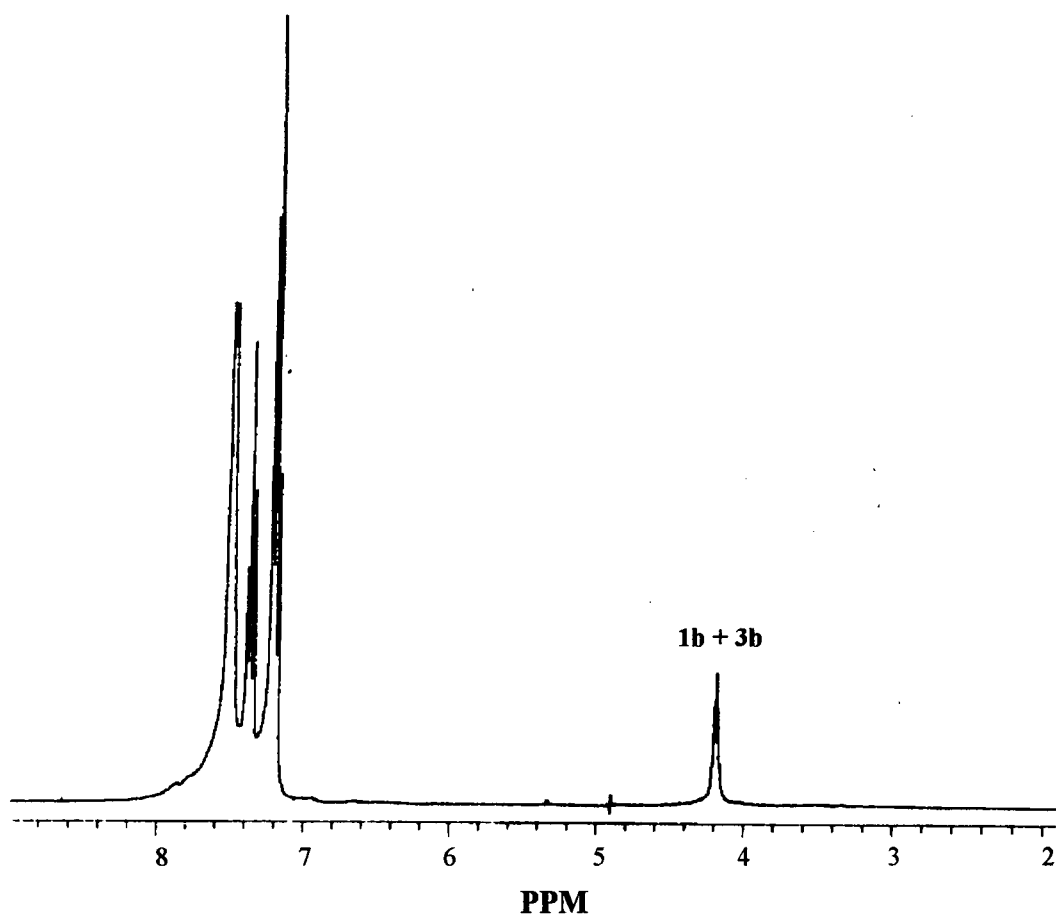


Fig. 3.5. The $^{31}\text{P}\{^1\text{H}\}$ NMR (121 MHz) spectrum of the isolated Pd products from the reaction of **2b** with dpm-d_2 at a 1:1 mole ratio in CD_2Cl_2 at R.T.

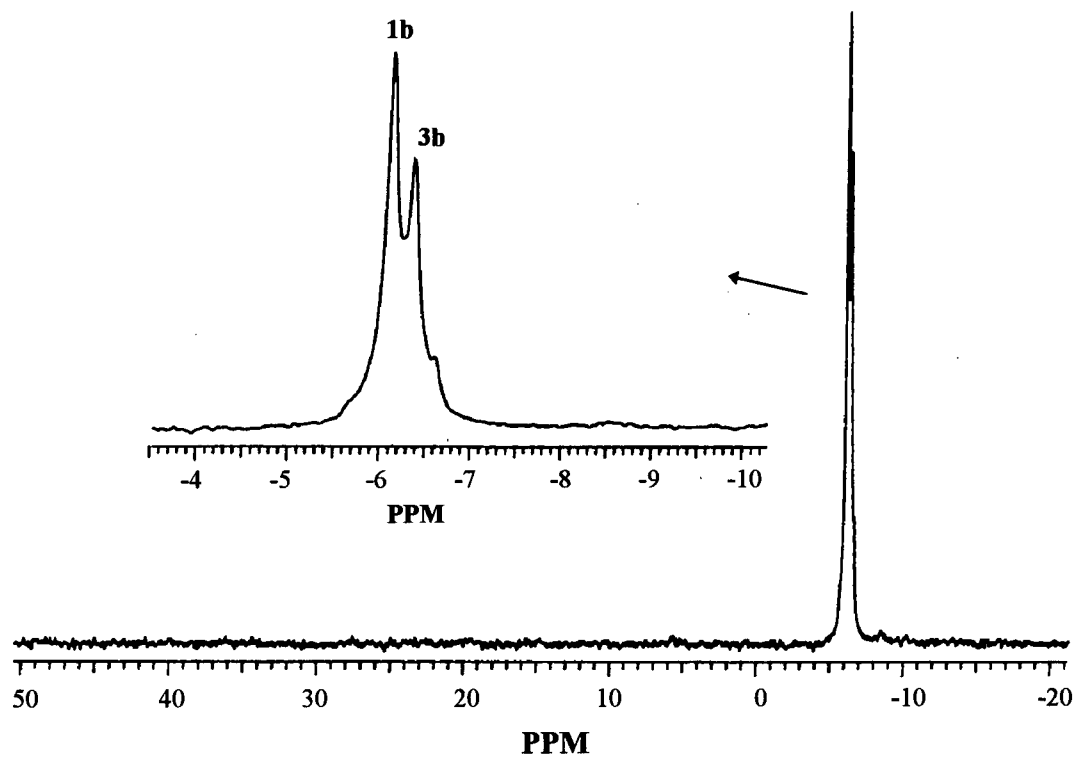


Fig. 3.6. The ^1H NMR (300 MHz) spectrum of the isolated phosphine monosulfide products from the reaction of **2b** with dpm-d_2 at a 1:1 mole ratio in CD_2Cl_2 at R.T.

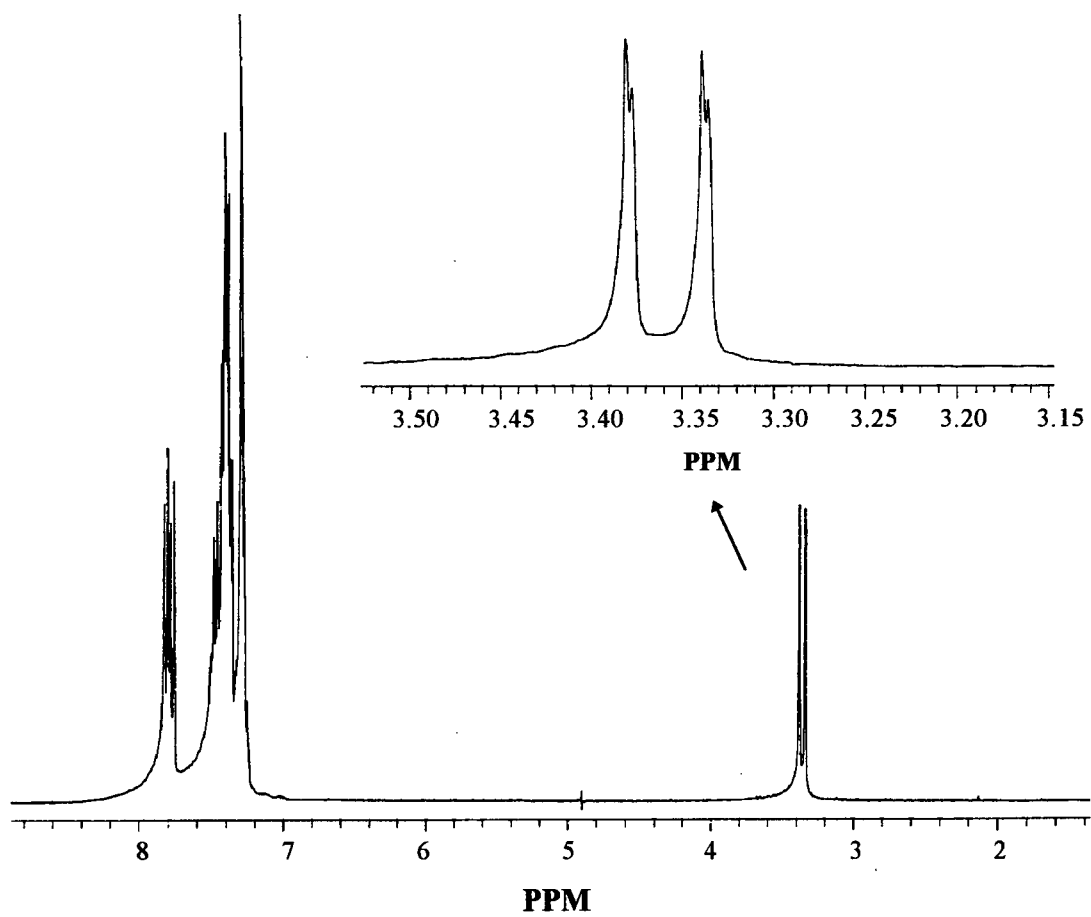


Fig. 3.7. The $^{31}\text{P}\{^1\text{H}\}$ NMR (121 MHz) spectrum of the isolated phosphine monosulfide products from the reaction of **2b** with dpm-d_2 at a 1:1 mole ratio in CD_2Cl_2 at R.T.

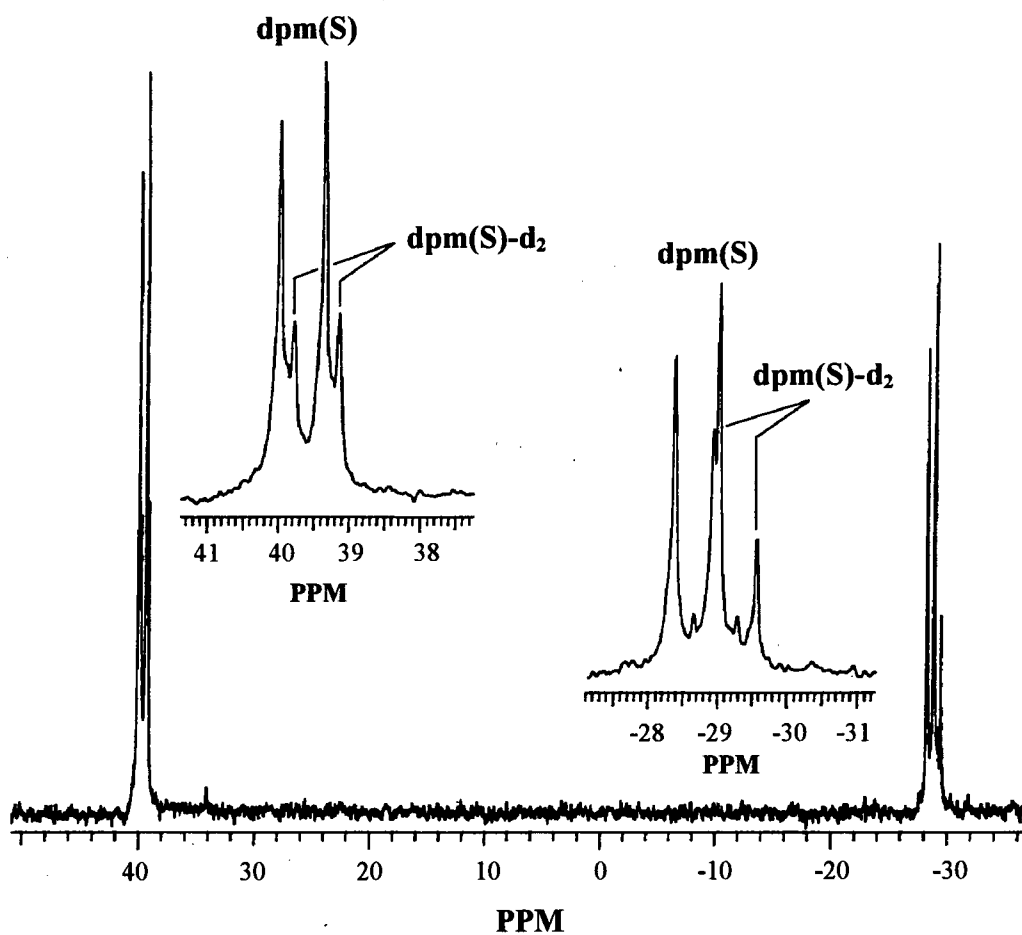


Fig. 3.8. The $^{31}\text{P}\{^1\text{H}\}$ NMR spectrum (121 MHz) of the completed *in situ* reaction between **2b** and dpm-d_2 (1.5 mole ratio) in CDCl_3 at R.T. (72 h); X = unknown.

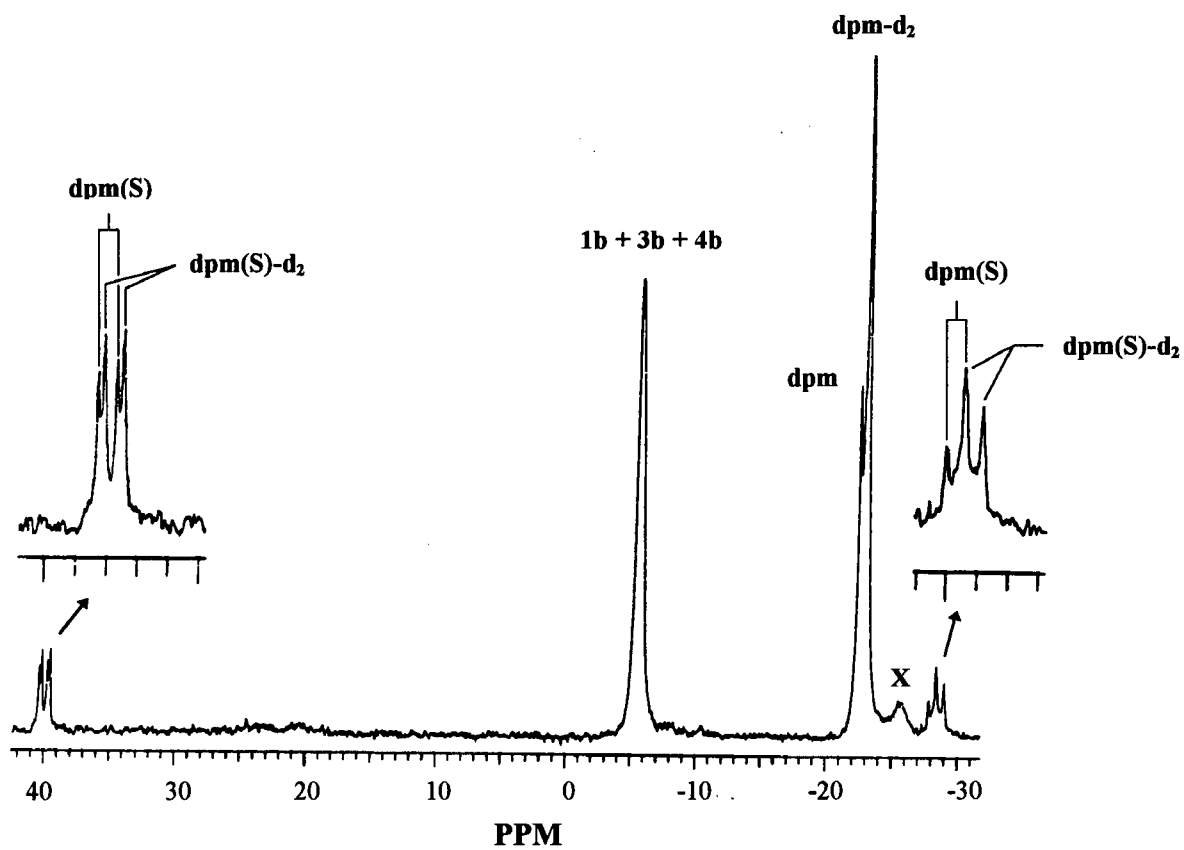
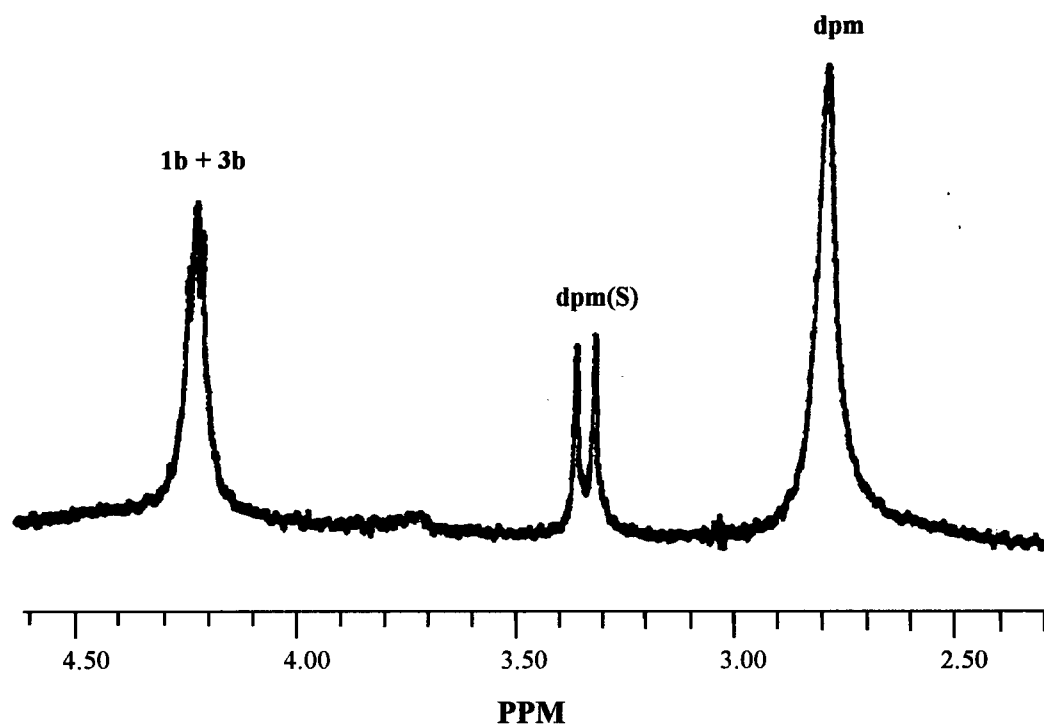


Fig. 3.9. The ^1H NMR (300 MHz) spectrum of the completed *in situ* reaction between **2b** and dpm-d_2 (1:5 mole ratio) in CDCl_3 at R.T. (72 h).

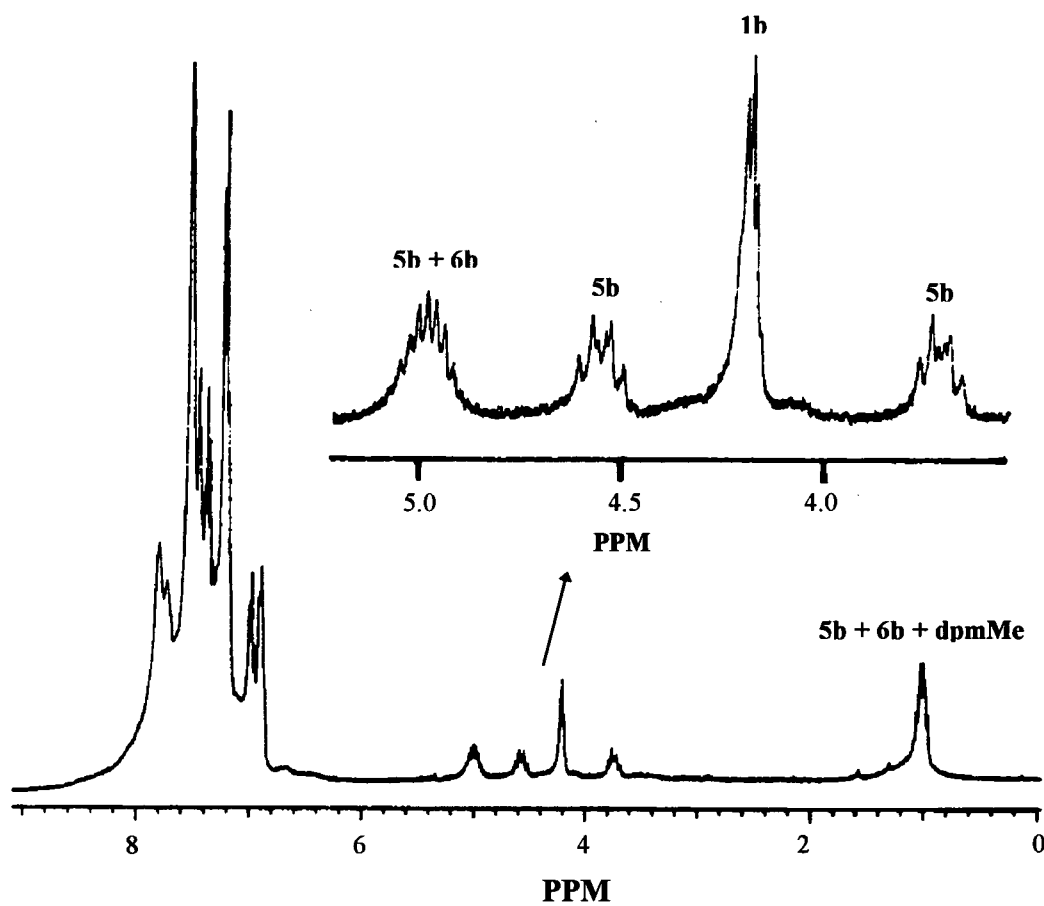


respectively. These results again reflect the combination of reaction 3.1.2 and the accompanying effects of diphosphine exchange of **1b** and **2b** with dpm-d₂ (see below).

Reaction of **2b** with dpmMe (1:1) after a few hours gave two immediately identifiable isolable Pd products, **1b** and Pd₂Br₂(dpm)(dpmMe) (**5b**),⁸ with the latter dominant; furthermore, some Pd₂Br₂(dpmMe)₂ (**6b**)⁸ is also probably present (Fig. 3.10). Pd₂Br₂(dpm)(dpmMe) (**5b**) is characterized by four multiplets in the ¹H NMR:⁸ a triplet of quartets centered at δ 4.98 (CH), a doublet of triplets at δ 1.00 (Me), and a doublet of triplets for each of the two CH₂ protons at δ 3.72 and at 4.55. Pd₂Br₂(dpmMe)₂ (**6b**) is characterized in the ¹H NMR spectrum⁸ by a quartet of quintets at δ 4.98 (CH) and a doublet of quintets at δ 1.00 (Me); these multiplets overlap those due to **5b**, and the presence of a small amount (~10%) of **6b** is suspected because of the slightly greater than expected intensities of the δ 4.98 and 1.00 signals. The ³¹P{¹H} NMR spectrum shows the singlet at δ -6.15 for **1b** and a complex AA'BB' pattern for **5b** in the δ +18 to -10 region, analogous to that recorded for Pd₂Cl₂(dpm)(dpmMe),⁸ the broad singlet expected for **6b** at δ 16.1⁸ could be buried within the AA'BB' pattern. The ³¹P{¹H} NMR spectrum of the isolated diphosphine products shows just two sets of AB doublets: one set due to dpm(S) and the other, downfield at δ 51.9 and -13.4, due to dpmMe(S); the ratio of dpm(S) to dpmMe(S) is ~ 3:1, this result being consistent with the presence of more **5b** than **1b** in the isolated Pd products.

In terms of quantifying the extent of S-extraction via originally coordinated and added diphosphine, it was necessary to study diphosphine exchange with **1b** and **2b**. Thus **1b** was reacted with 1 mole equivalent of dpm-d₂ in CDCl₃; a ¹H NMR triplet at δ 2.81 due to the CH₂ protons of dpm is seen 'immediately', the integrated area being about half that of the quintet at δ 4.24 due to the CH₂ protons of the various Pd species present (**1b**, **3b**, and possibly **4b**). The ³¹P{¹H} NMR spectrum shows the singlet of **1b** at δ -5.5 (which could also correspond to some

Fig. 3.10. The ^1H NMR spectrum (300 MHz) of the isolated Pd products from the reaction **2b** and dpmMe (1:1 mole ratio) in CD_2Cl_2 at R.T.



4b), the tight AB quartet of **3b** (δ -5.7), and a singlet at δ -22.5 due to dpm. The spectra were invariant with time. Similarly, the ^1H NMR spectrum of **2b** in the presence of 1 mole equivalent of dpm- d_2 shows (prior to any S-extraction) immediate generation of a triplet at δ 2.81 due to dpm, which overlaps the δ 2.90 signal of **2b**. As well, new peaks appear in the $^{31}\text{P}\{^1\text{H}\}$ NMR spectrum: an AB quartet δ 5.95, attributed to $\text{Pd}_2\text{Br}_2(\mu\text{-S})(\text{dpm})(\text{dpm-d}_2)$ (**7b**), overlaps the singlet of **2b** at δ 6.14 and the singlet of $\text{Pd}_2\text{Br}_2(\mu\text{-S})(\text{dpm-d}_2)_2$ (**8b**) at δ 6.00, and a singlet at δ -22.5 due to dpm is seen beside the singlet of dpm- d_2 at δ -23.0 (Fig. 3.11).

Diphosphine exchange of **1b** with dpmMe was not studied in detail but was shown to occur, at a much slower rate in contrast to the rapidly established equilibrium of **1b** or **2b** with dpm- d_2 . In a single *in situ* NMR experiment where **1b** was reacted with 1 mole equivalent of dpmMe, the final ^1H and $^{31}\text{P}\{^1\text{H}\}$ NMR spectra (which are then invariant with time after ~ 3 days) indicate that significant amounts of $\text{Pd}_2\text{Br}_2(\text{dpm})(\text{dpmMe})$ (**5b**), $\text{Pd}_2\text{Br}_2(\text{dpmMe})_2$ (**6b**), and dpm are formed (with some **1b** and dpmMe remaining) (Figs. 3.12 and 3.13). The suggestion that **6b** is present is again based on 'increased intensities' of the δ_{H} 4.98 and 1.00 signals (Fig. 3.12) and a possible buried δ_{P} 16.1 singlet (Fig. 3.13) (see above). Analysis of the various non-phenyl protons signals in the ^1H NMR spectrum gives the following absolute integrated values for **1b**, dpmMe, **5b**, dpm, and **6b** as 0.98, 0.91, 2.55, 2.27, and 0.58, respectively (with respect to the 60 phenyl protons of **1b** + dpmMe). Also, in contrast to the rapidly established equilibrium of **2b** with dpm- d_2 , **2b** does not undergo detectable diphosphine exchange with dpmMe (prior to any S-abstraction) as evidenced by NMR spectra.

The catalysis of reaction 3.1.3 was examined at R.T. using **1b** and **2b**. Gas chromatography and NMR spectroscopy were used to analyze for the products, H_2 and dpm(S), respectively. In preliminary studies, contrasting results were obtained where products were

Fig. 3.11. The $^{31}\text{P}\{^1\text{H}\}$ NMR (121 MHz) spectrum of **2b** on addition of 1 mole equivalent of dpm-d_2 ; the spectrum was recorded at R.T. immediately after sample preparation in CDCl_3 .

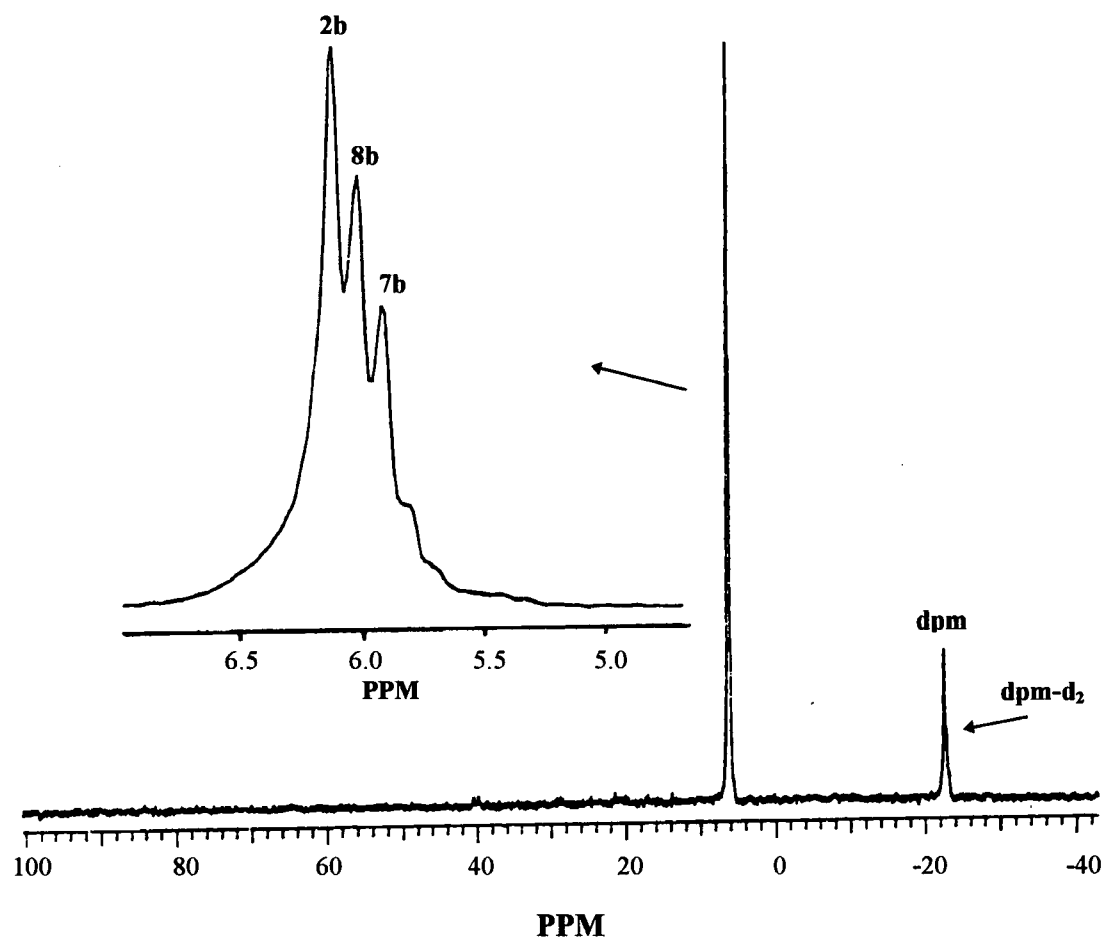


Fig. 3.12. The ^1H NMR spectrum (300 MHz) recorded at R.T. in CDCl_3 of **1b** on addition of 1 mole equivalent of **dpmMe** (72 h).

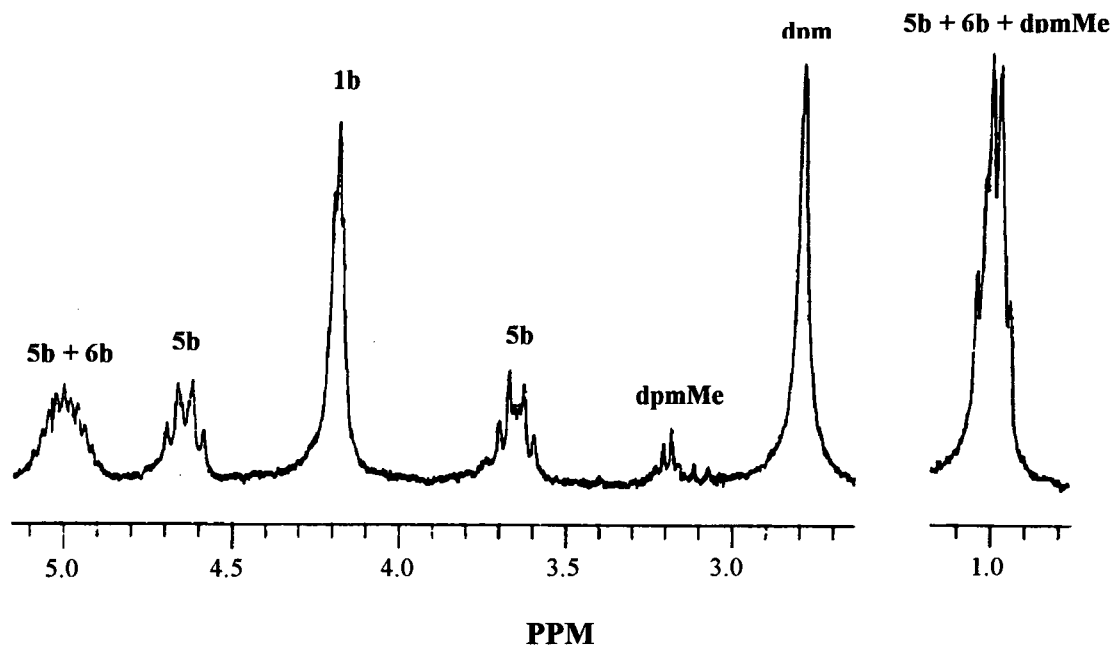
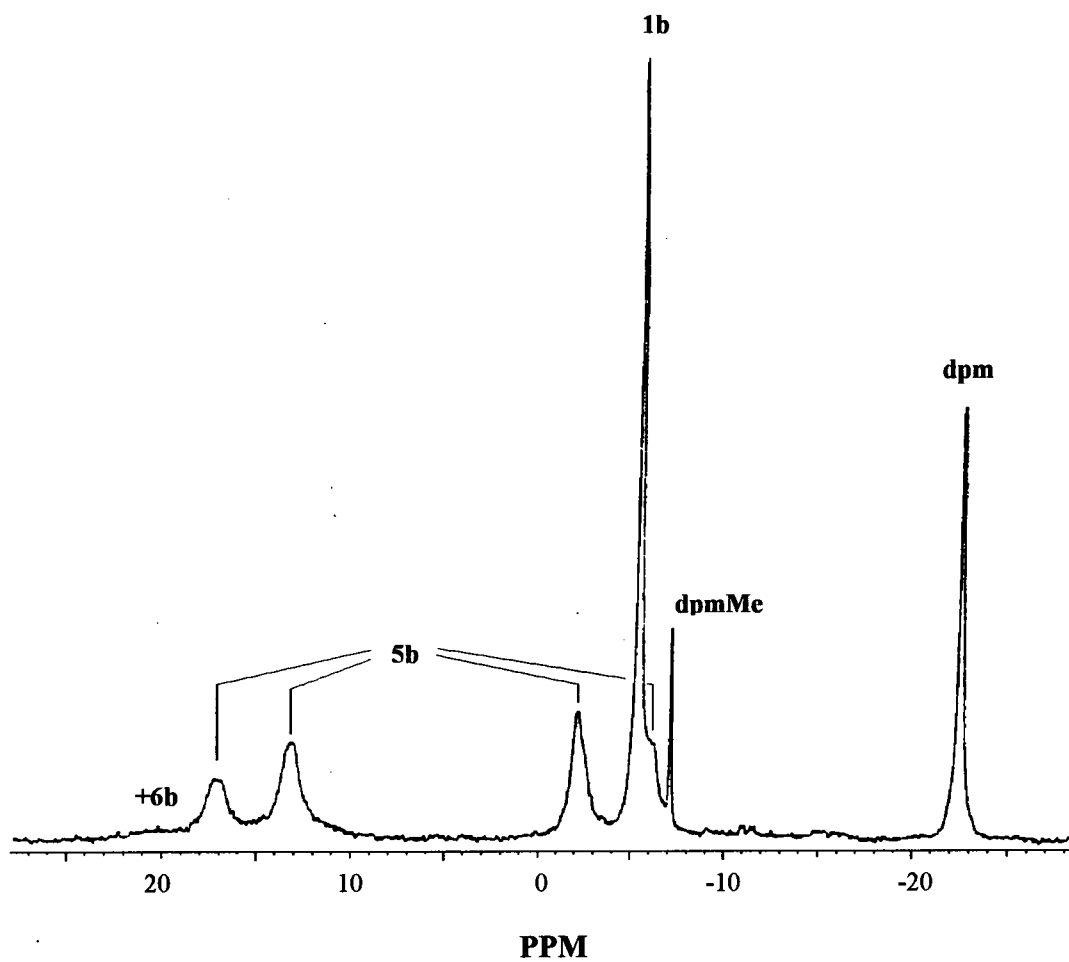


Fig. 3.13. The $^{31}\text{P}\{^1\text{H}\}$ NMR spectrum (121 MHz) recorded at R.T. in CDCl_3 of **1b** on addition of 1 mole equivalent of **dpmMe** (72 h).



observed in some studies but not in others. A series of experiments were then carried out where **1b** ranged from $(8.76 - 263) \times 10^{-5}$ M, [dpm] from $(3.64 - 52.0) \times 10^{-3}$ M, and $[\text{H}_2\text{S}] = 0.013$ M or 1.0 M (Table 3.3). The reaction ($\text{H}_2\text{S} + \text{dpm} \rightarrow \text{H}_2 + \text{dpm}(\text{S})$) was allowed to proceed for up to 72 h prior to analysis. In experiments 1 and 3 to 9, very little or no dpm(S) or H_2 products were seen. Moreover, UV-vis, ^1H and $^{31}\text{P}\{^1\text{H}\}$ NMR spectroscopic analyses revealed in all cases the presence of Pd species characterized by: three absorption maxima at 358, 422, and 522 nm in the UV-vis spectrum (Fig. 3.14); a multiplet, triplet, and singlet in a 10:1:2 integration ratio at δ 7.0-8.0, 4.72 and 3.37, respectively, in the ^1H NMR spectrum; and a singlet at δ -4.71 and a series of resonances resembling an AA'BB' pattern from δ 22 to 0 in the $^{31}\text{P}\{^1\text{H}\}$ NMR spectrum (Figs. 3.15 and 3.16). The same results were seen when non-cylinder, synthesized H_2S was used (expt. 8) or when **2b** was used as the catalyst (expt. 10). [In the latter study, although dpm(S) was observed in a 5% yield, no H_2 was detected.] The unknown Pd species was subsequently isolated and tested for catalytic activity; under similar experimental conditions (expt. 11), no products were found. In expt. 2 where a lower concentration of dpm was used, H_2 was detected and dpm(S) was found to be formed in ~47% yield after 24 h. A UV-vis spectrum was obtained at the end of the experiment and revealed absorption maxima at 340 and 426 nm (Fig. 3.17). This experiment (on the same scale) was repeated in an NMR tube fitted with a PTFE J. Young valve. After 24 h, ^1H and $^{31}\text{P}\{^1\text{H}\}$ NMR spectra showed the presence of H_2 (at δ 4.64) and dpm(S) in about 15 and 20% yields, respectively. **1b** and **2b** were the only Pd species seen, but their relative amounts were not determined because of the extremely low concentration conditions used. After 72 h, the yields of these products increased to approx. 40 and 50%, respectively. No more changes occurred in the system thereafter, and $^{31}\text{P}\{^1\text{H}\}$ NMR spectra revealed that decomposition of the catalyst had taken place.

Table 3.3. Conditions used in the study of the catalysis of reaction 3.1.3 in CHCl_3 at R.T. using $\text{Pd}_2\text{Br}_2(\text{dpm})_2$ (**1b**) or $\text{Pd}_2\text{Br}_2(\mu\text{-S})(\text{dpm})_2$ (**2b**).

Experiment	Amount of catalyst (mM)	Amount of dpm (M)	[H_2S] (M)	Time period (h)	Product formation	
					dpm(S) ^a	H_2
1	0.088 1b	0.026	1.0	24	trace	no
2	0.35 1b	0.0036	1.0	24	~47%	yes
3	0.35 1b	0.026	1.0	24	trace	no
4	0.088 1b	0.013	1.0	24	trace	no
5	0.88 1b	0.026	1.0	72	no	no
6	1.75 1b	0.052	0.013	24	no	no
7	2.63 1b	0.052	1.0	72	no	no
8	2.63 1b	0.052	1.0 ^b	72	trace	no
9	0.66 1b	0.026	1.0	5	no	no
10	2.56 2b	0.052	0.013	24	~5% ^c	no
11	<i>d</i>	0.052	1.0	24	no	no

^a Based on dpm reactant.

^b Non-cylinder H_2S , prepared from $\text{CaS} + \text{HCl}(\text{aq.})$.

^c Stoichiometric (see text).

^d 10 mg of an unknown Pd species isolated from expts. 5 to 10.

Fig. 3.14. The UV-vis spectrum of the isolated catalytically inactive species (in CHCl_3).

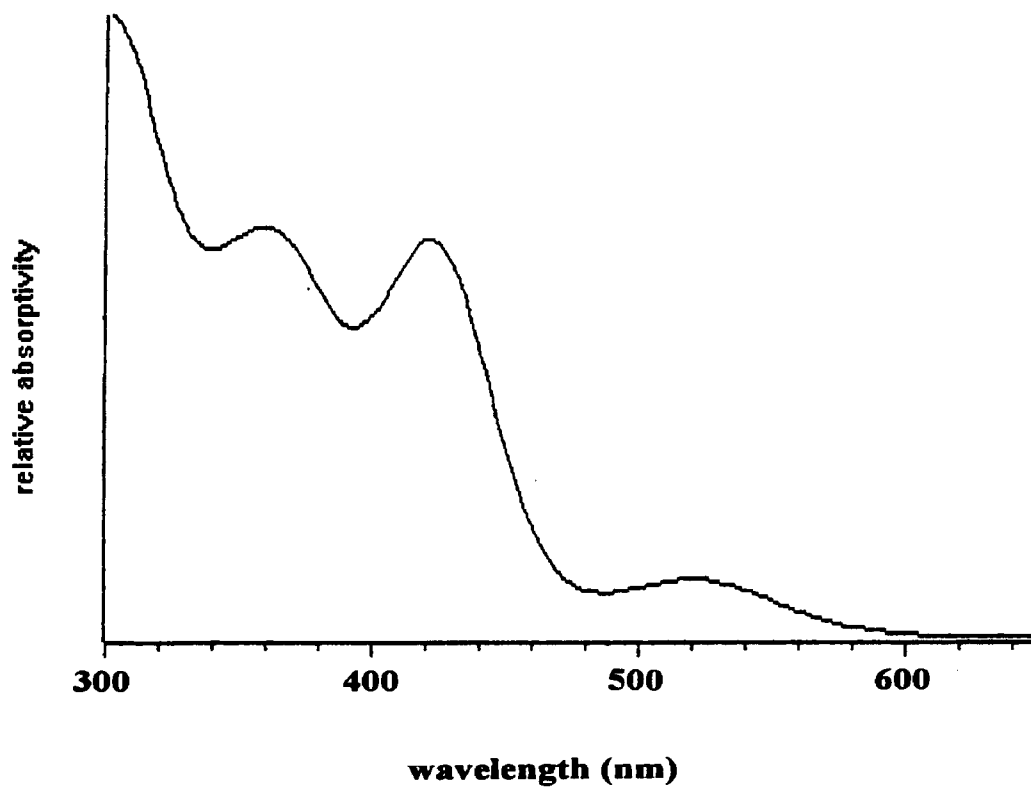


Fig. 3.15. The ^1H NMR spectrum (300 MHz) recorded at R.T. in CDCl_3 of the isolated catalytically inactive species.

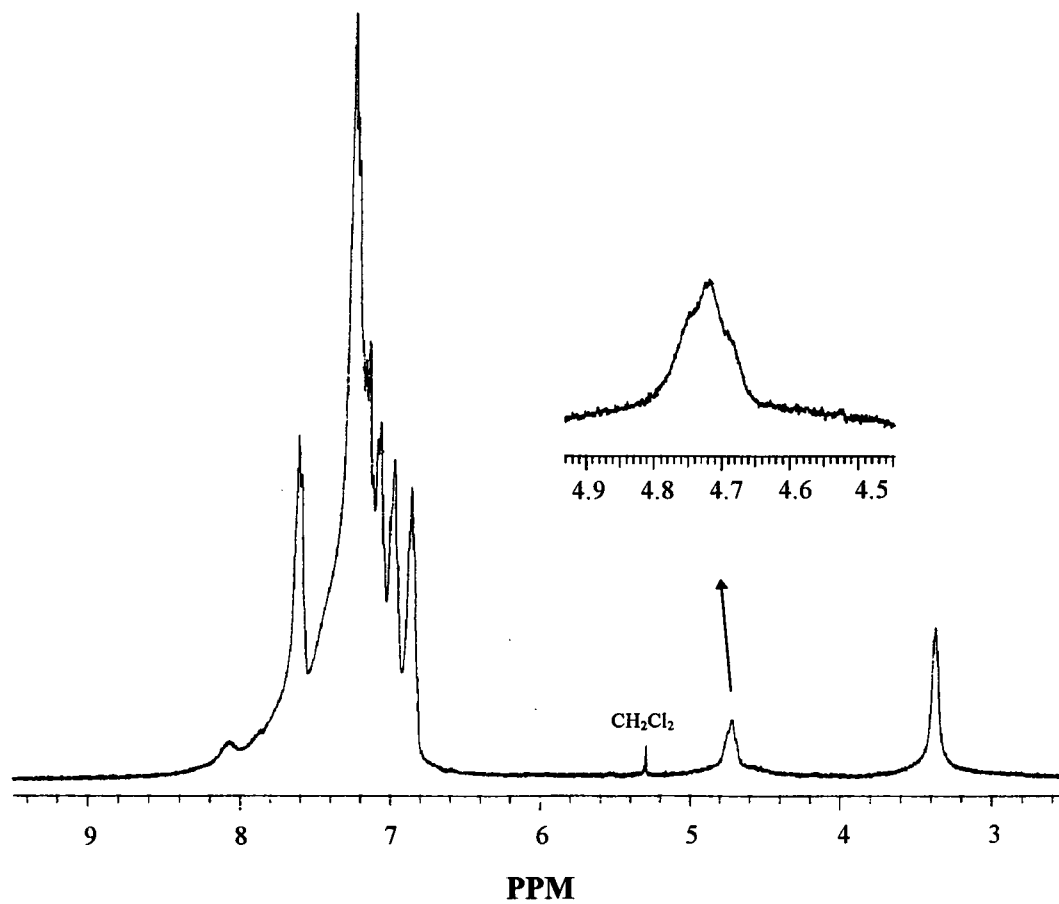


Fig. 3.16. The $^{31}\text{P}\{^1\text{H}\}$ NMR spectrum (121 MHz) recorded at R.T. in CDCl_3 of the isolated catalytically inactive species.

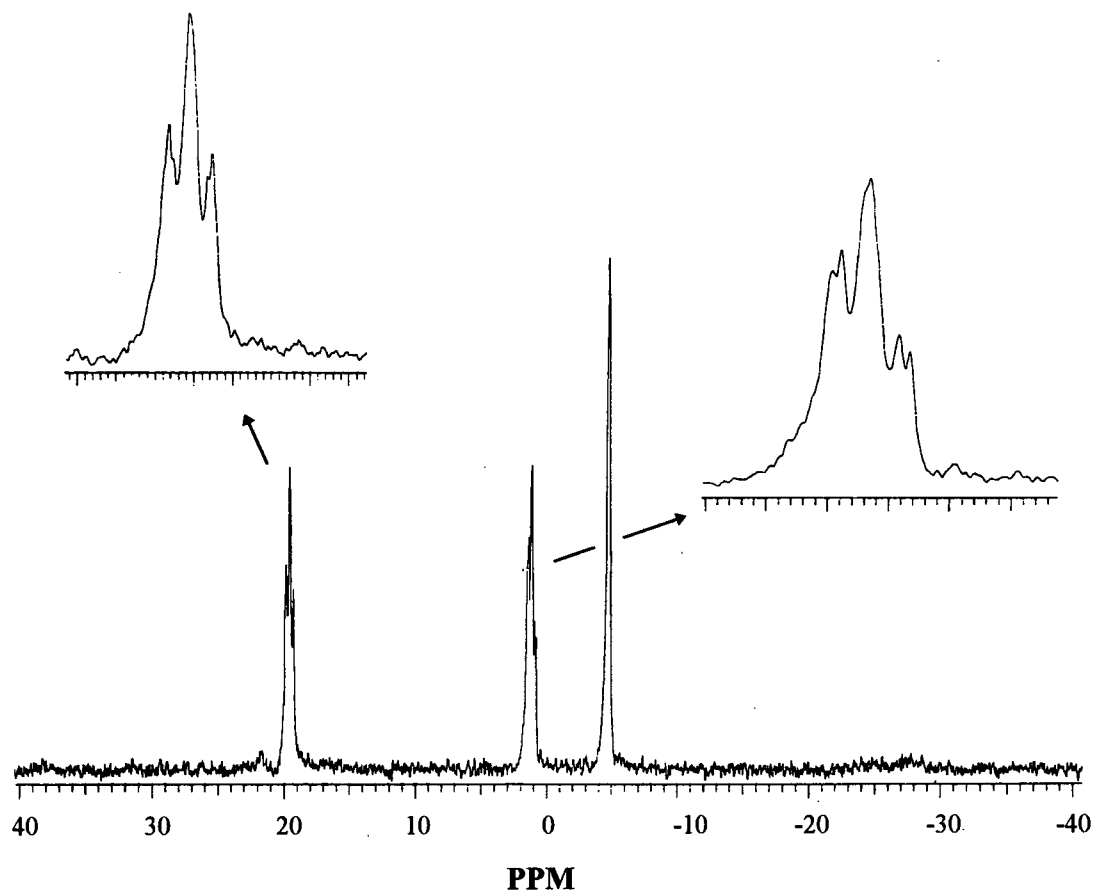
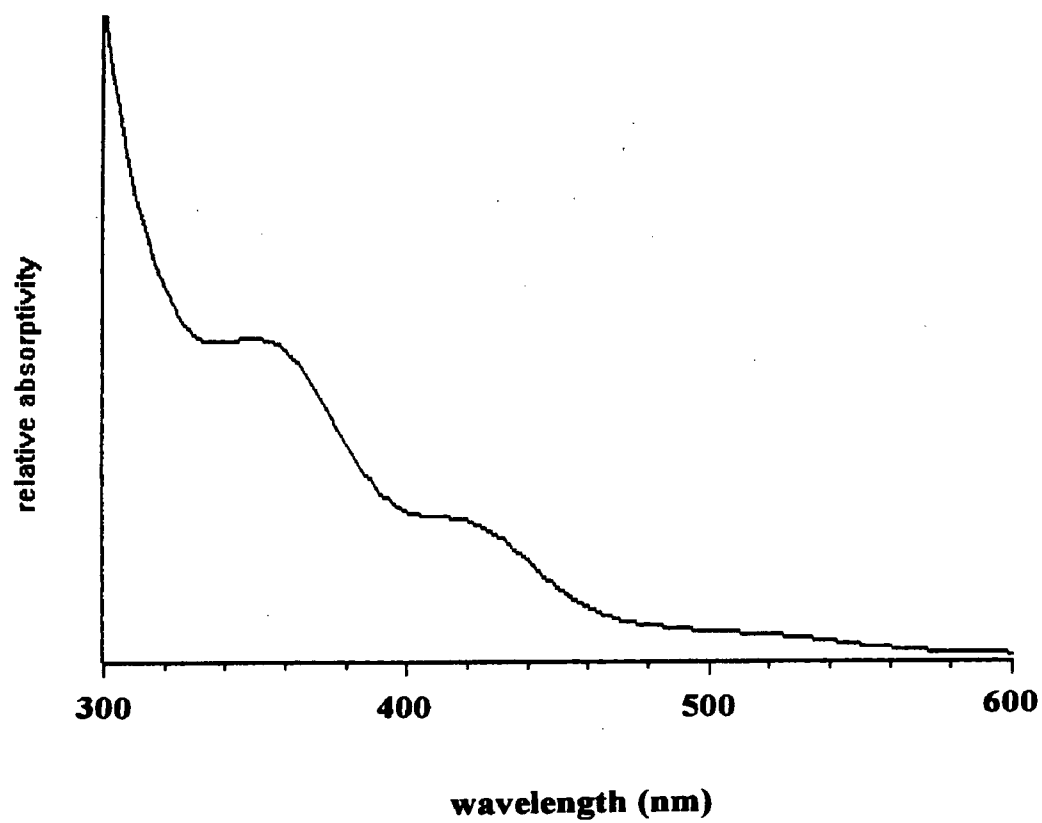
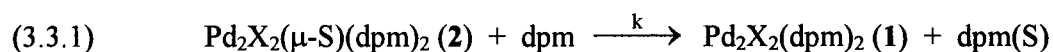


Fig. 3.17. The UV-vis spectrum obtained from catalytic studies of dpm + H₂S using **1b** in CHCl₃ after 24 h (Expt. 2).

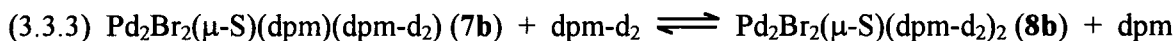
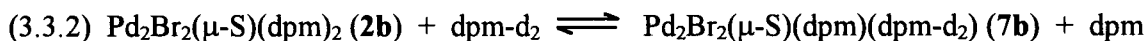


3.3 Discussion

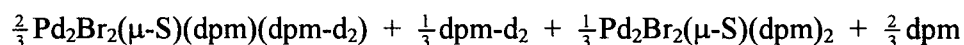
Kinetic results show that, at least for the chloride and bromide systems, the rate of the reconversion reaction (**2**→**1**) has a first-order dependence on both **2** and dpm. No intermediates were seen in low temperature NMR studies and this result, along with the observed isosbesticity in UV/vis spectroscopic studies, show that reaction 3.3.1 can be represented as shown, making no distinction in the identity of the dpm ligands:



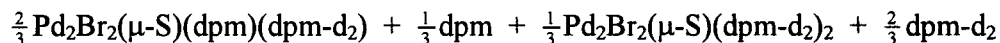
Labeling Experiments and Statistical Analysis. Labeling experiments with dpm-d₂ have demonstrated that diphosphine exchange takes place with both **2** and **1**, with rapid equilibria being established. The systems are complex because of the numerous rapidly established reactions occurring; the distribution of products, as a consequence, is considered to be statistical according to the stoichiometries of the reactants. For example, for the reaction of **2b** with dpm-d₂, prior to S-abstraction, the following rapid equilibria are established:



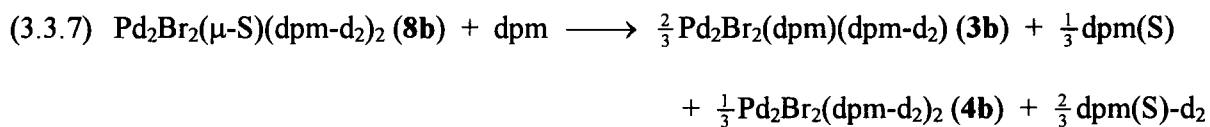
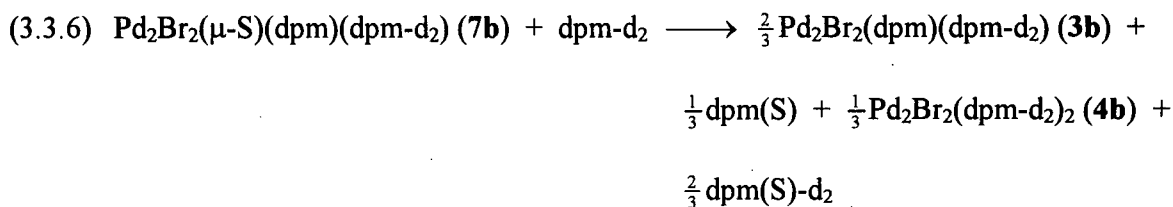
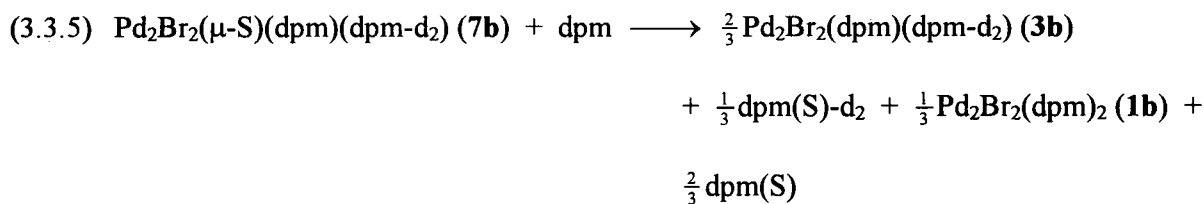
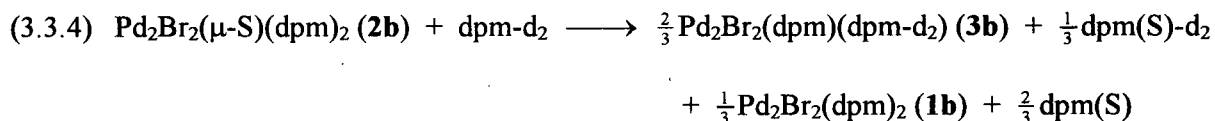
For equilibrium 3.3.2, for an initial 1:1 ratio of **2b** and dpm-d₂, the following distribution of species will be present at equilibrium:

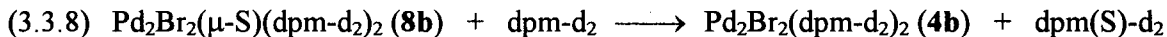


Similarly for equilibrium 3.3.3 at an initial 1:1 ratio of **7b** and dpm-d_2 , the distribution of species will be:

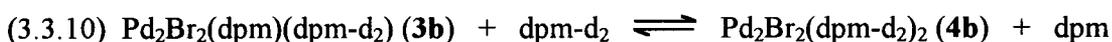


The S-abstraction then occurs via the slower reactions 3.3.1, and 3.3.4 - 3.3.8:

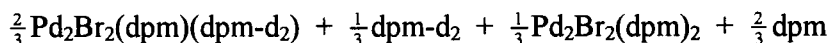




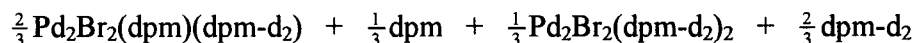
and then the rapid equilibria 3.3.9 and 3.3.10 are established within **1b** type species:



with the following distribution of species present at equilibrium for reaction 3.3.9 for an initial 1:1 ratio of **1b** and dpm-d_2 :

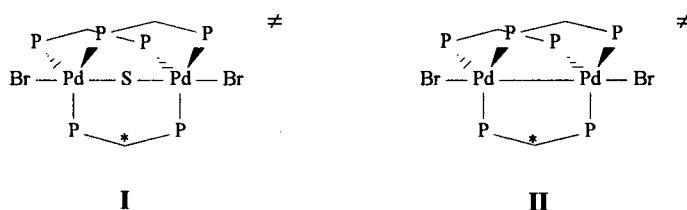


and similarly for equilibrium 3.3.10:



To contend with the many reactions, each set of rapid equilibria, 3.3.2 and 3.3.3, and 3.3.9 and 3.3.10, occurring essentially with equal probability, and to compare with the experimental results, a computer program (see Appendix III) was written and tested to simulate the reconversion reaction with dpm-d_2 ; the program displays the different statistical outcomes resulting from using different reactant ratios of **2b** and dpm-d_2 . The program is based on the premise that the diphosphine

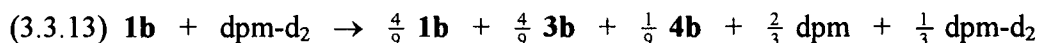
exchange and S-abstraction reactions proceed via transition states of a certain configuration where three diphosphines ligands are equivalent. To consider one possibility, **I** would be a reasonable and easily visualized transition state for the exchange and the S-abstraction reaction within **2b**, although the much slower S-abstraction (*vs.* exchange) requires, of course, differences in the transition states for the two processes; **II** seems reasonable for the exchange within **1b** type species. (**I** and **II** are chosen just as models to introduce the statistical nature of the reactions; more realistic chemical formulations are considered below).



(The phenyl groups are omitted for clarity; the * implies $-\text{CD}_2-$)

The simple overall second-order process for reaction 3.3.1 could proceed, for example, via **I**, containing three equivalent diphosphine bridges, with the reactant diphosphine initially coordinating at a vacant axial site of the square planar Pd centers within the A-frame complex **2b**. Product formation is then envisaged as sulfur abstraction by any one of the bridging phosphines with equal probability; this picture leads to statistical product distributions that correspond closely to those observed. For example, modeling of the S-abstraction within a 1:1 reaction between **2b** and dpm-d_2 gives the following predicted overall stoichiometry:

Thus, in a simulated ^1H NMR spectrum, the theoretical ratios of the integrated peak areas (CH_2 protons) of the Pd products to $\text{dpm}(\text{S})$, dpm to $\text{dpm}(\text{S})$, and dpm to the Pd products are, respectively, 1.2, 2.4, and 2.0 to 1. There is reasonable experimental agreement for the last two ratios, but a discrepancy is seen for the first; however, more importantly, the correct trends are observed: the integrated peak area of the Pd products is greater than that of $\text{dpm}(\text{S})$ but less than that of dpm . The $^{31}\text{P}\{^1\text{H}\}$ NMR spectrum (Fig. 3.8), on the other hand, clearly shows the approximately 1:1 ratio of $\text{dpm}(\text{S})$ to $\text{dpm}(\text{S})\text{-d}_2$, thus, providing stronger support for such transition states. Finally, in diphosphine exchange studies of type **1b** species with dpm-d_2 , the proposal of a transition state such as **II** is reasonable in that the expected statistical outcome of the exchange between **1b** and dpm-d_2 (1:1) is as follows:



and the theoretical ratio of the CH_2 protons of the Pd products to those of dpm is 2:1; experimentally, this ratio is found, thus providing very strong support for a transition state with equivalent diphosphines.

NMR spectra have shown that dpmMe also undergoes diphosphine exchange with **1b** at a 1:1 ratio, and that the exchange is slow, taking ~ 3 d for equilibrium to be established; the equilibrium favors the formation of $\text{Pd}_2\text{Br}_2(\text{dpm})(\text{dpmMe})$ (**5b**):





The equilibrium constants at room temperature are calculated from the spectral integration values (Fig. 3.12) and are found to be $K_1 \approx 6$ and $K_2 \approx 0.6$. NMR results show that **2b** does not undergo rapid diphosphine exchange with dpmMe as it does with dpm-d₂, but it is uncertain whether or not some slower exchange does occur on the timescale of the exchange of **1b** with dpmMe, which is also that of the S-abstraction by this phosphine. Nevertheless, whether or not exchange does happen, the resulting product distributions of the reaction between **2b** and dpmMe are expected to differ from that of the dpm case because the phosphines are different. An approximate 3 : 1 ratio of dpm(S) to dpmMe(S) is seen in the $^{31}\text{P}\{^1\text{H}\}$ NMR spectrum, complementing the result that greater amounts of **5b** and **6b** than **1b** are observed. The preliminary experimental findings suggest that, as with dpm, the S-abstraction reaction with dpmMe probably proceed via a transition state with close to equivalent diphosphine ligands.

Transition States and Intermediates. More insight into the nature of the transition state and intermediates is gleaned on consideration of reactivity of **2b** with other phosphines. Several other tertiary phosphines, including PPh_3 ,⁵ PPh_2Me ,⁵ and $\text{Ph}_2\text{P}(\text{CH}_2)_3\text{PPh}_2$ (dpp), were reacted with **2b**, but surprisingly no sulfur abstraction was observed, *i.e.* no phosphine sulfides were formed, and no **1b** was generated. With $\text{Ph}_2\text{P}(\text{CH}_2)_2\text{PPh}_2$ (dpe), however, small amounts of **1b** and dpm(S) were formed, but the major Pd species generated are as yet unidentified as the spectra are complicated; no dpe(S) was seen (Figs. 3.18 and 3.19). *In situ* treatment of **2b** with dpp (1:1) at R.T. resulted in a slow reaction (over ~3 d) and complex $^{31}\text{P}\{^1\text{H}\}$ and ^1H NMR spectra, attributable to an as yet uncharacterized species W (or mixture of species) (Fig. 3.20). (The formation of **1b** is

Fig. 3.18. The ^1H NMR spectrum (300 MHz) recorded at R.T. in CDCl_3 of **2b** on addition of 1 mole equivalent of dpe (72 h).

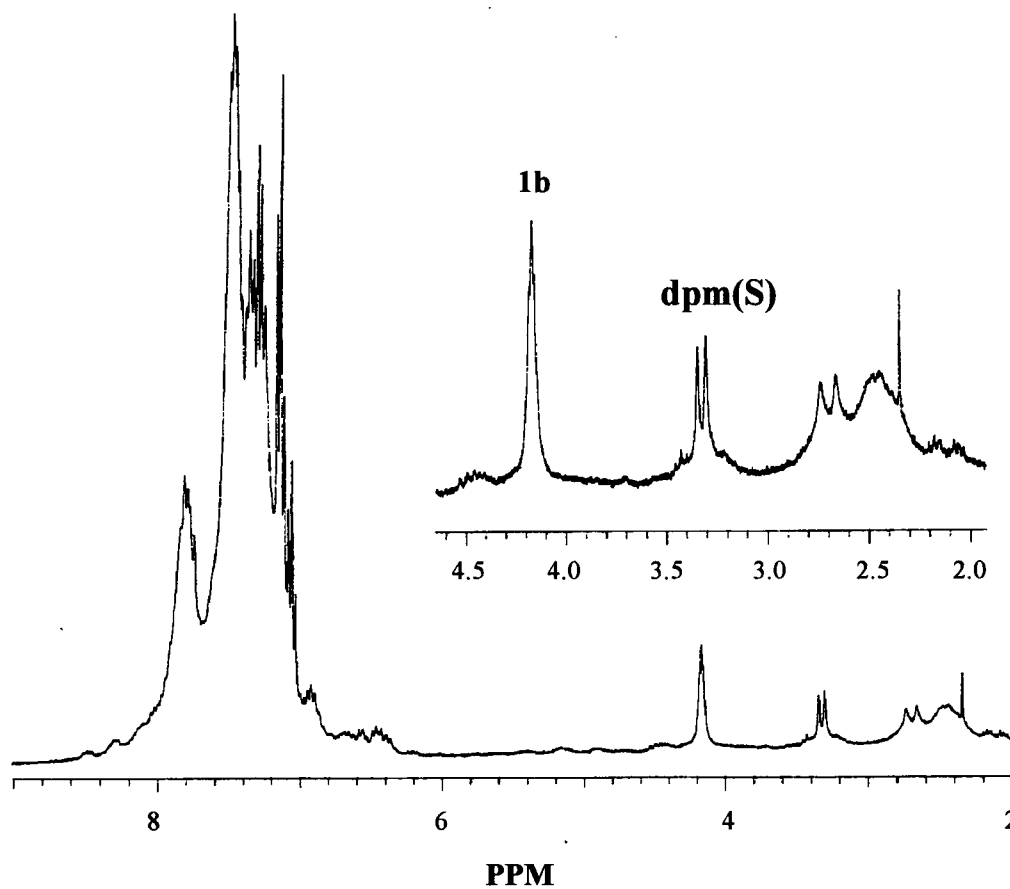


Fig. 3.19. The $^{31}\text{P}\{^1\text{H}\}$ NMR spectrum (121 MHz) recorded at R.T. in CDCl_3 of **2b** on addition of 1 mole equivalent of dpe (72 h).

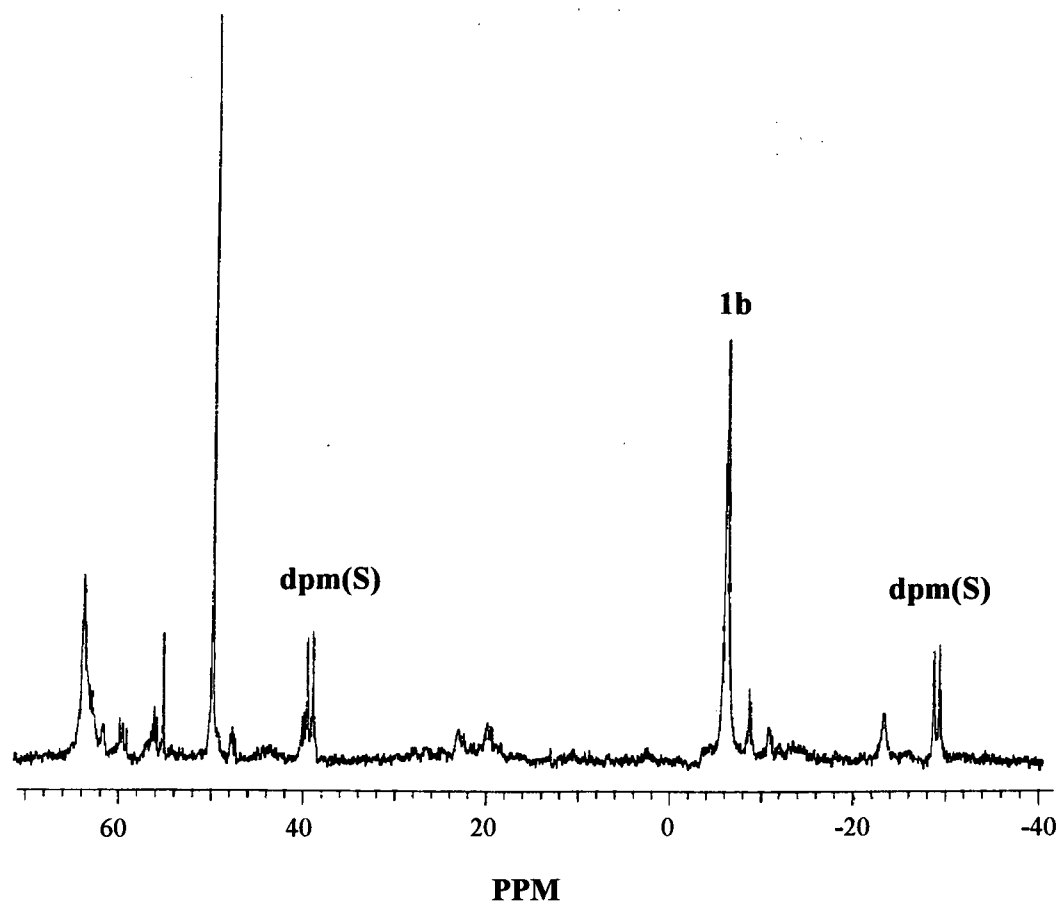
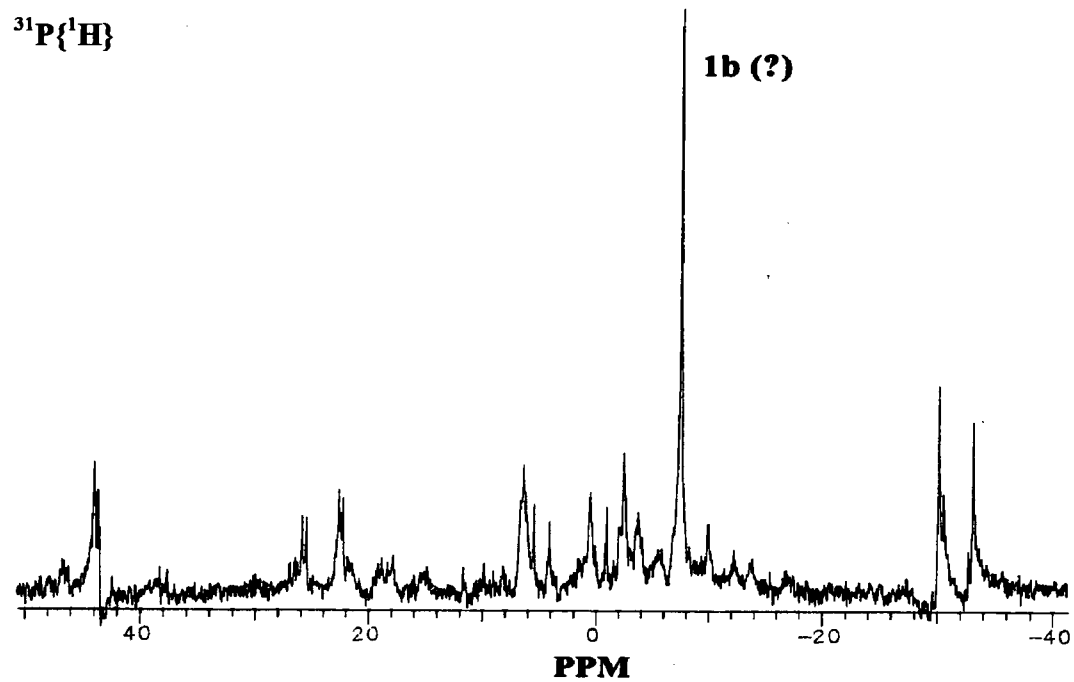
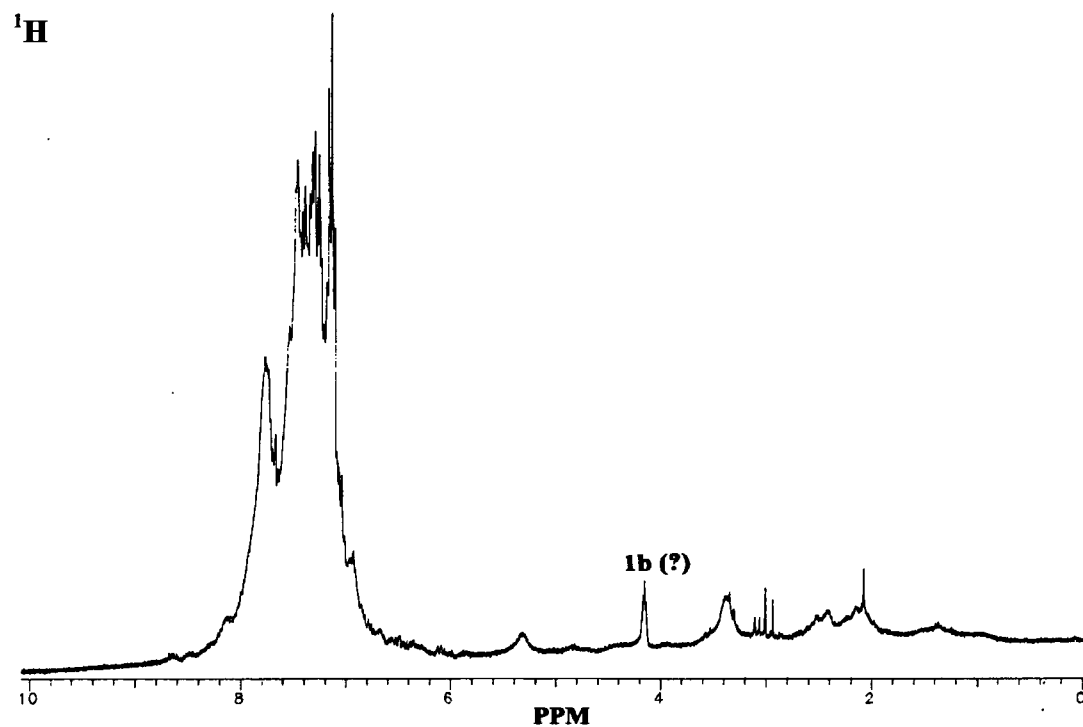


Fig. 3.20. The ^1H (300 MHz) and $^{31}\text{P}\{^1\text{H}\}$ (121 MHz) NMR spectra recorded at R.T. in CDCl_3 of **2b** on addition of 1 mole equivalent of dpp (72 h) (species W).



questionable because, although the ^1H NMR spectrum shows a prominent quintet at δ 4.2 attributable to **1b**, the corresponding singlet at δ -6.15 is not seen in the $^{31}\text{P}\{^1\text{H}\}$ NMR spectrum. Instead, a distinctive singlet at δ -7.20 is seen; accuracy in $^{31}\text{P}\{^1\text{H}\}$ NMR spectra is usually within ± 0.05 ppm.) Remarkably, treatment of this solution with ~ 2 mole equivalent of dpm resulted in slow but quantitative formation of dpm(S). The NMR spectra are still complex; however, addition of ~ 3 mole equivalent more of dpm yielded clean spectra with an AA'BB' pattern seen in the $^{31}\text{P}\{^1\text{H}\}$ attributed to dimeric Pd species with bridging dpm and dpp ligands (Figs. 3.21 and 3.22). The 'W solution' could contain species with monodentate, 'dangling' dpp, but no δ_{P} resonances in the region for free dpp ($\delta_{\text{P}} \sim -18$)⁹ were seen; di- or polynuclear species formed by bridging dpp seem plausible. The uniqueness of dpm (and dpmMe) in quantitatively abstracting the sulfur could be satisfyingly pictured via a transition state such as **I**; dpm (and presumably dpmMe) could generate this state in which the S atom is in a trigonal prismatic arrangement of P atoms, all of these being forced closer to the sulfur than the P atoms within **2b**. Presumably, if the longer chain dpp bridges the two Pd atoms, it does so in a configuration not very different to the ground state of **2b** and which gives no sulfur abstraction. There could be sufficient flexibility in dpm and dpmMe to generate transition states such as **II**, the supposed pathway for diphosphine ligand exchange with **1b**. This flexibility could exist for dpe, but presumably this ligand prefers to form a 5-membered chelate ring at a single Pd site; this could induce conversion of a μ -dpm to an η^1 -dpm with subsequent abstraction of S by the latter (see below).

It should be noted that complexes of the type $\text{Pd}_2\text{Cl}_4(\mu\text{-Bu}^t\text{P}(\text{CH}_2)_n\text{PBu}^t)_2$ ($n=7,10$) are known;¹⁰ these contain square-planar, d^8 Pd(II) moieties, and no metal-metal bond is involved. Species containing η^1 -diphosphine ligands are well documented,¹¹⁻¹³ including η^1 -dpm in complexes of the type $[\text{Pt}_2(\text{L})(\mu\text{-dpm})_2(\eta^1\text{-dpm})]^+$, L = alkyl or H.¹³ The possibility of dpm (and

Fig. 3.21. The ^1H NMR spectrum (300 MHz) recorded at R.T. in CDCl_3 of species W on addition of 3 mole equivalent of dpp (72 h).

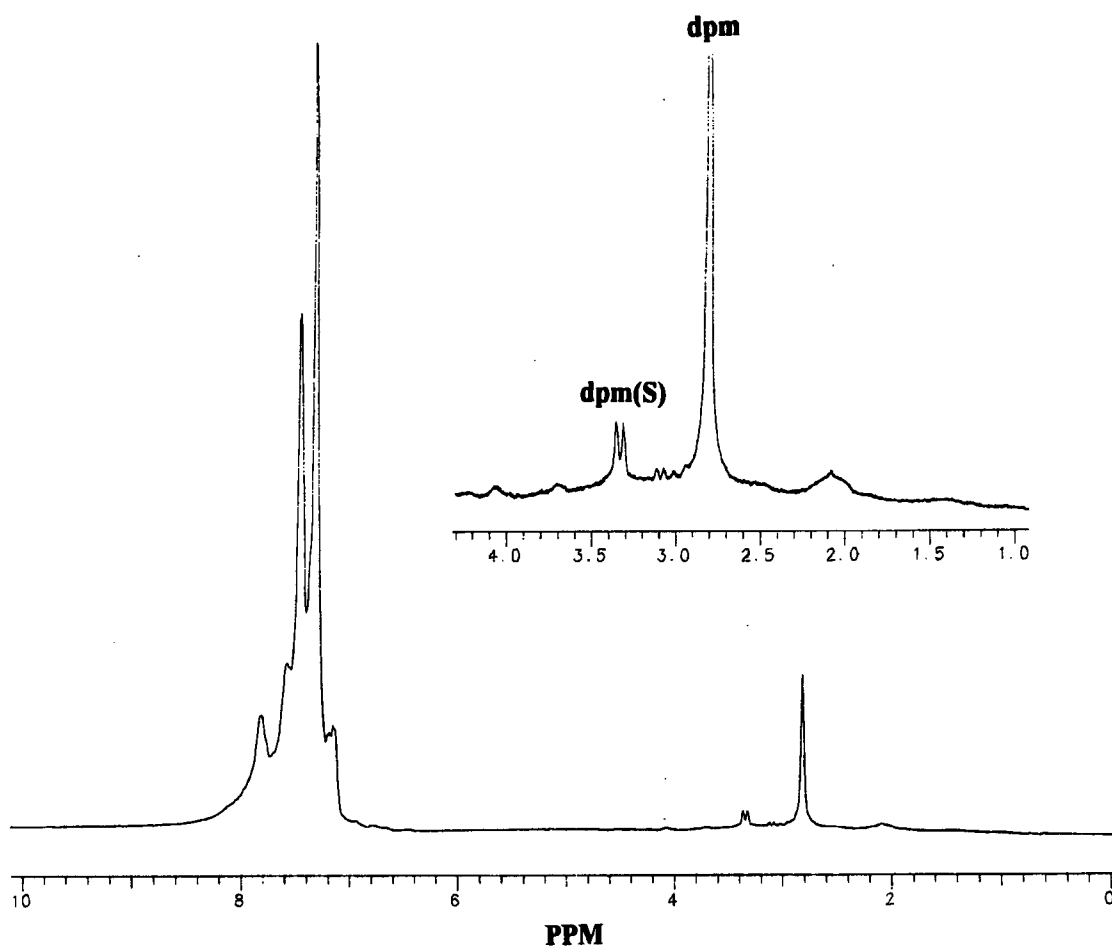
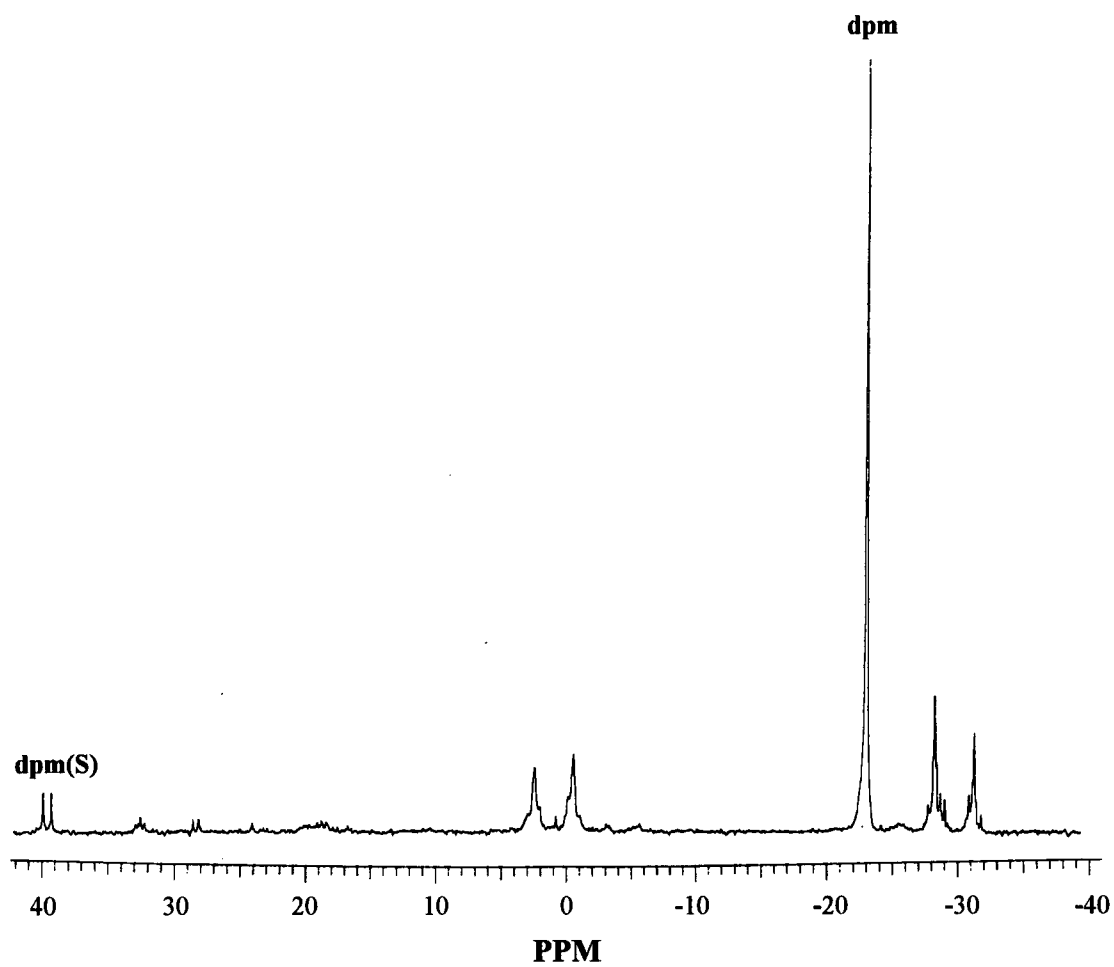
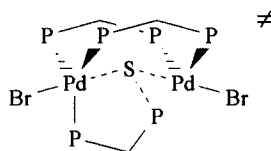


Fig. 3.22. The $^{31}\text{P}\{^1\text{H}\}$ NMR spectrum (121 MHz) recorded at R.T. in CDCl_3 of species W on addition of 3 mole equivalent of dpp (72 h).



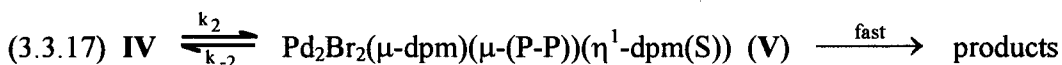
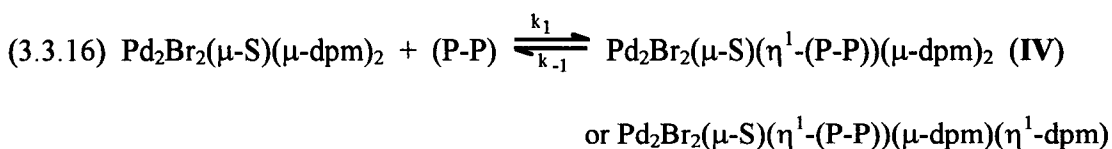
dpmMe) reacting with **2b** by binding in an η^1 -fashion at one Pd center with the 'free end' then abstracting sulfur seems the most obvious pathway for formation of the diphosphine monosulfide which would involve incipient formation of a 5-membered ring; the findings of the product distribution using dpm-d₂ and dpmMe could be accommodated via rapid fluxionality between the η^1 - and μ -diphosphines prior to S-abstraction. Such fluxionality offers the obvious pathway to diphosphine exchange with rapid on- and off-rates for the η^1 -ligands (see below). That other phosphines do not abstract the sulfur implies the requirement of a 5-membered ring for this process. Although **I** was offered as an easily visualized transition state for the S-abstraction, a more realistic chemical picture is shown in **III**; if the diphosphines are indistinguishable (essentially so if dpm-d₂ is used as the entering diphosphine), the transition state is effectively one of 3-fold degeneracy and the "averaged" transition state picture approximates to that shown in **I**.



III

Consideration of the various findings reveals that dpm reacts relatively rapidly with **2b** (to give exchange and S-abstraction) and with **1b** (exchange), and yet dpmMe and dpp (and dpm(S) (see below)) react more slowly. Presumably, all the chelating phosphines must first react at a metal center as η^1 -nucleophiles; the difference in apparent rates cannot be due to electronic or steric effects (indeed, regarding the latter, dpm might be more 'encumbered' than dpp), and thus

some rationale is needed. The series of steps shown in eqs. 3.3.16 and 3.3.17 can account for the observations:



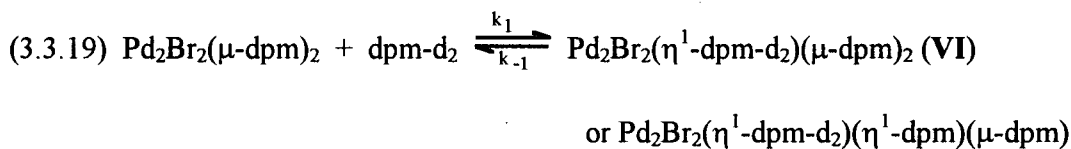
III would be a reasonable transition state en route from **IV** to **V**. It seems reasonable that for all the P-P systems, the k_1 values are comparable; the findings require that for dpm or dpm-d₂, the k_1/k_{-1} equilibrium is established rapidly but the k_2 step can compete sufficiently with the k_{-1} step to result in S-abstraction, *i.e.* the bite of the dpm ligand makes it highly favorable for forming the 5-membered $\text{Pd-S-P-CH}_2\text{-P}$ ring. Diphosphine exchange with dpm (or dpm-d₂) within type **2b** species is pictured as proceeding via reaction 3.3.16, with an originally coordinated diphosphine having the same probability of leaving as the incoming diphosphine. The S-abstraction occurs via eq. 3.3.17 as discussed above; all three dpm ligands within **IV** (because of the rapidly established k_1/k_{-1} equilibrium) have an equal probability of abstracting the S. The discussion necessitates that species **IV** and **V** are genuine intermediates. A steady state treatment for **IV** gives the following rate expression for S-abstraction:

$$(3.3.18) \quad \text{Rate} = \frac{k_1 k_2}{k_{-1} + k_2} [\mathbf{2b}] [\text{P-P}]$$

consistent with our experimental findings, *e.g.* with $k_{Br} = k_1 k_2 (k_{-1} + k_2)^{-1}$. For the other phosphines, the k_2 step cannot compete effectively with the k_{-1} step, and the k_{-1} value for these phosphines must also be greater than the k_1 value for dpm/dpm-d₂ because the exchange (*e.g.* with dpmMe) is established much more slowly. The rate law for S-abstraction using other phosphines thus approximates to $(k_1/k_{-1})k_2[2b][P-P]$.

The experimental findings show that the dpm/dpm-d₂ exchange for **2b** at R.T. is established in less than seconds for solutions typically $\sim 10^{-2}$ M in both complex and phosphine, while the S-abstraction occurs with a rate constant of $\sim 0.03 \text{ M}^{-1}\text{s}^{-1}$. Qualitatively, typical, somewhat arbitrary values that would satisfy the above analysis are $k_1 \sim 10^3 \text{ M}^{-1}\text{s}^{-1}$, $k_{-1} \sim 10^2 \text{ s}^{-1}$, and $k_2 \sim 10^{-3} \text{ s}^{-1}$; the S-abstraction via **IV** is $\sim 10^{-5}$ times less probable than loss of the η^1 -dpm.

Within type **1b** species, the rapid exchange involving dpm-d₂ can be accounted for by an equilibrium (eq. 3.3.19) analogous to that giving the exchange within type **2b** species, loss of η^1 -dpm from **VI** giving the exchange process.



The transition state for this exchange could be akin to that shown in **II** but with one Pd-P bond at each metal being stretched towards an η^1 -(P-P) configuration en route to **VI**. This picture satisfactorily explains the observations for dpm-d₂. The slow exchange of dpmMe with **1b** (as with **2b**) implies that loss of an η^1 -dpmMe from a species such as **VI** (as with **IV**) occurs much more readily than loss of η^1 -dpm, possibly because of steric factors.

Of note also is that *in situ* treatment of **2b** with dpm(S) (1:1) in CDCl₃ yields over several days an uncharacterized species Y (Fig. 3.23) that on subsequent reaction with dpm (1:1) slowly generates **1b** and two mole equivalents of dpm(S). [Note: the NMR spectra of isolated Y have the same characteristics as those of *in situ* generated Y.] Y could be a species such as Pd₂Br₂(μ-S)(μ-dpm)₂(η¹-dpm(S)) or Pd₂Br₂(μ-S)(η¹-dpm)(μ-dpm)(η¹-dpm(S)), while subsequent reaction with dpm could slowly replace the coordinated dpm(S) and lead then to an intermediate such as **IV** with P-P = dpm. No reaction occurs between **2b** and dpm(S)₂. Support for species Y being a single compound comes from elemental and mass spectrometric analyses of an isolated species. The FAB mass spectrum (Fig. 3.24) shows a prominent mass ion peak at 1429 m/z attributed to a species with loss of two bromine atoms, e.g. Pd₂(μ-S)(μ-dpm)₂(η¹-dpm(S))⁺, while elemental analysis shows excellent agreement between theoretical and experimental values.

Attempts to grow crystals of species Y (via solvent layering techniques) for structural information were unsuccessful due to facile formation of oils even at low temperatures (-40 °C). Of interest, it was found that **2a** and **2c** react with dpm(S) in an analogous way giving species X and Z, respectively; the ¹H and ³¹P{¹H} NMR spectra are exactly the same as those seen in the reaction of **2b** with dpm(S) (Fig. 3.23). [Note: attempts to analyze the complex NMR spectra using, for example, a spin simulation program, were unsuccessful.] Furthermore, the UV-vis spectra of all three species (isolated from their respective reactions) show only one absorption maximum at 464 nm in the range 300 to 600 nm (Fig. 3.25). These results suggest that species X, Y, and Z may be ionic in nature; further studies to elucidate the structures are required.

Of interest, we find that **2c**, Pd₂I₂(μ-S)(dpm)₂, reacts with I₂ in CDCl₃ at R.T. according to eq. 3.3.20 (see Chapter 4); the NMR data (Table 3.1) of the Pd₂ intermediate correspond well to

Fig. 3.23. The ^1H (300 MHz) and $^{31}\text{P}\{^1\text{H}\}$ (121 MHz) NMR spectra recorded at R.T. in CDCl_3 of **2b** on addition of 1 mole equivalent of $\text{dpm}(\text{S})$ (72 h) (species Y).

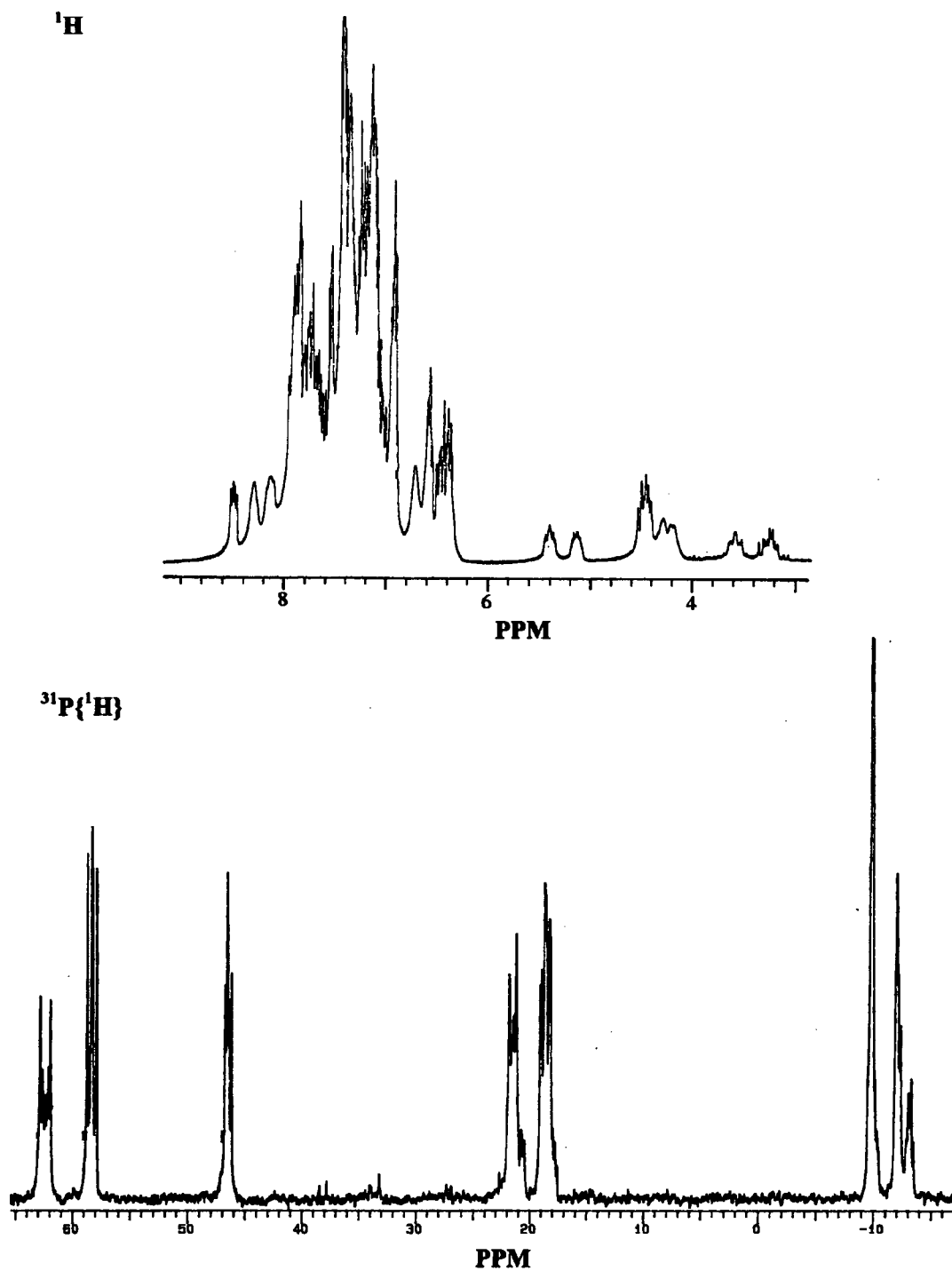


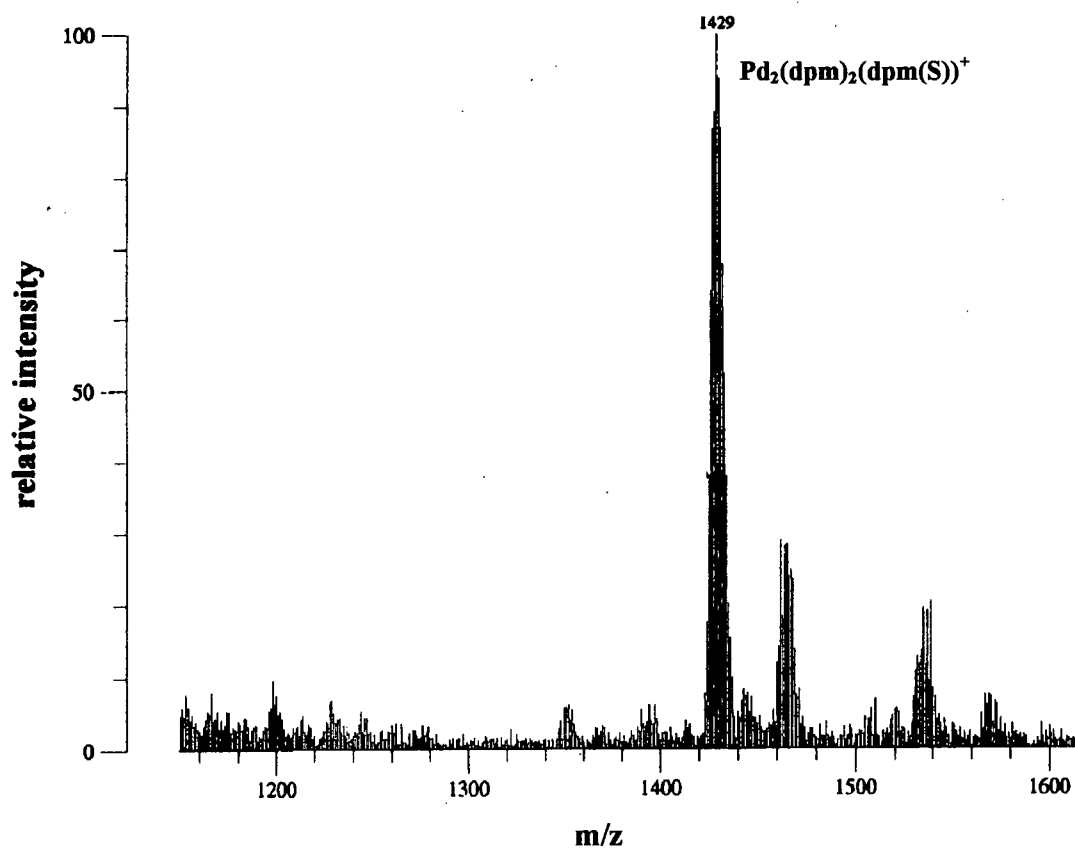
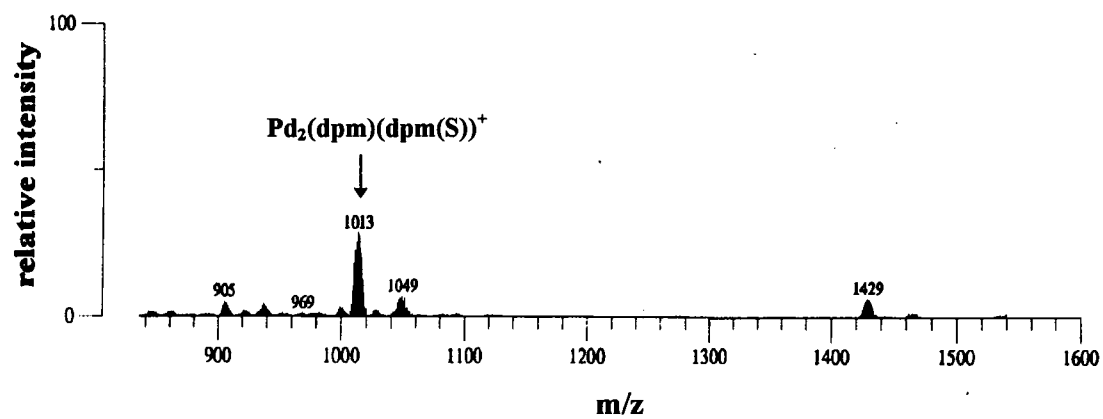
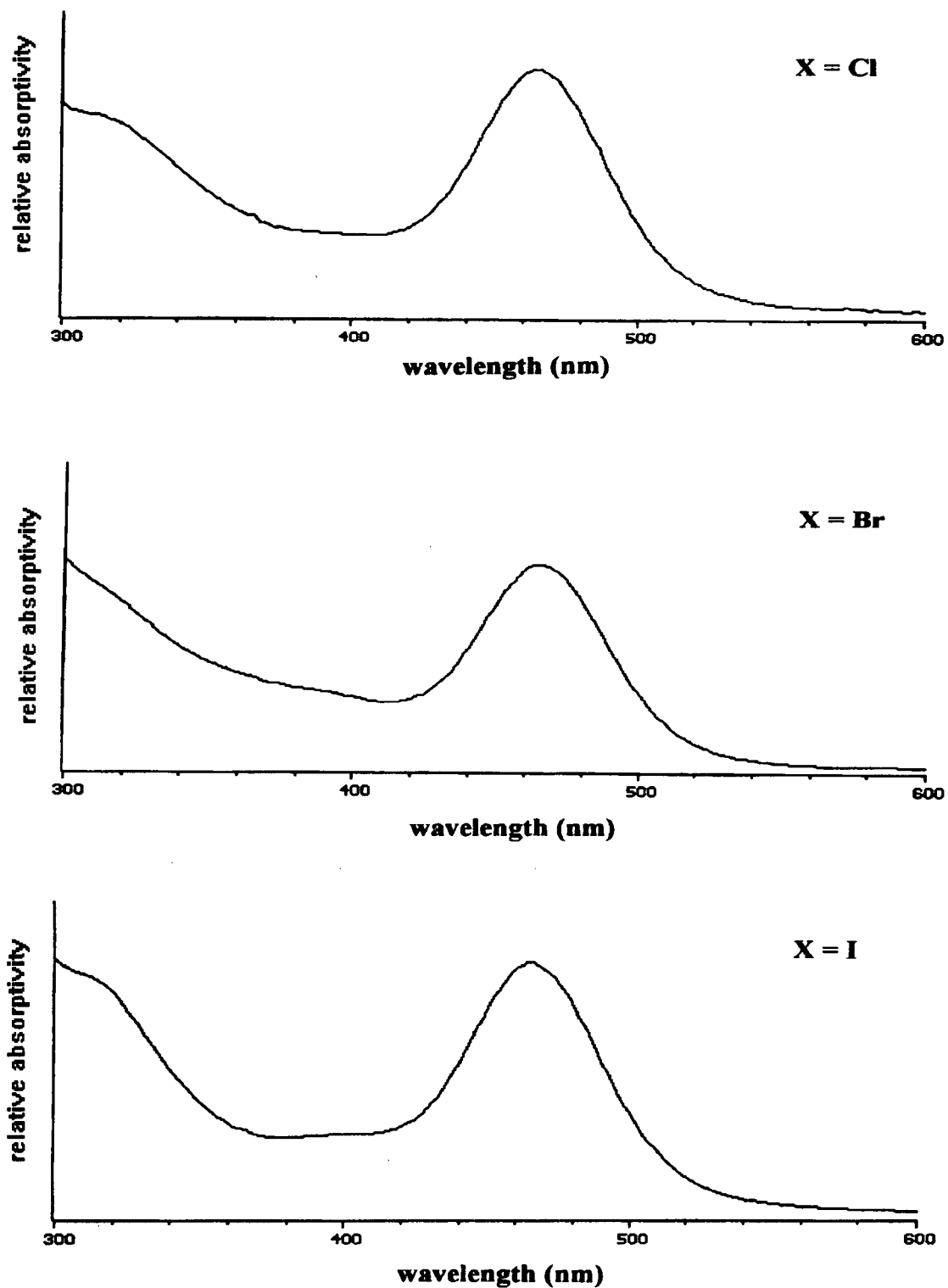
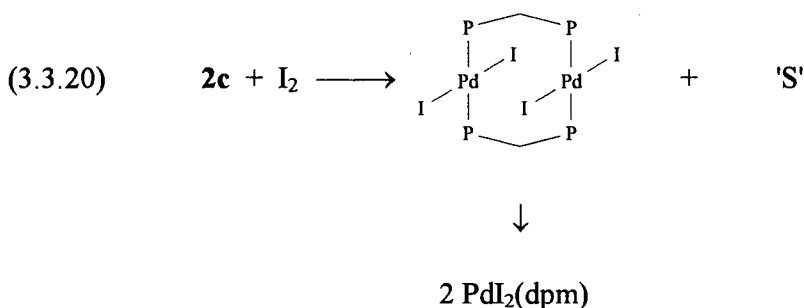
Fig. 3.24. Mass spectrum (FAB, matrix = thioglycerol + CHCl_3) obtained of species Y.

Fig. 3.25. The UV-vis spectra of species isolated from reactions of $\text{Pd}_2\text{X}_2(\mu\text{-S})(\text{dpm})_2$ (**2**) with 1 mole equivalent of $\text{dpm}(\text{S})$ in CHCl_3 ($\text{X} = \text{Cl}$ (species X), Br (species Y), I (species Z)).



those of the tetraiodo species, characterized previously by Hunt and Balch¹⁴ in a study of the reaction of I_2 with $Pd_2I_2(dpm)_2$ (**1c**).



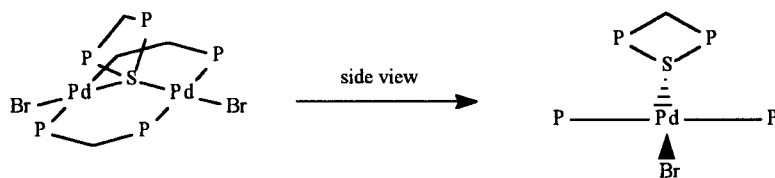
That transannular addition can occur across an A-frame complex, reaction 3.3.20, albeit with destruction of the A-frame, offers some support for reactivity via a transition state such as **I** or **III**, the diphosphine addition resembling in the broadest sense the addition of two iodide ligands. Thus, in eq. 3.3.20 the bridged sulfide is formally oxidized by I_2 to elemental sulfur, with the electron transfer presumably proceeding from the (μ -S) through the metal atoms toward the attacking I_2 reagent, and a transition state akin to **I** or **III** but with the P-P replaced by I-I. Indeed, the conversion of the **2** to **1** species could, in principle, involve incipient formation of a S-atom (*cf.* eq. 3.3.20) that is then scavenged as a phosphine monosulfide.

The reactivity trend for reaction 3.3.1, $X = Cl > Br > I$, can be rationalized in terms of transition state **I**. The activation parameters for the chloro and bromo systems reveal that the dominant factor governing reactivity is the entropy term (-127 and -144 for the chloro and bromo systems, respectively). A large, unfavorable ΔS^\ddagger value is reasonable for the addition of the dpm ligand to **2b** to generate **I** or **III** and this is expected to be more difficult when the auxiliary ligand is the bulkier bromide (*vs.* chloride), because of interactions with the phenyl groups. For the iodo

system, ΔS^\ddagger is predicted to be still more negative. The essentially constant ΔH^\ddagger value for the chloro and bromo systems tends to imply that the energy required to form a transition state such as **I** or **III** is similar in the two systems; any contribution from the *trans*-effect of the halides (Br > Cl)¹⁵ must be small.

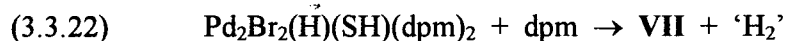
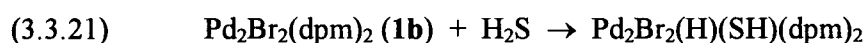
Catalytic Conversion of H₂S. As noted in the Introduction, the demonstration of the conversion of **1** to **2**, and the reconversion using dpm, constitutes a catalytic cycle for reaction 3.1.3 which could be catalyzed by complex **1** or **2**. Some experiments were carried out confirming the existence of the catalysis. Difficulties, however, were encountered in these studies due to one (or several) catalytically inactive species being formed under conditions of high [dpm]. In almost all studies using **1b** as the catalyst, little or no product formation was seen (Table 3.3, expts. 1, 3 to 9). When **2b** was used, dpm(S) was formed in ~5% yield (stoichiometric); however, no H₂ was detected (expt. 10); the monosulfide is likely formed during initial reaction of **2b** with dpm (*i.e.* the reconversion reaction). Indeed, with [**2b**] = 2.6×10^{-3} M and [dpm] = 0.052 M, in principle, the concentration of dpm(S) formed via the reconversion reaction is $\sim 2.6 \times 10^{-3}$ M which corresponds to 5% dpm conversion. Product formation was seen in one study (expt. 2) where H₂ was detected and dpm(S) was found to be formed in ~47% yield. Here, [dpm] = 3.6×10^{-3} M initially, and 1.7×10^{-3} M was converted to dpm(S) after 24 h; [**1b**] = 3.5×10^{-4} M and hence, true catalysis is observed. Turn over numbers based on this study is calculated to be ~ 5 d⁻¹. (Previous studies in CH₂Cl₂ have noted that a 10^{-3} M solution of **1b** at R.T. under 1 atm H₂S converted 0.02 M dpm completely to dpm(S) in a few hours; total turn over numbers were ~ 20 .¹⁹) The presence of H₂ was unequivocally established by corresponding NMR experiments; here, H₂ and dpm(S) were formed in ~40 and 50% yields, respectively, after 3 d (why there is a difference in reaction

timescales is unclear, although there was a difference of $\sim 5^\circ$ in the room temperature recorded (23 vs. 18 $^\circ\text{C}$). UV-vis spectrophotometry was used for a qualitative assessment of the nature of the species in solution; as confirmed by NMR spectroscopy, the UV-vis spectrum (Fig. 3.17) is characteristic of a system containing both **1b** and **2b** (cf. Fig. 3.1). The catalytically inactive species was seen in previous studies by $^{31}\text{P}\{^1\text{H}\}$ NMR and was thought to be the active species during the catalysis.⁵ In the present thesis work, the inactive species was isolated and characterized using UV-vis spectrophotometry and NMR spectroscopy. The UV-vis spectrum shows three well-defined absorption maxima (Fig. 3.14); NMR spectra are not complex (Figs. 3.15 and 3.16). In the ^1H NMR spectrum, two resonances, a triplet and a singlet, are seen in the range δ 3 to 5 with an integration ratio of 1:2 and are indicative of protons of CH_2 groups. Furthermore, the phenyl protons integrate for 10 H with respect to both the triplet and singlet resonances. In the $^{31}\text{P}\{^1\text{H}\}$ NMR spectrum, a singlet and a series of resonances resembling an AA'BB' pattern are observed in a 1:2 integration ratio. The implication is that multiple numbers of diphosphine ligands are present, possibly multiples of three. A complex which satisfactorily meets these requirements could be a dimeric Pd complex bridged also by the sulfur atom of a $\text{dpm}(\text{S})$, species **VII**:



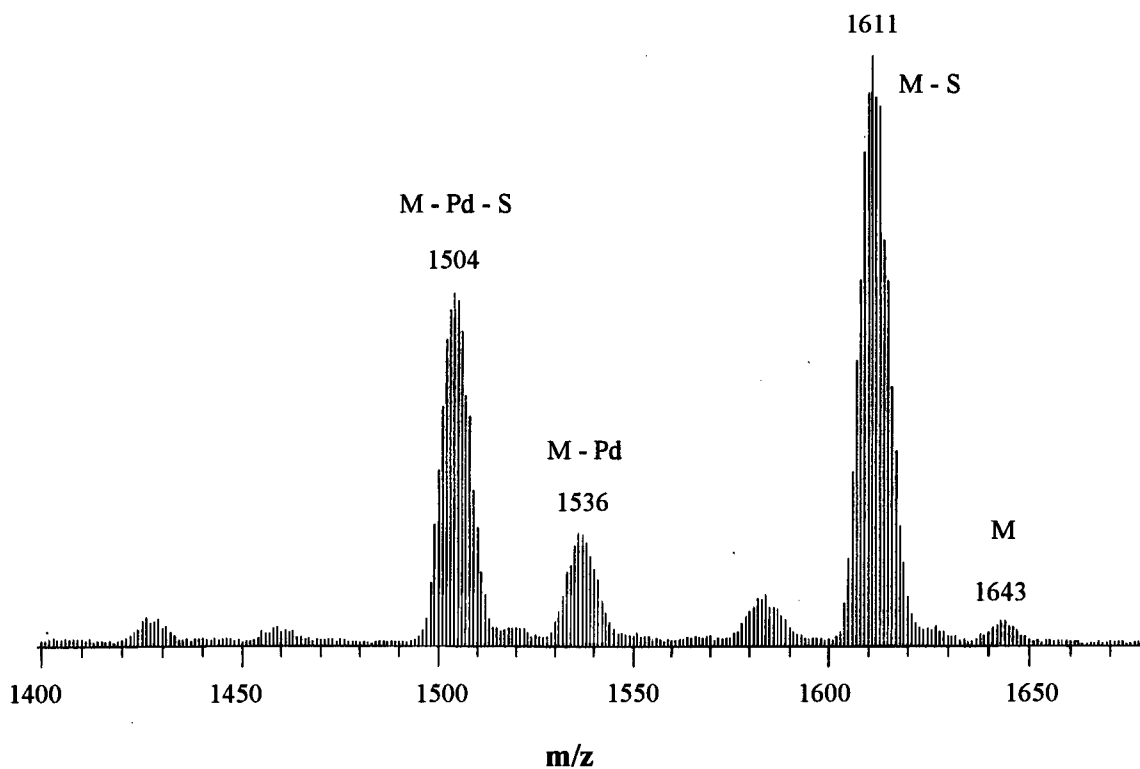
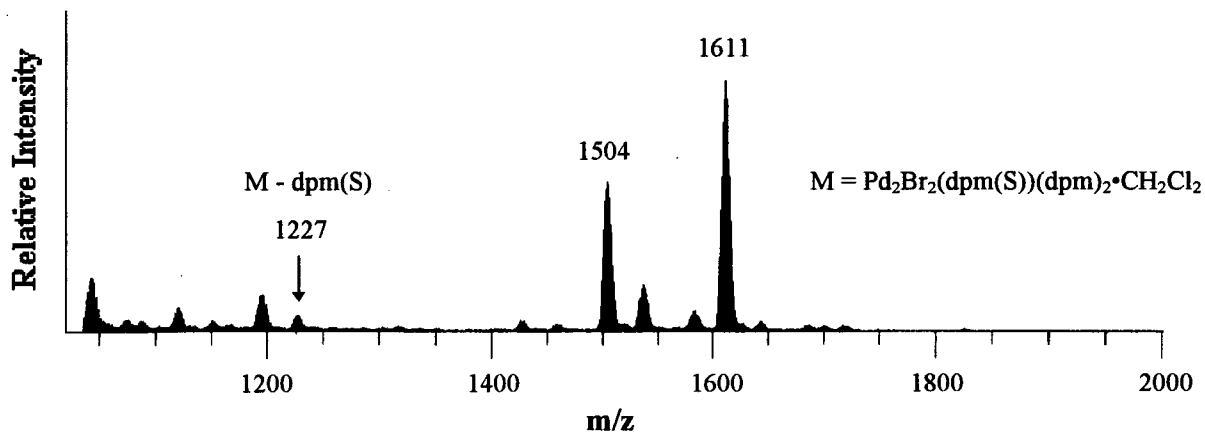
(the phenyl groups are omitted for clarity)

Elemental analysis for a species formulated as **VII** shows excellent agreement between theoretical and experimental results. Crystals of this species were grown (via solvent layering techniques) but the poor crystallinity precluded an X-ray crystallographic study; however, mass spectrometric analysis indicates a parent ion peak at 1643 m/z (Fig. 3.26) corresponding to a species that can be formulated as **VII** with 1 CH₂Cl₂ solvate molecule. Because the catalytically inactive Pd species is invariably produced under conditions where the [dpm] is high, formation of **VII** perhaps proceeds via reaction of dpm with the hydrido(mercapto) intermediate² formed from **1b** with H₂S. For example,



H₂ is included in eq. 3.3.22 by virtue of mass balance; failure to detect it may be due to its low concentration. Although further studies are warranted, the conclusion is that catalysis can proceed simply via coupling of reactions 3.1.1 and 3.1.2.

Fig. 3.26. Mass spectrum (FAB, matrix = thioglycerol + CHCl_3) of the catalytically inactive species VII with the region from 1400 to 1650 m/z expanded.



3.4 Experimental section

The materials used, synthetic procedures for the ligands and complexes, and instrumentation used for ^{31}P and ^1H NMR, and UV/vis spectra have been described in Chapter 2. The dpm (Aldrich), 1,2-bis(diphenylphosphino)ethane (dpe) (Strem), 1,3-bis(diphenylphosphino)propane (dpp) (Strem), and sulfur (Aldrich) were pure and were used as received. Dpm(S), dpmMe, and the complexes $\text{PdCl}_2(\text{PhCN})_2$, $\text{Pd}_2(\text{dba})_3\cdot\text{CHCl}_3$, **1a** - **1c**, and **2a** - **2c** were synthesized using published methods as outlined in Chapter 2. All experiments were performed under N_2 unless otherwise specified.

3.4.1 Preparation of dpm-d₂

Lithium diphenylphosphide, LiPPh_2 , (22.6 g, 0.118 mol, in 250 mL THF)¹⁶ was slowly added dropwise to a solution of CD_2Cl_2 (5 g, 0.059 mol, in 50 mL THF) over a period of ~2 h. The solvent of the resulting yellow mixture was rotovaped off before 200 mL of CH_2Cl_2 was added to re-dissolve the crude product. The CH_2Cl_2 solution was washed with 4 x 100 mL of H_2O , and then dried over CaSO_4 . Removal of the solvent gave a light yellow solid which was dissolved in 50 mL of a CH_2Cl_2 -hexane (1:2) mixture and chromatographed through a column (8 x 40 cm) of silica gel with the same solvent as eluent. The first ~250 mL of eluate was discarded and then the eluate was collected as 4 x 20 mL fractions and analyzed using TLC. The required product was the last substance to emerge; ~500 mL of eluate was then collected. The solvents were removed to give a crystalline white solid; yield ~5 g (22%). The compound was characterized using ^1H and $^{31}\text{P}\{^1\text{H}\}$

NMR spectroscopy (Table 3.1). Anal. Calcd for $C_{25}H_{20}D_2P_2$: C, 77.72; H, 5.74. Found: C, 77.70; H, 5.77.

3.4.2 Preparation of dpm(S)-d₂

Dpm-d₂ (100 mg, 0.259 mmol) and S₈ (8.30 mg, 0.032 mmol) were dissolved in hot hexanes (~10 mL) and the solution was refluxed overnight. The solution was then cooled down to room temperature (R.T.; ~20°C) and white crystals subsequently formed (within several hours). The solid was collected and identified as dpm(S)-d₂ using NMR spectroscopy (Table 3.1); yield ~50 mg (46%). Anal. Calcd for $C_{25}H_{20}D_2P_2S$: C, 71.76; H, 5.30. Found: C, 71.71; H, 5.38.

3.4.3 Preparation of dpmMe(S)

DpmMe (100 mg, 0.251 mmol) and S₈ (8.00 mg, 0.031 mmol) were dissolved in hot ethanol (~5 mL) and the solution was refluxed briefly (~10 min). The solution was then cooled to R.T. and white crystals subsequently formed (within 1 h). The solvent was removed leaving a white solid above an oily, white film. The solid was gently scraped off, dried *in vacuo*, and identified as dpmMe(S) using NMR spectroscopy (Table 3.1); yield ~30 mg (28%). Anal. Calcd for $C_{26}H_{24}P_2S$: C, 72.54; H, 5.62. Found: C, 71.89; H, 5.54.

3.4.4 Preparation of dpm(S)₂, dpe(S), dpe(S)₂, dpp(S), and dpp(S)₂

Syntheses of these diphosphine mono- and di-sulfides were carried out by refluxing the appropriate diphosphine with sulfur in hexanes. For example, disulfides were prepared by refluxing dpm (100 mg, 0.26 mmol), dpe (100 mg, 0.25 mmol), or dpp (100 mg, 0.24 mmol) and sulfur (16 mg, 0.52 mmol) in hexanes (10 mL) for 2 h. Monosulfides were similarly prepared using 8 mg (0.025 mmol) sulfur; a mixture of products (mono- and di-sulfides) including unreacted diphosphine was typically seen. Removal of solvent by rotary evaporation gave white solids which were dried *in vacuo* prior to thin-layered chromatographic analyses (eluant: 1:2 = CH₂Cl₂ : hexanes by volume) and NMR spectroscopic analyses in CDCl₃. Dpm(S)₂: ¹H NMR (20 °C, CDCl₃): δ 7.0 - 8.0 m (20H, Ph), δ 3.98 t (2H, CH₂, J_{PH} = 14.0 Hz); ³¹P{¹H} NMR (20 °C, CDCl₃): δ 35.3 s. Dpe: ¹H NMR (20 °C, CDCl₃): δ 7.0 - 8.0 m (20H, Ph), δ 2.09 m (4H, CH₂); ³¹P{¹H} NMR (20 °C, CDCl₃): δ -12.6 s. Dpe(S): ¹H NMR (20 °C, CDCl₃): δ 7.0 - 8.0 m (20H, Ph), δ 2.47, 2.28 m (4H, CH₂); ³¹P{¹H} NMR (20 °C, CDCl₃): δ 44.3, -12.9 AB pattern (J_{PP} = 47.5 Hz). Dpe(S)₂: ¹H NMR (20 °C, CDCl₃): δ 7.0 - 8.0 m (20H, Ph), δ 2.71 p d (4H, CH₂); ³¹P{¹H} NMR (20 °C, CDCl₃): δ 44.3 s. Dpp: ¹H NMR (20 °C, CDCl₃): δ 7.0 - 8.0 m (20H, Ph), δ 2.18 m (4H, CH₂), δ 1.59 m (2H, CH₂); ³¹P{¹H} NMR (20 °C, CDCl₃): δ -17.5 s. Dpp(S): ¹H NMR (20 °C, CDCl₃): δ 7.0 - 8.0 m (20H, Ph), δ 2.56 m (2H, CH₂), δ 1.99 m (2H, CH₂), δ 1.76 m (2H, CH₂); ³¹P{¹H} NMR (20 °C, CDCl₃): δ 41.8 s, δ -18.9 s. Dpp(S)₂: ¹H NMR (20 °C, CDCl₃): δ 7.0 - 8.0 m (20H, Ph), δ 2.56 m (4H, CH₂), δ 2.00 m (2H, CH₂); ³¹P{¹H} NMR (20 °C, CDCl₃): δ 41.8 s.

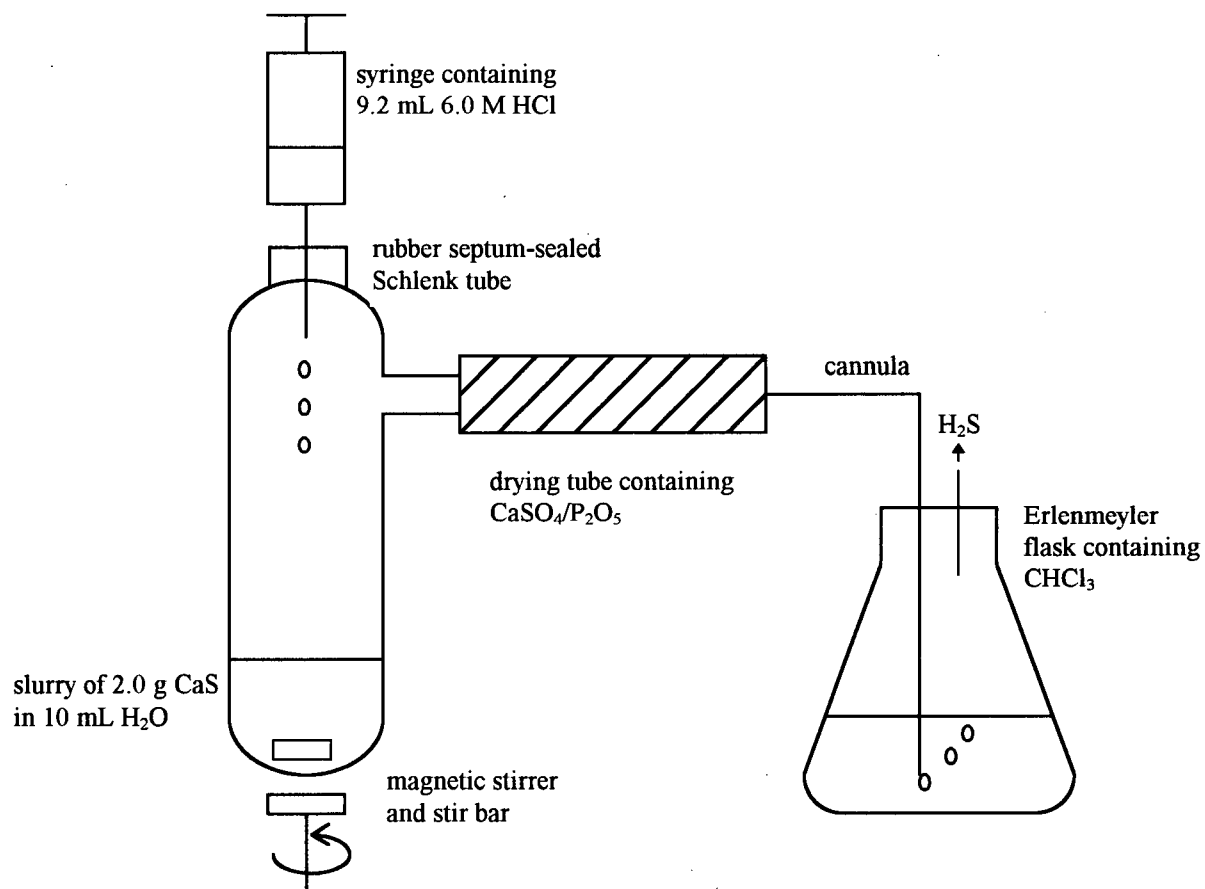
3.4.5 Preparation of H₂S

H₂S was separately prepared for studies of reaction 3.1.3 (see Section 3.4.10). The experimental setup is schematically shown in Fig. 3.27. To a stirred slurry of CaS (2.0 g, 0.028 mol) in distilled H₂O (10 mL) was added aq. HCl (6.0 M, 9.2 mL, 0.056 mol) dropwise via syringe over a period of 10 min. The resulting, instantly formed H₂S was dried using CaSO₄/P₂O₅ prior to bubbling through CHCl₃.

3.4.6 Preparation of Pd₂Br₂(dpm-d₂)₂·2H₂O (4b)

PdCl₂(PhCN)₂ (0.41 g, 1.01 mmol), Pd₂(dba)₃·CHCl₃ (0.55 g, 0.53 mmol), and dpm-d₂ (0.82 g, 2.1 mmol) were refluxed in CDCl₃ (50 mL) for 30 min. After being cooled, the resulting red solution was filtered to remove any insoluble materials, and the filtrate reduced in volume to ~10 mL. The yellow-orange product, which precipitated after the addition of Et₂O (25 mL), was then filtered, washed with acetone (2 x 10 mL) to remove any Pd(II) monomer, and dried *in vacuo*. The yield of the product, Pd₂Cl₂(dpm-d₂)₂ is ~1.0 g (90%). Some of this complex (0.25 g, 0.24 mmol) was re-dissolved in ~10 mL of CDCl₃ and a solution of NaBr (0.25 g, 2.4 mmol) in aqueous methanol added (~5 mL CH₃OD : ~0.5 mL D₂O). The resulting solution was filtered, and concentrated under vacuum until red crystals formed. Et₂O (40 mL) was added to complete the precipitation. The solid was filtered and quickly washed with aqueous methanol (2 x 10 mL) and Et₂O (2 x 10 mL) and then dried *in vacuo*; yield 0.26 g (96%). **4b** was characterized using NMR spectroscopy (Table 3.1). Anal. Calcd for C₅₀H₄₀Br₂D₄P₄Pd₂·2H₂O: C, 50.84; H, 4.06. Found: C, 50.75; H, 3.83. (The presence of H₂O was evidenced by ¹H NMR).

Fig. 3.27. Schematic diagram showing experimental setup for preparation of H_2S from reaction of CaS with aq. HCl .



3.4.7 Preparation of Pd₂Br₂(μ-S)(dpm-d₂)₂ (**8b**)

Pd₂Cl₂(dpm-d₂)₂ (0.50 g, 0.48 mmol) (see above) was dissolved in CDCl₃ (50 mL) and H₂S gas was bubbled through the solution for 20 min at R.T.; the colour changed from orange-red to brown with accompanying precipitation of a brown solid that was completed by gradual addition of Et₂O (50 mL). The product, Pd₂Cl₂(μ-S)(dpm-d₂)₂, was filtered, washed successively with acetone (2 x 10 mL), and Et₂O (10 mL), and then dried *in vacuo*; yield 0.50 g (97%). The solid was re-dissolved in CDCl₃ (50 mL) and a solution of NaBr (0.5 g, ~ 5 mmol) in aqueous methanol (10 mL CH₃OD : 1 mL D₂O) was added. The resulting mixture was filtered, and concentrated under vacuum until brown crystals formed. Et₂O (30 mL) was added to complete the precipitation. The solid was filtered, washed with aqueous methanol (2 x 10 mL) and Et₂O (2 x 10 mL), and then dried *in vacuo*; yield 0.52 g (95%). **8b** was characterized by NMR spectroscopy (Table 3.1). Anal. Calcd for C₅₀H₄₀Br₂D₄P₄Pd₂S: C, 50.95; H, 3.77. Found: C, 50.27; H, 3.80.

3.4.8 Kinetic measurements

The kinetics of the reconversion reaction (**2** → **1**) in CHCl₃ (for X = Cl, Br, I) were monitored spectrophotometrically in a thermostated Perkin-Elmer 552A instrument using quartz cells of path lengths of 1.0 cm fitted with a rubber septum. A 2.00 mL solution of dpm of appropriate concentration was placed in the cell and thermostated at the required temperature (20 - 35 °C); the complex **2** was then injected as a solution (0.125 mL). The cell was shaken to ensure complete mixing prior to monitoring optical density changes at some appropriate, fixed

wavelength. The concentration of **2** ranged from $(0.81 - 13.0) \times 10^{-5}$ M, and that of dpm from $(6.5 - 26.1) \times 10^{-3}$ M; thus pseudo-first-order conditions were maintained and standard log(absorbance difference) vs. time plots gave excellent linearity for at least 2.5 - 3 half-lives, from which the pseudo-first-order rate constants, k_{obs} , were readily evaluated.

3.4.9 Mechanistic studies

a) NMR-scale. Variable temperature and equilibrium studies were performed on the NMR-scale by reacting complexes with appropriate amounts of diphosphine. Thus, for example, **1b** (10 mg, 0.009 mmol) or **2b** (10 mg, 0.0085 mmol) was reacted at R.T. in CDCl_3 or CD_2Cl_2 (0.5 mL) with dpm- d_2 or dpmMe in either a 1:1 or a 1:5 mole ratio (in 0.1 mL solution). The samples were analyzed using ^1H and $^{31}\text{P}\{^1\text{H}\}$ NMR spectroscopy immediately and after periods of time up to 72 h. Under low temperature conditions, accurately weighed out samples of **2a**, **2b**, or **2c** were dissolved in the appropriate solvent (~ 0.5 mL) in a septum-sealed NMR tube which was placed in a dry ice/acetone slush bath (-78 °C). A 0.1 mL solution of dpm (5 mol. equiv. excess) was then injected and the shaken sample was analyzed immediately and after periods of time up to 72 h. The temperature was then raised in 20° increments to a final 20 °C and the spectra recorded at each temperature.

b) Synthetic-scale. The bromide **2b** (100 mg, 0.085 mmol) was reacted with either dpm- d_2 (32.9 mg, 0.085 mmol) or dpmMe (34.0 mg, 0.085 mmol) in 20 mL of CH_2Cl_2 or CHCl_3 , the reaction being monitored by thin-layer chromatography and/or UV-vis spectroscopy. Employing Schlenk techniques, the experiments were conducted on a scale such that products could be isolated in

sufficient amounts for analyses of both the Pd complexes and the dpm compounds. Upon completion of the synthesis (approx. 2 h), the solution was reduced in volume to ~ 5 mL before 20 mL of Et₂O was added to precipitate the palladium product(s). The filtrate was passed through a column of silica to remove all traces of metal compounds with the eluate collected. The solvent was rotovaped off to give a colourless oil, which was dissolved in minimal hot ethanol; cooling in a dry ice/acetone bath induced precipitation of a white solid, the diphosphine monosulfide. The ethanol solvent was slowly removed under vacuum and at low temperatures to avoid reformation of the oil. All products were dried *in vacuo* prior to analyses using ¹H and ³¹P{¹H} NMR spectroscopy in CDCl₃.

c) Reaction of 2b with dpe, dpp, dpm(S), and dpm(S)₂. Reaction of **2b** with other diphosphines was explored for possible sulfur abstraction. In a typical experiment, **2b** (10 mg, 0.0085 mmol) and the appropriate amount of diphosphine (*i.e.* 3.4 mg dpe, 3.5 mg dpp, 3.5 mg dpm(S), 3.8 mg dpm(S)₂; all diphosphines 0.0085 mmol) were placed in an NMR tube fitted with a PTFE J. Young valve, and CDCl₃ (~0.5 mL) was vacuum transferred in. All samples were analyzed using NMR spectroscopy immediately and after periods of time up to 72 h. For reactions with dpm(S), **2a** (9.2 mg, 0.0085 mmol) and **2c** (11 mg, 0.0085 mmol) were also used with analyses being carried out analogously.

In the above reactions with dpm(S), the solvent was removed by rotary evaporation (after completion of the reaction as evidenced by the disappearance of **2** and dpm(S) signals from NMR measurements) and the resulting residue was analyzed using NMR and UV-vis spectroscopy and mass spectrometry. Microanalysis was performed for the residue isolated from the **2b** + dpm(S) reaction. Calcd for Pd₂Br₂(μ-S)(dpm)₂•dpm(S), C₇₅H₆₆Br₂P₆S₂Pd₂: C, 56.66; H, 4.18. Found: C,

56.93; H, 4.40. Attempts to grow crystals of this species for X-ray crystallographic analysis, for example by diffusion of hexanes (10 mL) or Et₂O (10 mL) into a 6 mL CH₂Cl₂ solution of 10 mg of the complex at R.T. or -40 °C, were unsuccessful.

3.4.10 Catalytic conversion of H₂S

The catalysis of reaction 3.1.3 was briefly studied at R.T. using **1b** and **2b**. The conditions used are outlined in Table 3.3; the concentrations of H₂S used were determined from knowledge of Henry's constant (1.3 M/atm)¹⁷ and vapour pressure data (see Appendix IV).¹⁸ In a typical experiment, appropriate amounts of **1b** or **2b** and dpm were placed in a rubber septum sealed Schlenk tube (volume = 37.0 or 165.0 mL) and CHCl₃ was vacuum transferred using liquid N₂. The reaction mixture was thawed before H₂S was introduced. For studies at 1 atm, [H₂S] = 1.0 M. Low concentrations of H₂S were achieved by injecting the appropriate volume (see Appendix IV for sample calculations). Concentrations of **1b** ranged from (8.76 - 263) × 10⁻⁵ M, that of **2b**, 2.56 × 10⁻³ M, and those of dpm (3.64 - 52.0) × 10⁻³ M. The reaction was allowed to proceed for periods of 5, 24, or 72 h before the contents were analysed. The head space was analysed for hydrogen using gas chromatography. UV-vis spectra were obtained for qualitative assessment of Pd species. For reaction mixtures with high catalyst concentrations (*i.e.* > 8.76 × 10⁻⁴ M), Et₂O (20 mL) was added to precipitate the Pd species which were then filtered, washed with Et₂O (2 × 10 mL), dried *in vacuo*, and subsequently analysed using NMR and UV-vis spectroscopy and microanalysis. (Calcd for Pd₂Br₂(dpm)₂(μ-dpm(S)) • 2CH₂Cl₂, C₇₅H₆₆Br₂P₆SPd₂ • 2CH₂Cl₂: C, 53.53; H, 4.08. Found: C, 53.53; H, 4.00 (the presence of CH₂Cl₂ was evidenced by ¹H NMR spectroscopy). Crystals of this species, obtained by diffusion of hexanes (10 mL) into a 6 mL

CH₂Cl₂ solution of 10 mg of the complex at R.T., were subjected to X-ray analysis but the structure could not be determined.) The filtrate was passed through a column of silica to remove all traces of metal compounds with the eluate collected. The solvent was removed by rotary evaporation giving a white solid and/or colourless oil; analyses of these phosphine products were done using NMR spectroscopy. Percent conversion of dpm to dpm(S) was determined by comparison of the respective integrated areas.

A single *in situ* NMR experiment was carried out using an NMR tube (volume = 3.7 mL) fitted with a PTFE J. Young valve. Complex **1b** (0.0014 g, 0.0012 mmol) and dpm (0.0049 g, 0.013 mmol) were placed in the NMR tube and CDCl₃ (3.5 mL) was vacuum transferred using liquid N₂. H₂S was subsequently introduced to achieve a total pressure of 1 atm. The mixture was then left at R.T. for periods of time up to 72 h before being analyzed using NMR spectroscopy.

3.5 References for Chapter 3

- (1) Lee, C-L.; Besenyi, G.; James, B. R.; Nelson, D. A.; Lilga, M. A. *J. Chem. Soc., Chem. Commun.* **1985**, 1175.
- (2) Barnabas, A. F.; Sallin, D.; James, B. R. *Can. J. Chem.* **1989**, *64*, 2009.
- (3) Besenyi, G.; Lee, C-L.; Gulinski, J.; Rettig, S. J.; James, B. R.; Nelson, D. A.; Lilga, M. A. *Inorg. Chem.* **1987**, *26*, 3622.
- (4) Wong, T.Y.H.; Barnabas, A.F.; Sallin, D.; James, B.R. *Inorg. Chem.* **1995**, *34*, 2278.
- (5) Barnabas, A. F., M. Sc. Dissertation, University of British Columbia, Vancouver, 1989.
- (6) (a) Grim, S. O.; Mitchell, J. D. *Syn. React. Inorg. Metal-Org. Chem.* **1974**, *4*, 221. (b) Grim, S.O.; Walton, E. D. *Inorg. Chem.* **1980**, *19*, 1982.
- (7) Lyke, S. E.; Lilga, M. A.; Ozanich, R. M.; Nelson, D. A.; James, B. R.; Lee, C-L. *Ind. Eng. Chem. Prod. Res. Dev.* **1986**, *25*, 517.
- (8) Lee, C-L.; Yang, Y. P.; Rettig, S. J.; James, B. R.; Nelson, D. A.; Lilga, M. A. *Organometallics* **1986**, *5*, 2220.
- (9) James, B. R.; Mahajan, D. *Can. J. Chem.* **1979**, *57*, 180.
- (10) (a) Al-Salem, N. A.; Empall, H. D.; Markham, R.; Shaw, B. L.; Weeks, B. J. *Chem. Soc., Dalton Trans.* **1979**, 1972. (b) Shaw, B. L. In *Catalytic Aspects of Metal Phosphine Complexes, Adv. in Chem. Series*: Alyea, C., Meek, D.W., Eds.; Am. Chem. Soc.: Washington, 1982; Vol. 196, Ch. 6.
- (11) Ball, R. G.; Domazetis, G.; Dolphin, D.; James, B. R.; Trotter, J. *Inorg. Chem.* **1981**, *20*, 1556.
- (12) Keiter, R. L.; Rheingold, A. L.; Hamerski, J. J.; Castle, C. K. *Organometallics* **1983**, *2*, 1635.
- (13) (a) Brown, M. P.; Yavari, A.; Hill, R. H.; Puddephatt, R. J. *J. Chem. Soc., Dalton Trans.* **1985**, 2421. (b) Azam, K. A.; Brown, M. P.; Hill, R. H.; Puddephatt, R. J.; Yavari, A. *Organometallics* **1984**, *3*, 697.
- (14) Hunt, C. T.; Balch, A. L. *Inorg. Chem.* **1981**, *20*, 2267.

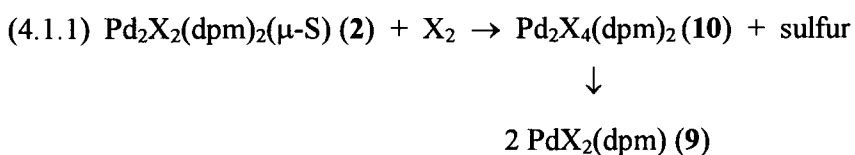
- (15) Appleton, T. G.; Clark, H. L.; Manzer, L. E. *Coord. Chem. Rev.* **1973**, *10*, 335.
- (16) Luther III, G. W.; Beyerle, G. *Inorg. Synth.* **1977**, *17*, 186.
- (17) Fogg, P.G.T.; Young, C.L. (Eds.). *Solubility data series*. Vol. 32. Pergamon Press, Oxford. 1988. p.279.
- (18) *Handbook of Chemistry and Physics*. 56th ed. Chemical Rubber Co., Cleveland, OH. 1979. p. D-191.
- (19) Sallin, D.; Barnabas, A.F.; James, B.R. Unpublished data.

CHAPTER 4

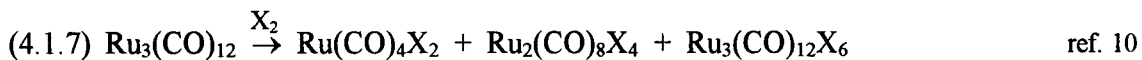
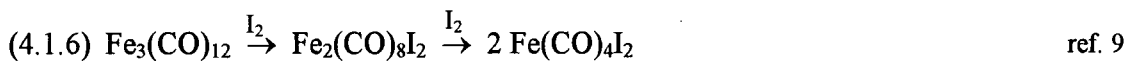
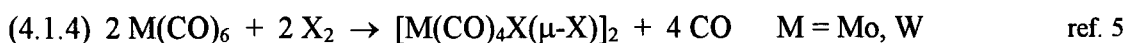
Kinetic and Mechanistic Aspects of Sulfur Abstraction from $\text{Pd}_2\text{X}_2(\mu\text{-S})(\text{dpm})_2$ Using Halogens

4.1 Introduction

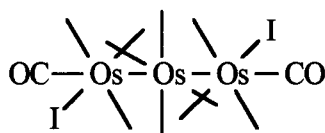
During the course of this thesis work, it was discovered that the bridged sulfur atom of **2** could be removed effectively using halogens (eq. 4.1.1).¹ The chemistry parallels that of reactions between **1** and X₂ previously studied by Hunt and Balch² in that transannular oxidative addition occurs with the formation of tetrahalodipalladium(II) intermediates en route to production of mononuclear species (eq. 4.1.2). Kinetic and mechanistic details of reaction 4.1.1 were performed and are summarized in this chapter; there is a correlation of the results with the limited semi-quantitative kinetic data reported for reaction 4.1.2.²



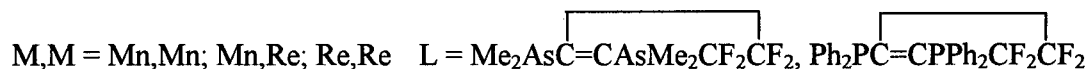
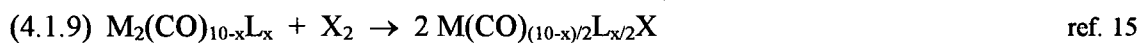
Numerous examples of electrophilic additions of halogens to transition metal complexes can be found in the literature including studies detailing kinetic and mechanistic investigations. For example, the mono-, di-, and trinuclear transition metal carbonyl complexes of group 6, 7, and 8 elements have been shown to undergo facile oxidative addition reactions.



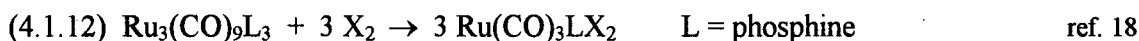
With the di- and trinuclear complexes, transannular oxidative addition takes place such that the products contain equal numbers of halide ligands at each of the reacted metal centers. There is increasing metal-metal bond stability towards oxidation on descending the transition metal group, Fe, Ru, and Os, and di- and trinuclear halide products are prominent with the heavier metals. An X-ray crystallographic study of $\text{Os}_3(\text{CO})_{12}\text{I}_2$ has revealed a linear Os_3 entity as illustrated and thus demonstrating ring opening upon oxidative addition across two Os centers.¹²



Kinetic and mechanistic studies have been carried out for reactions 4.1.3¹³ and 4.1.5¹⁴ including studies on a series of substituted dinuclear species (eqs. 4.1.9 and 4.1.10).



Similarly, halogenation of substituted dinuclear Fe and trinuclear Ru carbonyl complexes have been examined kinetically (eqs. 4.1.11 and 4.1.12).

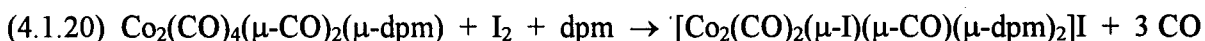
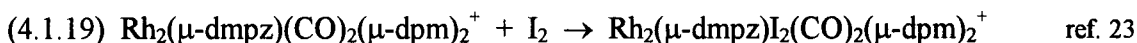
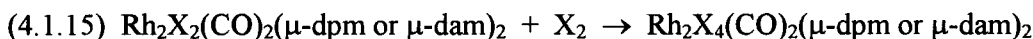


Reports on halogenation reactions involving main group metals can also be found and these center on the use of Sn (eqs. 4.1.13 and 4.1.14).

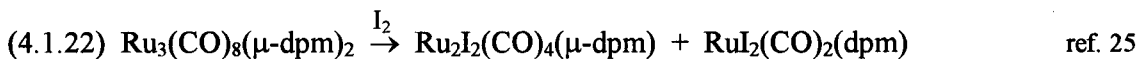
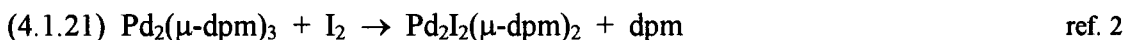




Within transition metal - dpm complexes, halogenations have been studied mostly with Rh complexes containing one or two bridging dpm ligands (eqs. 4.1.15 to 4.1.22); however, to date no kinetic reports can be found concerning such reactions of transition metal - dpm complexes. In general, metal - metal bond formation accompanies transannular oxidative addition; in the case of reaction 4.1.18 addition of I₂ occurs at one Rh center, and this is attributed to the larger steric bulk of the Γ ligand, compared to Br⁻ (eq. 4.1.17), in accommodating the steric requirements of the dpm ligand.

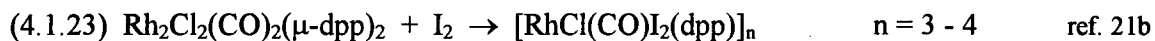


ref. 24



Other examples of halogen addition to one metal center in dinuclear complexes include Rh compounds containing bridging bis(diphenylphosphino)propane (dpp) and bis(diphenylphosphino)butane (dpb) ligands (eqs. 4.1.23 and 4.1.24). Addition across the two

metal centers cannot take place as they are too far apart (4 to 6 Å). The products have not been definitively characterized and may be polymers; infrared spectroscopy was used to establish the nature of the reaction as the change in the ν_{CO} was consistent with oxidative addition at one metal center (the greater change in oxidation state (I to III vs. I to II) results in a lesser degree of backbonding to the π^* molecular orbitals of CO).



Double transannular oxidative addition can also take place, and in reaction 4.1.25 consecutive metal - metal bond forming and breaking occurs.



There is only one report describing the oxidative addition of iodine to a metal sulfide complex with concomitant formation of elemental sulfur. Again, as with reactions 4.1.23 through 4.1.25, no kinetic or mechanistic studies have been reported.



4.2 Results

Complexes $\text{Pd}_2\text{X}_2(\text{dpm})_2$ (**1**), $\text{Pd}_2\text{X}_2(\mu\text{-S})(\text{dpm})_2$ (**2**), and $\text{PdX}_2(\text{dpm})$ (**9**) are well-characterized. NMR spectroscopic data were given in earlier chapters, but for the convenience of the reader, the data are again summarized in Table 4.1. Kinetic data can be found in Appendix V.

A preliminary ^1H and $^{31}\text{P}\{^1\text{H}\}$ NMR study of reaction 4.1.1 ($\text{X} = \text{I}$) in CDCl_3 at R.T. revealed, in general, a well-behaved system (Fig. 4.1) (the formation of small amounts of $\text{PdI}_2(\text{dpm}(\text{S}))$ (**11c**) will be discussed later (p. 152)). On addition of a purple iodine solution to an equimolar brown solution of **2c**, the $^{31}\text{P}\{^1\text{H}\}$ NMR singlet of **2c** rapidly decreased in intensity while a new $^{31}\text{P}\{^1\text{H}\}$ NMR singlet, corresponding to an observed green-black intermediate, at δ -1.2, concomitantly increased rapidly in intensity. This new singlet subsequently decreased slowly in intensity while the $^{31}\text{P}\{^1\text{H}\}$ NMR singlet of **9c** was observed to form and grow in intensity. Completion of the reaction (~1h) was evidenced by the eventual disappearance of the intermediate and the unchanging **9c** singlet. The intermediate is also characterized by a 1:4:6:4:1 quintet at δ 5.14 in the ^1H NMR spectrum and is identified as the tetraiododipalladium(II) (**10c**) species previously seen in the reaction between $\text{Pd}_2\text{I}_2(\text{dpm})_2$ (**1c**) and I_2 .² A repeated NMR study of this reaction served to establish firmly the NMR chemical shifts of the **10c** intermediate; the J_{PH} coupling was observed to be 3.7 Hz. The final orange-red solution of **9c** contained a very small amount of yellow particulate matter (~0.1 mg), attributed to elemental sulfur from thin-layered chromatographic studies (CHCl_3 eluent), and which prompted a synthetic-scale study to search for and substantiate the production of elemental sulfur. Reaction of **2c** and I_2 on the synthetic-scale yielded immediately an initial green-black solution that slowly changed colour to a final orange-red (~3h). A pale yellow precipitate was formed which was collected (~1 mg) and analyzed using

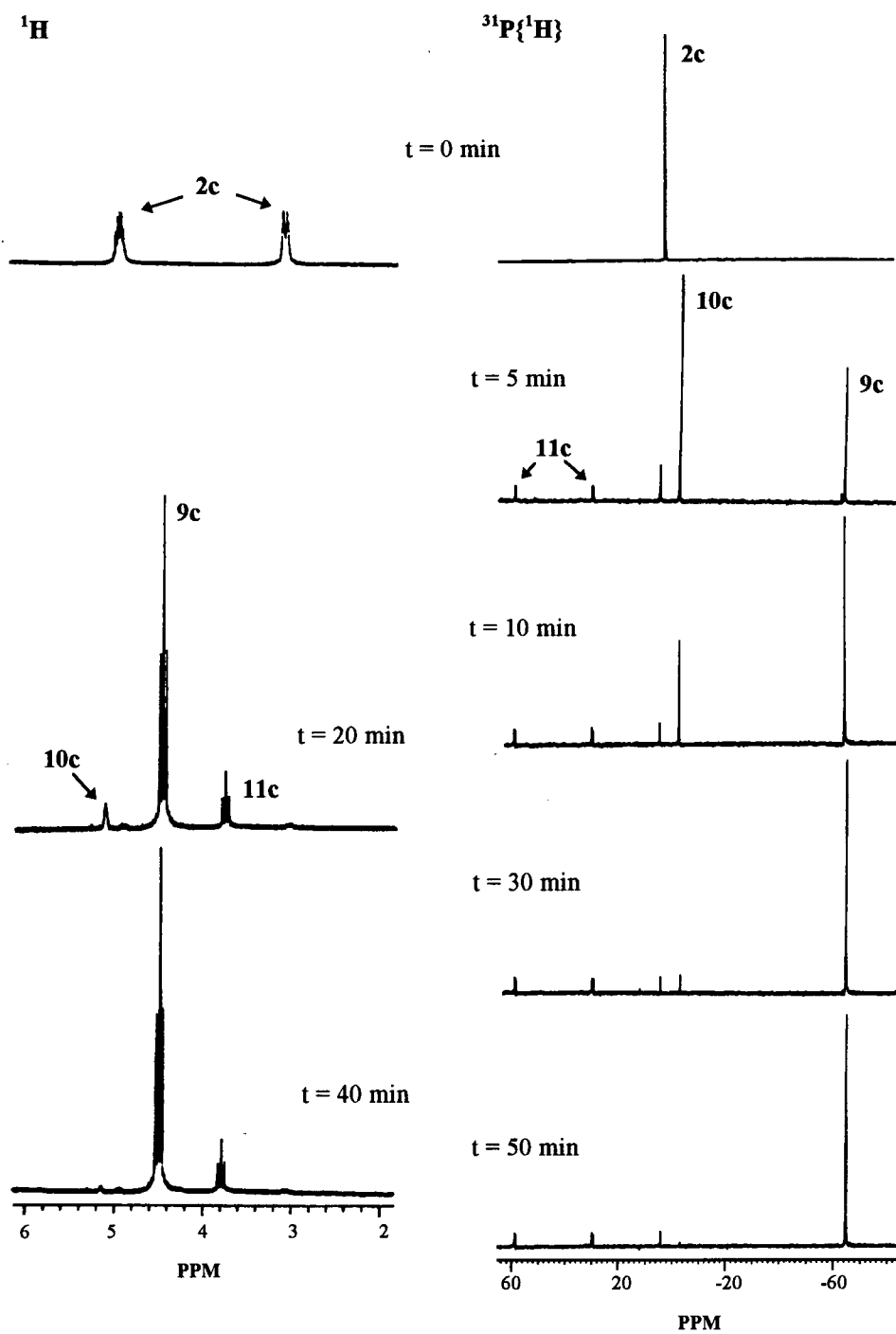
Table 4.1. NMR data for the palladium complexes.

Compound ^a	δ (¹ H) ^b	δ (³¹ P{ ¹ H}) ^c
Pd ₂ Cl ₂ (dpm) ₂ (1a)	4.17 ^{d,e} (4.0)	-5.5 ^d
Pd ₂ Br ₂ (dpm) ₂ (1b)	4.19 ^{d,e} (4.0)	-6.15 ^d
	4.24 ^e	-5.5
Pd ₂ I ₂ (dpm) ₂ (1c)	4.23 ^{d,e} (4.0)	-11.3 ^d
Pd ₂ Cl ₂ (μ -S)(dpm) ₂ (2a)	2.79 ^{d,f} (12.6, 3.5)	5.52 ^d
	4.73 ^f (12.6, 6.1)	
Pd ₂ Br ₂ (μ -S)(dpm) ₂ (2b)	2.88 ^{d,f} (12.8, 3.2) (2.90)	5.96 ^d
	4.83 ^f (12.8, 7.6)	6.14
Pd ₂ I ₂ (μ -S)(dpm) ₂ (2c)	3.06 ^{d,f} (14.0, 3.0)	6.08 ^d
	4.95 ^f (14.0, 6.0)	
PdCl ₂ (dpm) (9a)	4.21 ^g (10.8)	-54.7
PdBr ₂ (dpm) (9b)	4.37 ^g (10.5)	-56.2
PdI ₂ (dpm) (9c)	4.42 ^g (10.0)	-63.2
Pd ₂ Cl ₄ (dpm) ₂ (10a)	4.55 ^{d,e,h} (4.6)	8.5 ^{d,h}
Pd ₂ Br ₄ (dpm) ₂ (10b)	4.6 ^{d,h}	4.90 ^{d,h}
Pd ₂ I ₄ (dpm) ₂ (10c)	5.14 ^e (3.7)	-1.52
	5.18 ^{d,e,h} (4.0)	-0.73 ^{d,h}
PdCl ₂ (dpm(S)) (11a)	4.07 ⁱ	54.9, 30.9 (18.3) ^j
PdBr ₂ (dpm(S)) (11b)	4.02 ⁱ	56.6, 32.1 (20.4) ^j
PdI ₂ (dpm(S)) (11c)	3.71 ⁱ	61.1, 31.2 (25.5) ^j
Pd ₂ I ₂ (μ -SO)(dpm) ₂	4.98 ^k (12, 13.5)	19 to -7 AA'BB'
	4.18 ^k (15, 9)	
	2.58 ^l	
	2.26 ^l	
PdCl ₂ (dpm(S) ₂)	5.54 ^g (14)	37.3

^a The μ -symbol for the bridging diphosphine ligand(s) is omitted for convenience throughout this Table and the text. ^b In CDCl₃, unless stated otherwise, at 20 °C with respect to TMS; J_{HH} and/or J_{PH} values in Hertz are given in parentheses; signals for CH₂ protons. ^c Unless otherwise stated, singlets in CDCl₃ at 20 °C with respect to 85% H₃PO₄, downfield being positive. ^d In CD₂Cl₂. ^e Quintet. ^f Doublets of quintets

for each of 2 sets of CH₂ protons. ^g Triplet. ^h Taken from ref. 2. ⁱ Pseudo-triplet. ^j AB pattern, J_{pp} values in Hertz given in parentheses. ^k Doublets of triplets for each of 2 sets of CH proton. ^l Multiplet for each of 2 sets of CH proton.

Fig. 4.1. Preliminary ^1H (300 MHz) and $^{31}\text{P}\{^1\text{H}\}$ (121 MHz) NMR study of the reaction of $\text{Pd}_2\text{I}_2(\mu\text{-S})(\text{dpm})_2$ (**2c**, 1.6×10^{-2} M) with 1 mole equivalent I_2 in CDCl_3 at R. T.; **9c** = $\text{PdI}_2(\text{dpm})$, **10c** = $\text{Pd}_2\text{I}_4(\text{dpm})_2$, **11c** = $\text{PdI}_2(\text{dpm}(\text{S}))$.



TLC, UV-vis spectroscopy, and mass spectrometry; the results were compared with those of an authentic sample of sulfur. Degrees of retention (R_f -values) as well as electronic absorption spectral characteristics were found to be identical; the mass spectrum of the yellow solid excellently illustrates an ionization pattern, indicative only of sulfur, with the major parent peak located at 256 m/z and the other major peaks all separated by 32 units of mass (Fig. 4.2). The identity of the yellow solid was further proven to be sulfur by its reaction with $\text{Pd}_2\text{I}_2(\text{dpm})_2$ (**1c**) which gave only **2c** as evidenced by ^1H and $^{31}\text{P}\{^1\text{H}\}$ NMR spectroscopy. Finally, with the identity known, the yield of elemental sulfur from the synthetic reaction was determined to be ~80 %.

Kinetic studies. (a) Conventional UV-vis spectrophotometric measurements. The kinetics of the slow decomposition of $\text{Pd}_2\text{I}_4(\text{dpm})_2$ (**10c**) were measured by means of conventional UV-vis absorption spectroscopy; the rates were independent of the initially added I_2 . Species **2c** is brown and has absorption maxima at 368 and 485 nm, while **9c** is orange and has a single absorption maximum at 429 nm in the visible region. Treatment of a CHCl_3 solution of **2c** with a solution of I_2 immediately gave a green-black solution which gradually changed to a final yellow-orange. An illustrative example of accompanying spectral changes is shown in Fig. 4.3 where the spectrum recorded immediately after the two reactants have mixed ($t = 30$ s, dashed line) shows an absorption maximum at 362 nm with a shoulder at 484 nm. Below 420 nm and above 484 nm, the absorbance rapidly decreases while simultaneously increasing rapidly in the region between such that the next spectrum recorded ($t = 150$ s) corresponds to the stage of the reaction where **10c** has fully formed and is now decomposing. The spectral changes accompanying decomposition of **10c** are also characterized by two isosbestic points at 420 and 510 nm. Optical density was monitored as a function of time at 396 nm where the total spectral change is ~1 absorbance unit. Iodine and

Fig. 4.2. Mass spectrum (electron impact) of the yellow precipitate isolated from the synthetic-scale reaction of $\text{Pd}_2\text{I}_2(\mu\text{-S})(\text{dpm})_2$ (**2c**) with I_2 in CHCl_3 at R.T.

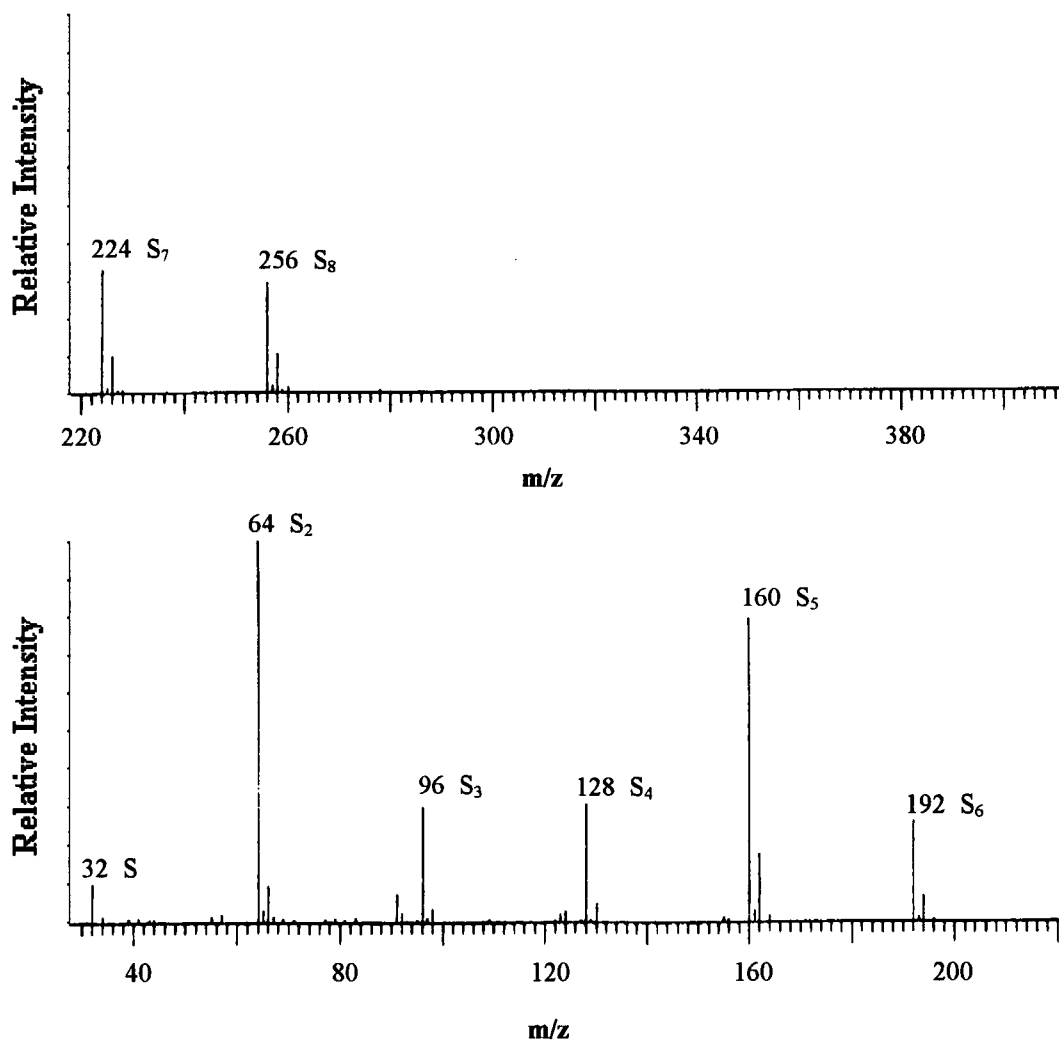
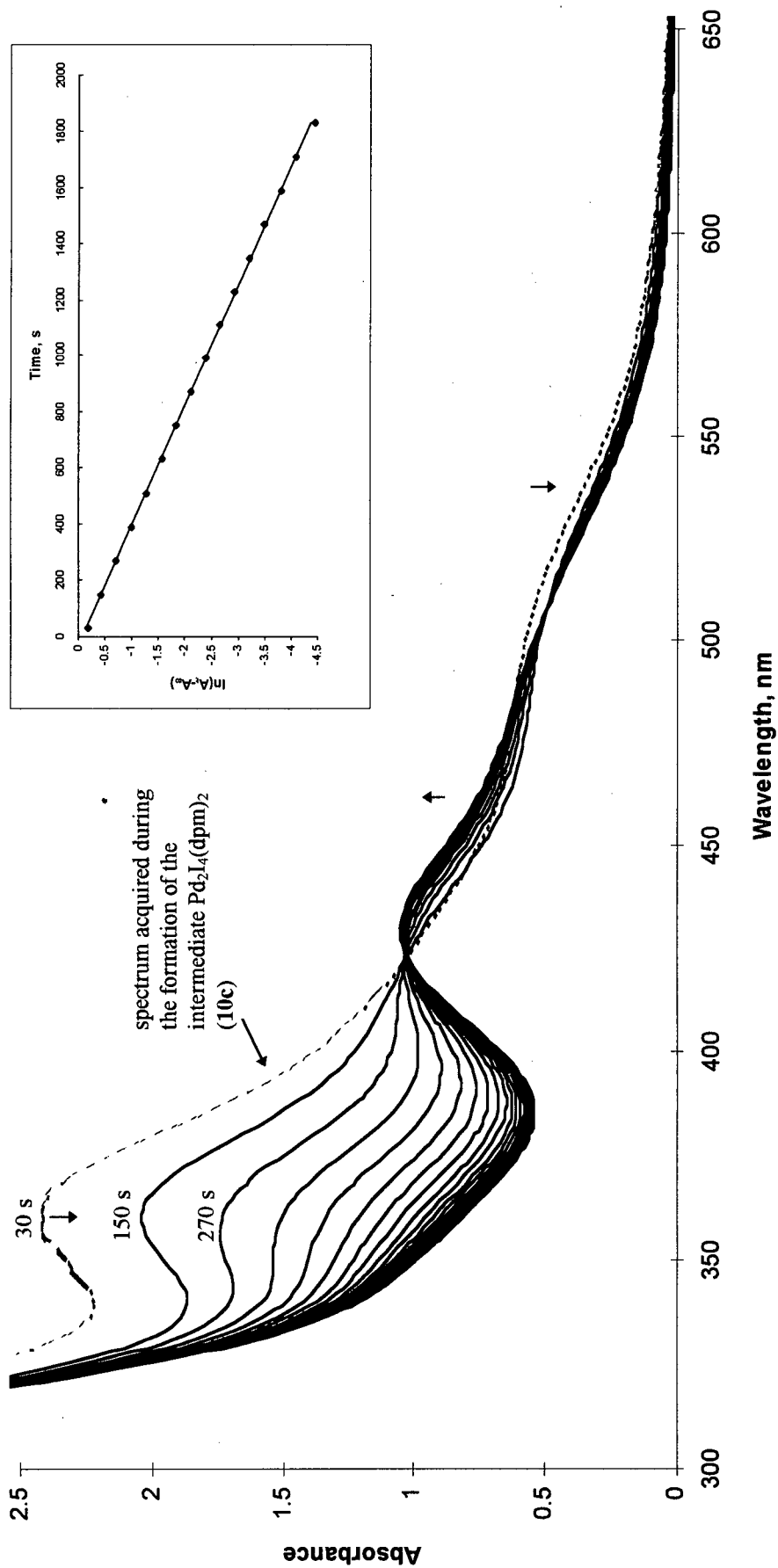


Fig. 4.3. Visible absorption spectral changes (320 - 650 nm region) as a function of time ($\Delta t = 120$ s) for a CHCl_3 solution of $\text{Pd}_2\text{I}_2(\mu\text{-S})(\text{dpm})_2$ (**2c**, 9.4×10^{-5} M) on addition of I_2 (3.8×10^{-4} M) at 25°C . Inset: a rate-plot analyzed for a first-order dependence on $\text{Pd}_2\text{I}_4(\text{dpm})_2$ (**10c**); A_t and A_∞ represent the absorption at 396 nm at times t and ∞ , respectively.



sulfur have no absorptivities at this wavelength (Fig. 4.4). The first-order rate constants, k_{obs} , obtained were found to be independent of both $[\text{I}_2]$ from $(3.8\text{-}7.5)\times 10^{-4}$ M (Fig. 4.5) and $[\mathbf{2c}]$ from $(1.6\text{-}9.9)\times 10^{-5}$ M. Noting that $\mathbf{2c}$ is rapidly converted fully to $\mathbf{10c}$, the rate law takes the simple form

$$(4.2.1) \quad \text{rate} = -\frac{d[\text{Pd}_2\text{I}_4(\text{dpm})_2]}{dt} = k_{\text{obs}}[\text{Pd}_2\text{I}_4(\text{dpm})_2] = k_{\text{D}}[\text{Pd}_2\text{I}_4(\text{dpm})_2]$$

where k_{D} is the unimolecular rate constant for the decomposition of the intermediate. The temperature dependence data for k_{D} were obtained at a single $[\text{I}_2]$ of 7.5×10^{-4} M and $[\mathbf{2c}] = 9.4 \times 10^{-5}$ M; an Eyring plot of the data (Table 4.2) from 20-35 °C gives an excellent straight line and the activation parameters $\Delta H_{\text{D}}^\ddagger = 80 \pm 1$ kJ mol⁻¹ and $\Delta S_{\text{D}}^\ddagger = -26 \pm 3$ J mol⁻¹ K⁻¹ (Fig. 4.6).

(b) Stopped-flow spectrophotometric measurements. The kinetics of the initial rapid reaction between $\mathbf{2c}$ and I_2 in forming the intermediate $\mathbf{10c}$ were measured in CHCl_3 using stopped-flow spectroscopy under pseudo-first-order conditions. Inspection of the spectral results from conventional UV-vis measurements (for example, see Fig. 4.3) led to the choice of 510 nm as the appropriate wavelength to monitor the reaction as the decrease in absorbance here eventually ceased (isosbesticity was then observed) indicating complete formation of $\mathbf{10c}$. Optical density changes were monitored as a function of time, and a representative plot of absorbance vs. time is shown in Fig. 4.7 with the corresponding pseudo-first-order rate-plot shown in Fig. 4.8. The observed pseudo-first-order rate constants, k_{obs} , were found to be strictly first-order with respect to

Fig. 4.4. Electronic absorption spectra of S_8 (conc. = 1.25×10^{-3} M; λ , nm (ϵ , $M^{-1} \text{ cm}^{-1}$) = 244 (828), 266 (910)) and I_2 (conc. = 3.94×10^{-4} M; λ , nm (ϵ , $M^{-1} \text{ cm}^{-1}$) = 512 (879)) in $CHCl_3$ at R.T.

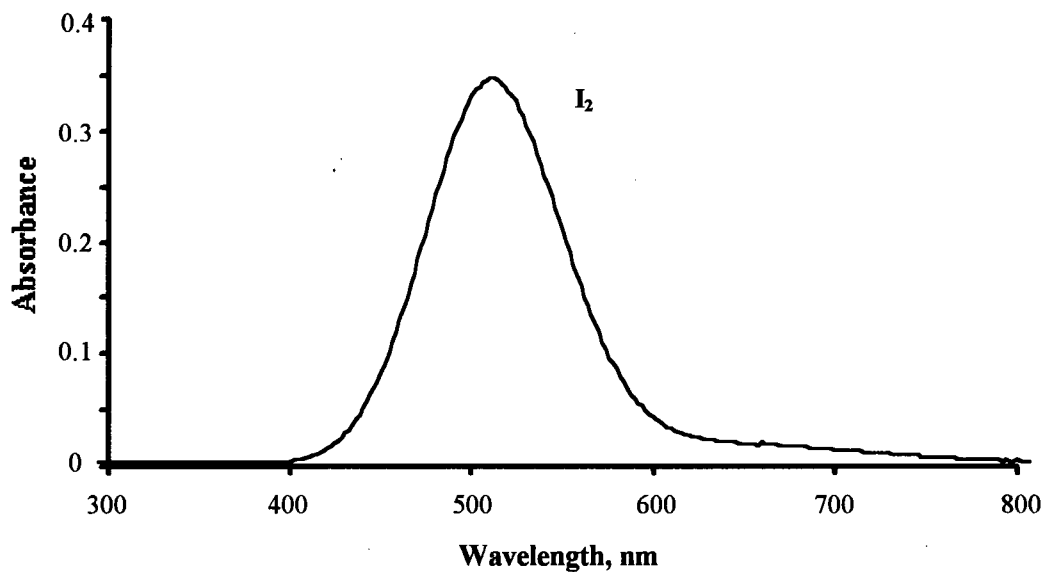
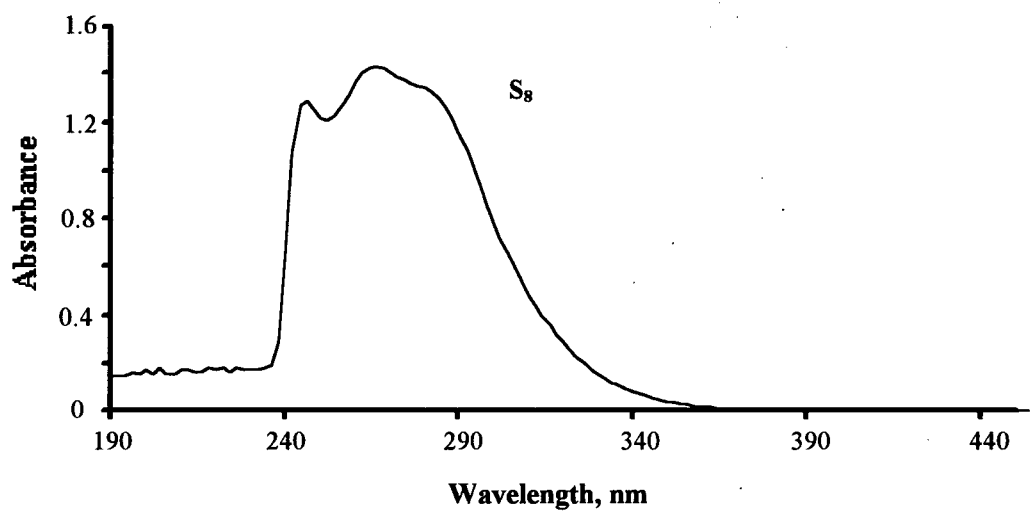


Fig. 4.5. The dependence of the first-order rate constant, k_{obs} , on $[\text{I}_2]$ for the decomposition of the intermediate $\text{Pd}_2\text{L}_4(\text{dpm})_2$ (**10c**) (formed from reaction with 9.4×10^{-5} M $\text{Pd}_2\text{I}_2(\mu\text{-S})(\text{dpm})_2$ (**2c**)) in CHCl_3 at 25°C .[†]

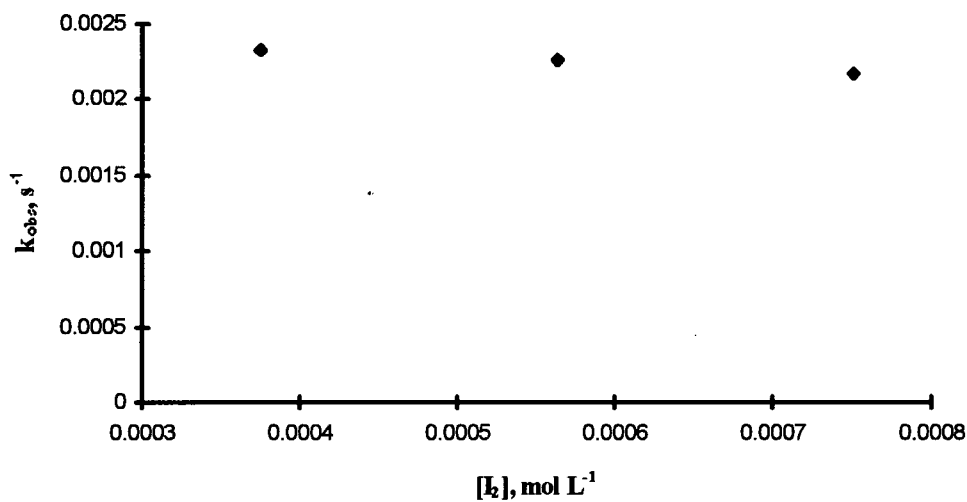
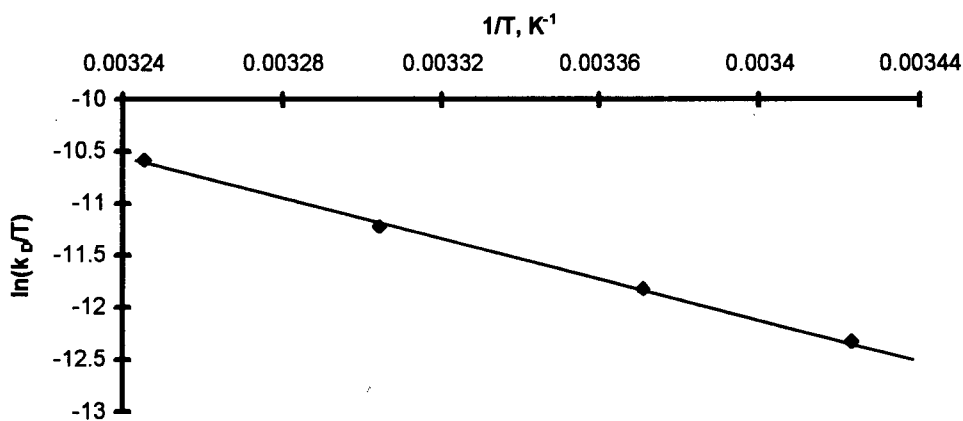


Fig. 4.6. Eyring plot of the temperature dependence for the unimolecular rate constants, k_{D} , for the decomposition of $\text{Pd}_2\text{L}_4(\text{dpm})_2$ (**10c**).



[†] Note: use of $[\text{I}_2] = 3.8 \times 10^{-4}$ M gave kinetics which analyzes excellently for first-order; the second-order rate-plot is non-linear.

Table 4.2. Temperature dependence for the bimolecular (k_f) and unimolecular (k_D) rate constants for the formation and decomposition of the intermediate, $\text{Pd}_2\text{L}_4(\text{dpm})_2$ (**10c**), respectively, in CDCl_3 .^a

Temperature, K	$k_f, \text{M}^{-1}\text{s}^{-1}$	k_D, s^{-1}
293	179	2.2×10^{-3}
298	235 (240) ^b	4.0×10^{-3} ^c
303	290	7.8×10^{-3} ^c
308	370	13.1×10^{-3} ^c

^a initial $[\mathbf{2c}] = 9.4 \times 10^{-5} \text{ M}$.

^b Five-fold excess of ${}^n\text{Bu}_4\text{NI}$ present.

^c Obtained at a single $[\text{I}_2] = 7.5 \times 10^{-4} \text{ M}$.

Fig. 4.7. Absorption spectral changes at $\lambda = 510$ nm as a function of time for the formation of $\text{Pd}_2\text{I}_4(\text{dpm})_2$ (**10c**) in CHCl_3 at 25°C from reaction of $\text{Pd}_2\text{I}_2(\mu\text{-S})(\text{dpm})_2$ (**2c**) (9.9×10^{-5} M) with I_2 (4.9×10^{-4} M).

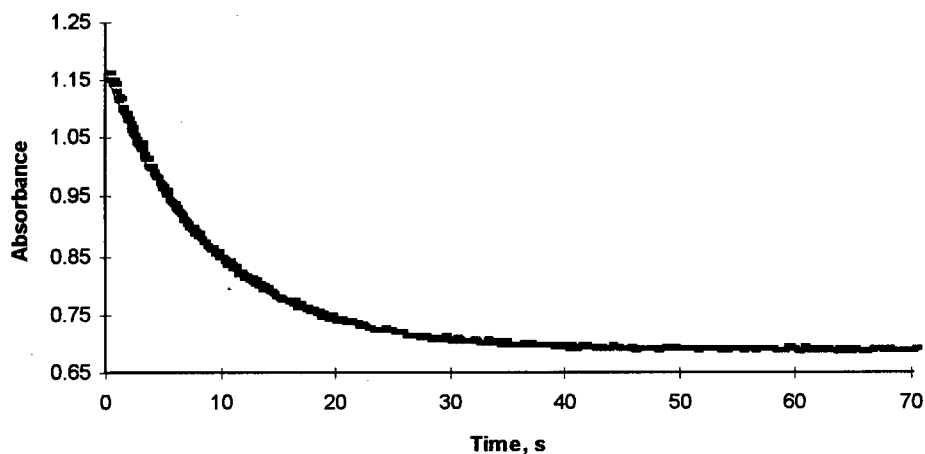
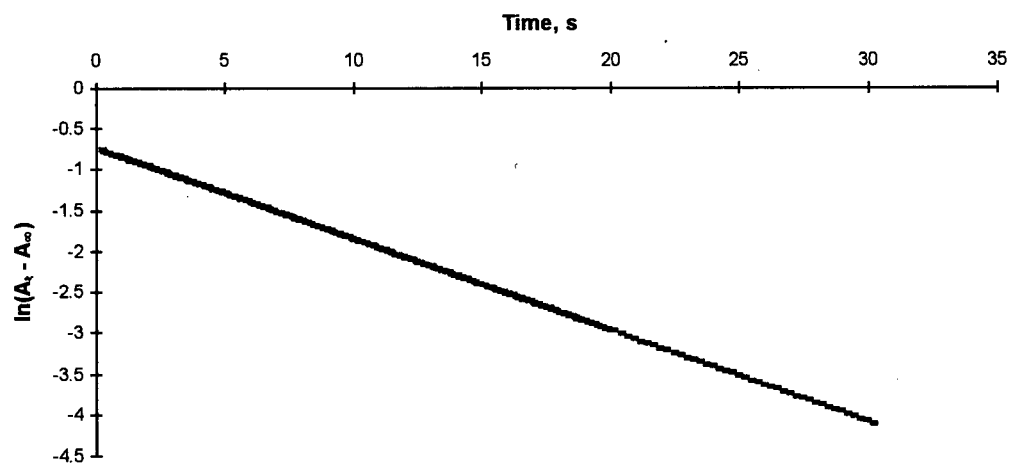


Fig. 4.8. Rate-plot analyzed for a pseudo-first-order dependence on $\text{Pd}_2\text{I}_2(\mu\text{-S})(\text{dpm})_2$ (**2c**) (initial conc. = 9.9×10^{-5} M) during reaction with I_2 (initial conc. = 4.9×10^{-4} M) in CHCl_3 at 25°C to form the intermediate $\text{Pd}_2\text{I}_4(\text{dpm})_2$ (**10c**); A_t and A_∞ represent the absorbance at 510 nm at times t and ∞ , respectively.



I_2 ((3.8-7.5) $\times 10^{-4}$ M) and independent of [2c] from (1.6-9.9) $\times 10^{-5}$ M. Thus, the rate law is as follows

$$(4.2.2) \quad \text{rate} = \frac{-d[2a]}{dt} = k_{\text{obs}}[2a] = k_1[I_2][2a]$$

where k_1 is the bimolecular rate constant obtained from a plot of the dependence of k_{obs} on $[I_2]$ (Fig. 4.9). The temperature dependence data for k_1 were obtained similarly from the plots at other temperatures; an Eyring plot of the data (Table 4.2) from 20-35 °C gives an excellent straight line and the activation parameters $\Delta H_1^\ddagger = 32 \pm 1 \text{ kJ mol}^{-1}$ and $\Delta S_1^\ddagger = -91 \pm 3 \text{ J mol}^{-1} \text{ K}^{-1}$ (Fig. 4.10). No ionic role for Γ was found; for example, addition of a five-fold excess of ${}^n\text{Bu}_4\text{NI}$ gave an unchanged k_1 value at 25 °C (Table 4.2).

The kinetics measured here correlate well with observations from low temperature NMR studies (see below). Using the activation parameters, the rate constant for the formation of the intermediate at -42 °C is calculated to be $4.12 \text{ M}^{-1} \text{ s}^{-1}$ and the corresponding calculated $t_{1/2}$ is 30.1 s. The intermediate was observed to be completely formed in ~3 min and this time period equates to six half-lives corresponding to ~98 % conversion.

Formation of $\text{PdI}_2(\text{dpm}(\text{S}))$ (11c). (a) Variable temperature NMR-scale studies. Closer examination of the preliminary NMR findings of the reaction between 2c and I_2 at R.T. reveals the presence of additional ${}^1\text{H}$ and ${}^{31}\text{P}\{{}^1\text{H}\}$ NMR resonances that are “unaccounted for” (Fig. 4.1). Specifically, a distinctive 1:2:1 triplet at δ 3.71 is observed in the ${}^1\text{H}$ NMR spectrum with corresponding doublets at δ 61.1 and δ 31.3 in the ${}^{31}\text{P}\{{}^1\text{H}\}$ NMR spectrum. These signals were

Fig. 4.9. The dependence of the pseudo-first-order rate constants, k_{obs} , for the formation of $\text{Pd}_2\text{L}_4(\text{dpm})_2$ (**10c**) on $[\text{I}_2]$ from reaction with $\text{Pd}_2\text{I}_2(\mu\text{-S})(\text{dpm})_2$ (**2c**, $9.9 \times 10^{-5} \text{ M}$) in CHCl_3 .

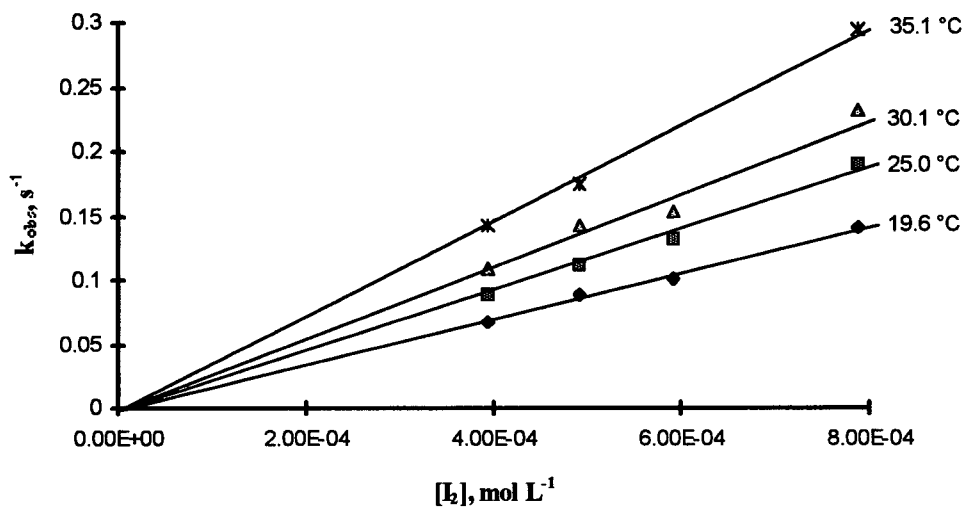
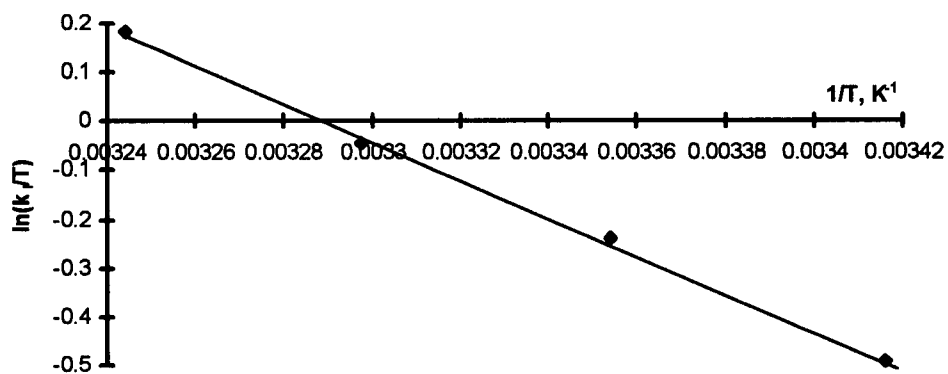


Fig. 4.10. Eyring plot of the temperature dependence for the bimolecular rate constants, k_1 , for the formation of $\text{Pd}_2\text{L}_4(\text{dpm})_2$ (**10c**) from reaction of $\text{Pd}_2\text{I}_2(\mu\text{-S})(\text{dpm})_2$ (**2c**) with I_2 in CHCl_3 .



later identified as belonging to the mononuclear complex **11c** which was separately synthesized and characterized. The ^1H and $^{31}\text{P}\{^1\text{H}\}$ NMR spectra accordingly show the same resonances corresponding to the CH_2 protons and the two P atoms, respectively. As the two P atoms are inequivalent resulting in an AB pattern, the CH_2 proton resonance is more accurately described as a pseudo-triplet. This by-product was observed consistently in relatively small amounts; Table 4.3 summarizes the work carried out in part to determine the factors that govern the formation of **11c** and to elucidate the nature of its origin. Similar NMR-scale experiments at R.T. under anaerobic and aerobic (1 atm air or 1 atm O_2) conditions gave the same product distribution, **11c** being present to ~17 %. At this point, it is noted that re-analysis of the products from the reaction on the synthetic-scale revealed that **11c** was also formed but to an extent of ~5 %. Furthermore, when **2c** and I_2 were reacted at concentrations used in the UV-vis or stopped-flow spectroscopic studies (*i.e.* 10^{-4} M), **11c** was not detected (after a work-up procedure). Variable temperature NMR-scale studies were performed, and at temperatures including 0, 40, and 80 °C, **11c** was observed to form in 15, 25, and 21% yield, respectively. At -42 °C, however, **11c** was not formed (both **2c** and I_2 initially at -42 °C) and its absence prompted mechanistic studies to determine the fate of the sulfur atom when initially released from **2c** (see next section). At this temperature, the intermediate **10c** was observed to be formed completely within 3 min, and no subsequent decomposition was seen; furthermore, no other observable intermediates were detected. When the temperature of the same sample was raised to -15 °C, the intermediate began to decompose to **9c**, and again no other detectable species were seen in the ^1H and $^{31}\text{P}\{^1\text{H}\}$ NMR spectra. Finally, the temperature was raised to R.T., and **9c** was again the only product seen in the NMR spectra; a yellow solid (~0.1 mg) seen in the NMR sample was identified using UV-vis spectroscopy and thin-layered

Table 4.3. Reaction of $\text{Pd}_2\text{X}_2(\mu\text{-S})(\text{dpm})_2$ (**2**) with X_2 under various conditions; yield of by-product $\text{PdX}_2(\text{dpm}(\text{S}))$ (**11**).

Reaction ^a	Conditions ^b	$\text{PdX}_2(\text{dpm}(\text{S}))$ yield (%)
$\text{Pd}_2\text{I}_2(\mu\text{-S})(\text{dpm})_2 + \text{I}_2$ NMR-scale; chloroform	1.6×10^{-2} M; 22 °C; 1 atm N_2	17, 18, 21
	1.6×10^{-2} M; 22 °C; 1 atm air	17
	1.6×10^{-2} M; 22 °C; 1 atm O_2	17
	1.6×10^{-2} M; -42 °C; 1 atm N_2	not detected
	1.6×10^{-2} M; 0 °C; 1 atm N_2	15
	1.6×10^{-2} M; 40 °C; 1 atm N_2	25
	1.6×10^{-2} M; 80 °C; 1 atm N_2	21
$\text{Pd}_2\text{I}_2(\mu\text{-S})(\text{dpm})_2 + 0.5 \text{I}_2$ ^c NMR-scale; chloroform	1.6×10^{-2} M; 22 °C; 1 atm N_2	25 ^d
$\text{Pd}_2\text{I}_2(\mu\text{-S})(\text{dpm})_2 + 2 \text{I}_2$ NMR-scale; chloroform	1.6×10^{-2} M; 22 °C; 1 atm N_2	not detected
$\text{Pd}_2\text{I}_2(\mu\text{-S})(\text{dpm})_2 + \text{I}_2$ NMR-scale; acetonitrile	8×10^{-4} M; 22 °C; 1 atm N_2	32
$\text{Pd}_2\text{I}_2(\mu\text{-S})(\text{dpm})_2 + \text{I}_2$ synthetic-scale; chloroform	2.0×10^{-3} M; 22 °C; 1 atm N_2	5
$\text{Pd}_2\text{I}_2(\mu\text{-S})(\text{dpm})_2 + \text{I}_2$ kinetic studies-scale; chloroform	9.9×10^{-4} M; 22 °C; 1 atm N_2	not detected
$\text{Pd}_2\text{I}_2(\mu\text{-SO})(\text{dpm})_2 + \text{I}_2$ NMR-scale; chloroform	1.6×10^{-2} M; 22 °C; 1 atm N_2	35
$\text{Pd}_2\text{Br}_2(\mu\text{-S})(\text{dpm})_2 + \text{Br}_2$ ^c NMR-scale; chloroform	1.7×10^{-2} M; 22 °C; 1 atm N_2	33 ^d

^a Unless otherwise stated, the reactions are 100% complete, and were studied after 24 h.

^b Concentrations refer to the Pd complex.

^c Reaction was incomplete but, once the halogen was consumed, there were no further changes.

^d Yield relative to $\text{PdBr}_2(\text{dpm})$ (**9b**) or $\text{PdI}_2(\text{dpm})$ (**9c**).

chromatography as elemental sulfur. No **11c** was formed if this “warming up” procedure was monitored from -42 to ~22 °C.

To determine the ease with which **11c** forms during the reaction of **2c** with I₂, NMR samples were prepared by the simultaneous injection of equal volumes of equimolar CDCl₃ solution of **2c** and I₂ initially at R.T. into NMR tubes held at -42 or -78 °C. The low temperatures either stopped or slowed down the reaction, which was examined by ¹H and ³¹P{¹H} NMR spectroscopy at the respective temperatures; in both samples, **9c** and **11c** were seen immediately in very small amounts (< ~1 %). There was no further change in spectral characteristics for the “solidified” sample analyzed at -78 °C; the sample analyzed at -42 °C, however, continued to show slow formation of the intermediate **10c** with completion within ~3 min. No further changes in the NMR resonances of **9c** and **11c** were seen.

(b) Mechanistic studies. The various Pd species present in the system during the reaction of **2c** with I₂ were each tested for possible reactivity with sulfur to help determine how the PdI₂(dpm(S)) (**11c**) was formed. Reaction of Pd₂I₂(dpm)₂ (**1c**) with S₈ in CDCl₃ at R.T. after 24 h gave only the μ-S adduct **2c** as evidenced by ¹H and ³¹P{¹H} NMR spectroscopy. With **9c** and **10c**, no reactivity was observed under purely thermal conditions. Specifically, in NMR-scale experiments in CDCl₃, ten-fold excesses of sulfur were employed with **9c** from 20 to 90 °C; ¹H and ³¹P{¹H} NMR studies after 24 h revealed no new signals. Using photolytic conditions, however, **11c** was quantitatively formed at R.T. after ~2 d of irradiation with a medium pressure Hg vapour lamp (450 W). Under the same conditions, **9c** in the absence of S₈ was unchanged. Possible reactivity of **10c** with sulfur was studied at -42 °C where **10c**, formed by reaction of **1c** with I₂, is stable at this temperature (see above); addition of an equimolar solution of S₈ to **10c** in CDCl₃ produced no change as indicated

by ^1H and $^{31}\text{P}\{^1\text{H}\}$ NMR data after 24 h. The NMR sample was subsequently placed at R.T. to allow **10c** to decompose; only **9c** was formed.

NMR-scale reactions in CDCl_3 at R.T. of **2c** with I_2 using different stoichiometric ratios were also carried out (Table 4.3). In the reaction of **2c** with 0.5 mole equivalent of I_2 , **9c** and **11c**, in addition to unreacted **2c**, were observed after 24 h; the yield of **11c** was 25% relative to **9c**. Reaction of **2c** with 2 mole equivalents of I_2 , however, yielded after 24 h **9c** only; **11c** was not observed. Corresponding TLC studies revealed the presence of elemental sulfur in the former reaction and surprisingly its absence in the latter.

A single R.T. NMR-scale reaction of $\text{Pd}_2\text{I}_2(\mu\text{-SO})(\text{dpm})_2$ with 1 mole equivalent of I_2 in CDCl_3 was performed. The ^1H and $^{31}\text{P}\{^1\text{H}\}$ NMR spectra revealed the presence of both **9c** and **11c** in about 65 and 35% yields, respectively; unreacted $\text{Pd}_2\text{I}_2(\mu\text{-SO})(\text{dpm})_2$ was not observed. A corresponding TLC study revealed the presence of elemental sulfur.

Because of the ease with which **11c** forms during the early stages of the reaction of **2c** with I_2 (see above), low temperature ESR experiments were performed (in attempts to detect, for example, S_1 and/or S_2 radicals) by injecting equal volumes of equimolar CDCl_3 solutions of **2c** and I_2 initially at R.T. into an ESR tube held in liquid N_2 . The ESR spectrum of the mixture, which solidified immediately (~ 1 s), was then recorded at 104 K and did not reveal the presence of any signals. The sample was briefly warmed to liquefy the mixture and was immediately placed back in liquid N_2 afterwards (~ 1 min total time); the recorded ESR spectrum again revealed no signals.

Crystal structure of $\text{PdI}_2(\text{dpm}(\text{S}))\cdot 0.5 \text{CH}_2\text{Cl}_2$ (11c** $\cdot 0.5 \text{CH}_2\text{Cl}_2$).** Crystal data, information relating to data collection, refinement details, bond distances and angles, and atomic coordinates for $\text{PdI}_2(\text{dpm}(\text{S}))\cdot 0.5 \text{CH}_2\text{Cl}_2$ are given in Appendix VI.

The molecular structure of $\text{PdI}_2(\text{dpm}(\text{S}))$, ignoring the greatly disordered solvent molecule, is shown in Fig. 4.11. The Pd atom in the complex is located in an approximately square-planar coordination environment; there is slight tetrahedral distortion around the metal centre with I(1) and P(1) lying slightly above the plane [0.0079(7) and 0.075(2) Å, respectively] and I(2) and S slightly below the plane [0.0085(7) and 0.084(2) Å, respectively]. The $\text{Ph}_2\text{PCH}_2\text{P}(\text{S})\text{Ph}_2$ ligand coordinates via the phosphorus and the S atom so as to form a five-membered chelate ring. This chelate ligand lies in a twisted conformation so that P(2) is above the coordination plane, 0.698 Å. The P(1)-C(1) and P(2)-C(1) bond distances and P(1)-C(1)-P(2) bond angle are 1.860(8) Å, 1.814(8) Å, and $107.8(4)^\circ$, respectively, which are within the normal ranges typically seen for P-C single bonds^{28,29} and P-C-P angles.^{29,30} The P(2)-S and Pd-S bond distances are 2.007(3) and 2.331(2) Å, respectively, and are not unusual.²⁹⁻³¹ The Pd-I(1) bond distance *trans* to the Pd-P(1) bond is 2.6419(9) Å, while the Pd-I(2) bond distance *trans* to the Pd-S(1) bond is much shorter (2.6006(9) Å). The difference is in keeping with the apparently greater *trans* influence of phosphorus versus sulfur.³¹⁻³³

The poor crystallinity of $\text{PdCl}_2(\text{dpm}(\text{S}))$ precluded an accurate X-ray crystallographic analysis; however, refinement of data on this compound to $R = 0.18$ revealed an approximately square-planar coordination of the ligands around the Pd atom and an envelope configuration of the five-membered $\text{dpm}(\text{S})$ chelate ring (Fig. 4.12).

Reaction of $\text{Pd}_2\text{Br}_2(\mu\text{-S})(\text{dpm})_2$ (2b) and Br_2 . Corresponding kinetic and mechanistic studies in CHCl_3 were attempted on the bromide system. However, complications arose due to the reactivity of Br_2 with the solvent³⁴ and irreproducible results were obtained. UV-vis spectral characteristics of Br_2 in CHCl_3 at R.T. changed dramatically on the same time scale as the reaction

Fig. 4.11. ORTEP drawing and stereoview of $\text{PdI}_2(\text{dpm}(\text{S}))$ (**11c**). Hydrogen atoms are omitted.

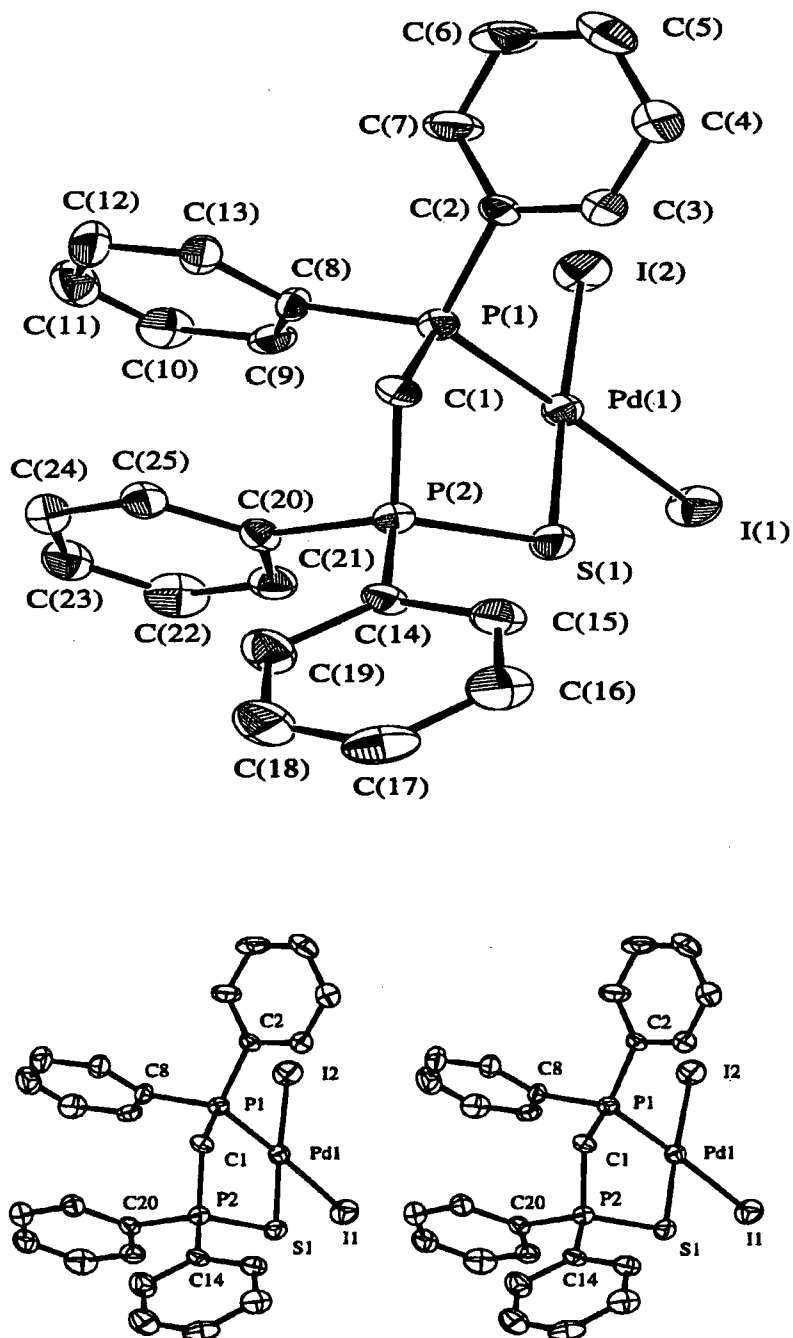
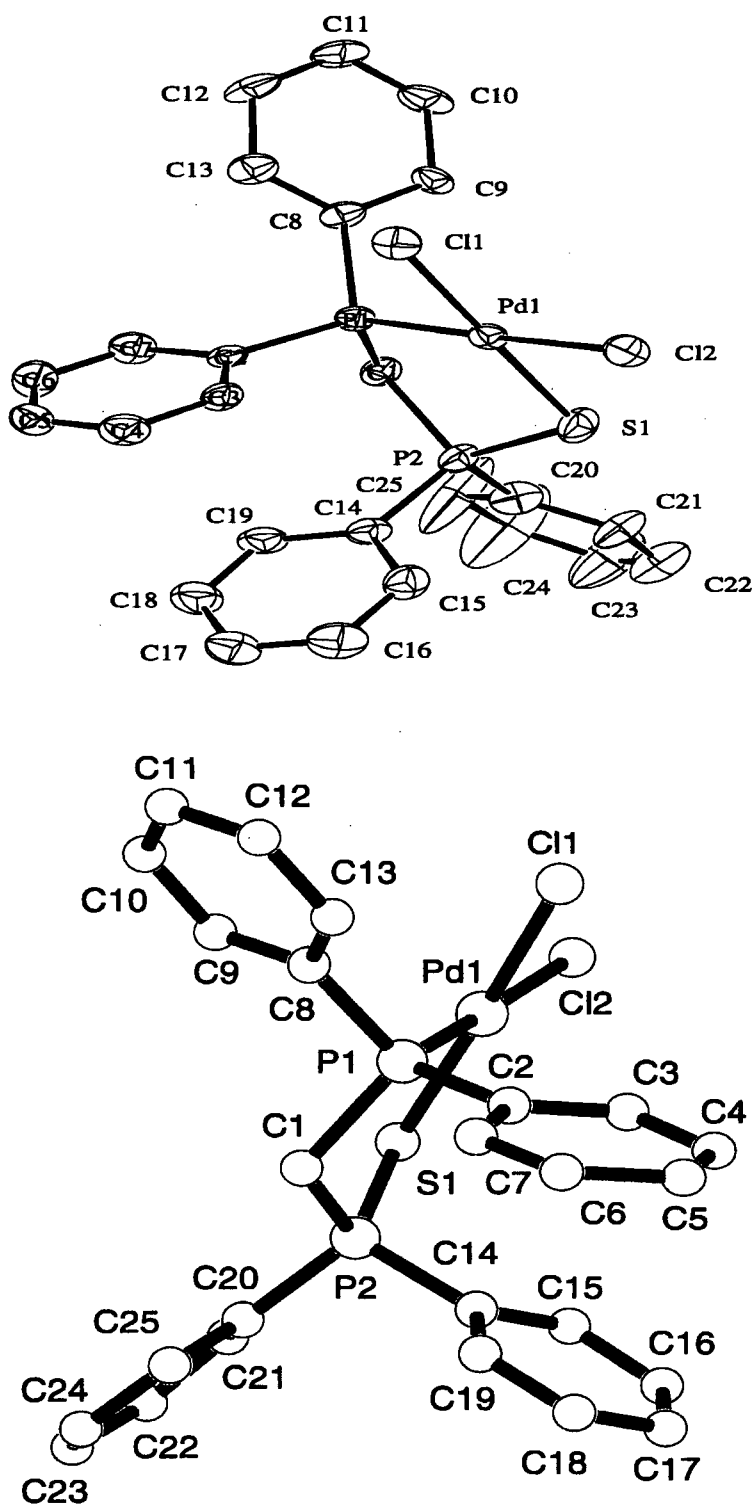


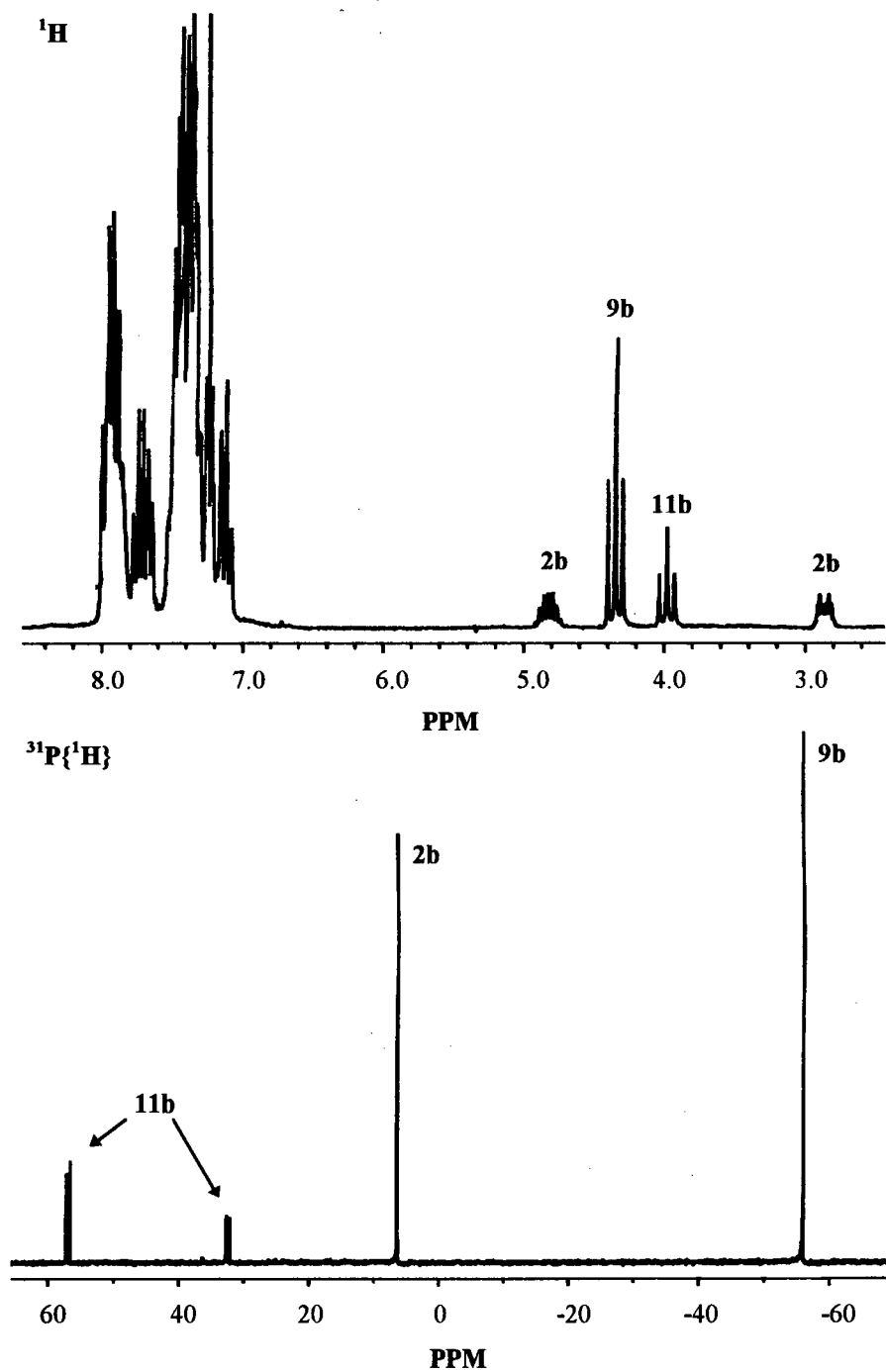
Fig. 4.12. ORTEP and PLUTO drawings of PdCl₂(dpm(S)) (11a). Hydrogen atoms are omitted.



between **2b** and Br₂; no change was observed for I₂ in CHCl₃. Nevertheless, a single qualitative NMR experiment revealed products analogous to those of the iodide system; namely, PdBr₂(dpm) (**9b**) and PdBr₂(dpm(S)) (**11b**) were observed to form in approximately 67 and 33% yields (Fig. 4.13). However, the reaction was incomplete as starting material **2b** was still seen even though a 1:1 mole ratio of reactants was used. Yellow particulate matter attributed to elemental sulfur was not visually observed; however, TLC studies were able to establish the presence of this product.

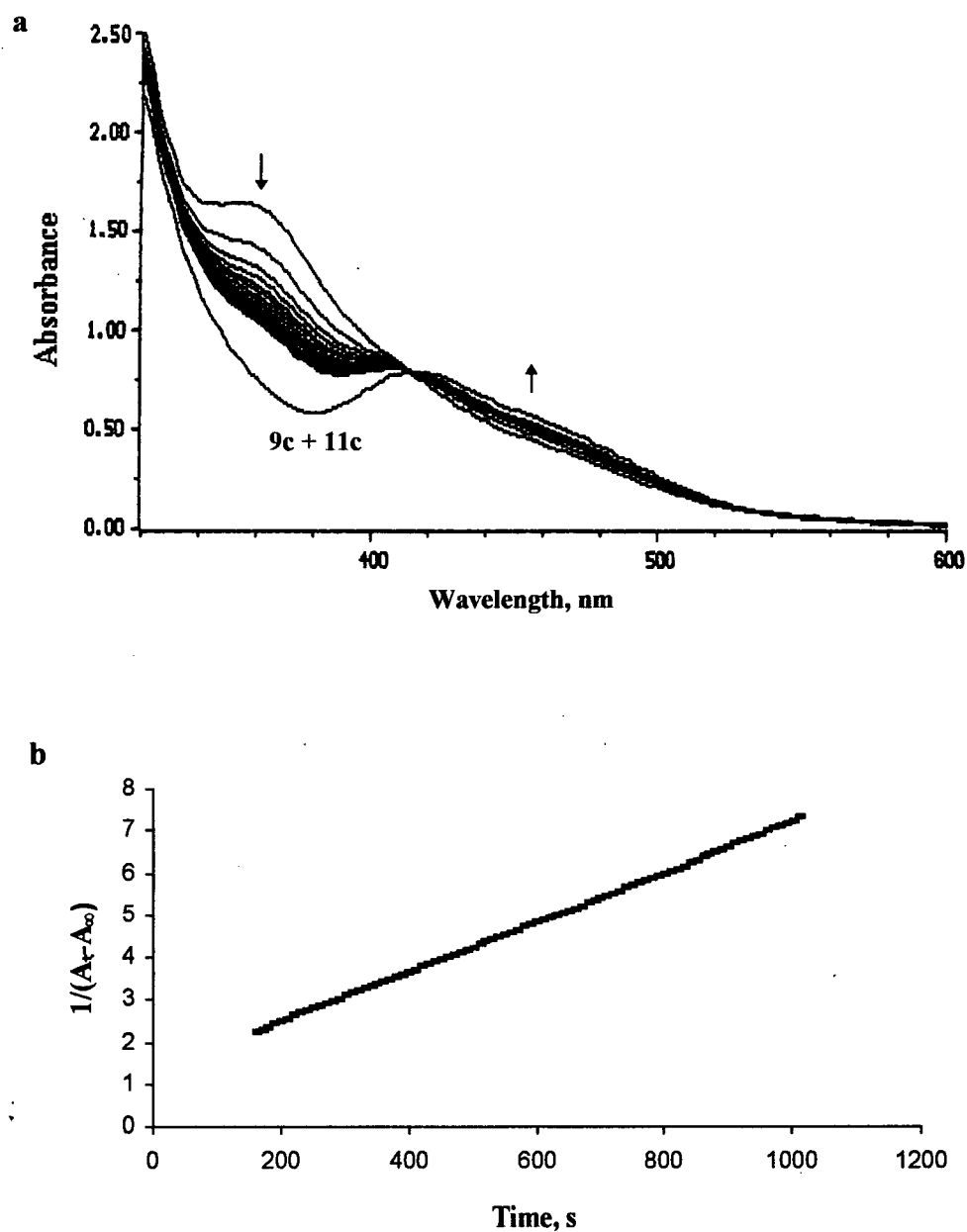
Solvent effects. Kinetic and mechanistic investigations of the reaction of **2c** with I₂ in various solvents were attempted. Of the solvents tested, none was found suitable for comparative studies. Either insolubility of **2c** was encountered or reactivity (adduct formation?) with I₂ was observed (*i.e.* acetone, acetonitrile, alcohol, benzene, carbon tetrachloride, dimethylacetamide, dimethylformamide, ethyl acetate, and toluene). Acetonitrile was used, however, for a qualitative NMR study because of its relatively slow reactivity toward I₂ (compared with the other solvents). In a single NMR study in which **2c** and I₂ were reacted in a 1:1 mole ratio at R.T. in CD₃CN, **10c** was observed to form immediately (in seconds) and disappear rapidly (few minutes) with concomitant formation of **9c** and **11c** in approximately 68 and 32 % yields, respectively. The presence of **10c** was evidenced by the 1:4:6:4:1 quintet at δ 5.08 in the ¹H NMR spectrum and the singlet at δ 1.54 in the ³¹P{¹H} NMR spectrum; **2c** was not seen. Again, **9c** and **11c** were characterized by a 1:2:1 triplet (δ 4.74) and a 1:2:1 pseudo-triplet (δ 4.15), respectively, in the ¹H NMR spectrum. In the ³¹P{¹H} NMR spectrum, only the singlet of **9c** at δ -55.7 was seen. The PdI₂(dpm(S)) species was probably too low in concentration to be detected (**2c** has limited solubility in CD₃CN: $\sim 8 \times 10^{-4}$ M from 0.5 mg in ~ 0.5 mL). TLC studies carried out on the NMR sample established the presence of elemental sulfur. Corresponding conventional UV-vis studies at

Fig. 4.13. ^1H (300 MHz) and $^{31}\text{P}\{^1\text{H}\}$ NMR spectra of the “completed” reaction (24 h) of $\text{Pd}_2\text{Br}_2(\mu\text{-S})(\text{dpm})_2$ (**2b**) with 1 mole equivalent of Br_2 in CDCl_3 at R.T.; **9b** = $\text{PdBr}_2(\text{dpm})$, **11b** = $\text{PdBr}_2(\text{dpm}(\text{S}))$.



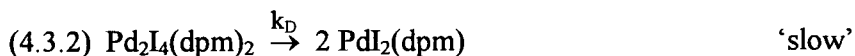
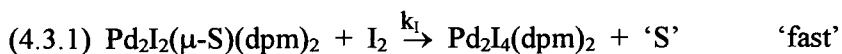
R.T. were carried out using only equimolar quantities of **2c** (9.4×10^{-5} M) and I_2 , as excess I_2 used for pseudo-first-order conditions led to rapid decomposition of **9c** in this solvent, as evidenced by subsequent NMR studies. Addition of a light brown CH_3CN solution of I_2 to a brown CH_3CN solution of **2c** immediately produced a yellow solution (presumably containing **10c**) characterized by two absorption maxima at $\lambda = 294$ and 360 nm (Fig. 4.14a, absorption maximum at $\lambda = 294$ nm not shown). Thereafter, the absorbances of these bands decreased over time, and an isosbestic point at $\lambda = 414$ nm was observed. The reaction was complete after ~ 20 min, and the final UV-vis spectrum was invariant with time. The solution was subsequently analyzed using NMR spectroscopy which revealed the presence of only **9c** and **11c** in about 70 and 30% yields, respectively (*cf.* NMR-scale study done at $\sim 8 \times 10^{-4}$ M **2c**). The kinetic data collected at $\lambda = 360$ nm where $\epsilon_{9c} = \epsilon_{11c} = 2.0 \times 10^3 \text{ M}^{-1} \text{ cm}^{-1}$ (sulfur has no absorptivity here) surprisingly analyze for approximately second-order with $k_{obs} \sim 4 \times 10^{-3} \text{ M}^{-1} \text{ s}^{-1}$ for the decomposition of **10c** (Fig. 4.14b). Kinetic studies of the rapid formation of the **10c** from **2c** and I_2 were attempted, but the reaction occurred too quickly to be amenable by stopped-flow spectrophotometry. Moreover, complications due to the reactivity of I_2 with the solvent interfered with the experimental setup.

Fig. 4.14. a) Visible absorption spectral changes (320-600 nm region) as a function of time for a CH₃CN solution of Pd₂I₂(μ-S)(dpm)₂ (**2c**) (9.4×10^{-5} M) on addition of I₂ (9.4×10^{-5} M) at 23.5 °C; **9c** = PdI₂(dpm). b) A rate-plot analyzed for an approximate second-order dependence on Pd₂I₄(dpm)₂ (**10c**); A_t and A_∞ represent the absorption at 360 nm at times t and ∞, respectively.

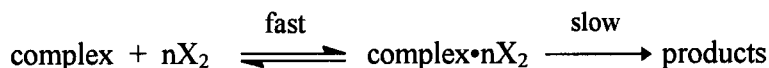


4.3 Discussion

Reaction of $\text{Pd}_2\text{I}_2(\mu\text{-S})(\text{dpm})_2$ (**2c**) with I_2 proceeds in two kinetically observable stages as described in eqs. 4.3.1 and 4.3.2 to yield $\text{PdI}_2(\text{dpm})$ (**9c**) and elemental sulfur. Transannular oxidative addition via electrophilic attack of I_2 occurs rapidly with formation of $\text{Pd}_2\text{I}_4(\text{dpm})_2$ (**10c**) and presumably monatomic sulfur. Thereafter, slower unimolecular decomposition of **10c** generates the monomeric product **9c**. The elemental sulfur product, S_8 , was visually detected and definitively identified using mass spectrometry, thin-layered chromatography, UV-vis spectrophotometry, and by its reaction with $\text{Pd}_2\text{I}_2(\text{dpm})_2$ (**1c**) to give only **2c** (see below).

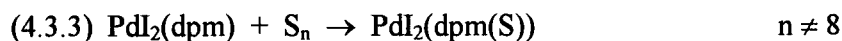


The chemistry parallels in part that observed by Hunt and Balch for the reaction of **1c** with I_2 which also proceeds via **10c** (eq. 4.1.2).² Although no quantitative kinetic studies were carried out, a qualitative $t_{1/2}$ value for decomposition of **10c** was determined from NMR data (see below).² Other similar chemistry can be seen in the halogenation of the substituted metal carbonyls cited in the Introduction.^{15,18,20} rapid pre-equilibria occur with the formation of adducts which then undergo slower intramolecular conversion to halogen-containing products.

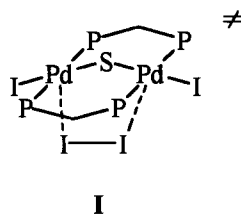


In the present system, depending on experimental conditions, the by-product $\text{PdI}_2(\text{dpm}(\text{S}))$ (**11c**) could also form (eq. 4.3.3) (see below) and as a consequence the yield of elemental sulfur could be affected. For example, in NMR- and synthetic-scale studies where concentrations are about 10^{-2} and 10^{-3} M, respectively, **11c** was found to form in ~17 and ~5% yields, respectively. The yield of sulfur was ~80% in each case; the unaccounted 10% in the synthetic-scale reaction is

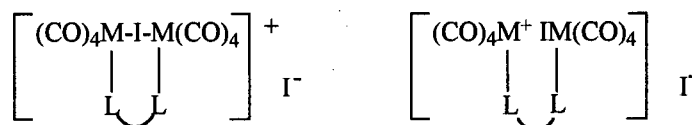
probably due to incomplete recovery from the sides of the reaction vessel as the remaining sulfur there was difficult to remove. In UV-vis spectroscopic studies, however, where concentrations are of the order of 10^{-4} M, **11c** does not form, and thus lowering concentrations permits more complete formation of elemental sulfur.



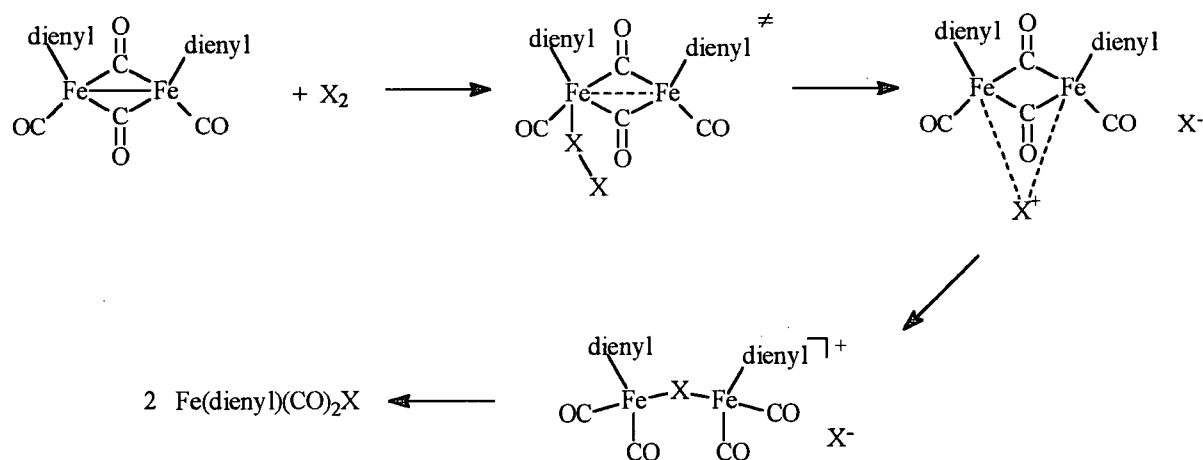
Formation of the intermediate, Pd₂I₄(dpm)₂ (10c). The kinetics of reaction 4.3.1, studied using stopped-flow spectroscopy, revealed a first-order dependence on both **2c** and I₂. The absence of any observable intermediates during low temperature NMR studies and the excellent linearity of the Eyring plot^{15a,20c,35} are good indications of an uncomplicated system. Formation of **10c** can be conveniently pictured as proceeding via a transition state such as **I**. Electron density is visualized as proceeding from the bridged S atom through the metal centers to the attacking I₂; the net result is the oxidation of the sulfide ligand to sulfur and the accompanying reduction of I₂ to iodide. The associative mechanism implied here is commonly seen for square planar, d⁸ metal complexes.³⁶



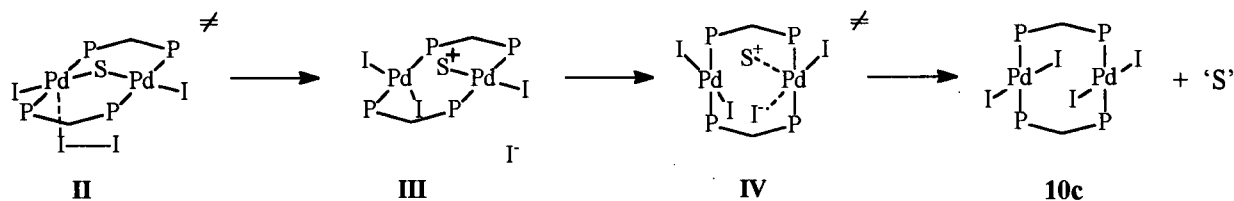
There is ample precedence for involvement of ionic species in transannular oxidative addition of halogens.^{16c,17} For example, in reaction 4.1.10, conceivable intermediates such as the following are suggested.^{16c}



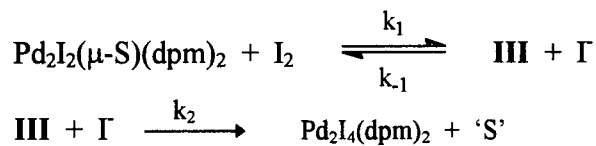
Likewise, in reaction 4.1.11, the intermediate formed following electrophilic attack at one Fe center is thought to be a halogenonium species, which rearranges to give an isolated bridging halide species that subsequently undergoes nucleophilic attack by X^- to give the product.¹⁷



The kinetic data and spectroscopic data do not rule out such possibilities in the Pd-system studied here. Rather than simultaneous electrophilic attack of two iodine atoms at the two Pd centers, an initial electrophilic attack at one metal center is more probable,^{14,20} and a transition state such as **II** is therefore not unreasonable. Associative substitution could then give formation of intermediate **III**, and then nucleophilic attack of Γ^- at the second Pd center, perhaps via transition state **IV**, could lead to **10c**.



The theoretical rate equation derived for the series **II** through **10c**, for example,



with steady state treatment for **III**, gives

$$\text{rate} = (k_1 k_2 / (k_{-1} + k_2)) [2\mathbf{c}][\text{I}_2]$$

which is also consistent with the experimental findings; the measured rates were independent of added iodide, but this clearly does not rule out the possibility of ionic intermediates.

The activation parameters, $\Delta H_1^\ddagger = 32 \text{ kJ mol}^{-1}$ and $\Delta S_1^\ddagger = -91 \text{ J mol}^{-1} \text{ K}^{-1}$, are typical of those seen for oxidative addition at either one or two metal centres.³⁷⁻⁴⁰ Furthermore, these values are comparable to those reported for halogenation studies of some dinuclear complexes, as well as halogenation of alkenes and alkynes^{41,42} which are viewed as proceeding via halogenonium intermediates (Table 4.4). In the present study, it is not certain whether the parameters refer to reaction via transition states **I** or **II**.

Decomposition of the intermediate, Pd₂I₄(dpm)₂. The kinetics of the decomposition of **10c**, reaction 4.3.2, studied using conventional UV-vis spectroscopy, revealed first- and zero-order dependences on **10c** and I₂, respectively. The observed isosbesticity in these measurements, the absence of any detectable intermediate species in low temperature NMR studies, and the excellent linearity in the Eyring plot indicate a well-behaved system. These results complement those of Hunt and Balch who have studied the reaction of **1** with X₂.² Specifically, reaction of **1c** with I₂ rapidly formed **10c** which underwent slow unimolecular decomposition to give **9c**. From a qualitative assessment of the NMR data, they reported $t_{1/2} = 360 \text{ s}$ at 15 °C in CD₂Cl₂ which compares to $t_{1/2} = 850 \text{ s}$ in CHCl₃ in the present study, determined using the rate constant $k_D = 8.14 \times 10^{-4} \text{ s}^{-1}$ obtained from extrapolation of the k_D values in Table 4.2 to 15 °C. As noted previously in Chapter 3, the rates of reactions in these solvents commonly differ by a factor of 2

Table 4.4. Activation parameters for some halogenation studies of dinuclear metal complexes and unsaturated systems.

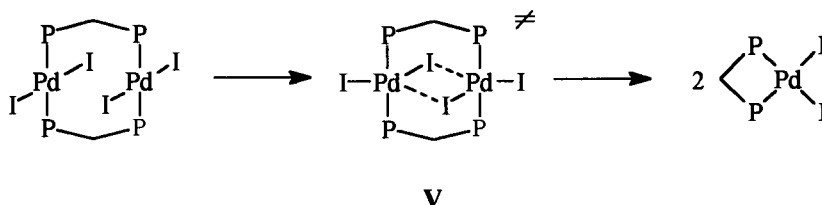
System (ref)	ΔH^\ddagger (kJ mol ⁻¹)	ΔS^\ddagger (J mol ⁻¹ K ⁻¹)
Reaction 4.1.9 (15)	21 - 43	-78 to -120
Reaction 4.1.10 (16c)	28 - 40	-46 to -58
Reaction 4.1.13 (19)	48 - 61	-61 to -122
Alkenes, alkynes (41,42)	20 - 60	-120 to -160

Table 4.5. Polarity (Q) of selected solvents at 25 °C (measured by $(\epsilon-1)/(2\epsilon+1)$ where ϵ is the dielectric constant^{20c}) (see text, p. 172).

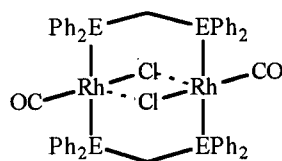
Solvent	Dielectric constant, ϵ	Polarity, Q
CCl ₄	2.24	0.226
CHCl ₃	4.81	0.359
CH ₂ Cl ₂	9.08	0.422
CH ₃ CN	36.2	0.480

with reactions occurring faster in the more polar CH_2Cl_2 . Thus, the findings are in good agreement with those of Hunt and Balch (see later).

Decomposition of **10c** can be envisaged as proceeding via transition state **V**:



It should be noted that structure **V** is a realistic one for **10c**, but the face-to-face dimeric structure is preferred because of the rarity of five-coordinate $\text{Pd}(\text{II})$.² Substitution reactions of square planar, d^8 metal complexes are generally associative rather than dissociative and, as Hunt and Balch have suggested, it is unlikely therefore that **10c** simply fragments by direct Pd-P bond rupture but rather, halide bridges form to give trigonal bipyramidal geometry at the Pd centres prior to Pd-P bond breaking.² Furthermore, the presence of π -bonding phosphines should contribute positively to the transition state as removal of electron density from the metal results in a more positive metal that could more readily accept the entering, fifth ligand.⁴³ That halide bridges could form from **10c** is supported by several examples.² For instance, the complexes $\text{Rh}_2\text{Cl}_2(\text{CO})_2(\mu\text{-dpm or } \mu\text{-dam})_2$ have face-to-face dimeric structures but the Rh coordination planes are so tipped that both Cl^- ligands are folded in towards the adjacent Rh atoms, and molecular models indicate that the formation of halo-bridged structures is entirely reasonable.^{44,45}



$\text{E} = \text{P or As}$

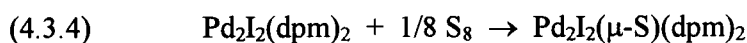
Of note, decomposition of these Rh complexes to monomeric species does not occur; their stabilities are attributed to the weak metal-metal bonding interactions that exist in related Rh(I) dimeric complexes^{21a} and which presumably do not exist in the Pd(II) dimer.

The activation parameters, $\Delta H_D^\ddagger = 80 \text{ kJ mol}^{-1}$ and $\Delta S_D^\ddagger = -26 \text{ J mol}^{-1} \text{ K}^{-1}$, obtained in the present study are consistent with the proposed mechanism. The small entropic change seems reasonable for a unimolecular re-arrangement of **10c** to **V** as the iodide ligands are already in “close vicinity”, while the relatively large enthalpy term probably reflects the energy required to overcome the proximity and strain effects in forming the halide bridges. The proposed mechanism probably also applies to $\text{Pd}_2\text{Br}_4(\text{dpm})_2$ (**10b**) and $\text{Pd}_2\text{Cl}_4(\text{dpm})_2$ (**10a**) but no kinetic measurements for their decompositions are available. Of note, **10a** and **10b** were also observed as intermediates in the reactions of **1a** and **1b** with HCl and HBr, respectively.⁴⁶ Kinetic studies of the reaction of **2b** with Br_2 , presumably proceeding via **10b**, were attempted in the present study but reactivity of Br_2 with the solvent (presumably alkane halogenation)³⁴ interfered with reproducibility of the results. A qualitative NMR study, however, revealed that the bromide system reacts faster than the iodide system; as in many systems, the greater reactivity is commonly attributed to Br_2 being a less selective electrophile than I_2 ,^{20c} and this is reflected in a smaller entropy of activation, for example, for the formation of **10b**.^{20c} Although solvent iodination does not occur,⁴⁷ it seems unlikely that iodine atoms have a role in the system as reaction 4.3.1 also takes place in the absence of light and/or at low temperatures.

Solvent effects. The reaction of **2c** with I_2 was briefly examined in acetonitrile, where again rapid formation and subsequent slow decomposition of the intermediate **10c**, to give the products **9c** and elemental sulfur, were observed. The first stage was not kinetically observable, the formation of

10c occurring too quickly to be amenable for study even by stopped-flow spectroscopy. The second stage, however, was studied using conventional UV-vis spectroscopy, and although isosbesticity was observed indicating a well-behaved system, the rate of decomposition was approximately second-order in **10c**. This finding is not easily rationalized using the limited data available, although reactivity of I₂ with the solvent, as noted previously, could be a contributing factor. Nevertheless, the observed rapidity of the reaction of **2c** with I₂ in acetonitrile in comparison to the rate in CHCl₃ (and CH₂Cl₂) may be due to the increase in solvent polarity (Table 4.5). In general, increase in the polarity of a solvent causes reaction rates to accelerate by stabilizing the charge separation or the development of charges in the transition state (*e.g.* for transition states **II**, **IV**, and **V**).^{20c,48,49} Presumably, the rate of formation of PdI₂(dpm(S)) is similarly affected as this by-product was formed in ~32% yield (*cf.* ~17% in CHCl₃) (see later).

Formation of Pd₂I₂(μ-S)(dpm)₂ (2c**); reaction of Pd₂I₂(dpm)₂ (**1c**) with S₈.** Reaction of **2c** with I₂ produces elemental sulfur, one identification being made by its reaction with **1c** to form only **2c**, as evidenced by NMR spectroscopy (eq. 4.3.4).

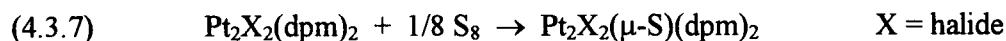
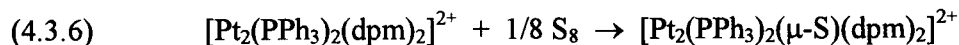


Although extensive studies on this particular reaction were not carried out, there are numerous reports on reactions of transition metal complexes with elemental sulfur⁵⁰ including several studies describing similar chemistry. For example, Balch et al. have studied reaction 4.3.5 for which an X-ray crystal structure of Pd₂Cl₂(μ-S)(dpm)₂ was obtained.⁵¹

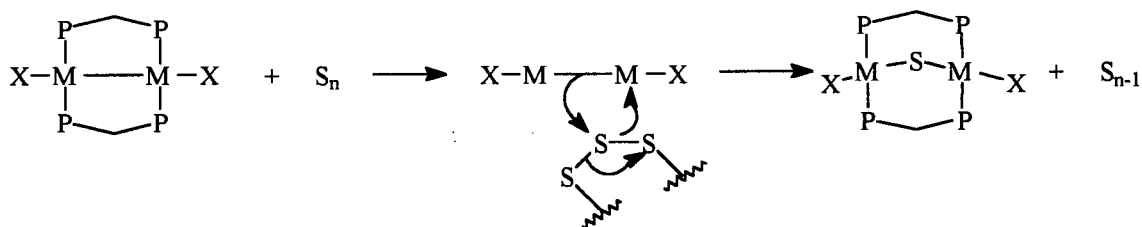


Espenson et al. investigated the A-frame formation reactions of [Pt₂(PPh₃)₂(dpm)₂]²⁺ and Pt₂X₂(dpm)₂ (reactions 4.3.6 and 4.3.7) for which some kinetic and mechanistic studies were

done.^{52,53} They demonstrated that all or nearly all the sulfur atoms of S₈ can be utilized, and suggested that the two reactions have different reaction profiles, with reaction 4.3.6 proceeding via an intermediate containing a monodentate “dangling” dpm ligand and an intact Pt-Pt bond, and reaction 4.3.7 via a transition state with opposite characteristics.



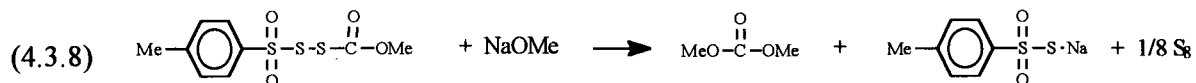
The issue of how S₈ reacts remains unclear although Espenson et al. suggested that sulfur fragments smaller than S₈ (metastable molecules that have been identified (see below)) could also undergo similar insertive reactions; in view of the suggestion that metal - metal bond cleavage occurs in the transition state (*i.e.* there is electron pair transfer out of the metal - metal bond⁵³), the following is a plausible mechanistic scheme with $n \leq 8$ for reactions 4.3.4, 4.3.5, and 4.3.7. The resulting S_{n-1} fragment could undergo yet another insertive reaction.



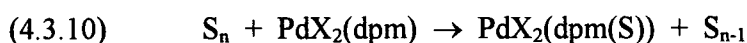
Formation of PdI₂(dpm(S)) (11c). The fate of the sulfur atom produced from the reaction of **2** with X₂ (*i.e.* reaction 4.3.1) is of interest because of the formation of the by-product PdX₂(dpm(S)) observed only in synthetic- and NMR-scale studies. Table 4.3 summarizes the work carried out in part to determine the factors that govern the formation of the by-product.

Mass spectrometry was used in part to identify positively the elemental sulfur produced, the mass spectrum excellently illustrating the ionization pattern with the parent mass peak observed

at 256 m/z and all other peaks at 32 mass units apart (Fig. 4.2). Although the exact mechanism is not known, S_8 is commonly pictured to form via a series of rapid concatenation reactions, possibly through S_1 atoms as recently suggested by Williams and Harpp⁵⁴ in their study of the MeO^- induced decomposition of methoxycarbonylsulfenic 4-toluenethiosulfonic anhydride in 2,3-dimethyl-1,3-butadiene (eq. 4.3.8).



In these studies, diatomic sulfur could not be detected and thus concatenation of monatomic sulfur was proposed; however, frozen-state, ESR spectroscopic investigations in the present study not only failed to detect S_2 but also S_1 or any paramagnetic species. S_1 and S_2 are species which can be detected by ESR spectroscopy, for example, in the gas phase.^{56,57} Nevertheless, as will be seen later, the yield of by-product **11c** results from competition of two reactions, the concatenation reaction to form S_8 , perhaps via monatomic S (eq. 4.3.9), and the reaction of an S_n species ($n < 8$) with $\text{PdX}_2(\text{dpm})$ to form $\text{PdX}_2(\text{dpm}(\text{S}))$ (eq. 4.3.10).

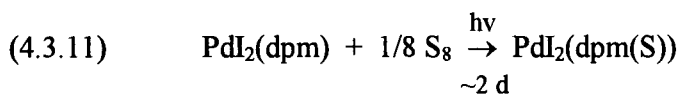


It is noted that in addition to S_1 , S_2 , and S_8 , sulfur species S_3 through S_{26} , including allotropic forms, have been identified and, whereas S_1 through S_5 are stable only in the vapour phase, S_6 , S_7 , and S_9 through S_{26} are metastable cyclic species in solution that eventually (over "considerable" time) convert to the thermodynamically stable S_8 form.^{57,58} In the solid phase, however, S_9 through S_{26} are known to have kinetic stabilities comparable to that of S_8 . Although it is uncertain whether S_6 or S_7 are also present in the $2c + I_2$ system, it is unlikely that sulfur species higher than S_8 are also formed.

The identity of the by-product was established by the reaction of $\text{PdCl}_2(\text{PhCN})_2$ with $\text{dpm}(\text{S})$. Using a 1:1 mole ratio, ligand exchange afforded $\text{PdCl}_2(\text{dpm}(\text{S}))$ (**11a**) from which $\text{PdBr}_2(\text{dpm}(\text{S}))$ (**11b**) and $\text{PdI}_2(\text{dpm}(\text{S}))$ (**11c**) were then obtained using the appropriate halide source. Of note, use of $\text{dpm}(\text{S})$ in excess resulted in formation of the ionic species $[\text{Pd}(\text{dpm}(\text{S}))_2]\text{Cl}_2$ for which an X-ray crystal structure was obtained (see Appendix VII). As with $[\text{Pd}(\text{dpm}(\text{S}))_2]\text{Cl}_2$, the X-ray crystal structures of **11a** and **11c** show coordination of $\text{dpm}(\text{S})$ through the phosphorus and sulfur atoms with the resulting five-membered ring in an envelope configuration (Figs. 4.11 and 4.12). A comparison was made (see Results, p. 158) with the recently reported structure of $\text{RhI}(\text{CO})(\text{dpm}(\text{S}))$, which is the first literature X-ray crystal structure containing a $\text{dpm}(\text{S})$ ligand,²⁹ although the $\text{PdCl}_2(\text{dpm}(\text{S}))$ structure was completed in this thesis work in 1993. There exist examples in the literature of non-structured transition metal complexes containing chelating $\text{dpm}(\text{S})$, as well as chelating $\text{R}_2\text{P}(\text{Y})\text{CH}_2\text{PR}_2$ ligands where one or more phenyl groups are substituted with other alkyl groups, and where $\text{Y} = \text{O}, \text{S}, \text{or Se}$.⁵⁹

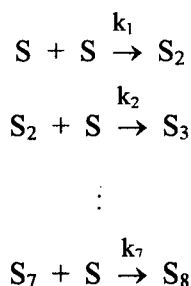
Reaction of $\text{Pd}_2\text{I}_2(\mu\text{-S})(\text{dpm})_2$ (**2c**) with I_2 was explored under various conditions as summarized in Table 4.3, and the yield of the by-product $\text{PdI}_2(\text{dpm}(\text{S}))$ (**11c**) can be satisfactorily explained in terms of the two competing reactions 4.3.9 and 4.3.10. From the non-reactivity of S_8 with **2c**, **9c** (under purely thermal conditions), or **10c**, it follows that an S_n species where $n < 8$ must be responsible. Reaction of **2c** with I_2 at -42°C where **10c** is stable did not yield **11c** after 24 h; **11c** was not observed even when the temperature was raised to R.T. thereafter. Thus, the conclusion here is that S_n does not react with **10c**. S_n also does not react with **2c**, as the by-product yield from reaction with excess **2c** is comparable to that from reactions with equimolar quantities of **2c** and I_2 . The possibility left from this process of elimination is that of reaction S_n with **9c** forms **11c**. Strong support for this suggestion comes from reaction of S_8 with **9c** under photolytic

conditions where **11c** can be quantitatively formed (reaction 4.3.11). In the absence of S_8 , **9c** was found to be unchanged.

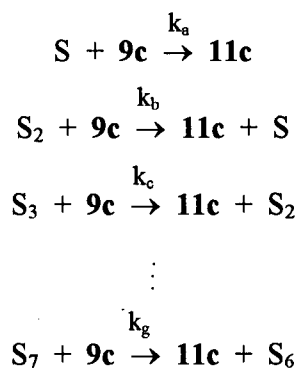


In the present **2c** + I_2 system, some **11c** forms even in the absence of light, and because the Pd-P bond ($\approx 400 \text{ kJ mol}^{-1}$)⁶⁰ is approx. 200 kJ mol^{-1} stronger than the S-S bond,⁵⁷ reaction 4.3.11 presumably proceeds via ring opening^{50j} of S_8 to form a reactive S_n species which then reacts with **9c**. The strong impetus to form S_8 in the competing rapid concatenation reaction 4.3.9 is in keeping with observations that **11c** forms only during the early reaction stages and ceases to form once reaction 4.3.9 is complete even though **9c** continues to form from the decomposition of **10c**.

The results in Table 4.3 can be rationalized semi-quantitatively by considering rates of reaction. Assume that reaction 4.3.9 proceeds via monatomic sulfur:



Reaction 4.3.10 is rewritten to include all possibilities:



A full rate derivation would be extremely complicated; however, two further assumptions can be made. As previously discussed, spectroscopic data reveal elemental sulfur forms very quickly and

intermediate species such as S_1 and S_2 are not observable; furthermore, $11c$ forms only during the early stages (until S_8 is fully formed) and only in minor amounts relative to, for example, elemental sulfur. Thus, it is reasonable to assume that $k_1, k_2, \dots, k_7 \gg k_a, k_b, \dots, k_g$, and that the intermediate species S_1 through S_7 are very reactive and are therefore present at very small concentrations such that the steady state approximation can be applied giving the expression $[S_n] = k_1[S]/k_n$ ($n = 2 - 7$).[†]

The rate of formation of S_8 can then be shown to have the following form:

$$(4.3.12) \quad \text{rate\#1} = k_1[S]^2$$

The rate of formation of $11c$ would be as follows:

$$(4.3.13) \quad \text{rate\#2} = [9c](k_a[S] + k_b[S_2] + k_c[S_3] + \dots + k_g[S_7])$$

Application of $[S_n] = k_1[S]/k_n$ on eq. 4.3.13 gives

$$(4.3.14) \quad \begin{aligned} \text{rate\#2} &= [9c](k_a[S] + (k_b k_1/k_2)[S] + (k_c k_1/k_3)[S] + \dots + (k_g k_1/k_7)[S]) \\ &= k[9c][S], \text{ where } k = k_a + k_b k_1/k_2 + k_c k_1/k_3 + \dots + k_g k_1/k_7 \end{aligned}$$

Eq. 4.3.14 is quite general and easily accommodates any unrealistic possibility (*i.e.* where the rate constant k varies).

Species $9c$ forms from the unimolecular decomposition of $10c$, and thus reaction 4.3.14 can be written as follows:

$$(4.3.15) \quad \text{rate\#2} = k[S](2[10c]_o)(1 - \exp(-kDt))$$

where $[10c]_o$ is the $[10c]$ when it is fully formed (before any appreciable decomposition to $9c$). On consideration of initial rates, eqs. 4.3.14 and 4.3.15 become:

$$(4.3.16) \quad \text{rate\#1}_o = k_1[S]_o^2$$

$$(4.3.17) \quad \text{rate\#2}_o = 2k[S]_o[10c]_o$$

[†] The back reactions (with $k_{-1}, k_{-2}, \dots, k_{-7}$) are not considered. For further explanation of the steady state approximation as it applies here, see Frost, A.A.; Pearson, R.G. "Kinetics and Mechanism, 2nd Ed.", John Wiley & Sons, London, 1963, ch. 8, p. 172.

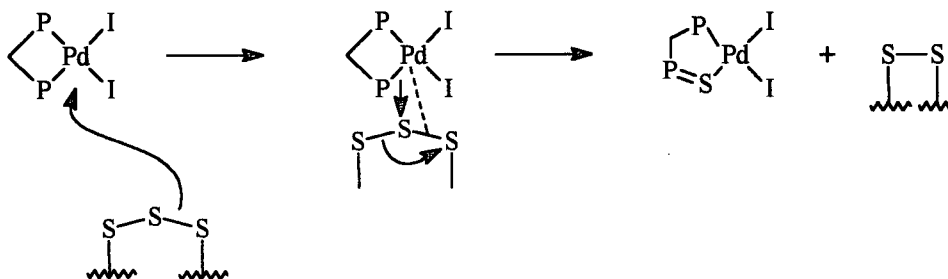
where $[S]_o$ is the initial (total) concentration of monatomic S. Eliminating $[S]_o$ from eqs. 4.3.16 and 4.3.17 gives the following ratio (R).

$$(4.3.18) \quad R = [(\text{rate}\#1_o)^{1/2}/[\text{rate}\#2_o]] = k_1^{1/2}/(2k[10c]_o)$$

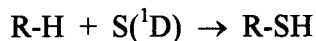
Hence, on using lower concentration conditions (*i.e.* proceeding from synthetic- to NMR- to kinetic-scale studies), R increases as $[10c]_o$ decreases, and lower yields of by-product are observed (with correspondingly higher yields of elemental sulfur). For the bromide system, the higher by-product yield could be explained by higher k values (*i.e.* reaction 4.3.10 proceeds at a greater rate), although the greater decomposition rate of **10b** (relative to that of **10c**) could be a contributing factor. In acetonitrile, the rates of both reactions 4.3.9 and 4.3.10 are perhaps similarly affected (*i.e.* increased) but because of the square root factor, R decreases overall and the yield of **11c** increases. Finally, in the reaction of $\text{Pd}_2\text{I}_2(\mu\text{-SO})(\text{dpm})_2$ with I_2 , which also presumably proceeds via the intermediate **10c**, R decreases perhaps because the rate of reaction 4.3.9 decreases because of the slower decomposition of the free SO species (which gives elemental sulfur and dioxygen⁶¹).

It is interesting to note that while the presence of O_2 has no effect on the yield of **11c**, excess amounts of I_2 result in its lack of formation. For example, in an NMR-scale reaction of **2c** with 2 mole equivalents of I_2 , **11c** was not observed to form and the only Pd species seen was the **9c** product. Iodine exhibits no reactivity with **11c** or with S_8 , and thus the absence of **11c** can be attributed to a scavenging process by I_2 for an S_n species to form, for example, the known iodosulfanes, S_nI_2 where $n \geq 2$.⁶² Presumably, this scavenging process also takes place (in addition to reactivity with the solvent) in the bromide system and probably at a greater rate, as unreacted **2b** is observed despite equimolar conditions.

Although speculative, the mechanism for the formation of **11c** could resemble that for reaction 4.3.4, the reaction proceeding via initial nucleophilic attack of an S_n species at the Pd centre and the resulting S_{n-1} species undergoing yet another insertive reaction.



It is unlikely that **11c** forms simply by insertion of monatomic sulfur into the Pd-P bond as reactions of this type usually require excited sulfur atoms, $S(^1D)$, commonly generated under photolytic conditions (*e.g.* by photolysis of COS).⁶³ $S(^1D)$ insertion reactions are known; for example, the gas- or liquid-phase photolysis of COS in the presence of alkanes produces thiol products.⁶⁴



In the present study, ground state sulfur atoms, $S(^3P)$, are probably formed, but these have been shown to be inert toward such insertive reactions.⁶³ Rather, it is surmised that reaction 4.3.10 proceeds as a result of the torsional strain that cyclic S_n species are known to have,⁵⁷ although involvement of chain-like S_n reactive species cannot be discounted.⁶⁵ Why a second insertion reaction does not occur to form, for example, $\text{PdI}_2(\text{dpm}(\text{S})_2)$ is unclear. Perhaps the energetics favour a five-membered ring as opposed to a six-membered ring that might contain axial phenyl group interactions; in the X-ray crystal structure of **11c** (Fig. 4.11), the axial phenyl groups are seen to be positioned away from one another:



Synthesis of $\text{PdCl}_2(\text{dpm}(\text{S})_2)$, by reaction of $\text{PdCl}_2(\text{PhCN})_2$ with $\text{dpm}(\text{S})_2$, was attempted but because of thermal instability of the product, its identity has not been unequivocally established. Of note, transition metal complexes containing chelating $\text{dpm}(\text{S})_2$ as well as $\text{dpm}(\text{Se})_2$ are known.^{59c,72}

4.4 Experimental section

The materials used, synthetic procedures for the ligands and complexes, and instrumentation used for ^1H and $^{31}\text{P}\{^1\text{H}\}$ NMR, ESR, and UV/vis spectra, were described in Chapter 2. $\text{Dpm}(\text{S})$, $\text{dpm}(\text{S})_2$, and the complexes $\text{PdCl}_2(\text{PhCN})_2$, $\text{Pd}_2(\text{dba})_3\cdot\text{CHCl}_3$, $\text{Pd}_2\text{I}_2(\mu\text{-SO})(\text{dpm})_2$, **1a - 1c**, **2a - 2c**, and **9a - 9c** were synthesized using published methods as outlined in Chapter 2. All experiments were performed under N_2 unless otherwise specified.

4.4.1 Preparation of $\text{PdCl}_2(\text{dpm}(\text{S}))$ (**11a**)

$\text{PdCl}_2(\text{PhCN})_2$ (0.10 g, 0.26 mmol) and $\text{dpm}(\text{S})$ (0.11 g, 0.26 mmol) were stirred in CH_2Cl_2 (20 mL) at room temperature (R.T.). Within several minutes, the colour changed from an initial yellow to a final orange with accompanying precipitation of a yellow solid. Stirring was continued for 1 h before the volume was reduced to ~ 10 mL to complete the precipitation. The yellow solid was filtered off, washed with Et_2O (2 x 10 mL), and dried *in vacuo*; yield 0.15 g (97%). ^1H NMR (20 °C, CDCl_3): δ 7.0 - 8.0 m (20H, Ph), δ 4.07 p.t (2H, CH_2). $^{31}\text{P}\{^1\text{H}\}$ NMR (20 °C, CDCl_3): δ 54.9, 30.9 (AB pattern, $J_{\text{PP}} = 18.3$ Hz). UV/vis: λ : 372 (1500). Anal. Calcd for $\text{C}_{25}\text{H}_{22}\text{Cl}_2\text{P}_2\text{PdS}$: C, 50.57; H, 3.73. Found: C, 50.56; H, 3.74. Crystals of the complex were grown via diffusion of hexanes (10 mL) or Et_2O (10 mL) into a 6 mL CH_2Cl_2 solution of 10 mg **11a** at R.T., and subjected to X-ray crystallographic analysis.

4.4.2 Preparation of PdBr₂(dpm(S)) (11b)

PdCl₂(dpm(S)) (0.10 g, 0.17 mmol) was dissolved in ~20 mL CH₂Cl₂ and a solution of ⁿPr₄NBr (0.67 g, 2.52 mmol) in CH₂Cl₂ added. The solution which instantly turned yellow-red was stirred at R.T. for 1 h before the volume was reduced to ~10 mL. Et₂O (2 x 10 mL) was added to precipitate a yellow-red solid which was filtered off and washed with a Et₂O/CH₂Cl₂ mixture (2 x 10 mL; 60:40 by volume Et₂O:CH₂Cl₂) followed by Et₂O (2 x 10 mL). The resulting yellow solid was then dried *in vacuo*; yield 0.110 g (96%). ¹H NMR (20 °C, CDCl₃): δ 7.0 - 8.0 m (20H, Ph), δ 4.02 p.t (2H, CH₂). ³¹P{¹H} NMR (20 °C, CDCl₃): δ 56.6, 32.1 (AB pattern, J_{PP} = 20.4 Hz). UV/vis: λ : 396(2180), 374 sh (2095). Anal. Calcd for C₂₅H₂₂Br₂P₂PdS•CH₂Cl₂: C, 40.68; H, 3.15. Found: C, 41.23; H, 3.11. Despite repeated drying procedures, the CH₂Cl₂ solvent as evidenced by ¹H NMR spectroscopy was not removed.

4.4.3 Preparation of PdI₂(dpm(S)) (11c)

PdCl₂(dpm(S)) (0.10 g, 0.17 mmol) was dissolved in ~20 mL CH₂Cl₂ and a solution of ⁿBu₄NI (0.93 g, 2.52 mmol) in CH₂Cl₂ added. The remainder of the procedure is as for **11b**. Yield 0.13 g (97%). ¹H NMR (20 °C, CDCl₃): δ 7.0 - 8.0 m (20H, Ph), δ 3.71 p.t (2H, CH₂). ³¹P{¹H} NMR (20 °C, CDCl₃): δ 61.1, 31.3 (AB pattern, J_{PP} = 25.5 Hz). UV/vis: λ : 478(3000), 420 sh (1735). Anal. Calcd for C₂₅H₂₂I₂P₂PdS•0.5CH₂Cl₂: C, 37.39; H, 2.83. Found: C, 36.88; H, 2.73. A brown crystal of the complex, obtained by diffusion of hexanes (10 mL) into a 6 mL CH₂Cl₂ solution of 10 mg **11c** at R.T., was analyzed using X-ray crystallography.

4.4.4 Preparation of PdCl₂(dpm(S)₂)

PdCl₂(PhCN)₂ (0.10 g, 0.26 mmol) and dpm(S)₂ (0.12 g, 0.26 mmol) were stirred in CH₂Cl₂ (10 mL) at R.T. The colour of the solution immediately changed from an initial yellow to a final orange-red. After a few minutes; the initially clear solution turned cloudy with accompanying precipitation of an orange-red solid. The reaction mixture was stirred for 1 h before Et₂O (20 mL) was added to complete the precipitation. The solid was filtered off, washed with Et₂O (2 x 10 mL), and dried *in vacuo*; yield 0.13 g (80%). This compound is not thermally stable; attempts to dry it, for example at 40 °C, resulted in its decomposition as evidenced by NMR measurements. Furthermore, the compound has limited solubility in CH₂Cl₂ and CHCl₃ but is soluble in DMSO. ¹H NMR (20 °C, DMSO-d₆): δ 7.0 - 8.0 (20H, Ph), δ 5.54 t (2H, CH₂, J_{PH} = 14 Hz). ³¹P{¹H} NMR (20 °C, DMSO-d₆): δ 37.3 s. UV/vis (20 °C, CH₂Cl₂): λ: 418 (1.0), 322 (13.5) (relative intensities).

4.4.5 Kinetic studies

a) Conventional UV-vis measurements. The kinetics of the slow decomposition of the intermediate, Pd₂I₄(dpm)₂ (**10c**) (formed from **2c**, see below), in CHCl₃ were spectrophotometrically monitored in a stoppered thermostated quartz cell (volume 1.5 mL). A 1.00 mL solution of **2c** of appropriate concentration was placed in the cell and thermostated at the required temperature (20 - 35 °C). A 0.050 mL solution of iodine was injected and the cell was briefly shaken to ensure complete mixing prior to monitoring optical density changes at some appropriate, fixed wavelength (396 nm). The concentration of **2c** ranged from (1.6 - 9.9) x 10⁻⁵ M,

and that of I₂ from $(3.8 - 7.5) \times 10^{-4}$ M; pseudo-first-order conditions were maintained and standard log (absorbance difference) vs. time plots gave excellent linearity for at least 2.5 - 3 half-lives. The pseudo-first-order rate constants, k_{obs} , were readily evaluated from the semi-log plots or were automatically calculated by means of a direct mathematical function fit of the actual data by the quantification software provided (see Chapter 2).

Corresponding kinetic measurements in acetonitrile were conducted at 23.5 °C using a 1:1 mole ratio of **2c** (9.4×10^{-5} M) to I₂ (9.4×10^{-5} M). Optical density changes were monitored at 360 nm.

b) Stopped-flow measurements. The kinetics of the rapid formation of the intermediate, Pd₂L₄(dpm)₂ (**10c**), in CHCl₃ were measured spectrophotometrically using a stopped-flow apparatus. Two 1-mL loading syringes were filled with solutions of the appropriate concentrations of **2c** and I₂, respectively (as noted above in (a)), and thermostated at the required temperature (20 - 35 °C). Optical density changes were monitored at a fixed wavelength of 510 nm (an isosbestic point **only** with respect to the decomposition of the intermediate). Reported pseudo-first-order rate constants were determined from the average of four replicate experiments using a standard non-linear regression algorithmic fitting equation provided by the accompanying kinetic software (see Chapter 2).

4.4.6 Mechanistic studies

a) NMR-scale. The sulfur abstraction reaction (**2c** → **9c**, eq. 4.1.1) in CDCl₃ was monitored at R.T. using ¹H and ³¹P{¹H} NMR spectroscopy. A 0.10 mL solution of I₂ (0.002 g, 0.0079 mmol)

was injected into a septum-sealed NMR tube with a 0.40 mL solution of **2c** (0.010 g, 0.0079 mmol). The sample was briefly shaken to ensure complete mixing before being placed in the NMR probe; spectra were recorded approx. every 10 min for 1 h. Variable temperature NMR-scale experiments also were performed at -42, 0, 20, 40, and 80 °C under anaerobic (*i.e.* vacuum) and aerobic (*i.e.* 1 atm air or 1 atm O₂) conditions. In a typical experiment here, **2c** (0.010 g, 0.0079 mmol) and I₂ (0.0020 g, 0.0079 mmol) were placed in an NMR tube fitted with a PTFE (poly(tetrafluoroethylene)) J. Young valve (Aldrich) and ~0.5 mL CDCl₃ was vacuum transferred using liquid N₂. The sample was then briefly placed in a dry ice / acetonitrile bath (-42 °C)⁶⁶ to ensure complete mixing of reactants before being placed in the appropriate constant temperature bath for 24 h prior NMR analysis. The O₂/air dependence was examined only at R.T. The reaction was also examined at low temperatures; the samples were prepared by the simultaneous injection of equal volumes (0.25 mL) of equimolar solutions of **2c** and I₂ at R.T. into NMR or ESR tubes held at -42, -78, or -196 °C. Spectroscopic analyses at the respective temperatures were performed “immediately” and (for NMR spectroscopic analyses) after periods of approx. 2 min for a total of ~30 min. Finally, the reaction was investigated using different stoichiometric ratios of **2c** to I₂. Specifically, 1:2 **2c** (0.010 g, 0.0079 mmol) to I₂ (0.0040 g, 0.016 mmol) and 1:0.5 **2c** (0.010 g, 0.0079 mmol) to I₂ (0.010 g, 0.0040 mmol) ratios of reactants were studied in CDCl₃ (~0.5 mL) at R.T. with NMR spectroscopic analyses performed after 24 h.

Corresponding NMR studies in acetonitrile were conducted at R.T. using a 1:1 mole ratio. Because **2c** has limited solubility in CD₃CN, at best ~8 x 10⁻⁴ M concentrations can be achieved (*e.g.* 0.5 mg (3.9 x 10⁻³ mmol) in ~0.5 mL CD₃CN). A 0.10 mL solution of I₂ (0.1 mg, 3.9 x 10⁻³ mmol) was injected, and the sample was analyzed “immediately” and after periods of approx. 5 min for a total time of ~30 min.

The bromide system (**2b** → **9b**) was briefly examined at R.T. in CDCl₃. To a 0.50 mL solution of **2b** (0.010 g, 0.0085 mmol) placed in an NMR tube fitted with a PTFE J. Young valve was added Br₂ (0.44 μL, 0.0085 mmol) via vacuum transfer. The sample was analyzed after 1 h.

TLC studies of each NMR sample were carried out using CHCl₃ eluent to analyze for elemental sulfur (see below).

b) Synthetic-scale. Schlenk techniques were employed, the iodo complex **2c** (0.050 g, 0.039 mmol) being reacted with I₂ (0.010 g, 0.039 mmol) in 20 mL of CHCl₃; the reaction was monitored by UV-vis spectroscopy. After 24 h, the supernatant red liquid was decanted off leaving a pale yellow solid. The solid was washed with acetone (2 x 10 mL) and dried *in vacuo* before being collected (yield ~0.001 g), and then analyzed using mass spectrometry (electron impact), UV-vis spectroscopy (Et₂O), and thin-layered chromatography (CHCl₃ eluent). The results were compared with those of an authentic sample of elemental sulfur. The solvent was removed under vacuum from the supernatant and the resulting red-orange solid (**9c**) was dried *in vacuo* prior to ¹H and ³¹P{¹H} NMR analyses in CDCl₃. A similar experiment was also performed where the concentrations of **2c** and I₂ were the same as those used in the UV-vis or stopped-flow studies; specifically, **2c** (0.005g, 0.0039 mmol) and I₂ (0.001g, 0.0039 mmol) were reacted in 40 mL of CHCl₃.

c) Reaction of Pd₂I₂(dpm)₂ (1c**) with sulfur.** Reaction of **1c** with elemental sulfur was carried out in CDCl₃ on the NMR-scale whereby a 0.20 mL solution of sulfur (0.13 mg, 0.0040 mmol) was injected into a septum-sealed NMR tube containing a 0.30 mL solution of **1c** (5.0 mg, 0.0040 mmol). The sample was analyzed “immediately”, 1 h, and 24 h after preparation by NMR

spectroscopy. Reaction of **1c** with the yellow solid obtained from **(b)** above was carried out in an analogous way except the solid (~1 mg) was directly added to a 0.50 mL solution of **1c**.

d) NMR-scale examination of the reaction of PdI₂(dpm) (9c**) with sulfur.** Possible reaction between PdI₂(dpm) (**9c**) and sulfur was studied in CDCl₃ at 20, 50, and 90 °C under purely thermal or photolytic conditions. Samples were prepared under vacuum in NMR tubes fitted with J. Young valves: **9c** (0.0050 g, 0.0067 mmol) was placed in the NMR tube with a 10-fold excess of elemental sulfur (0.0022 g), and ~0.5 mL of CDCl₃ was vacuum transferred using liquid N₂. The samples were then left at the appropriate temperatures for 24 h prior to NMR analyses. Photolysis was carried out only at 20 °C where the samples were irradiated for periods up to 2 d using a medium pressure Hg vapour lamp (450 W).

e) NMR-scale examination of the reaction of Pd₂I₄(dpm)₂ (10c**), with sulfur.** A 0.30 mL CDCl₃ solution of Pd₂I₂(dpm)₂ (**1a**) (0.0050 g, 0.0040 mmol) was prepared in a septum-sealed NMR tube at -42 °C and a 0.20 mL CDCl₃ solution of I₂ (0.0010 g, 0.0040 mmol) was injected in. The sample was shaken and maintained at -42 °C for 15 h to permit complete conversion to **10c** (as monitored by NMR spectroscopy). A 0.050 mL CDCl₃ solution of sulfur (0.0001 g, 0.004 mmol) was then injected and the mixture shaken and held at -42 °C for another 24 h prior to NMR analysis. The sample was then placed at R.T. for 24 h, and re-analyzed.

f) NMR-scale examination of the reaction of Pd₂I₂(μ-SO)(dpm)₂ with I₂. Reaction of Pd₂I₂(μ-SO)(dpm)₂ with I₂ was carried out in CDCl₃ whereby a 0.20 mL solution of I₂ (0.0020 g, 0.0078 mmol) was injected into a septum-sealed NMR tube containing a 0.30 mL solution of Pd₂I₂(μ-

SO)(dpm)₂ (0.010 g, 0.0078 mmol). The sample was analyzed “immediately”, 1 h, and 24 h after preparation by NMR spectroscopy. TLC studies were carried out thereafter to analyze for elemental sulfur.

4.4.7 X-ray crystallographic analysis of PdI₂(dpm(S))•0.5CH₂Cl₂

A single crystal having approx. dimensions of 0.05 x 0.20 x 0.30 mm was mounted in a glass capillary. All intensity measurements were made on a Rigaku AFC6S diffractometer with graphite monochromated Mo-K α radiation ($\lambda = 0.71069 \text{ \AA}$). Accurate cell constants along with orientation matrices were obtained from a least squares refinement of the setting angles of 25 reflections in the range $14.2 < 2\theta < 24.7^\circ$. Intensity data were collected at 21 °C using the ω -2 θ scan technique. The intensities of 3 representative reflections were measured after every 200 reflections and no decay correction was applied. The data were corrected for Lorentz and polarization effects. The structure was solved by direct methods⁶⁷ and expanded using Fourier techniques.⁶⁸ The CH₂Cl₂ solvent is disordered about a centre of symmetry - the disorder was modeled by a single 0.5 occupancy carbon atom and 3 partially occupied Cl sites. The solvent C atom and 2 of the Cl atoms were refined with isotropic thermal parameters. Hydrogen atoms associated with the metal complex were fixed in calculated positions with C-H = 0.98 Å. Neutral atom scattering factors⁶⁹ and anomalous dispersion terms⁷⁰ were taken from the usual sources. All calculations were performed using TEXSAN.⁷¹

4.5 References for Chapter 4

1. Wong, T.Y.H.; Barnabas, A.F.; Sallin, D.; James, B.R. *Inorg. Chem.* **1995**, *34*, 2278.
2. Hunt, C.T.; Balch, A.L. *Inorg. Chem.* **1981**, *20*, 2267.
3. a) Noack, K. *Helv. Chim. Acta* **1962**, *45*, 1847. b) Mittasch, A. *Angew. Chem.* **1928**, *41*, 827.
4. Calderazzo, F.; L'Eplattenier, F. *Inorg. Chem.* **1967**, *6*, 1220.
5. a) Colton, R.; Tomkins, I.B. *Austral. J. Chem.* **1966**, *19*, 1143. b) Ankes, M.W.; Colton, R.; Tomkins, I.B. *Austral. J. Chem.* **1967**, *20*, 9.
6. a) Abel, E.W.; Wilkinson, G. *J. Chem. Soc.* **1959**, 1501. b) Brimm, E.O.; Lynch, M.A.; Sesny, W.J. *J. Am. Chem. Soc.* **1954**, *76*, 3831.
7. Hileman, J.C.; Huggins, D.K.; Kaesz, H.D. *Inorg. Chem.* **1962**, *1*, 933.
8. Hieber, W.; Schuk, R.; Fuchs, H.Z. *Anorg. Chem.* **1941**, 248, 243.
9. Cotton, F.A.; Johnson, B.F.G. *Inorg. Chem.* **1967**, *6*, 2113.
10. Johnson, B.F.G.; Johnston, R.D.; Josty, P.L.; Lewis, J.; Williams, I.G. *Nature* **1967**, *213*, 901.
11. Johnson, B.F.G.; Lewis, J. *J. Chem. Soc. (A)* **1968**, 2859.
12. Cook, N.; Smart, L.; Woodward, P. *J. Chem. Soc., Dalton Trans.* **1977**, 1744.
13. a) Noack, K.J. *Organomet. Chem.* **1968**, *13*, 411. b) Faron, M.F.; Camp, G.R. *Inorg. Chim. Acta* **1969**, *3*, 395. c) Dobson, G.R.; Jernigan, R.T.; Chang, P.-T. *J. Organomet. Chem.* **1973**, *54*, C33.
14. a) Haines, L.I.B.; Hopgood, D.; Poe, A.J. *J. Chem. Soc. (A)* **1968**, 421. b) Haines, L.I.B.; Poe, A.J. *J. Chem. Soc. (A)* **1969**, 2826.
15. a) Kramer, G.; Patterson, J.; Poe, A.J. *J. Chem. Soc., Dalton Trans.* **1979**, 1165. b) Kramer, G.; Patterson, J.; Poe, A.J.; Ng, L. *Inorg. Chem.* **1980**, *19*, 1161.
16. a) Crow, J.P.; Cullen, W.R.; Hou, F.L. *Chem. Commun.* **1971**, 1229. b) Crow, J.P.; Cullen, W.R.; Hou, F.L. *Inorg. Chem.* **1972**, *11*, 2125. c) Cullen, W.R.; Hou, F.L. *Inorg. Chem.* **1975**, *14*, 3121.
17. Haines, R.J.; du Preez, A.L. *J. Chem. Soc. (A)* **1970**, 2341.
18. Kramer, G.; Poe, A.J.; Amer, S. *Inorg. Chem.* **1981**, *20*, 1362.

19. Bott, R.W.; Eaborn, C.; Waters, J.A. *J. Chem. Soc.* **1963**, 681.
20. a) Chipperfield, J.R.; Ford, I.; Webster, D.E. *J. Chem. Soc., Dalton Trans.* **1975**, 2042. b) Chipperfield, J.R.; Hayter, A.C.; Webster, D.E. *J. Chem. Soc., Dalton Trans.* **1975**, 2048. c) Chipperfield, J.R.; Ford, J.; Hayter, A.C.; Lee, D.J.; Webster, D.E. *J. Chem. Soc., Dalton Trans.* **1976**, 1024.
21. a) Balch, A.L. *J. Am. Chem. Soc.* **1976**, 98, 8049. b) Balch, A.L.; Tulyathan, B. *Inorg. Chem.* **1977**, 16, 2840.
22. Faraone, F.; Bruno, G.; Schiavo, S.L.; Bombieni, G. *J. Chem. Soc., Dalton Trans.* **1984**, 533.
23. Oro, L.A.; Carmona, D.; Perez, P.L.; Esteban, M.; Tiripicchio, A.; Tiripicchio-Camellini, M. *J. Chem. Soc., Dalton Trans.* **1985**, 973.
24. Hanson, B.E.; Fanwick, P.E.; Mancini, J.S. *Inorg. Chem.* **1982**, 21, 3811.
25. Colombie, A.; Lavigne, G.; Bonnet, J.-J. *J. Chem. Soc., Dalton Trans.* **1986**, 899.
26. Schmidbauer, H.; Franke, R. *Inorg. Chim. Acta* **1975**, 13, 85.
27. Farrar, D.H.; Grundy, K.R.; Payne, N.C.; Roper, W.R.; Walker, A. *J. Am. Chem. Soc.* **1979**, 101, 6577.
28. Corbridge, D.E.C. "The Structure Chemistry of Phosphorus", Elsevier, Amsterdam, 1974, p. 7.
29. Baker, M.J.; Giles, M.F.; Orpen, A.G.; Taylor, M.J.; Watt, R.J. *J. Chem. Soc., Chem. Commun.* **1995**, 197.
30. Berry, D.E.; Browning, J.; Dixon, K.R.; Hitts, R.W. *Can. J. Chem.* **1988**, 66, 1272.
31. Balakrishna, M.S.; Klein, R.; Uhlenbrock, S.; Pinkerton, A.A.; Cavell, R.G. *Inorg. Chem.* **1993**, 32, 5676.
32. Appleton, T.G.; Clark, H.C.; Manzer, L.E. *Coord. Chem. Rev.* **1973**, 10, 335.
33. Zumdahl, S.S.; Drago, R.S. *J. Am. Chem. Soc.* **1968**, 90, 6669.
34. See for example: a) Streitwieser, Jr., A.; Heathcock, C.H. "Introduction to Organic Chemistry, 3rd Ed.", Macmillan, New York, 1985, ch. 6. b) Morrison, R.T.; Boyd, R.N. "Organic Chemistry, 3rd Ed.", Allyn and Bacon, Boston, 1973, ch. 3.

35. Permutter-Hayman, B. *Progr. Inorg. Chem.* **1976**, *20*, 229.
36. Basolo, F.; Pearson, R.B. "Mechanisms of Inorganic Reactions", Wiley, New York, 1967, pp. 351-453.
37. Vaska, L. *Acc. Chem. Res.* **1968**, *1*, 335.
38. Collman, J.P.; Roper, W.R. *Adv. Organomet. Chem.* **1968**, *7*, 54.
39. Halpern, J. *Pure Appl. Chem.* **1969**, *20*, 59.
40. a) Barnabas, A.F.; Sallin, D.; James, B.R. *Can. J. Chem.* **1989**, *67*, 2009. b) Xie, L.Y.; James, B.R. *Inorg. Chim. Acta* **1994**, *217*, 209.
41. Pincock, J.A.; Yates, K. *Can. J. Chem.* **1970**, *48*, 3332.
42. Pincock, J.A.; Yates, K. *Can. J. Chem.* **1970**, *48*, 2944.
43. a) Chatt, J.; Duncanson, L.A.; Venanzi, L.M. *J. Chem. Soc.* **1955**, 4456. b) Orgel, L.E. *J. Inorg. Nucl. Chem.* **1956**, *2*, 137.
44. Cowie, M.; Dwight, S.K. *Inorg. Chem.* **1980**, *19*, 3500.
45. Mague, J.T. *Inorg. Chem.* **1969**, *8*, 1975.
46. Barnabas, A.F. M.Sc. Dissertation, University of British Columbia, Vancouver, 1989.
47. Meislich, H.; Nechamkin, H.; Sharefkin, J. "Theory and Problems of Organic Chemistry, 2nd Ed.", McGraw-Hill, Toronto, 1991, ch. 4, p. 57.
48. Carey, F.A.; Sundberg, R.J. "Advanced Organic Chemistry, 3rd Ed. Part A: Structure and Mechanisms", Plenum Press, New York, 1993, ch. 4, p. 232.
49. Koppel, I.A.; Palm, V.A. "Advances in Linear Free Energy Relationships", N.B. Chapman and J. Shorter, Eds., Plenum Press, London, 1972, ch. 5.
50. See for example: a) Piper, T.S.; Wilkinson, G. *J. Am. Chem. Soc.* **1956**, *78*, 900. b) Khattab, S.A.; Marko, L.; Bor, G.; Marko, B. *J. Organomet. Chem.* **1964**, *1*, 373. c) Schunn, R.A.; Fritchie, Jr., C.J.; Prewitt, C.T. *Inorg. Chem.* **1966**, *5*, 892. d) Schrauzer, G.N.; Mayweg, V.P.; Finck, H.W.; Heinrich, W. *J. Am. Chem. Soc.* **1966**, *88*, 4604. e) Fackler, Jr., J.P.; Coucouvanis, D.; Fetchin, J.A.; Seidel, W.C. *J. Am. Chem. Soc.* **1968**, *90*, 2784. f) Balch, A.L. *J. Am. Chem. Soc.* **1969**, *91*, 6962. g)

- Epstein, E.F.; Bernal, I. *J. Organomet. Chem.* **1971**, *26*, 229. h) Ginsberg, A.P.; Lindsell, W.E. *Chem. Commun.* **1971**, 232. i) Giannotti, C.; Fontaine, C.; Septe, B.; Doue, D. *J. Organomet. Chem.* **1972**, *39*, C74. j) Giannotti, C.; Ducourant, A.M.; Chanaud, H.; Chiaroni, A.; Riche, C. *J. Organomet. Chem.* **1977**, *140*, 289, and references therein.
51. Balch, A.L.; Benner, L.S.; Olmstead, M.M. *Inorg. Chem.* **1979**, *18*, 2996.
52. Muralidharan, S.; Espenson, J.H. *J. Am. Chem. Soc.* **1984**, *106*, 8104.
53. Muralidharan, S.; Espenson, J.H.; Ross, S.A. *Inorg. Chem.* **1986**, *25*, 2557.
54. Williams, C.R.; Harpp, D.N. *Sulfur Lett.* **1993**, *16*, 63.
55. Brown, R.L. *J. Chem. Phys.* **1966**, *44*, 2827.
56. Wayne, F.D.; Davies, P.B.; Thrush, B.A. *Mol. Phys.* **1974**, *28*, 989.
57. Meyer, B. *Chem. Rev.* **1976**, *76*, 367.
58. Laitinen, R.S.; Pekonen, P.; Suontamo, R.J. *Coord. Chem. Rev.* **1994**, *130*, 1.
59. See for example: a) Grim, S.O.; Walton, E.D. *Inorg. Chem.* **1980**, *19*, 1982. b) Lusser, M.; Peringer, P. *Inorg. Chim. Acta* **1987**, *127*, 151. c) Bond, A.M.; Colton, R.; Ebner, J.; Ellis, S.R. *Inorg. Chem.* **1989**, *28*, 4509, and references therein.
60. Although a value for the Pd-P bond strength cannot be found, the bond energy is probably comparable to that of the Pt-P bond (417 kJ mol^{-1}). See, for example, Smoes, S.; Huguet, R.; Drowart, J. *Z. Naturforsch Teil A*, **1971**, *26*, 1934.
61. Meyer, B.; Jensen, D.; Oommen, T. "Sulfur in Organic and Inorganic Chemistry, Vol. 2", A. Senning, Ed., Marcel Dekker, New York, 1972, ch. 12.
62. Johnson, D.A. "Sulfur in Organic and Inorganic Chemistry, Vol. 2", A. Senning, Ed., Marcel Dekker, New York, 1972, ch. 13.
63. Strausz, O.P. "Sulfur in Organic and Inorganic Chemistry, Vol. 2", A. Senning, Ed., Marcel Dekker, New York, 1972, ch. 11.
64. Gunning, H.E.; Strausz, O.P. *Adv. Photochem.* **1966**, *4*, 143.
65. Schumann, H. "Sulfur in Organic and Inorganic Chemistry, Vol. 3", A. Senning, Ed., Marcel

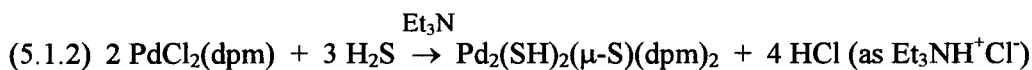
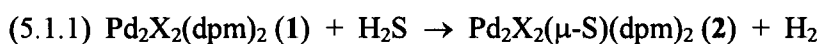
- Dekker, New York, 1972, ch. 21.
66. Gordon, A.J.; Ford, R.A. "The Chemist's Companion", John Wiley & Sons, Toronto, 1972, p. 451.
67. SIR92: Altomare, A.; Burla, M.C.; Camalli, M.; Cascarano, M.; Giacovazzo, C.; Guagliardi, A.; Polidori, G. *J. Appl. Cryst.*, in preparation.
68. DIRDIF92: Beurskens, P.T.; Admiraal, G.; Beurskens, G.; Bosman, W.P.; Garcia-Granda, S.; Gould, R.O.; Smits, J.M.M; Smykall, C. "The DIFDIF program system, Technical Report of the Crystallography Laboratory", University of Nijmegen, The Netherlands.
69. Cromer, D.T.; Waber, J.T. "International Tables for X-ray Crystallography, Vol. 4", The Kynoch Press, Birmingham, England, 1974, Table 2.2A.
70. Ibers, J.A.; Hamilton, W.C. *Acta Crystallogr.* **1964**, *17*, 781.
71. TEXSAN: Crystal Structure Analysis Package, Molecular Structure Corporation (1985 & 1992).
72. Peringer, P.; Schwald, J. *J. Chem. Soc., Chem. Commun.* **1986**, 1625.

CHAPTER 5

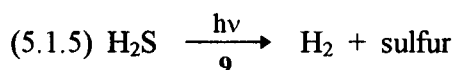
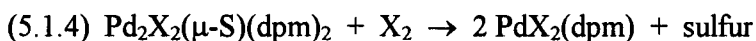
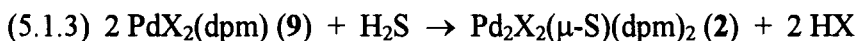
**Preliminary Studies on the Reaction of $\text{PdX}_2(\text{dpm})$ with H_2S in Dimethylsulfoxide;
Formation of $\text{Pd}_2\text{X}_2(\mu\text{-S})(\text{dpm})_2$**

5.1 Introduction

Previously in this laboratory, during investigations of the sulfur abstraction from H₂S with the Pd₂X₂(dpm)₂ complexes (**1**) (X = halide) (reaction 5.1.1), the mononuclear, Pd(II) complexes PdX₂(dpm) (**9**) were tested for reactivity toward H₂S. It was discovered that in benzene or in CH₂Cl₂, reaction of PdCl₂(dpm) (**9a**) with H₂S proceeded only in the presence of a base, for example Et₃N, to form the dinuclear complex Pd₂(SH)₂(μ-S)(dpm)₂ (reaction 5.1.2).¹



In the present thesis work, reaction 5.1.2 was explored further using DMSO as solvent in order to enhance the nucleophilicity of SH⁻ without the need for basic conditions,^{2,3} and reaction 5.1.3 was discovered. The important implications are seen with the X = I system; photodecomposition of HI, for example, with solar irradiation, produces H₂ and the I₂, which can react with **2** via reaction 5.1.4 (see Chapter 4). The net reaction would be the overall homogeneous, photocatalytic decomposition of H₂S to give H₂ and sulfur (reaction 5.1.5). Preliminary work was carried out to substantiate the catalytic nature of reaction 5.1.5, and the results are summarized in this chapter.



5.2 Results

NMR spectroscopic data for the complexes and other compounds relating to the studies described in this chapter are given in Table 5.1.

Reaction of PdX₂(dpm) (9) with H₂S. Reaction of PdX₂(dpm) (**9a**, 1.8 × 10⁻² M; **9b**, 1.5 × 10⁻² M; **9c**, 1.3 × 10⁻² M) with 0.5, 0.75, 1.0, or 1.5 mole equivalent H₂S was studied at R.T. in CDCl₃ and in DMSO-d₆ in both the absence and presence of light (either laboratory light or sunlight). In CDCl₃, **9** does not exhibit reactivity with H₂S, remaining unchanged even after 27 d exposure to light. Supplementary GC and TLC (CHCl₃ eluent) studies did not reveal the presence of H₂ or elemental sulfur, respectively. In DMSO-d₆, however, **9** reacts immediately with H₂S to form, depending on conditions, some Pd₂X₂(μ-S)(dpm)₂ (**2**) and HX(solv.); Table 5.2 summarizes the experimental results. Upon addition of H₂S, the orange solution of **9c** or the yellow solutions of **9b** or **9a** rapidly changed colour to brown. ¹H and ³¹P{¹H} NMR spectroscopic analyses revealed varying quantities of Pd₂X₂(dpm)₂ (**1**), Pd₂X₂(μ-S)(dpm)₂ (**2**), unreacted **9**, and an unknown species **Y**. The ¹H NMR singlet of H₂S at δ 1.99 is not seen. A broad singlet, however, is observed at various positions ranging from δ 3.79 to 6.14 in the iodide system and at δ 3.72 and 3.70 in the bromide and chloride systems, respectively; the residual H₂O peak invariably present in the DMSO-d₆ used is no longer seen at its usual position of δ 3.42 and is considered to be part of the broad singlet. Figures 5.1 - 5.3 show representative ¹H and ³¹P{¹H} NMR spectra for each of the three systems. The unknown species **Y** is halogen-independent and is characterized by a ³¹P{¹H} singlet at δ -40.4 and an unresolved broad ¹H triplet at δ 5.10. Furthermore, this unknown species in the iodide system is most prominent (45 to 80% with respect to all ³¹P{¹H} NMR-

Table 5.1. NMR data for Complexes and Other Compounds Discussed in Chapter 5.

Compound ^a	δ (¹ H) ^b	δ (³¹ P{ ¹ H}) ^c
Pd ₂ I ₂ (dpm) ₂ (1c)	4.23 ^{d,e} (4.0) 4.39 ^{e,f}	-11.3 ^d -10.6 ^f
Pd ₂ Cl ₂ (μ -S)(dpm) ₂ (2a)	2.79 ^{d,g} (12.6, 3.5) 4.73 (12.6, 6.1) 3.35, ^{f,g} 4.63	5.52 ^d 5.90 ^f
Pd ₂ Br ₂ (μ -S)(dpm) ₂ (2b)	2.88 ^{d,g} (12.8, 3.2) 4.83 (12.8, 7.6) 3.36, ^{f,g} 4.72	5.96 ^d 6.14 6.36 ^f
Pd ₂ I ₂ (μ -S)(dpm) ₂ (2c)	3.06 ^{d,g} (14.0, 3.0) 4.95 (14.0, 6.0) 3.49, ^{f,g} 4.87	6.08 ^d 6.52 ^f
PdCl ₂ (dpm) (9a)	4.21 ^h (10.8) 4.98 ^{f,h}	-54.7 -51.7 ^f
PdBr ₂ (dpm) (9b)	4.37 ^h (10.5) 5.04 ^{f,h}	-56.2 -51.5 ^f
PdI ₂ (dpm) (9c)	4.42 ^h (10.0) 5.17 ^{f,h}	-63.2 -54.6 ^f
PdCl ₂ (dpm(S)) (11a)	4.07 ⁱ 4.97 ^{f,i}	54.9, 30.9 (18.3) ^j 56.3, 34.0 ^{fj}
PdBr ₂ (dpm(S)) (11b)	4.02 ⁱ 4.97 ^{f,i}	56.6, 32.1 (20.4) ^j 57.6, 36.5 ^{fj}
PdI ₂ (dpm(S)) (11c)	3.71 ⁱ 4.86 ^{f,i}	61.1, 31.2 (25.5) ^j 61.1, 38.9 ^{fj}
Y (possibly Pd(SH) ₂ (dpm))	5.10 ^{f,k}	-40.4 ^f
Pd ₂ (Cl)(Br)(μ -S)(dpm) ₂	see footnote <i>l</i>	see footnote <i>l</i>
Pd ₂ I ₂ (SH) ₂ (dpm) ₂	5.16 ^{e,f}	-1.2 ^f
dpm(O) ₂	4.05 ^{f,h}	24.1 ^f
H ₂ S	0.82, 1.99 ^{f,m}	
H ₂ O	3.42 ^f	
H ₂	4.64 ^f	

^a The μ -symbol for the bridging diphosphine ligand(s) is omitted for convenience throughout this Table and the text. ^b In CDCl_3 , unless stated otherwise, at 20 °C with respect to TMS; J_{HH} (and J_{PH}) values in Hertz are given in parentheses; signals for CH_2 protons unless indicated otherwise. ^c Singlets in CDCl_3 at 20 °C with respect to 85% H_3PO_4 , downfield being positive. ^d In CD_2Cl_2 . ^e Quintet. ^f In DMSO-d_6 . ^g Doublets of quintets for each of 2 sets of CH_2 protons. ^h Triplet. ⁱ Pseudo-triplet. ^j AB pattern, J_{PP} values in Hertz given in parentheses. ^k Broad triplet. ^l See Figure 5.5. ^m Measured using 1 atm H_2S .

Table 5.2. Results from studies on the reaction of PdX₂(dpm) (**9a**, 1.8 x 10⁻² M; **9b**, 1.5 x 10⁻² M; **9c**, 1.3 x 10⁻² M) with H₂S at R. T. in DMSO-d₆; **1** = Pd₂X₂(dpm)₂, **2** = Pd₂X₂(μ-S)(dpm)₂, **11** = PdX₂(dpm(S)), **Y** = probably Pd(SH)₂(dpm).

System	1	2	9	11	Y	H ₂ ^a	sulfur ^b
9c + 1.5 H ₂ S NMR-technique ^c	0	25 ^d	0	0	75	-	-
9c + 1 H ₂ S NMR-technique	0	20	0	0	80	-	-
9c + 0.75 H ₂ S Schlenk-technique ^e	2	0	89	0	9	-	-
+5 d absence of light	2	0	89	0	9	no	-
9c + 0.5 H ₂ S NMR-technique	0	10	45	0	45	-	-
+2 d exposure to light	0	0	68	10	22	-	yes
9c + 0.5 H ₂ S Schlenk-technique	6	22	63	0	9	-	-
+5 d exposure to light	0	0	63	37	0	-	-
+27 d exposure to light	0	0	42	58	0	yes(?) ^f	-
9b + 0.5 H ₂ S Schlenk-technique	0	23	20	0	57	-	-
+8 d exposure to light	0	0	74	26	0	no	yes
9a + 0.5 H ₂ S Schlenk-technique	0	24	39	0	37	-	-
+5 d exposure to light	0	0	50	20	30	yes(?) ^f	-
9a + 1 H ₂ S NMR-technique	0	25	25	29	21	yes(?) ^f	-

^a Detection of H₂ using gas chromatography. ^b Detection of elemental sulfur using thin-layered chromatography (CHCl₃ eluent). ^c NMR-technique refers to injection of H₂S via syringe into DMSO-d₆ solution of **9** held in an NMR tube. ^d Estimated amounts (%) of all the Pd complexes determined from ³¹P{¹H} NMR spectra. ^e Schlenk-technique refers to injection of H₂S via syringe into DMSO-d₆ solution of **9** held in a Schlenk tube of 165.0 mL volume. ^f The presence of H₂ was not positively established (see text).

Fig. 5.1. Representative ^1H (200 MHz) and $^{31}\text{P}\{^1\text{H}\}$ (81 MHz) NMR spectra showing results from the immediate reaction at R.T. in DMSO-d_6 of $\text{PdI}_2(\text{dpm})$ (**9c**, 1.3×10^{-2} M) with 0.5 mole equivalent H_2S in the absence of light (Schlenk techniques were employed); **1c** = $\text{Pd}_2\text{I}_2(\text{dpm})_2$, **2c** = $\text{Pd}_2\text{I}_2(\mu\text{-S})(\text{dpm})_2$, **Y** = probably $\text{Pd}(\text{SH})_2(\text{dpm})$.

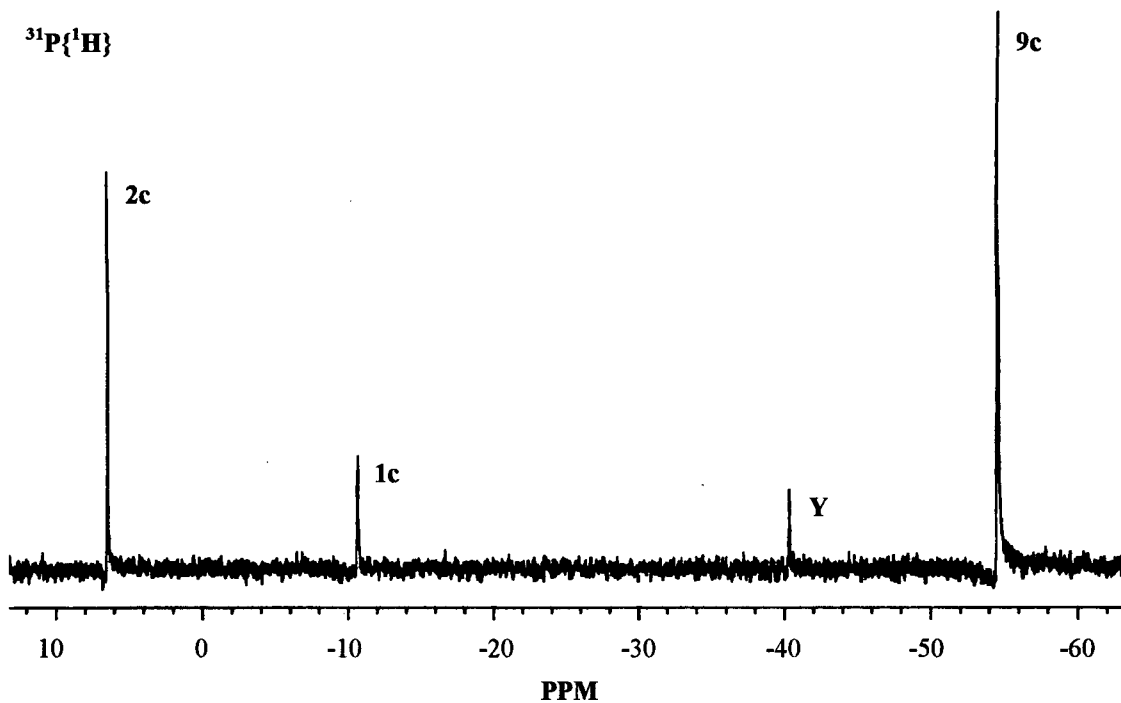
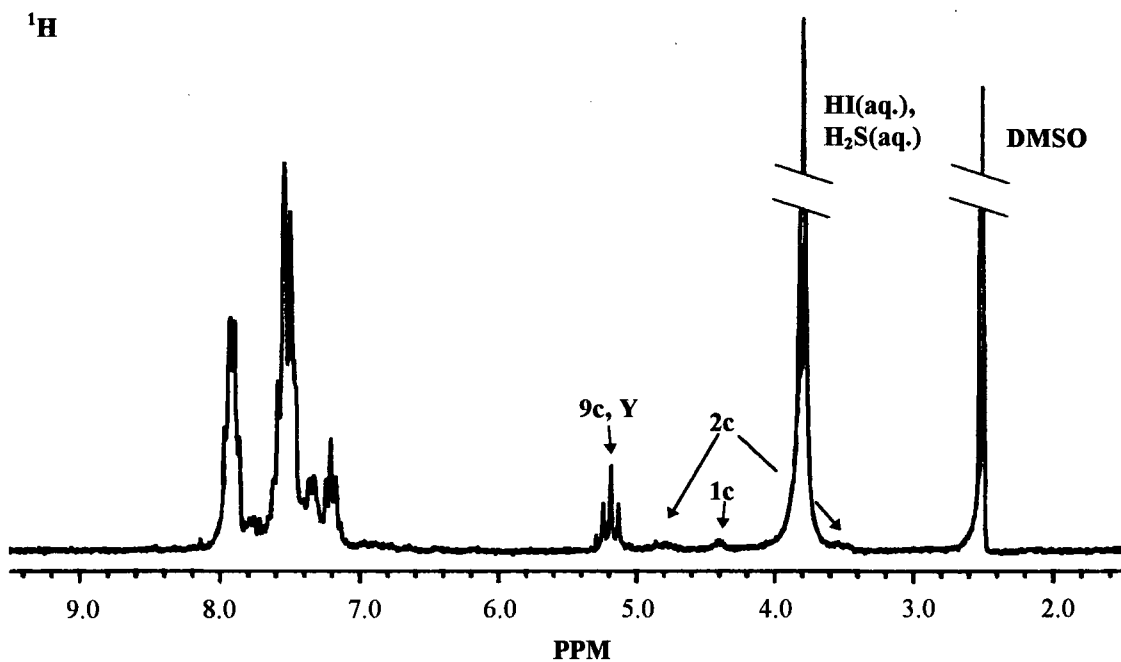


Fig. 5.2. Representative ^1H (300 MHz) and $^{31}\text{P}\{^1\text{H}\}$ (121 MHz) NMR spectra showing results from the immediate reaction at R.T. in DMSO-d_6 of $\text{PdBr}_2(\text{dpm})$ (**9b**, 1.5×10^{-2} M) with 0.5 mole equivalent H_2S in the absence of light (Schlenk techniques were employed); **2b** = $\text{Pd}_2\text{Br}_2(\mu\text{-S})(\text{dpm})_2$, **Y** = probably $\text{Pd}(\text{SH})_2(\text{dpm})$.

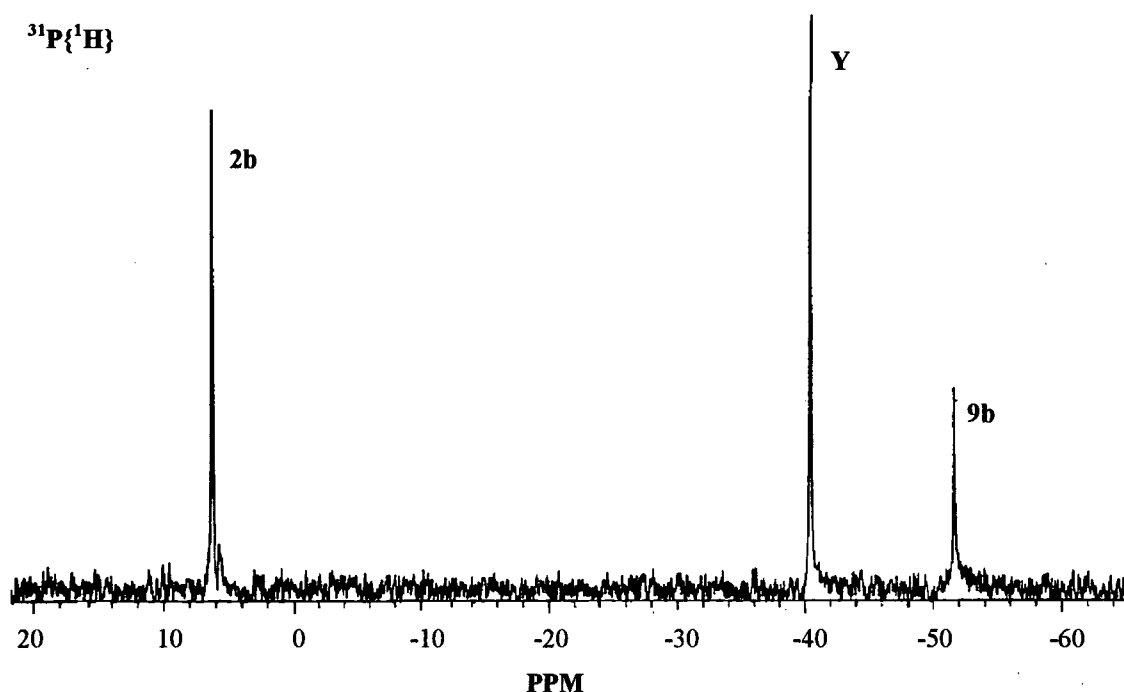
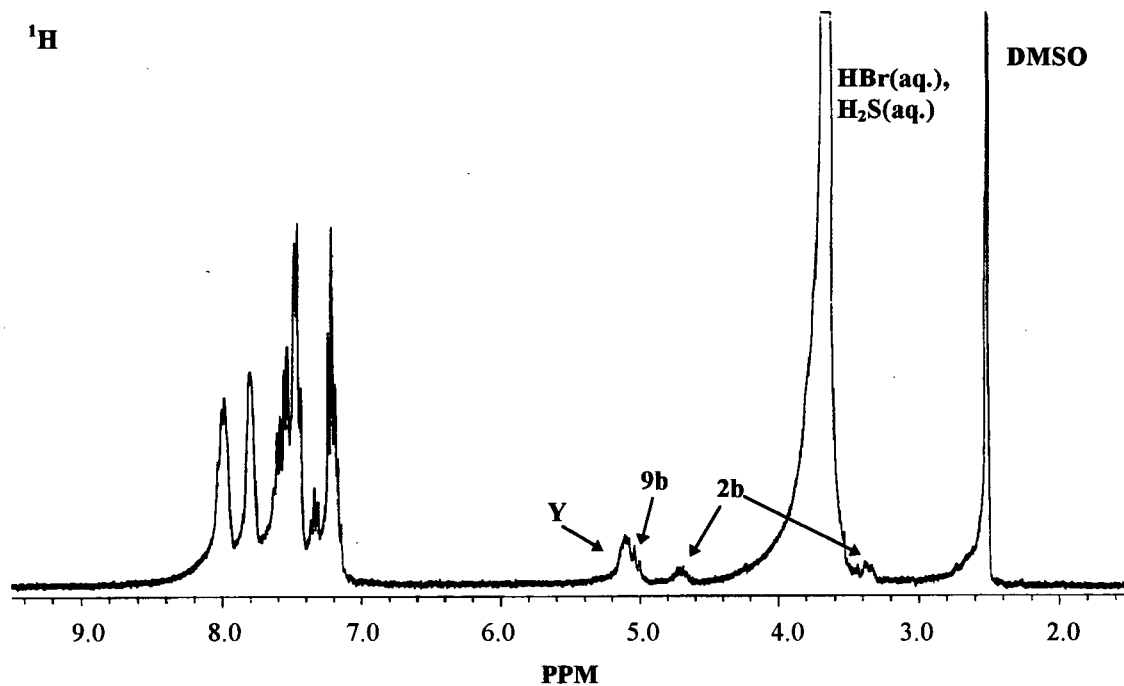
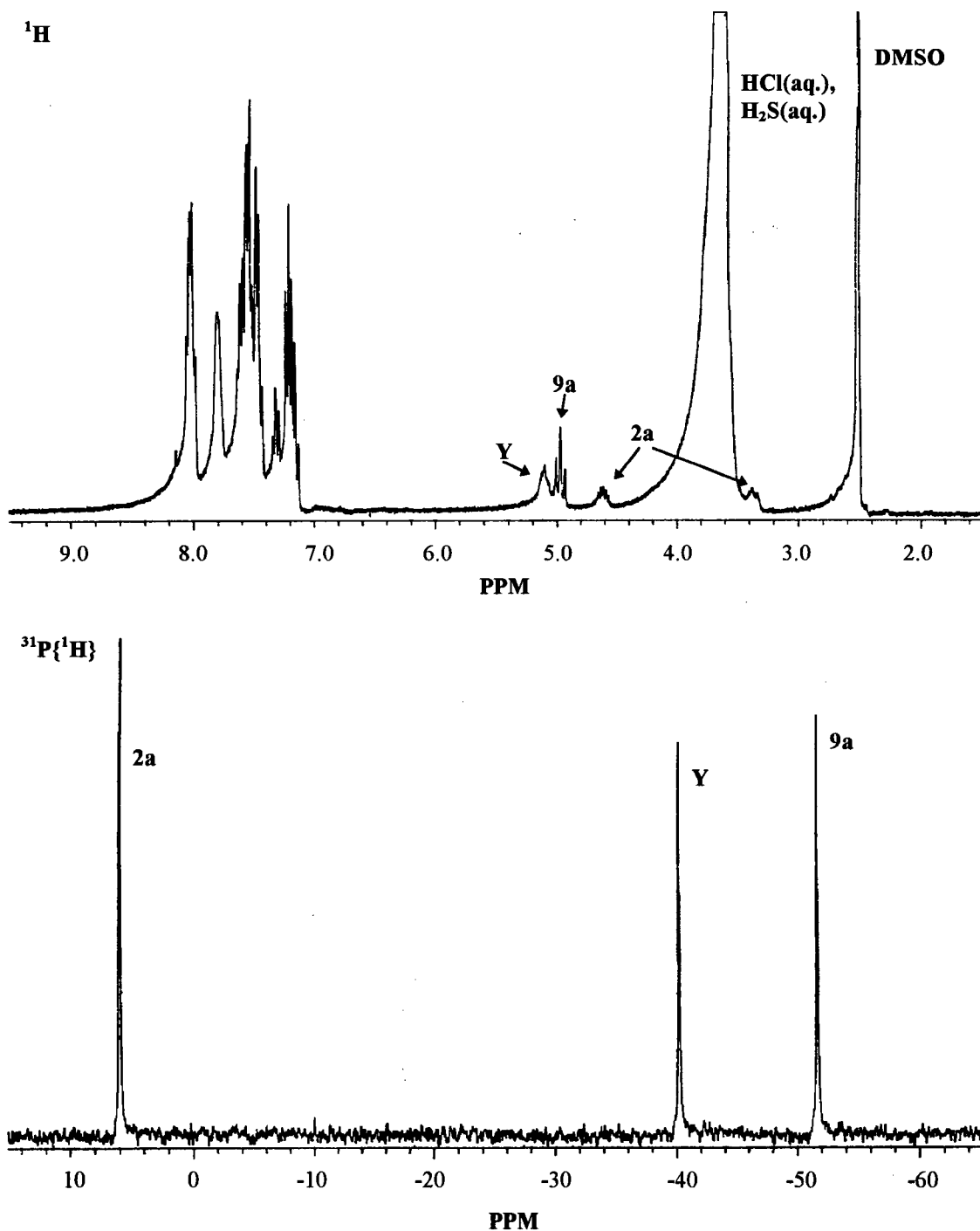
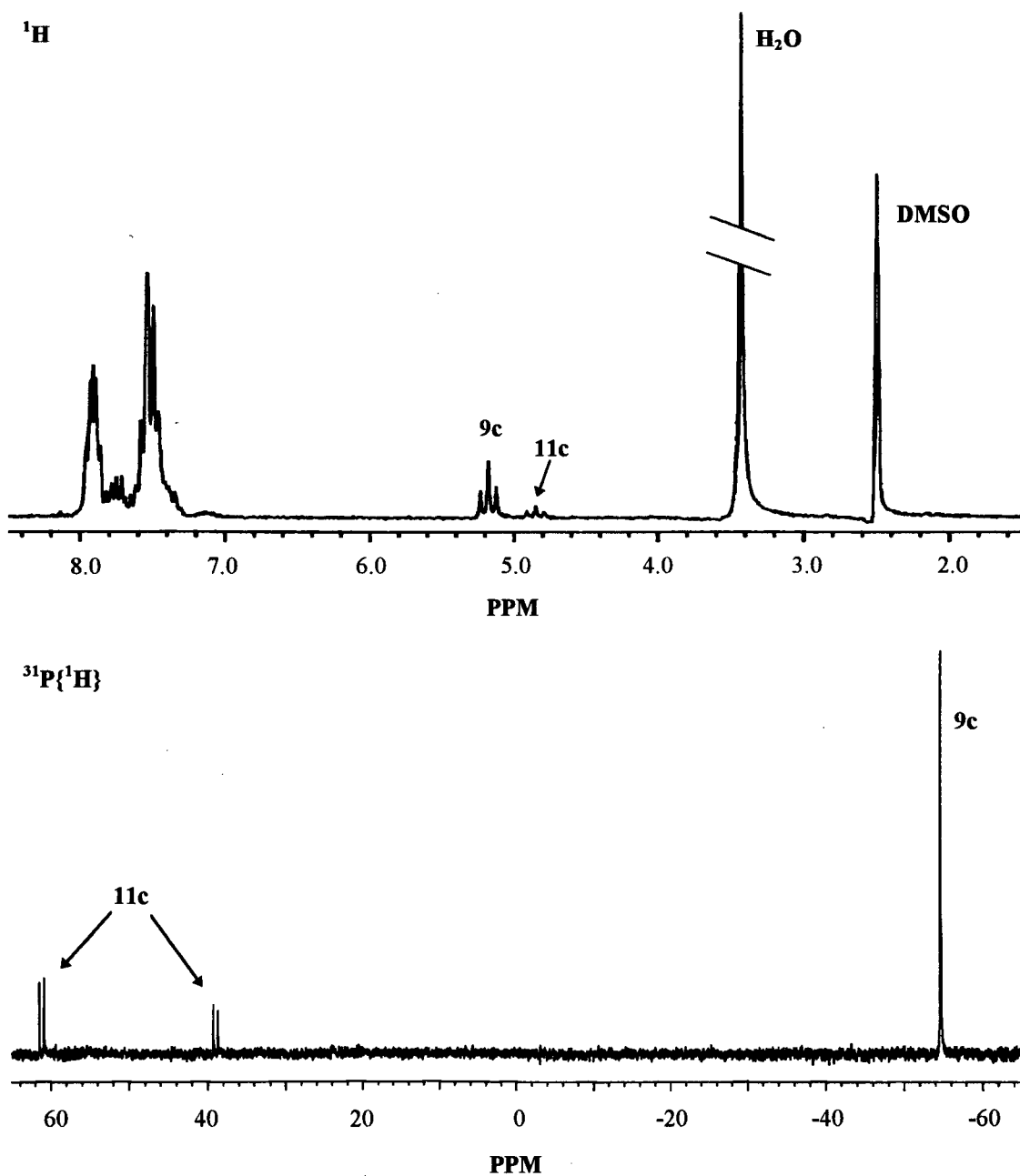


Fig. 5.3. Representative ^1H (300 MHz) and $^{31}\text{P}\{^1\text{H}\}$ (121 MHz) NMR spectra showing results from the immediate reaction at R.T. in $\text{DMSO-}d_6$ of $\text{PdCl}_2(\text{dpm})$ (**9a**, 1.8×10^{-2} M) with 0.5 mole equivalent H_2S in the absence of light; Schlenk techniques were employed; **2a** = $\text{Pd}_2\text{Cl}_2(\mu\text{-S})(\text{dpm})_2$, **Y** = probably $\text{Pd}(\text{SH})_2(\text{dpm})$.



detectable species) when H₂S is introduced into a solution of **9c** held in an NMR tube (typically of 2-3 mL volume). On the other hand, the yield of species **Y** is significantly reduced (9%) if H₂S is administered into a Schlenk tube of much greater volume (*i.e.* 165.0 mL) containing the same solution volume (0.50 mL) and concentration (1.3×10^{-2} M) of **9c**. In the bromide and chloride systems, species **Y** forms in larger yields of 57 and 37%, respectively, despite the use of similar Schlenk techniques. For systems where less than 1 mole equivalent H₂S is used, unreacted **9** ranges from 45 to 89% in the iodide system and 20 and 39% in the bromide and chloride systems, respectively. **9** reacts completely when 1 or more mole equivalent of H₂S is used, for example as shown for the iodide systems where 1 or 1.5 mole equivalent is introduced. Interestingly, Pd₂I₂(dpm)₂ (**1c**) forms in two iodide systems in which Schlenk techniques are employed; the corresponding bromide and chloride analogues are not observed in the respective systems. Exposure to light over a few days (either laboratory light or sunlight) results in the disappearance of **1** and **2**, the disappearance or reduction of species **Y**, an increase in **9**, and the appearance of PdX₂(dpm(S)) (**11**) (see Chapter 4). ¹H NMR spectra also reveal that in most systems the broad singlet mentioned above has reduced in intensity and shifted to higher fields; in some cases, the signal has completely disappeared and that of H₂O reappears. Figure 5.4 shows representative ¹H and ³¹P{¹H} NMR spectra of the iodide system (reaction of PdI₂(dpm) (**9c**, 1.3×10^{-2} M) with 0.5 mole equivalent H₂S using Schlenk techniques) after exposure to laboratory light for 5 d. A control study of the reaction of **9c** with 0.75 mole equivalent H₂S in the absence of light for 5 d (3rd entry in Table 5.2) revealed the necessity of light to affect further reaction. A few GC and TLC studies were carried out and, while the presence of elemental sulfur was always definitively identified after exposure to light by using TLC (CHCl₃ eluent) and comparing the degree of retention to that of an authentic sample of elemental sulfur, the presence of H₂ remained uncertain although in the gas

Fig. 5.4. Representative ^1H (200 MHz) and $^{31}\text{P}\{^1\text{H}\}$ (81 MHz) NMR spectra showing results from the exposure of the iodide system (reaction of $\text{PdI}_2(\text{dpm})$ (**9c**, 1.3×10^{-2} M) with 0.5 mole equivalent H_2S in the absence of light using Schlenk techniques) to laboratory light for 5 d; **11c** = $\text{PdI}_2(\text{dpm}(\text{S}))$.



chromatogram, a positive peak, with a retention time of 1.6 min and attributable to H₂, was sometimes seen.

Titration studies were carried out for the chloride system to substantiate and quantify the amount of HCl produced in reaction 5.1.3. **9a** (9.9×10^{-3} M) was reacted in DMSO (4.5 mL) at R.T. with 0.5 mole equivalent H₂S using Schlenk techniques. After 4 h, H₂O was added to precipitate the Pd species, which were subsequently filtered off. The filtrate was then titrated with a standardized NaOH solution (0.010 M); the number of moles of HCl was determined to be 1.8×10^{-5} , which corresponds to a 41% yield with respect to **9a**.

Reaction of PdX₂(dpm) (9) with elemental sulfur. Reaction of PdX₂(dpm) (**9a**, 3.6×10^{-2} M; **9b**, 3.0×10^{-2} M; **9c**, 2.7×10^{-2} M) with 1 mole equivalent S₈ was studied on the NMR-scale at R.T. and at 50 °C in DMSO-d₆, in the absence or presence of light (either laboratory light or sunlight), for periods up to 29 d. ¹H and ³¹P{¹H} NMR spectroscopic analyses revealed the formation of one product, PdX₂(dpm(S)) (**11**), and Table 5.3 summarizes the results of these studies. Reaction of **9** with S₈ is seen to take place under purely thermal conditions, and in the iodide system, the presence of light has an effect, increasing the yields of **11c** 10 to 15%. The yields of **11** decrease proceeding from the iodide to the bromide to the chloride system. For example, at R.T. in the absence of light, **11c** is present in 20% yield after 5 d, **11b**, 15% yield after 9 d, and **11a**, 10% yield after 10 d. The yields are significantly increased when the reactions are carried out at 50 °C where **11c** is formed in 45% yield after 18 h, **11b**, 30% yield after 1 d, and **11a**, 25% yield after 1 d.

Table 5.3. Results from studies on the reaction of PdX₂(dpm) (**9a**, 3.6 × 10⁻² M; **9b**, 3.0 × 10⁻² M; **9c**, 2.7 × 10⁻² M) with 1 mole equivalent of elemental sulfur in DMSO-d₆.

System	Conditions ^a	Unreacted PdX ₂ (dpm) (9) (%) ^b	PdX ₂ (dpm(S)) yield (11) (%) ^b
PdI ₂ (dpm) (9c) + 1/8S ₈	5 d; absence; R.T.	80	20
	5 d; presence; R.T.	70	30
	12 d; absence; R.T.	80	20
	12 d; presence; R.T.	65	35
	29 d; presence; R.T.	40	60
	18 h; absence; 50 °C	55	45
	2 d; absence; 50 °C	50	50
PdBr ₂ (dpm) (9b) + 1/8S ₈	9 d; absence; R.T.	85	15
	1 d; absence; 50 °C	70	30
PdCl ₂ (dpm) (9a) + 1/8S ₈	1 d; absence; R.T.	100	trace
	10 d; absence; R.T.	90	10
	1 d; absence; 50 °C	75	25

^a Absence and presence refer to experiments performed in the absence or presence of light (either laboratory- or sunlight), respectively. ^b The amounts of PdX₂(dpm) and PdX₂(dpm(S)) are determined from the relative integration values of the ¹H NMR triplet and pseudo-triplet signals, respectively, for the iodide system, and from the relative integration values of the ³¹P{¹H} NMR singlet and set of AB doublets, respectively, for the bromide and chloride systems.

Reaction of Pd₂I₂(μ-S)(dpm)₂ (2c) with I₂. Reaction of Pd₂I₂(μ-S)(dpm)₂ (**2c**) (1.6 × 10⁻² M) with 1 mole equivalent I₂ was studied at R.T. in DMSO-d₆. Addition of a red solution of I₂ to a brown solution of **2c** immediately produced a green-black solution which slowly changed to a final red-brown colour after ~20 min. The sample was analyzed after 24 h using NMR spectroscopy and thin-layered chromatography (CHCl₃ eluent). ¹H and ³¹P{¹H} NMR spectra revealed the presence of two species, **9c** and **11c** in 51 and 49% yields; TLC analysis revealed no sulfur present.

Reaction of Pd₂X₂(μ-S)(dpm)₂ (2) with HX. Reaction of Pd₂X₂(μ-S)(dpm)₂ (**2a**, 1.8 × 10⁻² M; **2b**, 1.7 × 10⁻² M; **2c**, 1.5 × 10⁻² M) with HX was studied at R.T. in CDCl₃ and in DMSO-d₆. The results of these studies are summarized in Table 5.4. In CDCl₃, 2 mole equivalents of HCl(g) and HBr(g) were added to solutions of **2a** and **2b**, respectively, and the samples were analyzed after 24 h using NMR spectroscopy. ¹H and ³¹P{¹H} NMR spectra revealed that **2a** and **2b** have completely reacted forming **9a** and **9b**, respectively, and H₂S. H₂S is characterized by a ¹H singlet signal at δ 0.82 and by its characteristic odor resembling rotten eggs. Exposure to light (laboratory light or sunlight) for 1 or 5 d had no effect on the reaction; corresponding GC and TLC studies revealed no H₂ or elemental sulfur.

Similar studies were also carried out using DMSO-d₆. For the chloride system, NMR spectroscopic analyses after 24 h revealed, in addition to unreacted **2a**, the presence of **9a**, **11a**, and a non-phosphorus-containing species characterized by a broad ¹H singlet at δ 6.26. For the bromide system, similar findings were obtained; **9b**, **11b**, and a species characterized by a broad ¹H singlet at δ 6.14 were observed, in addition to unreacted **2b**. Exposure of the DMSO systems to light (from an 18 W TLC Hg vapour lamp) for 17 h resulted in the complete disappearance of **2a** and **2b**; **9a**, **9b**, **11a**, and **11b** were still observed and in the same relative yields. Furthermore, the

Table 5.4. Results from studies on the reaction of $\text{Pd}_2\text{X}_2(\mu\text{-S})(\text{dpm})_2$ (**2a**, 1.8×10^{-2} M; **2b**, 1.7×10^{-2} M; **2c**, 1.5×10^{-2} M) with $\text{HX}(\text{g})$.

System	Conditions ^a	Observed species ^b
2a + 2 HCl	CDCl ₃ ; R.T. CDCl ₃ ; R.T.; 1 and 5 d exposure DMSO-d ₆ ; R.T. DMSO-d ₆ ; R.T.; 17 h exposure ^d	9a , H ₂ S 9a , H ₂ S 2a (14%), 9a (41%), 11a (45%), b.s. at δ 6.26 ^c 9a (49%), 11a (51%), sulfur, b.s. at δ 4.67 ^c
2b + 2 HBr	CDCl ₃ ; R.T. CDCl ₃ ; R.T.; 1 and 5 d exposure DMSO-d ₆ ; R.T. DMSO-d ₆ ; R.T.; 17 h exposure ^d	9b , H ₂ S 9b , H ₂ S 2b (58%), 9b (21%), 11b (21%), b.s. at δ 6.14 ^c 9b (50%), 11b (50%), sulfur, b.s. at δ 4.09 ^c
2c + HI ^e	DMSO-d ₆ ; R.T. ^f	9c (19%), 11c (41%), $\text{dpm}(\text{O})_2$ (40%), sulfur, H ₂ ^g
2b + 2 HCl	DMSO-d ₆ ; R.T. DMSO-d ₆ ; R.T.; 1 d exposure	$\text{Pd}_2(\text{Br})(\text{Cl})(\mu\text{-S})(\text{dpm})_2$, 2a (?), 2b (?), b.s. at δ 8.69 ^c $\text{Pd}_2(\text{Br})(\text{Cl})(\mu\text{-S})(\text{dpm})_2$, 2a (?), 2b (?) > $\text{Pd}(\text{Br})(\text{Cl})(\text{dpm})$, 9a (?), 9b (?) > $\text{Pd}(\text{Br})(\text{Cl})(\text{dpm}(\text{S}))$, 11a (?), 11b (?), b.s. at δ 5.86 ^c

^a Exposure refers to exposure of the sample to light (laboratory light or sunlight). ^b Observed species from ¹H and ³¹P{¹H} NMR spectroscopic and thin-layered and gas chromatographic analyses. Values in parentheses refer to approximate relative yields determined from ³¹P{¹H} NMR integration values.

^c Broad singlet observed in the ¹H NMR spectrum. ^d Exposure to light from an 18 W TLC Hg vapour lamp. ^e Hydrogen iodide (0.15 M) was introduced as HI(aq.) or HI(g). ^f Subsequent exposure to light for 5 d gave no further changes. ^g H₂ was detected only in reaction of **2c** with HI(g).

broad ^1H singlets at δ 6.26 and 6.14 were replaced by ones at δ 4.67 and 4.09 in the chloride and bromide systems, respectively. Corresponding GC and TLC studies revealed the absence of H_2 and presence of elemental sulfur, respectively, in both systems. Reaction of **2c** with HI was studied only in DMSO-d_6 . Due to the corrosive nature of aq. HI, 10 mole equivalents (10 μL 7.58 M aq. HI) were used (see Experimental Section). Use of aq. HI or HI(g) (prepared from aq. HI, see Experimental Section) gave similar results. ^1H and $^{31}\text{P}\{^1\text{H}\}$ NMR analyses after 24 h revealed that **2c** had completely reacted, and **9c**, **11c**, and $\text{dpm}(\text{O})_2$ had formed in 19, 41, and 40% relative yields, respectively. Exposure of this system to light for 5 d had no effect on the NMR spectral characteristics. Subsequent TLC studies revealed the presence of elemental sulfur. GC studies indicated the presence of H_2 only for the reaction of **2c** with HI(g); it was noted that when HI(g) was introduced into the system (*i.e.* an NMR tube containing a solution of **2c**) via vacuum transfer using liquid N_2 , a purple solid (attributable to I_2) was seen condensing on the inside walls of the NMR tube. Finally, reaction of **2b** with 2 mole equivalents of HCl(g) was investigated, and NMR spectroscopic analyses after 24 h revealed the formation of a species attributable to $\text{Pd}_2(\text{Cl})(\text{Br})(\mu\text{-S})(\text{dpm})_2$ which is characterized by multiplets at δ 3.37 and 4.65 in the ^1H NMR spectrum and an AA'BB' pattern from δ 7.0 to 3.0 in the $^{31}\text{P}\{^1\text{H}\}$ NMR spectrum (Fig. 5.5). In addition, a broad singlet at δ 8.69 in the ^1H NMR spectrum is observed. Whether **2a** and **2b** are also present cannot be ascertained. NMR analyses after 1 d exposure to light, however, revealed in addition to $\text{Pd}_2(\text{Cl})(\text{Br})(\mu\text{-S})(\text{dpm})_2$, the presence of a mixture consisting of perhaps $\text{Pd}(\text{Cl})(\text{Br})(\text{dpm})$, **9a**, **9b**, **11a**, **11b**, and $\text{Pd}(\text{Cl})(\text{Br})(\text{dpm}(\text{S}))$ (Fig. 5.6). The broad singlet in the ^1H NMR spectrum at δ 8.69 has disappeared and one at δ 5.86 has appeared.

In all of the systems studied in DMSO-d_6 , the odor of H_2S was not detected nor was the H_2S singlet seen at δ 1.99 in ^1H NMR spectra.

Fig. 5.5. ^1H (200 MHz) and $^{31}\text{P}\{^1\text{H}\}$ (81 MHz) NMR spectra showing results from the reaction of $\text{Pd}_2\text{Br}_2(\mu\text{-S})(\text{dpm})_2$ (**2b**, 1.7×10^{-2} M) with 2 mole equivalent HCl at R.T. in DMSO-d_6 ; spectra recorded 1 h after sample preparation.

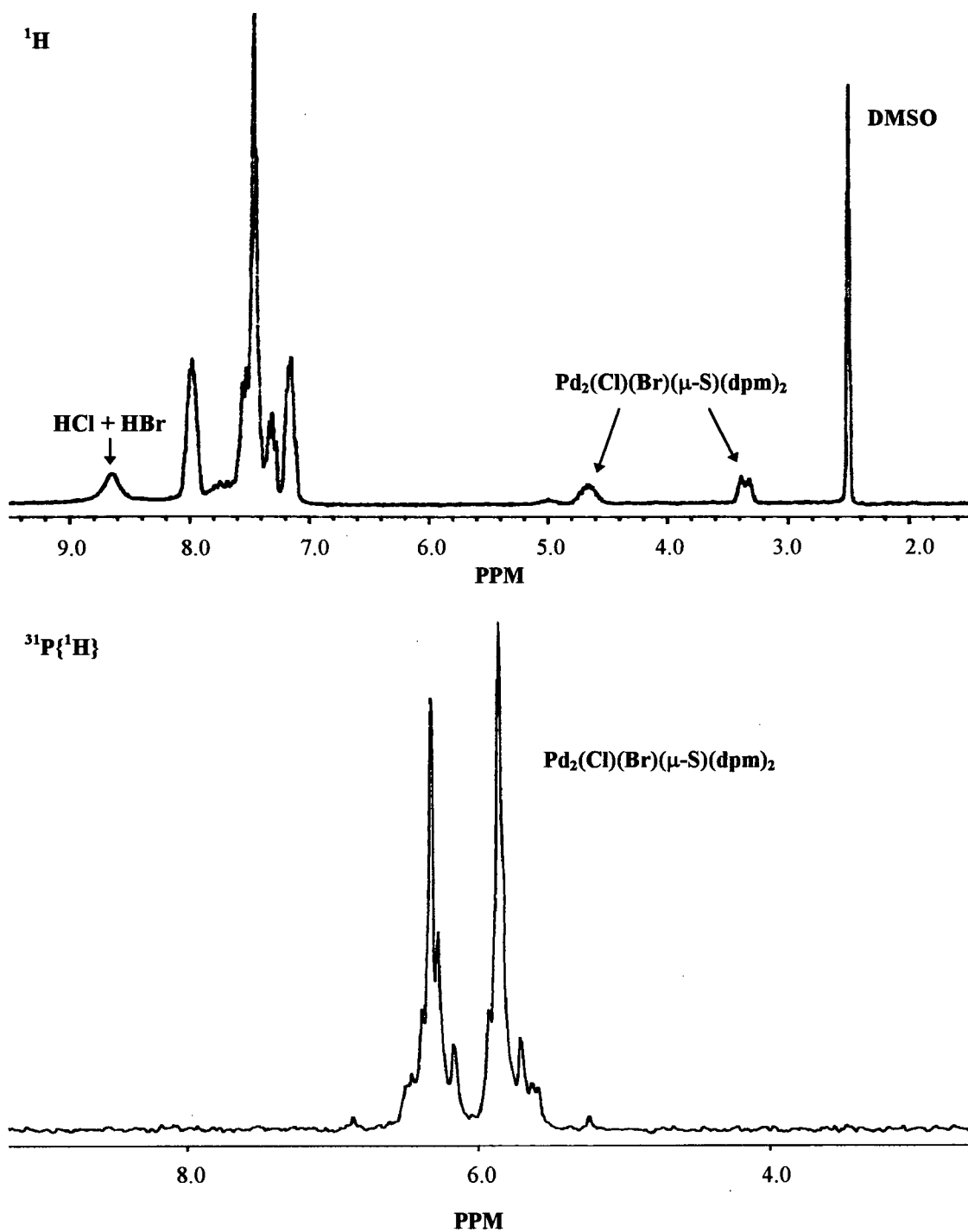
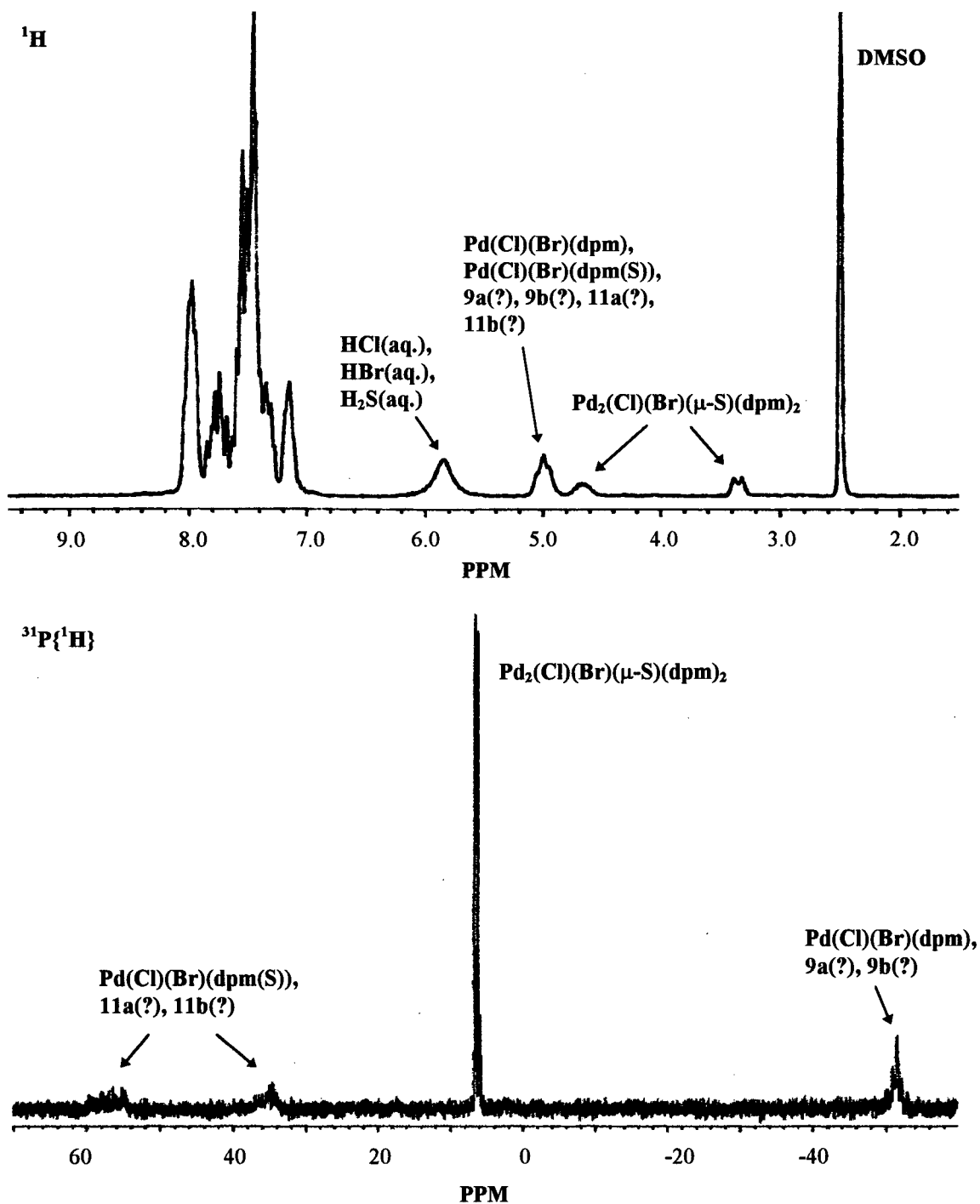


Fig. 5.6. ^1H (200 MHz) and $^{31}\text{P}\{^1\text{H}\}$ (81 MHz) NMR spectra showing results from the reaction of $\text{Pd}_2\text{Br}_2(\mu\text{-S})(\text{dpm})_2$ (**2b**, 1.7×10^{-2} M) with 2 mole equivalent HCl at R.T. in DMSO-d_6 ; spectra recorded after exposure of the system to laboratory light for 1 d; **9a** = $\text{PdCl}_2(\text{dpm})$, **9b** = $\text{PdBr}_2(\text{dpm})$, **11a** = $\text{PdCl}_2(\text{dpm}(\text{S}))$, **11b** = $\text{PdBr}_2(\text{dpm}(\text{S}))$.



Reaction of $\text{Pd}_2(\text{SH})_2(\mu\text{-S})(\text{dpm})_2$ with I_2 . Reaction of $\text{Pd}_2(\text{SH})_2(\mu\text{-S})(\text{dpm})_2$ (1.9×10^{-2} M) with 1 mole equivalent I_2 was studied at R.T. in CDCl_3 and in DMSO-d_6 . Addition of a purple (CDCl_3) or red (DMSO-d_6) solution of I_2 to a brown solution of $\text{Pd}_2(\text{SH})_2(\mu\text{-S})(\text{dpm})_2$ immediately produced a brown-black solution which slowly changed colour to a final brown after ~ 30 min. In CDCl_3 , ^1H and $^{31}\text{P}\{^1\text{H}\}$ NMR spectroscopic analyses revealed the formation of two detectable products, $\text{Pd}_2\text{I}_2(\mu\text{-S})(\text{dpm})_2$ (**2c**) and H_2S , the latter being characterized by smell and the ^1H singlet at δ 0.82. In DMSO-d_6 , **2c** was formed; the $\delta(\text{H}_2\text{S})$ signal at 1.99 was not seen in the ^1H NMR spectrum, but a broad singlet at δ 5.68 was observed (Fig. 5.7). Also, the characteristic odor of H_2S was not detected. Unreacted $\text{Pd}_2(\text{SH})_2(\mu\text{-S})(\text{dpm})_2$ was not seen. TLC analyses (CHCl_3 eluent) of all samples revealed the presence of elemental sulfur. Reaction of $\text{Pd}_2(\text{SH})_2(\mu\text{-S})(\text{dpm})_2$ with I_2 in CDCl_3 was also studied at -60 °C using NMR spectroscopy. "Immediate" NMR spectra revealed that $\text{Pd}_2(\text{SH})_2(\mu\text{-S})(\text{dpm})_2$ had completely reacted to form **2c**, H_2S , and an intermediate species characterized by a 1:4:6:4:1 ^1H quintet at δ 5.16 and a $^{31}\text{P}\{^1\text{H}\}$ singlet at δ -1.2. There was no change in the spectra when temperature was raised to -45 °C; at 10 °C, the intensities of the NMR signals were reduced (with respect to **2c**), and at 22 °C the intermediate had completely disappeared. Corresponding TLC studies again revealed the presence of elemental sulfur.

Reaction of $\text{PdX}_2(\text{dpm})$ (9**) with NaSH.** Reaction of $\text{PdX}_2(\text{dpm})$ (**9a**, 3.6×10^{-2} M; **9b**, 3.0×10^{-2} M; **9c**, 2.7×10^{-2} M) with 0.5 mole equivalent NaSH was studied at R.T. in DMSO-d_6 . After 24 h, ^1H and $^{31}\text{P}\{^1\text{H}\}$ NMR spectra revealed in addition to unreacted **9**, the presence of small amounts of $\text{Pd}_2\text{X}_2(\mu\text{-S})(\text{dpm})_2$ (**2**) and the unknown **Y** (Fig. 5.8).

Fig. 5.7. ^1H (300 MHz) and $^{31}\text{P}\{^1\text{H}\}$ (121 MHz) NMR spectra of the completed reaction between $\text{Pd}_2(\text{SH})_2(\mu\text{-S})(\text{dpm})_2$ (1.9×10^{-2} M) and 1 mole equivalent I_2 at R.T. in DMSO-d_6 ; $2\text{c} = \text{Pd}_2\text{I}_2(\mu\text{-S})(\text{dpm})_2$.

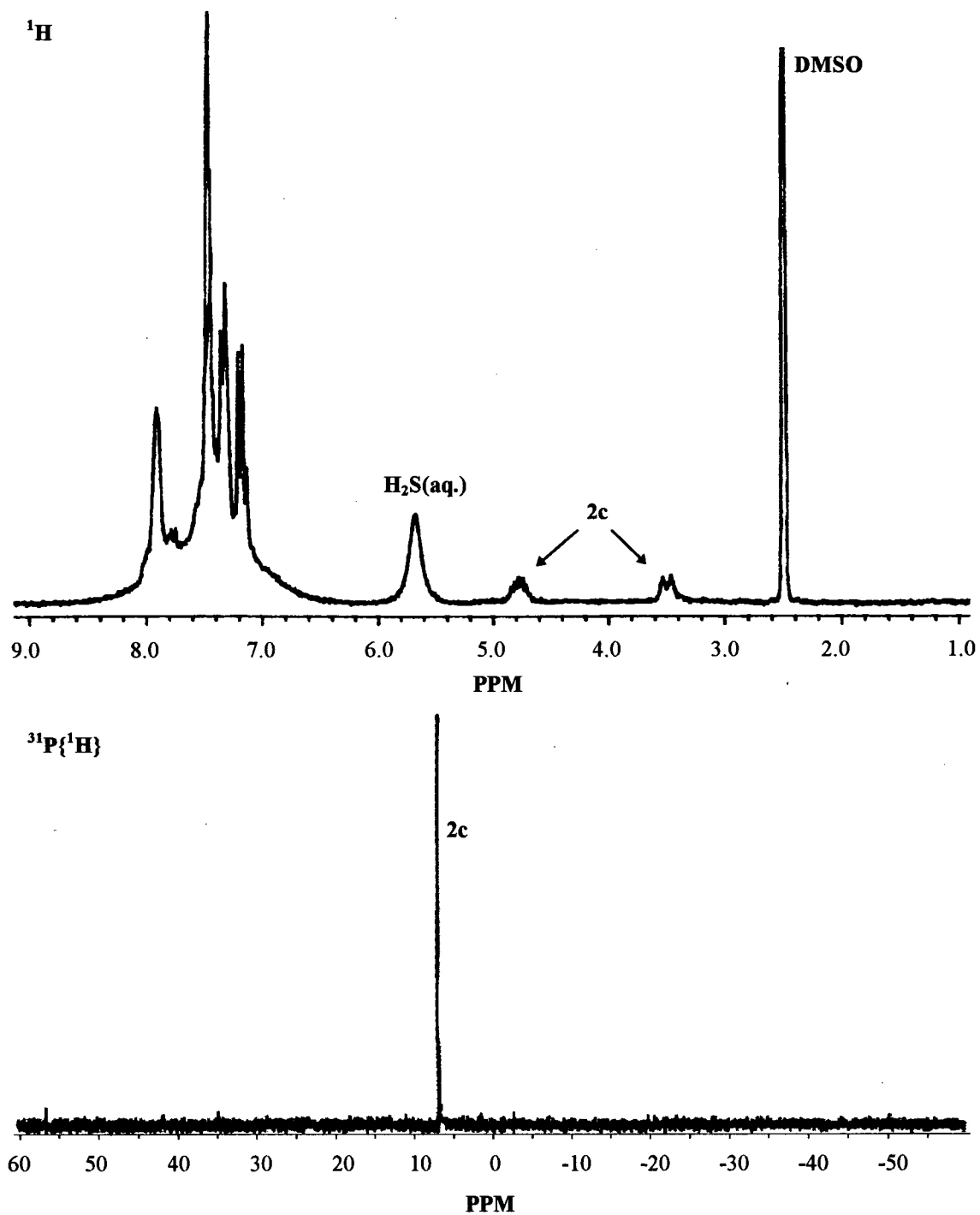
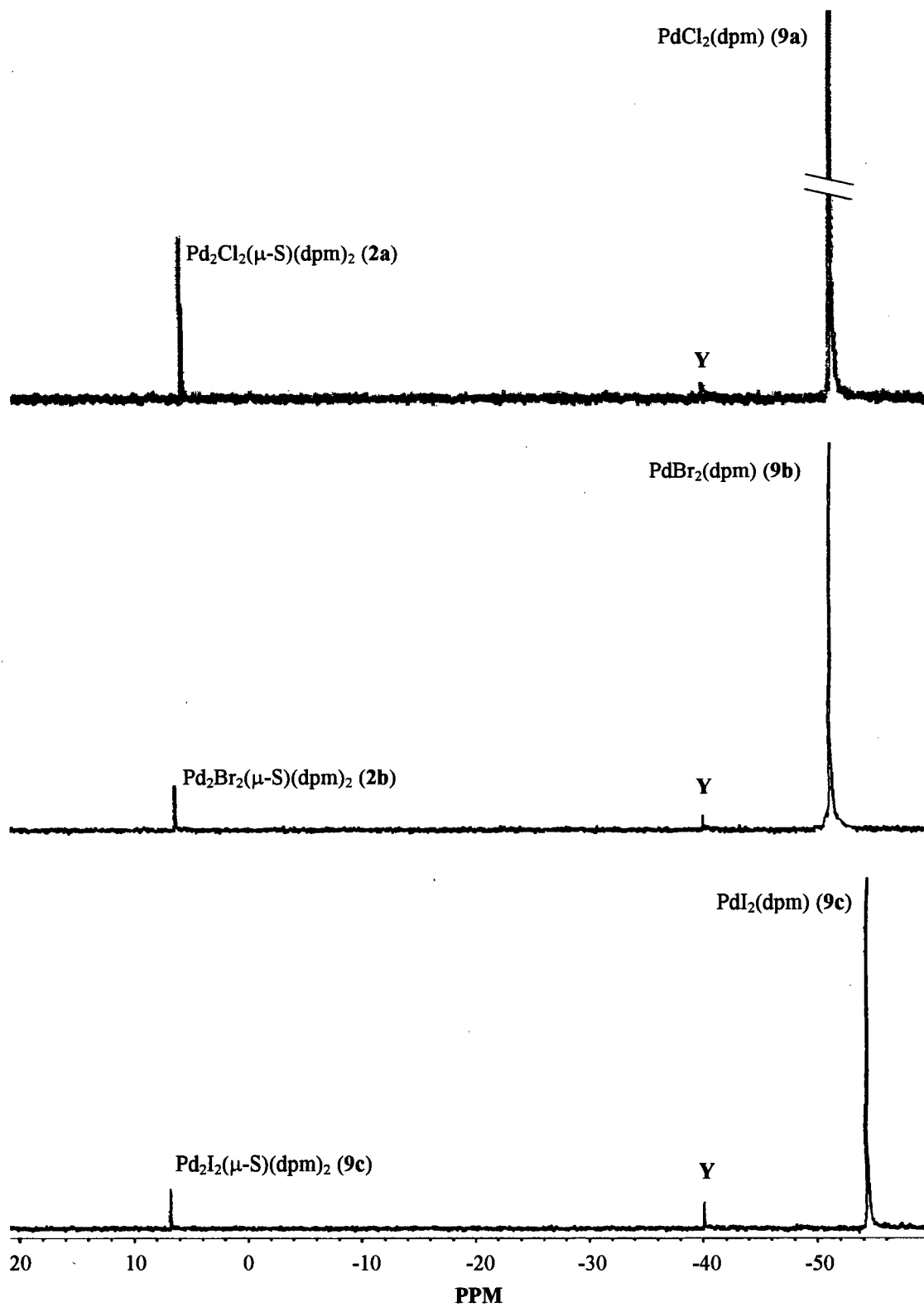


Fig. 5.8. $^{31}\text{P}\{^1\text{H}\}$ NMR spectra (121 MHz) showing the partial formation of $\text{Pd}_2\text{X}_2(\mu\text{-S})(\text{dpm})_2$ (**2**) from the reaction of $\text{PdX}_2(\text{dpm})$ (**9**) with 0.5 mole equivalent NaSH at R.T. in DMSO-d_6 ; Y = probably $\text{Pd}(\text{SH})_2(\text{dpm})$.



Photodecomposition studies of HI, HBr, and H₂S. Qualitative photodecomposition studies were carried out, and Table 5.5 summarizes the results. UV-vis spectroscopy was used to analyze for Br₂, I₂, and elemental sulfur (see Fig. 4.4, page 148), and gas chromatography for H₂. In CDCl₃, within 0.5 h after the introduction of aq. HI, the system acquired a purple colour indicative of I₂; the UV-vis spectrum shows an absorption maximum at 512 nm (Fig. 5.9). Exposure to laboratory light for 5 d resulted in an increase in the intensity of the purple colour and an increase in absorbance at 512 nm. GC analyses of the liquid and head space, however, revealed no detectable H₂. Similar results were obtained in analogous studies of aq. HI alone or dissolved in DMSO-d₆ except a dark red colour was observed instead; UV-vis spectroscopic studies in DMSO-d₆ revealed absorption maxima at 294 and 364 nm characteristic of I₃⁻ (compared with an authentic sample of NaI₃ prepared from NaI + I₂) (Fig. 5.10). There were again increases in intensities of colour and absorption after exposure to light.

Exposure of HI(g) to sunlight for 2 d also produced I₂ but no detectable H₂; irradiation with light from a 450 W medium pressure Hg lamp, however, resulted in complete decomposition to H₂ and I₂. H₂ was positively detected and the absorbance at 512 nm corresponded to ~0.020 mmol I₂, in excellent agreement with the theoretical yield of 0.020 mmol. Exposure of H₂S(g) to sunlight for 5 d produced no detectable H₂ or elemental sulfur.

In a single study in which aq. HBr was dissolved in DMSO-d₆ with the sample exposed to laboratory light for 12 h, the formation of Br₂ was evidenced by the appearance of a yellow colour and by comparison of the electronic absorption spectrum with that of an authentic sample of Br₂ (Fig. 5.11). Both spectra show an absorption maximum at 418 nm. H₂ was not detected in GC studies.

Table 5.5. Results from photodecomposition studies of HI, HBr, and H₂S.

System ^a	Conditions ^b	Decomposition products ^c
Aq. HI (10 μL) in 0.50 mL CDCl ₃	laboratory light; 0.5 h laboratory light; 5 d	I ₂ I ₂
Aq. HI (10 μL) in 0.50 mL DMSO-d ₆	laboratory light; 5 d	I ₂ (as I ₃ ⁻)
Aq. HI (0.50 mL)	sunlight; 1 d laboratory light; 5 d	I ₂ (as I ₃ ⁻) I ₂ (as I ₃ ⁻)
HI(g) (prepared from 10 μL aq. HI) ^{d,e}	sunlight; 2 d 450 W Hg lamp; 20 h	I ₂ H ₂ , I ₂
Aq. HBr (10 μL) in 0.50 mL DMSO-d ₆	laboratory light; 0.5 d	Br ₂
H ₂ S(g) (1.0 mL at STP) ^e	sunlight; 5 d	none detected

^a Samples were prepared in NMR tubes fitted with a PTFE J. Young valves. ^b Exposure to light for specified time period. ^c Decomposition products were detected using UV/vis spectroscopy (Br₂, I₂) and gas chromatography (H₂). ^d See Experimental Section. ^e Gaseous samples were used.

Fig. 5.9. Electronic absorption spectrum of I_2 in chloroform from the photodecomposition of aq. HI (0.040 mmol) (amount of I_2 not quantified).

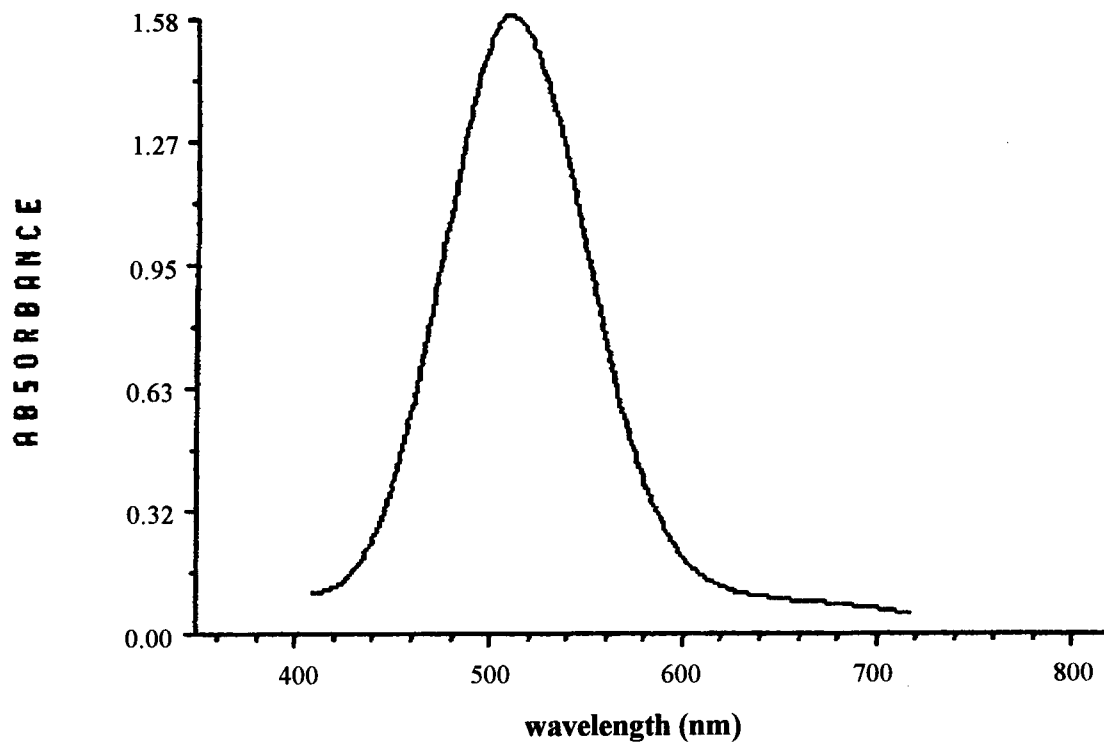


Fig. 5.10. Electronic absorption spectrum of NaI_3 in DMSO-d_6 (amount of NaI_3 not quantified).

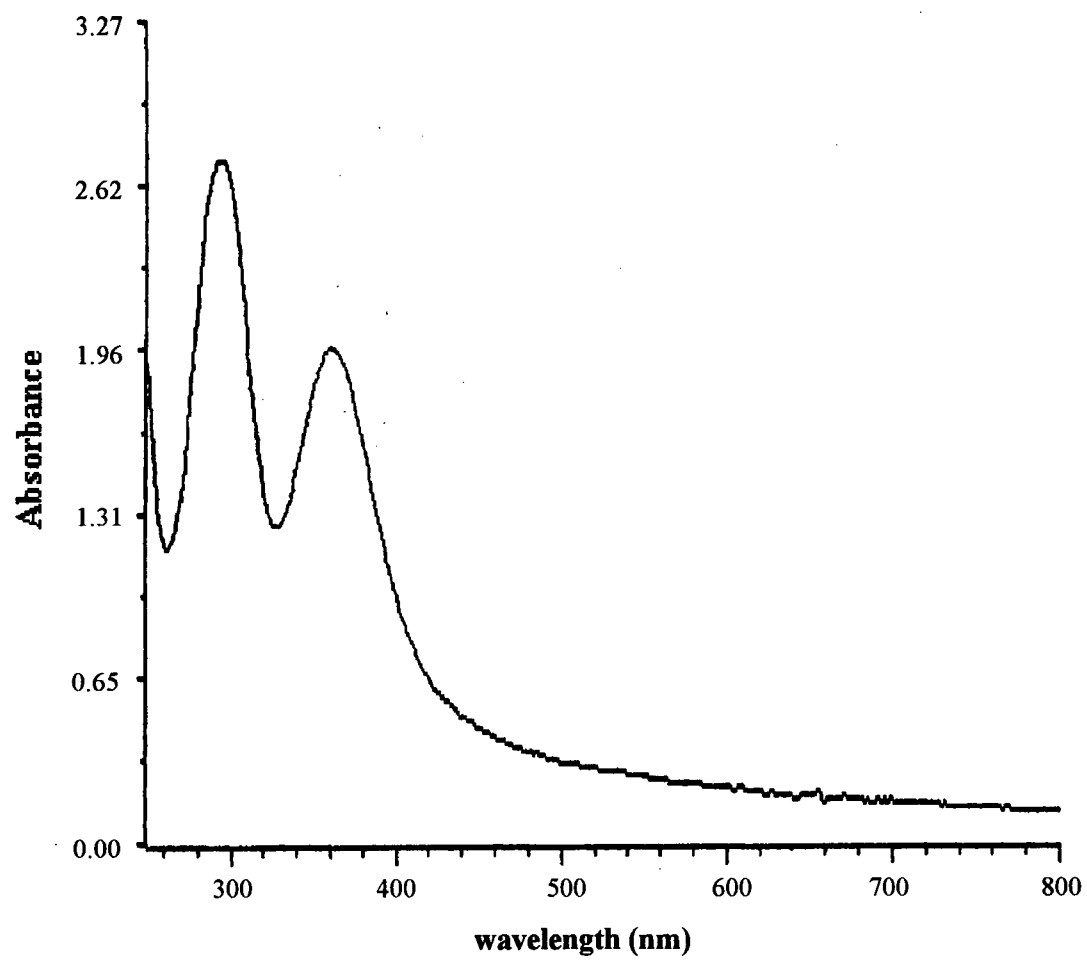
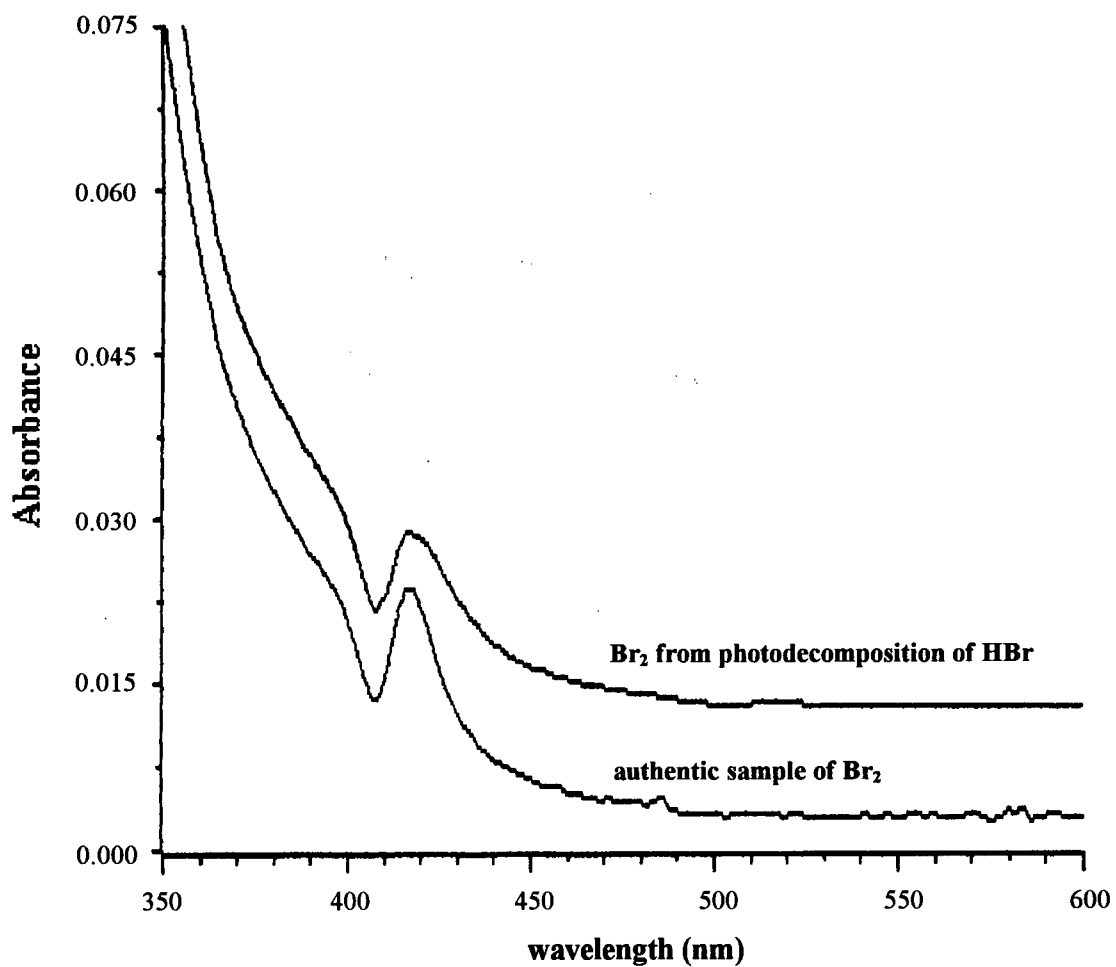
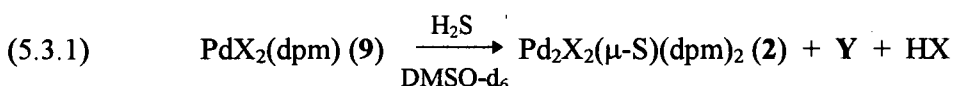


Fig. 5.11. Electronic absorption spectra of an authentic sample of Br_2 in DMSO-d_6 and Br_2 from photodecomposition of HBr ($10 \mu\text{L}$ 8.83 M HBr(aq.) dissolved in 0.5 mL DMSO-d_6 ; 12 h exposure to laboratory light) (amount of Br_2 not quantified).



5.3 Discussion

Preliminary investigations of the reaction of $\text{PdX}_2(\text{dpm})$ (**9**) with H_2S were carried out, and while **9** exhibits no reactivity toward H_2S in CDCl_3 , rapid reaction occurs in DMSO-d_6 forming $\text{Pd}_2\text{X}_2(\mu\text{-S})(\text{dpm})_2$ (**2**), a species **Y** which is probably $\text{Pd}(\text{SH})_2(\text{dpm})$ (see below), and HX (reaction 5.3.1).

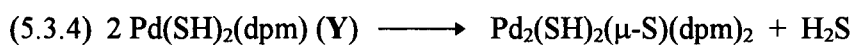
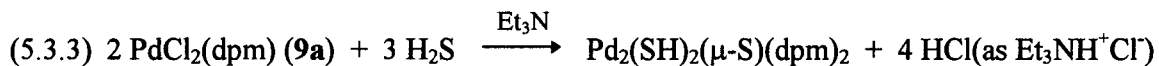
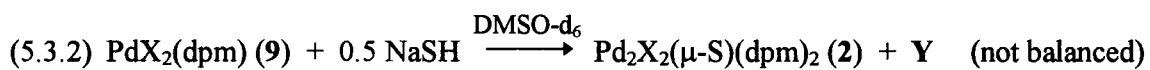


Reaction 5.3.1 was studied using NMR- and Schlenk-experimental techniques which refer to the addition of H_2S to solutions of **9** held in NMR and Schlenk tubes, respectively. The yields of **2**, **Y**, HX , and unreacted **9** were dependent on these experimental conditions; Tables 5.1 and 5.2 summarize NMR data and the results of these studies, respectively. The presence of HX was established by titration studies on the chloride system; a 41% yield was observed (initial $[\mathbf{9a}] = 9.9 \times 10^{-3} \text{ M}$) compared to 61% seen in an *in situ* NMR study where the initial $[\mathbf{9a}] = 1.8 \times 10^{-2} \text{ M}$ (see Table 5.2, entry 7). In all three Cl^- , Br^- , and I^- systems, ^1H NMR spectroscopic analyses showed broad singlets which vary in position from experiment to experiment even within duplicate runs. Furthermore, the DMSO-d_6 solvent used, despite extensive drying, invariably contained residual H_2O whose ^1H NMR signal disappeared after addition of H_2S . It is inferred that the broad singlets observed in reaction 5.3.1 belong to aquated HX (*i.e.* $\text{H}_3\text{O}^+\text{X}^-$); however, as will be discussed later, H_2S could also be present in the aquated form, $\text{H}_3\text{O}^+\text{SH}^-$, its ^1H NMR signal being part of the broad singlet. Of note, ^1H NMR analyses of aq. HI in DMSO-d_6 , for example, showed a broad singlet which also varies in position from sample to sample, and the ^1H NMR signal of H_2O was no longer seen.

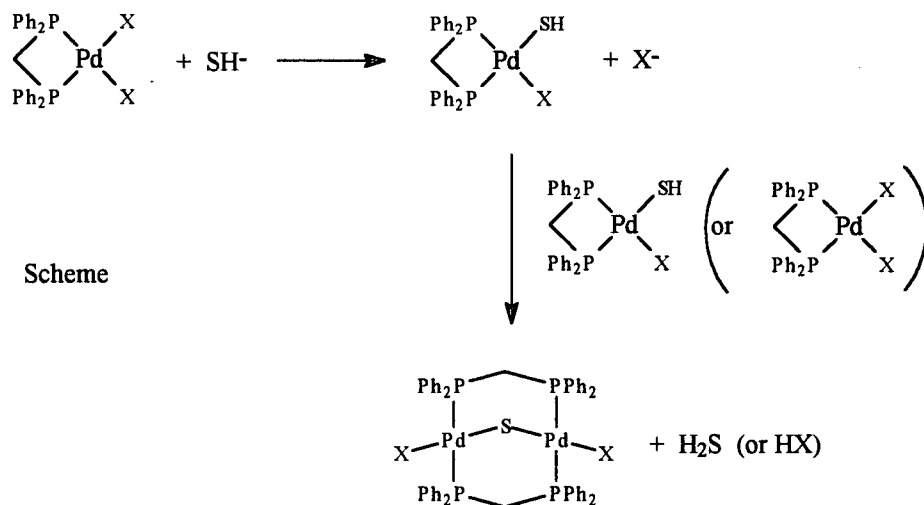
Species **Y** appears to be halide-independent as it possesses the same NMR characteristics in the three chloride, bromide, and iodide systems. Its yield, however, depended on the system and on the experimental technique used to study reaction 5.3.1. For example, in the iodide system, **Y** formed in higher yields when NMR-techniques were employed, while the use of Schlenk techniques greatly reduced the yield of **Y** but unreacted **9** was largely seen. In the chloride and bromide systems, Schlenk-techniques gave yields of **Y** that were comparable to those in the iodide system using NMR-techniques. Species **Y** is thought to be the mononuclear complex, $\text{Pd}(\text{SH})_2(\text{dpm})$, for which strong support comes from the reaction of **9** with 0.5 mole equivalent NaSH: this resulted in the formation of **2** and species **Y**, reaction 5.3.2, and the spectral data of **Y** are analogues to those of the $\text{PdX}_2(\text{dpm})$ species (see Table 5.1).

It is difficult to rationalize the limited results in terms of an intimate mechanism for reaction 5.3.1; however, analogies can be drawn from the previous study of the reaction of $\text{PdCl}_2(\text{dpm})$ (**9a**) with H_2S under basic conditions in C_6H_6 or CH_2Cl_2 to form the dinuclear complex $\text{Pd}_2(\text{SH})_2(\mu\text{-S})(\text{dpm})_2$ (reaction 5.3.3).¹ The presence of the Et_3N base serves to react with H_2S to provide an SH source, and indeed, reaction of **9a** with excess NaSH also forms $\text{Pd}_2(\text{SH})_2(\mu\text{-S})(\text{dpm})_2$.¹ It was suggested that product formation proceeded via nucleophilic substitution of the Cl^- ligands to form initially species **Y**, $\text{Pd}(\text{SH})_2(\text{dpm})$, which rapidly underwent self-association with elimination of H_2S , reaction 5.3.4.¹ Species **Y** was not detected, and formation of $\text{Pd}_2(\text{SH})_2(\mu\text{-S})(\text{dpm})_2$ presumably results from the tendency of dpm to bridge;⁴ there is ample precedence for similar dinucleation processes forming bridge sulfide complexes from mononuclear species containing terminal SH ligands.⁵ Complexes of the type $\text{M}(\text{SH})_2(\text{dpe})$ where $\text{M} = \text{Ni}, \text{Pd}$, and $\text{dpe} =$ bis(diphenylphosphino)ethane, as well as the complex $\text{Pt}(\text{SH})_2(\text{PPh}_3)_2$, are stable with respect to dinucleation.⁶ In the present study, $\text{Pd}_2(\text{SH})_2(\mu\text{-S})(\text{dpm})_2$ was not observed and, if **Y** is

$\text{Pd}(\text{SH})_2(\text{dpm})$, reaction 5.3.4 does not occur in DMSO; this is a more polar and more coordinating solvent than CH_2Cl_2 or C_6H_6 ,^{7,8} and would appear to prevent the dinucleation.

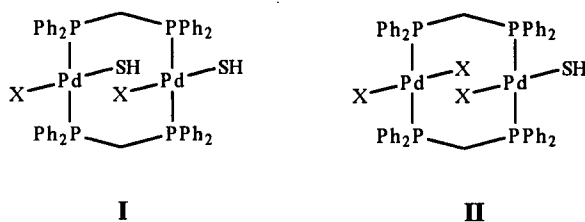


Formation of $\text{Pd}_2\text{X}_2(\mu\text{-S})(\text{dpm})_2$ (2) in the NaSH reaction is explained by invoking a similar mechanism. Nucleophilic substitution of one X⁻ ligand would give $\text{PdX}(\text{SH})(\text{dpm})$ which could then self-associate or react with 9 with elimination of H_2S or HX (Scheme). [Note: it is not clear how $\text{Pd}_2\text{I}_2(\text{dpm})_2$ (1c) was also formed in some studies (see Table 5.2), but a single experiment demonstrated that a DMSO- d_6 solution of 2c kept at 50 °C for 1 h generates 1c and several as yet unidentifiable species.]

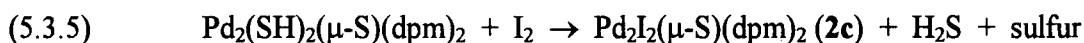


It is difficult to conceive how Y ($\text{Pd}(\text{SH})_2(\text{dpm})$) could be involved in the formation of 2, and Y is perhaps just a side-product that forms in higher yields under higher local solution

concentrations of H₂S (NMR- vs. Schlenk-techniques). In addition, the formation of Y is probably also governed by the nucleophilicity of SH⁻ versus I⁻, Br⁻, and Cl⁻ with the trend being SH⁻ > I⁻ > Br⁻ > Cl⁻;² in the chloride and bromide systems, more Y was formed despite the use of Schlenk-techniques. Although PdX(SH)(dpm) was not detected, indirect support for its existence comes from studies of the reaction of **9** with 0.5 mole equivalent NaSH that generates Pd₂X₂(μ-S)(dpm)₂ (**2**) (reaction 5.3.2); a mechanistic scheme similar to that above is envisaged with the coupling of PdX(SH)(dpm) proceeding via species such as **I** or **II**:

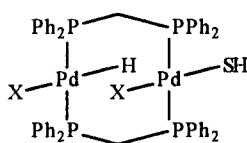


H₂S or HX is then pictured to form via a deprotonation/protonation process,⁹ where deprotonation of an SH⁻ ligand promotes sulfide bridge formation. The expected H₂S could not be detected within reaction 5.3.2 by smell or by NMR spectra as the reaction was <2% complete after 1 d, probably because of limited solubility of NaSH in DMSO; complex **2** could be seen only in the ³¹P{¹H} NMR spectra, the ¹H NMR spectra showing only unreacted **9**. H₂S, however, was detected both in NMR spectra and by its odor in closely related studies. For example, reaction of Pd₂(SH)₂(μ-S)(dpm)₂ with 1 mole equivalent I₂ was studied in CDCl₃ and in DMSO-d₆:



Oxidative addition of I₂ occurs, and in low temperature NMR studies in CDCl₃, an intermediate was detected, characterized by a 1:4:6:4:1 quintet in the ¹H NMR spectrum and a singlet in the ³¹P{¹H} NMR spectrum. Similar spectral characteristics were seen for the intermediate

$\text{Pd}_2\text{L}_4(\text{dpm})_2$ in reactions of **1** or **2** with I_2 (see Chapter 4), and it is therefore reasonable to attribute the intermediate in reaction 5.3.5 to a species such as **I**; however, a $\delta(\text{Pd-SH})$ signal, typically at δ between 1.5 and -1.5,¹ was not observed. Of note, a $\delta(\text{Pd-SH})$ signal was also not seen in the ^1H NMR spectrum of the structurally similar intermediate $\text{Pd}_2\text{X}_2(\text{H})(\text{SH})(\text{dpm})_2$ (**III**) formed during reaction of **1** with H_2S at low temperature,¹⁰ and here it was suggested that either the $\delta(\text{Pd-SH})$ signal was buried under the H_2S signal, or the acidic SH proton was undergoing rapid exchange with H_2S protons.^{10,11}

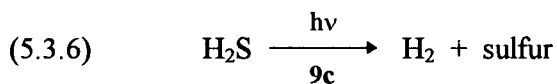


III

Reaction 5.3.5 is visualized to proceed in the same way that **2** reacts with X_2 (see Chapter 4), with the sulfur atoms produced during transannular oxidative addition undergoing concatenation to form elemental sulfur; elimination of H_2S , via a deprotonation/protonation involving the SH ligands, leads to formation of **2**. Interestingly, the expected H_2S signal at δ 1.99 in the ^1H NMR spectrum of the completed reaction in DMSO-d_6 was not observed, and the H_2S smell was not evident; instead, a broad singlet was seen at δ 5.68 and the H_2O singlet signal was absent. The broad singlet must be due to $\text{H}_3\text{O}^+\text{SH}$.

Important implications of reaction 5.3.1 are seen with the iodide system; photodecomposition of HI ¹² (bond strength is $\sim 295 \text{ kJ mol}^{-1}$; $\Delta G_f^\circ(\text{HI}(\text{g})) = 1.3 \text{ kJ mol}^{-1}$, $\Delta G_f^\circ(\text{HI}(\text{aq.})) = -55.9 \text{ kJ mol}^{-1}$), for example, produces H_2 and I_2 , and the latter can react with **2c**

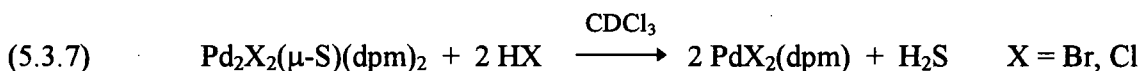
to give elemental sulfur, and complete the catalytic cycle with re-formation of **9c** (reaction 5.3.6, see section 5.1).



A few experiments were carried out in attempts to substantiate the catalysis implied in eq. 5.3.6, and Table 5.2 summarizes the results of photodecomposition studies. After the introduction of H₂S to DMSO-d₆ solutions of **9a**, **9b**, or **9c** (which generated **2**, **Y** and HX), the samples were placed in the presence of laboratory light or sunlight for up to 27 d. ¹H and ³¹P{¹H} NMR spectroscopic analyses revealed, in general, the disappearance of **2**, the disappearance or reduction of species **Y**, the disappearance of a species attributable aq. HX, an increase in **9**, and the appearance of PdX₂(dpm(S)) (**11**). The **11** complexes were previously seen in the study of the reaction of **2** with X₂ in CDCl₃ (see Chapter 4), and their formation was attributed to side-reactions of **9** with an S_n species (n<8); reaction of **9** with S₈ in CDCl₃ occurs only under photolytic conditions. In DMSO, **9** does slowly react with S₈ under purely thermal conditions, and the presence of light has little effect (Table 5.3); the observed reactivity trend is I>Br>Cl, which is the relative *trans* effect of the halide ligands. The disappearance of both **2** and the species attributable to aq. HX is consistent with photodecomposition of HX followed by reaction of **2** with the resulting X₂. GC analyses for H₂, however, remain inconclusive, a small positive peak in the chromatogram with a retention time corresponding to that of H₂ sometimes being seen. TLC analyses confirmed the presence of elemental sulfur. Reaction of **2c** with I₂ in DMSO-d₆ shows that transannular oxidative addition of I₂ occurs in this solvent to give after 1 d complete conversion to **9c** and **11c** (in a 1:1 ratio); interestingly, elemental sulfur does not form (in contrast to that observed in CHCl₃ - see Chapter 4), and considering that this reaction proceeds via the Pd₂L₄(dpm)₂ intermediate (as

evidenced by an observed green-black species - see Chapter 4), formation of **11c** occurs probably because of the S_n species ($n < 8$) being more stabilized in DMSO (than in $CHCl_3$) (see above).

Reactions of **2** with HX in $CDCl_3$ and in $DMSO-d_6$ were also investigated (Table 5.4). In $CDCl_3$, reaction of **2a** or **2b** with 2 mole equivalents of HCl or HBr, respectively, under purely thermal conditions produces H_2S and **9a** or **9b**, respectively:



Subsequent exposure to light yields no further changes in either system. As HCl and HBr do not exhibit acidic properties in $CDCl_3$,⁸ reaction 5.3.7 is pictured as proceeding via a series of HX additions across the Pd-S bonds with perhaps intermediate formation of $Pd_2X_3(SH)(dpm)_2$ (**II**) and then $Pd_2X_4(dpm)_2$; **9a** and **9b** would be subsequently formed by decomposition of $Pd_2X_4(dpm)_2$. Analogous reactions in $DMSO-d_6$ of HX with the chloride and bromide systems also proceed giving a mixture consisting of **9**, **11**, unreacted **2**, and non-Pd-containing species characterized by broad singlets in the 1H NMR spectra. These results imply that reaction 5.3.1 is more accurately described as an equilibrium:



The observed 1H NMR broad singlets could be due to a mixture of aquated (or solvated) HX and H_2S . The presence of **11** is difficult to explain but it is noted that during 1H and $^{31}P\{^1H\}$ NMR spectroscopic analyses, the samples were unavoidably exposed to laboratory light (the samples were submitted for analyses using the Bruker AC200E spectrometer that is equipped with an automatic sample changer). In separate photodecomposition studies, when aq. HBr in $DMSO-d_6$ was exposed to laboratory light for 12 h, Br_2 was formed (Table 5.5, Fig. 5.11). Thus, the formation of **11b** in the bromide system could result from reaction of **2b** with Br_2 (see Chapter 4); presumably, a similar reaction could take place in the chloride system to form **11a**. Exposure of

the type **2** complexes and HX to a Hg vapour lamp leads to the disappearance of **2a**, **2b**, and the species attributed to a mixture of HX(aq.) and H₂S(aq.) (replaced by new broad singlet - see Table 5.4); **9a**, **9b** and the corresponding **11a** and **11b** complexes were still observed (Table 5.4). GC did not reveal the presence of H₂ but elemental sulfur was seen by TLC. It is not clear why H₂ was not detected (by GC or NMR analyses) in these studies as well as in the separate photodecomposition studies of aq. HI and aq. HBr (Table 5.5), although in the latter studies sufficient amounts may not have been generated. Of note, in a single experiment where Pd₂Cl₂(dpm)₂ (**1a**) was reacted with H₂S in DMSO-d₆ on a similar NMR reaction scale, H₂ was positively identified by both GC and NMR analyses. In the iodide systems, however, H₂ was detected (by GC) in the reaction of **2c** with HI(g) (Table 5.4) but its presence is a result of decomposition of HI(g) during sample preparation because I₂ was observed to form on the inside wall of the NMR tube, well above the DMSO-d₆ solution of **2c**; **9c**, **11c**, sulfur, and dpm(O)₂ were also observed, but of interest a δ(H₂) signal in the ¹H NMR spectrum was not seen. The phosphine dioxide dpm(O)₂ is probably a consequence of excess I₂ (as well as trace O₂) in the system, as a single experiment in air in which **9c** was placed in the presence of 5 mole equivalents of I₂ revealed immediate decomposition to PdI₂(?) and dpm(O)₂; there is no reaction of **11c** with 5 mole equivalents of I₂ in air. Assuming that dpm(O)₂ results solely from PdI₂(dpm), the original yield of **9c** would be 59% with respect to **11c** (Table 5.4). Reaction of **2c** with aq. HI gave similar results but no H₂ was detected. In terms of possible mechanisms, reaction of **2** with HX in DMSO-d₆ could proceed as in reaction 5.3.7 in CDCl₃ but, in view of the acidic nature of HX in dimethylsulfoxide, via a series of nucleophilic additions of X⁻ to give again intermediates such as Pd₂X₃(SH)(dpm)₂ (**II**) and Pd₂X₄(dpm)₂, with the latter subsequently decomposing to **9**. However, having made this suggestion, it is not clear why reaction of **2b** with HCl immediately

forms exclusively a species thought to be $\text{Pd}_2(\text{Br})(\text{Cl})(\mu\text{-S})(\text{dpm})_2$ which slowly reacts further to give only trace amounts of $\text{Pd}(\text{Br})(\text{Cl})(\text{dpm})$, **9a**(?), **9b**(?), $\text{Pd}(\text{Br})(\text{Cl})(\text{dpm}(\text{S}))$ (*cis* or *trans*), **11a**(?), and **11b**(?). The presence and identities of the mononuclear species have not been unequivocally established but $^{31}\text{P}\{^1\text{H}\}$ NMR signals can be seen in regions indicative of chelating dpm and dpm(S) Pd complexes (Fig. 5.6).

Clearly, further studies are warranted, and if the existence of H_2 can be established, then reaction 5.3.6 could be the first homogeneously catalyzed decomposition of H_2S in solution to H_2 and elemental sulfur. For a workable system, however, means must be determined to limit or prevent the formation of species **Y** and by-product $\text{PdX}_2(\text{dpm}(\text{S}))$.

5.4 Experimental Section

The materials used, synthetic procedures for the ligands and complexes, and instrumentation used for ^{31}P and ^1H NMR spectroscopy, UV/vis spectrophotometry, and gas chromatography were described in Chapter 2. The complexes $\text{Pd}_2(\text{SH})_2(\mu\text{-S})(\text{dpm})_2$, **2a** - **2c**, and **9a** - **9c** were synthesized using published methods as outlined in Chapter 2. All experiments were performed under N_2 unless otherwise specified.

5.4.1 Preparation of gaseous HI

Hydrogen iodide gas was prepared from hydriodic acid (57% by weight, 7.58 M) using a procedure modified from that reported.^{12a} In a typical setup, P_2O_5 (~5 mg) and HI (aq.) (10 μL , 0.078 mmol) were separately placed in an NMR tube fitted with a PTFE J. Young valve, and the sample was then evacuated and left in the dark for ~3 d. Thereafter, the NMR tube was immersed in an ice-bath, and the HI gas (m.p. $-50.8\text{ }^\circ\text{C}$, b.p. $-35.4\text{ }^\circ\text{C}$) was vacuum transferred using liquid N_2 for use. Note: due to the corrosive nature of aq. HI, 10 μL were used as this quantity was convenient to handle by a 250 μL syringe; use of a 10 μL syringe to transfer smaller amounts resulted in immediate blockage in the needle.

5.4.2 Reaction of $\text{PdX}_2(\text{dpm})$ (**9**) with H_2S

Reaction of $\text{PdX}_2(\text{dpm})$ (**9**) with 0.5, 0.75, 1.0, or 1.5 mole equivalent H_2S was studied at R.T. on an NMR-scale in CDCl_3 and DMSO-d_6 . To a rubber septum-sealed NMR or Schlenk

(165.0 mL volume) tube, or an NMR tube fitted with a PTFE J. Young valve, was placed a 0.50 mL solution of **9** (**9a**, 5 mg, 0.0089 mmol; **9b**, 5 mg, 0.0076 mmol; **9c**, 5 mg, 0.0067 mmol). H₂S (**9a**: 108 μL at STP, 0.0045 mmol; **9b**: 92 μL at STP, 0.0038 mmol; **9c**: 81 μL (0.0034 mmol), 122 μL (0.0051 mmol), 162 μL (0.0068 mmol), and 243 μL (0.0102 mmol), all at STP) was slowly administered either by injection via syringe (in increments of 50 μL/min when using Schlenk-techniques) or by vacuum transfer. The sample was briefly shaken or continuously stirred, and was permitted to react in the absence of light for 1, 2, or 24 h prior to ¹H and ³¹P{¹H} NMR spectroscopic analyses. The sample was then placed under laboratory light or sunlight for periods of 1, 2, 5, 8, or 27 d; thereafter, the contents were analyzed using NMR and UV/vis spectroscopy and thin-layered (CHCl₃) and gas chromatography.

Titration studies were carried out for the chloride system. In a Schlenk tube (165.0 mL volume) fitted with a rubber septum was placed **9a** (25 mg, 0.045 mmol) dissolved in DMSO (4.5 mL). The solution was rapidly stirred, and H₂S (545 μL at STP, 0.022 mmol) was injected in increments of 100 μL/min. The mixture was continuously stirred for 2 h during which the initially yellow solution gradually turned red-brown. H₂O (15 mL) was then added, and a fine orange precipitate formed. This mixture was then de-gassed briefly to remove H₂S and washed with CH₂Cl₂ (2 x 10 mL) before being filtered through a column of Celite 545 (2 cm x 10 cm). The column was subsequently washed with H₂O (2 x 5 mL), and the washings were combined with the colourless, clear filtrate, which was then titrated with a standardized solution of NaOH (0.010 M) using phenolphthalein as indicator. For a blank titration, the above procedure was repeated but with no H₂S added.

5.4.3 Reaction of PdX₂(dpm) (**9**) with elemental sulfur

Reaction of PdX₂(dpm) (**9**) with 1 mole equivalent S₈ was studied at R.T. and at 50 °C on the NMR-scale in DMSO-d₆. PdX₂(dpm) (**9a**, 10 mg, 0.0178 mmol; **9b**, 10 mg, 0.0152 mmol; **9c**, 10 mg, 0.0134 mmol) and S₈ (**9a**: 0.57 mg, 0.0178 mmol; **9b**: 0.49 mg, 0.0152 mmol; **9c**, 0.43 mg, 0.0134 mmol) were placed in an NMR tube fitted with a rubber septum, and 0.50 mL DMSO-d₆ was introduced. The sample was briefly shaken to ensure complete mixing, and was then placed in the dark or under laboratory light or sunlight for periods of 1, 2, 5, 9, 10, or 29 d prior to NMR analyses.

5.4.4 Reaction of Pd₂I₂(μ-S)(dpm)₂ (**2c**) with I₂

Reaction of Pd₂I₂(μ-S)(dpm)₂ (**2c**) with 1 mole equivalent I₂ was studied on an NMR-scale at R.T. in DMSO-d₆. To a 0.40 mL solution of **2c** (10 mg, 0.0078 mmol) in a rubber septum-sealed NMR tube was injected a 0.10 mL solution of I₂ (2.0 mg, 0.0078 mmol). The sample was analyzed after 24 h using NMR spectroscopy and thin-layered chromatography (CHCl₃ eluent).

5.4.5 Reaction of Pd₂X₂(μ-S)(dpm)₂ (**2**) with HX

Reaction of Pd₂X₂(μ-S)(dpm)₂ (**2**) with HX was studied on an NMR-scale at R.T. in CDCl₃ and DMSO-d₆. A 0.50 mL solution of **2** (**2a**, 10 mg, 0.0092 mmol; **2b**, 10 mg, 0.0085 mmol; **2c**, 10 mg, 0.0078 mmol) was placed in a NMR tube fitted with a rubber septum or a PTFE J. Young valve, and HX (HCl(g), 446 μL at STP, 0.0184 mmol; HBr(g) at STP, 412 μL, 0.0170

mmol; HI(aq. or g), 0.078 mmol) was injected or vacuum transferred in. The sample was then analyzed “immediately” and after 24 h using NMR spectroscopy. Subsequently, the sample was placed under laboratory light, sunlight, or light from an 18 W TLC lamp for 1 or 5 d. Thereafter, the sample was again analyzed using NMR spectroscopy and thin-layered (CHCl_3 eluent) and gas chromatography. Reaction of **2b** with HCl was similarly studied. To a 0.50 mL DMSO-d_6 solution of **2b** (10 mg, 0.0085 mmol) placed in a rubber septum-sealed NMR tube was added HCl(g) (412 μL , 0.0170 mmol) via syringe. The remainder of the procedure is as described above.

5.4.6 Reaction of $\text{Pd}_2(\text{SH})_2(\mu\text{-S})(\text{dpm})_2$ with I_2

Reaction of $\text{Pd}_2(\text{SH})_2(\mu\text{-S})(\text{dpm})_2$ with 1 mole equivalent I_2 was studied on an NMR- scale at R.T. in CDCl_3 and DMSO-d_6 and at low temperatures in CDCl_3 . At R.T., a 0.40 mL solution of $\text{Pd}_2(\text{SH})_2(\mu\text{-S})(\text{dpm})_2$ (10 mg, 0.0093 mmol) was placed in an NMR tube fitted with a rubber septum, and a 0.10 mL solution of I_2 (2.4 mg, 0.0093 mmol) was injected. The sample was analyzed after 24 h using NMR spectroscopy. To study the reaction at low temperatures, the sample was similarly prepared but at $-60\text{ }^\circ\text{C}$ (liq. N_2 /chloroform slush bath).¹³ NMR analyses were then carried out “immediately” at $-60\text{ }^\circ\text{C}$; thereafter, the temperature was raised (-45 , 10 , and $20\text{ }^\circ\text{C}$) and NMR spectra were recorded at each new temperature. Corresponding TLC studies (CHCl_3 eluent) were subsequently performed for each sample.

5.4.7 Reaction of PdX₂(dpm) (9) with NaSH

Reaction of PdX₂(dpm) (9) with 0.5 NaSH was studied on an NMR-scale at R.T. in DMSO-d₆. PdX₂(dpm) (9a, 10 mg, 0.0178 mmol; 9b, 10 mg, 0.0152 mmol; 9c, 10 mg, 0.0134 mmol) was placed in an NMR tube fitted with a rubber septum, and a 0.50 mL suspension of NaSH (9a: 0.50 mg, 0.0089 mmol; 9b: 0.43 mg, 0.0076 mmol; 9c: 0.38 mg, 0.0067 mmol) was injected. The samples were analyzed after 24 h using NMR spectroscopy.

5.4.8 Photodecomposition studies of HI, HBr, and H₂S

HI, HBr, and H₂S were irradiated using laboratory light, sunlight, or intense light from a 450 W medium pressure Hg vapour lamp in order to determine the extent of photodecomposition to H₂ and I₂, Br₂, or elemental sulfur, respectively. Specifically, aq. HI (10 μL, 0.078 mmol) or HBr (10 μL, 0.088 mmol) was dissolved in 0.50 mL CDCl₃ or DMSO-d₆ held in a rubber septum-sealed NMR tube or an NMR tube fitted with a PTFE J. Young valve, and the sample was placed in the appropriate light source for periods of 0.5, 1, 2, or 5 d. Thereafter, the liquid and head space of the sample were analyzed for H₂ using gas chromatography. Similar studies were also performed for H₂S (1.0 mL at STP, 0.041 mmol) and aqueous and gaseous HI (prepared from 10 μL HI (aq.), see above) without prior dissolution into a solvent. UV/vis spectroscopy was also used to analyze all samples for I₂ and elemental sulfur. For the liquid samples, analyses were carried out in CHCl₃ using ~5 μL (droplet transferred using a glass pasteur pipette) of the liquid. For the gaseous samples, the NMR tube was briefly evacuated before CHCl₃ was used to dissolve any deposit (I₂, S₈) found on the inside walls of the tube.

5.5 References for Chapter 5

1. Besenyei, G.; Lee, C-L.; Gulinski, J.; Rettig, S.J.; James, B.R.; Nelson, D.A.; Lilga, M.A. *Inorg. Chem.* **1987**, *26*, 3622.
2. Carey, F.A.; Sundberg, R.J. "Advanced Organic Chemistry, 3rd Ed. Part A: Structure and Mechanisms", Plenum Press, New York, 1993, ch. 5, p. 284.
3. Support for the dissociation of H₂S in DMSO to give solvated H⁺ and SH⁻ ionic species comes from the similarities in solvent properties DMSO displays compared with other polar, aprotic solvents. See also: a) Plummer, M.A. *Hydrocarbon Proc.* **1987**, *38*. b) Collman, J.P.; Finke, R.G.; Cawse, J.N.; Brauman, J.I. *J. Am. Chem. Soc.* **1977**, *99*, 2515.
4. Puddephatt, R.J. *Chem. Soc. Rev.* **1983**, *99*.
5. Shaver, A.; Lai, R.D.; Bird, P.; Wickramasinghe, W. *Can. J. Chem.* **1985**, *63*, 2555, and references therein.
6. Schmidt, M.; Hoffmann, G.G.; Holler, R. *Inorg. Chim. Acta* **1979**, *32*, L19.
7. See for example: Carey, F.A.; Sundberg, R.J. "Advanced Organic Chemistry, 3rd Ed. Part A: Structure and Mechanisms", Plenum Press, New York, 1993, ch. 4, p. 232.
8. Huheey, J.E. "Inorganic Chemistry, 3rd Ed. Principles of Structure and Reactivity", Harper and Row, New York, 1983, ch. 8, p. 328.
9. a) Jessop, P.G.; Lee, C-L.; Rastar, G.; James, B.R.; Lock, C.J.L.; Faggiani, R. *Inorg. Chem.* **1992**, *31*, 4601. b) Lee, C-L.; Chisholm, J.; James, B.R.; Nelson, D.A.; Lilga, M.A. *Inorg. Chim. Acta* **1986**, *121*, L7. c) Jessop, P.G.; Rettig, S.J.; Lee, C-L.; James, B.R. *Inorg. Chem.* **1991**, *30*, 4617.
10. Barnabas, A.F.; Sallin, D.; James, B.R. *Can. J. Chem.* **1989**, *67*, 2009.
11. Jennings, M.C.; Payne, N.C.; Puddephatt, R.J. *J. Chem. Soc., Chem. Commun.* **1986**, 1809.
12. Although much has been published on the photodecomposition of HI, HBr, HCl, and H₂S in the gas phase, similar studies in solution appear to be lacking. See for example: a) Martin, R.M.; Willard, J.E. *J. Chem. Phys.* **1964**, *40*, 2999. b) Huebert, B.J.; Martin, R.M. *J. Phys. Chem.* **1968**, *72*, 3046.

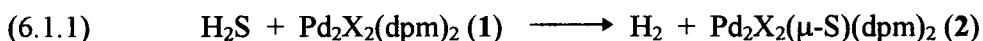
- c) Cadman, P.; Polanyi, J.C. *J. Phys. Chem.* **1968**, *72*, 3715. d) Compton, L.E.; Martin, R.M. *J. Phys. Chem.* **1969**, *73*, 3474. e) Oldershaw, G.A.; Porter, D.A.; Smith, A. *J. Chem. Soc. Faraday I* **1972**, *68*, 2218. f) Clear, R.D.; Riley, S.J.; Wilson, K.R. *J. Chem. Phys.* **1975**, *63*, 1340. g) Calvert, J.G.; Pitts, Jr., J.N. "Photochemistry", John Wiley & Sons, London, 1967, ch. 3, p. 196.
13. Gordon, A.J.; Ford, R.A. "The Chemist's Companion", John Wiley & Sons, Toronto, 1972, p. 451.

CHAPTER 6

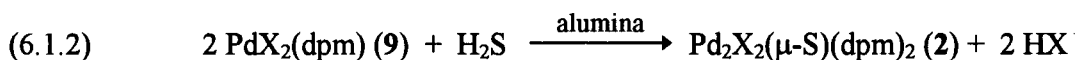
Reaction of $\text{PdX}_2(\text{dpm})$ with H_2S in the Presence of Alumina; Catalyzed Formation of $\text{Pd}_2\text{X}_2(\mu\text{-S})(\text{dpm})_2$

6.1 Introduction

The discovery of the homogeneous conversion of H_2S to H_2 in solution using complexes of the type $\text{Pd}_2\text{X}_2(\text{dpm})_2$ (**1**) (reaction 6.1.1)¹ led to some earlier attempts to heterogenize the reaction. Syntheses of $\text{Pd}_2\text{X}_2(\text{dpm})(\text{dpmMe})$ complexes where one of the bridging dpm ligands of **1** is replaced with dpmMe (1,1'-bis(diphenylphosphino)ethane), for example, were carried out with the aim of immobilizing the Pd complex via the methyl group to a solid support such as polystyrene.² With the finding that $\text{Pd}_2\text{X}_2(\text{dpm})(\text{dpmMe})$ can also react with H_2S to form quantitatively H_2 and the bridged-sulfide complex $\text{Pd}_2\text{X}_2(\mu\text{-S})(\text{dpm})(\text{dpmMe})$ ² and that H_2S can be catalytically converted to H_2 (see Section 1.3, p. 24),³ the prospect of heterogenization for the ease of product separation seemed even more favourable.

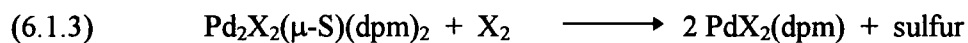


Kinetic and mechanistic studies on the S-abstraction process $\mathbf{2} \rightarrow \mathbf{1}$ using dpm (see Chapter 3), however, revealed that immobilization may not be appropriate or feasible because the bridging phosphine ligands of **2** are also involved in the S-abstraction; for example, reaction of **2** with added dpm- d_2 (or dpmMe) gives dpm(S) (or dpmMe(S)) products with distributions that are close to statistical regarding the availability of 3 chelating (P-P) moieties (see Section 3.3).³ Work on heterogenization was continued during the course of this thesis, and reaction 6.1.2 was discovered, occurring in the presence of alumina.



Reaction of **9** with H_2S was described in Chapter 5 and can take place in dimethylsulfoxide without the need for alumina; however, the formation of side-products, especially $\text{Pd}(\text{SH})_2(\text{dpm})$, was sometimes seen. Reaction 6.1.2 was studied in CHCl_3 , and the presence of alumina was

shown to be necessary. The reaction appears to proceed cleanly, in contrast to that when DMSO solvent was utilized. Important implications are again seen with the $X = I$ system; photodecomposition of HI, for instance, produces H_2 and the I_2 , and the latter can complete the catalytic cycle via reaction 6.1.3 (see Chapter 4).³



This chapter summarizes preliminary work on reaction 6.1.2; results of surface studies on the alumina used are also discussed.

6.2 Results

Reaction 6.1.2 was studied at R.T. in CDCl_3 on the NMR-scale, and NMR and X-ray photoelectron spectroscopies were used to analyze the solution and the alumina surface, respectively. Various experiments were carried out for the chloride system as outlined in the Experimental Section; Table 6.1 summarizes the content make-up for each type of experiment (hereafter also referred to as “sample”). The alumina used is of the γ -type, commonly used as chromatographic absorbents (powder (av. mesh size 200) or TLC plate forms (mesh size 60)). Samples 1 - 5 were prepared for NMR spectroscopic analyses only. For sample 1, there were no detectable changes in the colour of the solvent (colourless) or the alumina (white) after 24 h; the ^1H NMR spectrum recorded 24 h after sample preparation reveals in addition to the sharp singlets of residual CHCl_3 and H_2O at δ 7.24 and 1.54, respectively, a broad unresolved signal (possibly a doublet or triplet) at δ 1.2 (Fig. 6.1). These observations were also made for sample 2, the H_2S singlet at δ 0.82 (observed under the same conditions in the absence of alumina) not being seen. For samples 3 and 4 (prior to addition of H_2S), addition of **9a** yielded immediately a yellow solution, while the white alumina gradually turned orange after ~ 1 h. When a stoichiometric amount of H_2S (see eq. 6.1.2, $\text{H}_2\text{S} : \mathbf{9} = 0.5$) was introduced for sample 4, the alumina immediately turned orange-brown, and the solution at the same time changed from yellow to brown-yellow. ^1H and $^{31}\text{P}\{^1\text{H}\}$ NMR spectroscopic analyses of sample 3 revealed the presence of **9a**, with no other Pd species seen (Fig. 6.2a); for sample 4, trace amounts of $\text{Pd}_2\text{Cl}_2(\mu\text{-S})(\text{dpm})_2$ (**2a**) were observed (Fig. 6.2b). The order of adding **9a** and H_2S was reversed for sample 5 compared to that for sample 4; addition of a stoichiometric amount of H_2S first again produced no detectable changes in the system. Subsequent addition of **9a** (~ 1 h after the addition of H_2S) yielded an immediate colour

Table 6.1. Summary of the content make-up in Expts. 1 - 18; **9a** = PdCl₂(dpm).

Sample	Contents
1	CDCl ₃ (0.7 mL), γ -alumina powder (15 mg)
2	CDCl ₃ (0.7 mL), γ -alumina powder (15 mg), H ₂ S (110 μ L at STP, 0.0045 mmol)
3	CDCl ₃ (0.7 mL), γ -alumina powder (15 mg), 9a ^a
4	CDCl ₃ (0.7 mL), γ -alumina powder (15 mg), 9a , H ₂ S (110 μ L at STP, 0.0045 mmol)
5	CDCl ₃ (0.7 mL), γ -alumina powder (15 mg), H ₂ S (110 μ L at STP, 0.0045 mmol), 9a
6	CDCl ₃ (0.7 mL), γ -alumina powder (15 mg, pre-dried at 150 °C for 24 h), H ₂ S (110 μ L at STP, 0.0045 mmol), 9a
7	CDCl ₃ (1.0 mL), γ -alumina plate, ^b H ₂ S (0.5 mL at STP, 0.021 mmol), 9a
8	CDCl ₃ (1.0 mL), γ -alumina powder (11.5 mg) from 1.0 cm x 1.0 cm plate, 9a , H ₂ S (0.5 mL at STP, 0.021 mmol)
9	CDCl ₃ (1.0 mL), γ -alumina powder (15 mg, finely ground), 9a , H ₂ S (0.5 mL at STP, 0.021 mmol)
10	CDCl ₃ (1.0 mL), α -alumina powder (corundum, 15 mg), 9a , H ₂ S (0.5 mL at STP, 0.021 mmol)
11	10 mL CDCl ₃ solution of 9a (10 mg, 0.018 mmol), 10 mL MeOH solution of NaSH (1.0 mg, 0.018 mmol)

Table 6.1. (cont.)

12	CDCl ₃ (1.0 mL), γ -alumina plate
13	CDCl ₃ (1.0 mL), γ -alumina plate, 9a
14	CDCl ₃ (1.0 mL), γ -alumina plate, H ₂ S (0.5 mL at STP, 0.021 mmol)
15	CDCl ₃ (1.0 mL), γ -alumina plate, 9a , H ₂ S (0.5 mL at STP, 0.021 mmol)
16	CDCl ₃ (1.0 mL), γ -alumina plate, H ₂ S (0.5 mL at STP, 0.021 mmol), 9a
17	CDCl ₃ (1.0 mL), γ -alumina plate, S ₈ (12 mg, 0.047 mmol)
18	CDCl ₃ (1.0 mL), γ -alumina plate, HCl (0.5 mL at STP, 0.021 mmol)

^a 5 mg of **9a** (0.0089 mmol) was always used. ^b The γ -alumina plates were all 1.0 cm x 1.0 cm.

Fig. 6.1. Representative ^1H NMR spectrum (300 MHz) of samples 1 or 2 containing γ -alumina powder (15 mg) in CDCl_3 with and without the presence of H_2S (110 μL at STP), respectively.

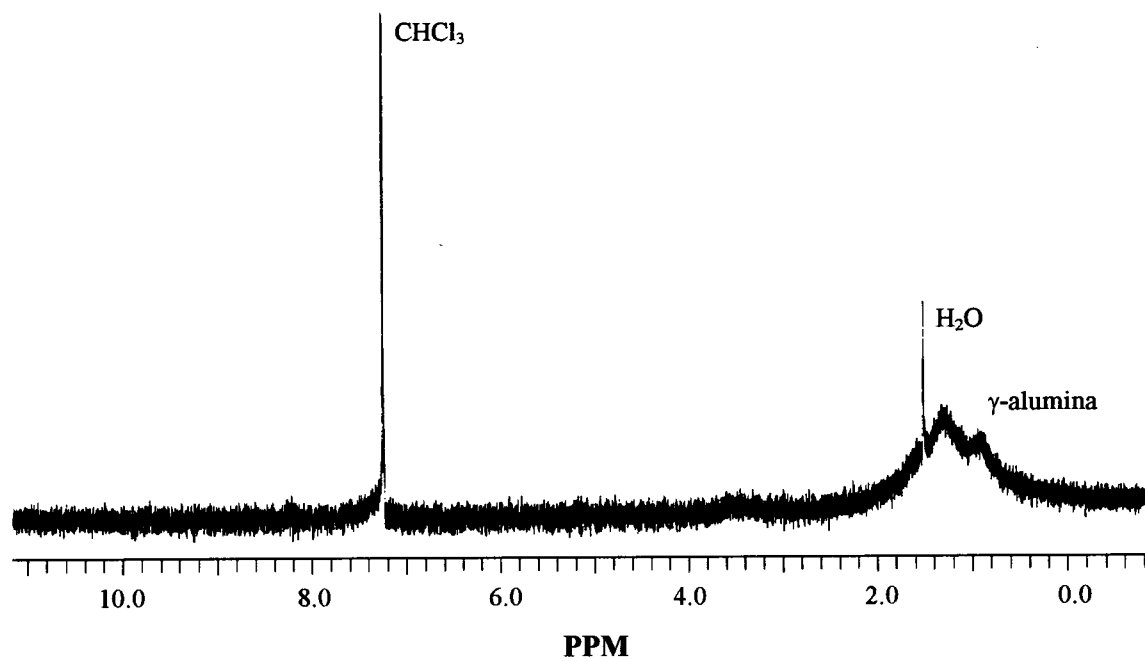
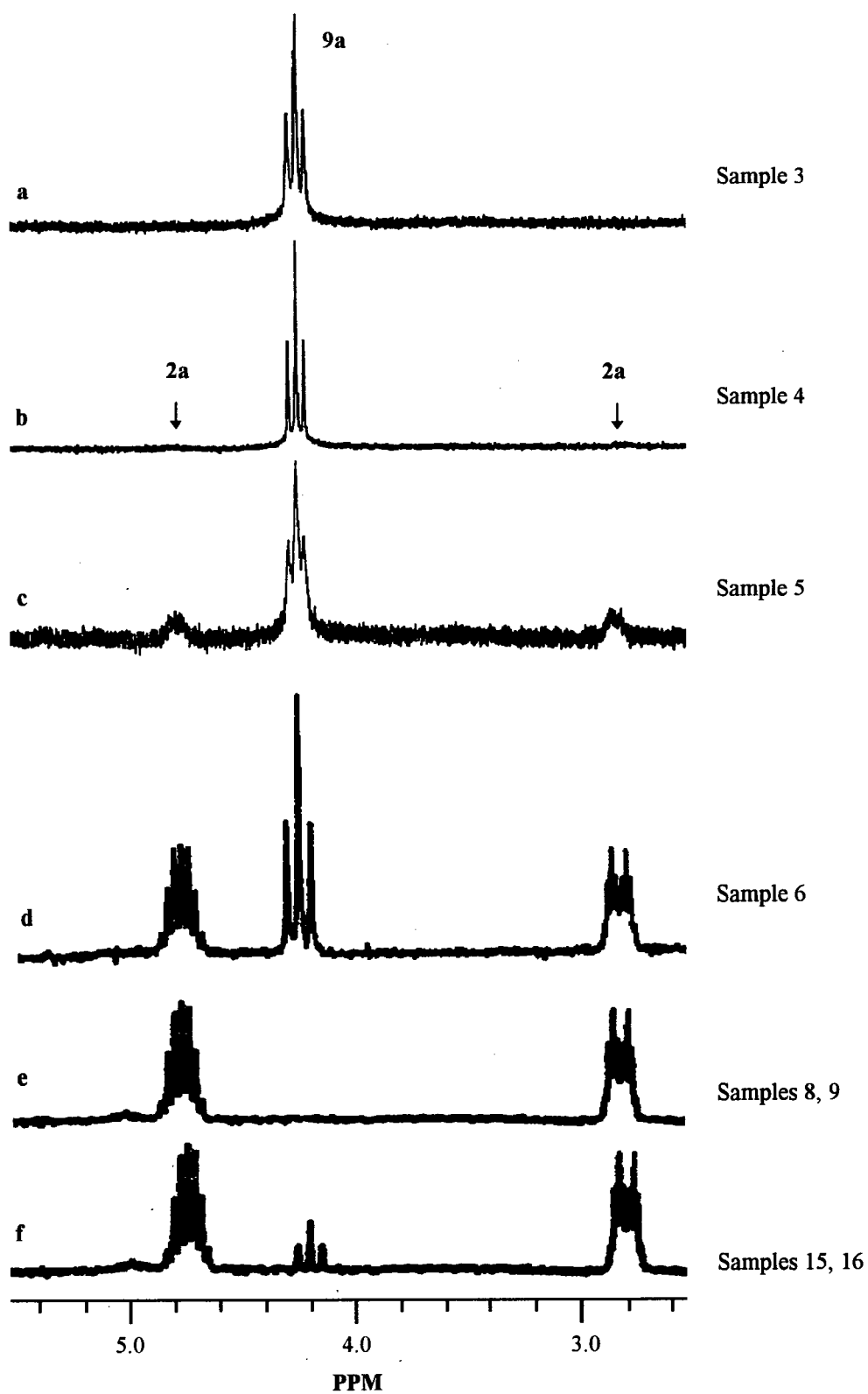
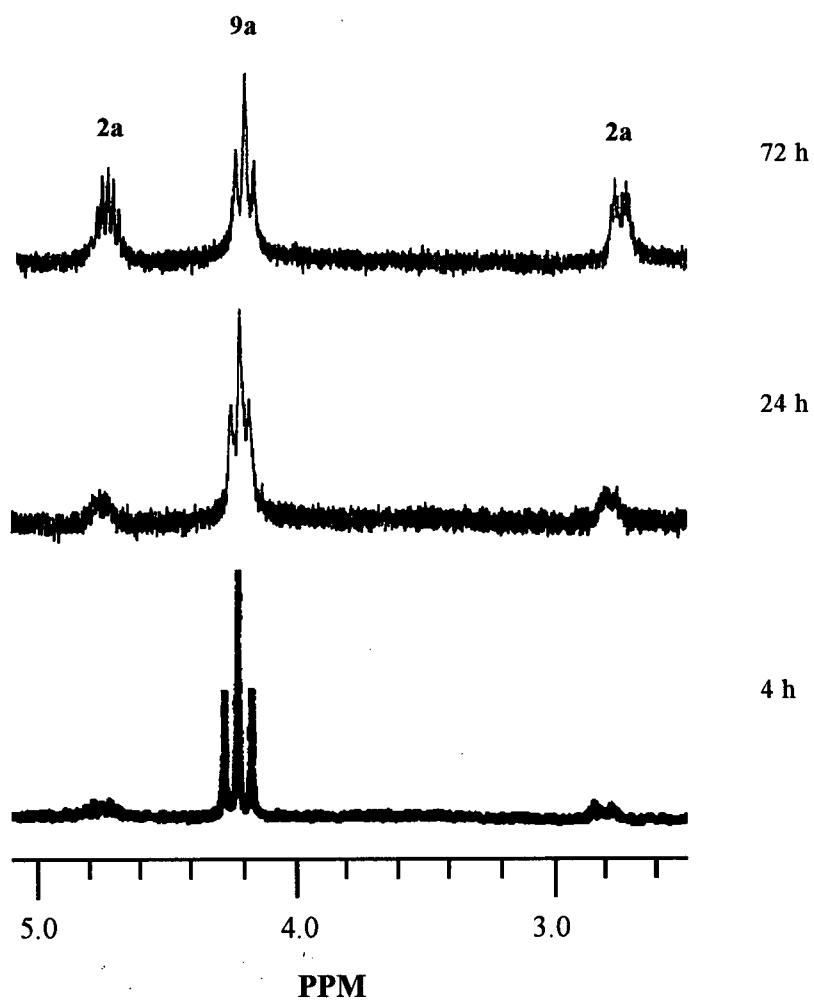


Fig. 6.2. ^1H NMR spectra (300 MHz) showing the extent of the reaction at R.T. of $\text{PdCl}_2(\text{dpm})$ (**9a**) with H_2S in CDCl_3 in the presence of γ -alumina under various experimental conditions; **2a** = $\text{Pd}_2\text{Cl}_2(\mu\text{-S})(\text{dpm})_2$.



change of both the white alumina and the colourless solution to orange-brown; qualitatively, there were no further visible changes over time. As observed for sample 4, ^1H and $^{31}\text{P}\{^1\text{H}\}$ NMR analyses for sample 5 also revealed the formation of **2a** but in more significant amounts, ~10% yield relative to **9a** (determined from the relative integrated areas of the respective CH_2 proton signals) (Fig. 6.2c). Sample 6 was prepared in the same way as sample 5 except that the alumina was pre-dried for 24 h at 150 instead of 75 °C. NMR analyses again revealed the formation of **2a** but in 60% yield (Fig. 6.2d). In these experiments (4 - 6), H_2S was again not seen in the ^1H NMR spectra. Experiment 7 was performed to determine if removal of H_2S pre-treated alumina from an H_2S (2.5 mole excess) solution, with subsequent drying of the alumina (under an Ar atmosphere) and its placement in a CDCl_3 solution containing only **9a**, could affect the dinucleation reaction. As with sample 3, the alumina slowly turned orange, and NMR analysis of the solution revealed only the starting material **9a**. It should be noted that in samples 3 - 7, undissolved **9a** (0.5 - 1 mg) was seen. Samples 8 - 10 were prepared using alumina powder scraped from a TLC plate, finely ground γ -alumina powder, and α -alumina, respectively; H_2S (2.5 mole excess) was then introduced into the system immediately after the mixture of **9a** and alumina in CDCl_3 was prepared. In experiments 8 and 9, the system immediately turned orange from an initial yellow, and NMR analyses after 4 h revealed that **9a** has completely reacted with **2a** as the only product detected (Fig. 6.2e). For experiment 10, however, the alumina turned yellow but NMR analyses after 4 h revealed **9a** and trace amounts of **2a** (Fig. 6.3); after 24 h, a 10% yield of **2a** was seen and, after 72 h, 50%. Experiment 11 was conducted to determine if **2a** could be formed from reaction of **9a** with 1 mole equivalent NaSH under conditions in which NaSH is slowly added to a solution of **9a** such that the local concentration of NaSH is kept low. During this experiment, the odor of H_2S was detected; NMR analyses again revealed that **9a** has completely reacted to form

Fig. 6.3. ^1H NMR spectra (300 MHz) showing the progress of the reaction at R. T. of $\text{PdCl}_2(\text{dpm})$ (**9a**, 8.9×10^{-3} M) with 2.5 mole equivalent H_2S in CDCl_3 in the presence of α -alumina (15 mg); **2a** = $\text{Pd}_2\text{Cl}_2(\mu\text{-S})(\text{dpm})_2$.



2a. Samples 12 - 18 were prepared mainly for surface studies; NMR spectroscopic analyses were carried out for samples 15 and 16. Samples 12 - 14 were control samples in which alumina plates (1.0 cm x 1.0 cm) were placed in CDCl_3 in the absence or presence of **9a** or H_2S (5 mole excess) and left at R.T. for ~4 h before analysis. For samples 12 and 14, there were no visible changes in the systems during this time period; the colour of the alumina plates remained white and the solvent colourless. For sample 13, however, the presence of **9a** yielded a yellow solution, and the initially white alumina plate slowly became orange over ~1 h; the presence of undissolved **9a** (~0.5 mg) was also observed. The plates were removed ~4 h after sample preparation and were analyzed using XPS with results shown in Figs. 6.4 to 6.7. For sample 12, the XPS spectrum (Fig. 6.4a) is characteristic of alumina⁴ (Fig. 6.4b) and shows peaks arising from the Al 2p, Al 2s, and O 1s photoelectrons with binding energies of 74.5, 119.8, and 531.8 eV, respectively; the XPS spectrum of the alumina powder used in samples 1 - 5 is identical to that shown in Fig. 6.4a. Also seen are the signals arising from the C 1s and N 1s photoelectrons with corresponding binding energies of 285.0 and 399.3 eV, respectively, as well as signals from the Auger electrons of O and C with kinetic energies of 507.5 and 260.7 eV, respectively. These spectral characteristics were also observed in all other samples (13 - 18) studied. For sample 13, the XPS spectrum (Fig. 6.5) shows additional signals arising from the Cl 2p, Pd 3d_{5/2}, and Pd 3d_{3/2} photoelectrons with corresponding binding energies of 198.2, 337.0, and 342.5, respectively; the Pd 3d_{5/2}, Pd 3d_{3/2}, and Cl 2p photoelectron signals are shown in more detail in Figs. 6.6 and 6.7. For sample 14, a S 2p photoelectron signal is observed with a binding energy of 169.1 eV (Fig. 6.7). Samples 15 and 16, as for samples 4 and 5, differ in the order of addition of **9a** and H_2S (2.5 mole excess). For sample 15, introduction of **9a** yielded a yellow solution and an initially white alumina plate which slowly changed to orange over a period of ~1 h; some undissolved **9a** (~0.5 mg) was still seen. When

Fig. 6.4. X-ray photoelectron spectra of γ -alumina: a) experimental; b) literature, taken from ref. 4, pertaining to a surface cleaned by bombardment with Ar.

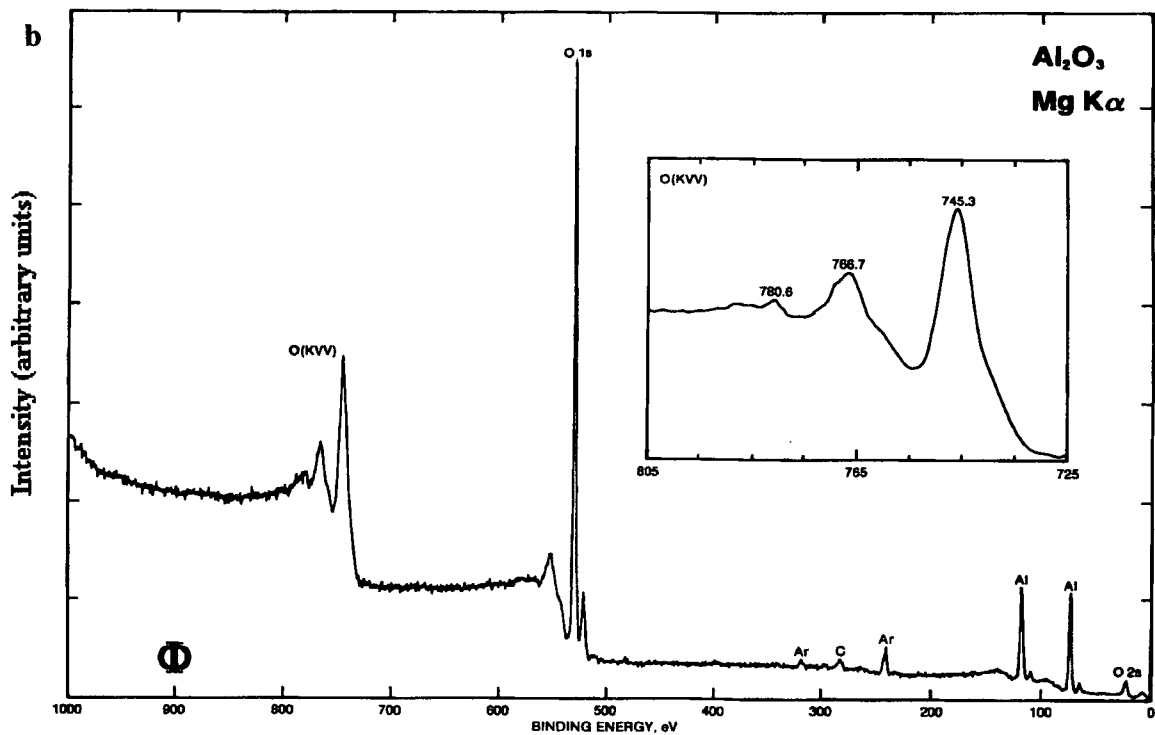
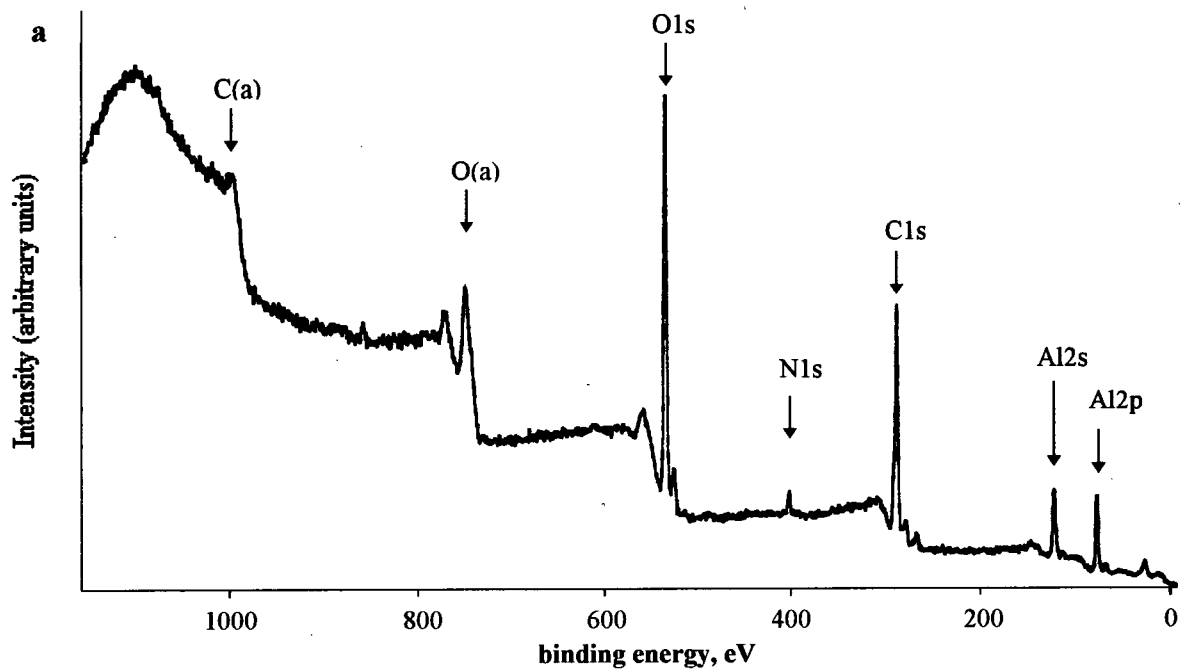


Fig. 6.5. X-ray photoelectron spectrum (Mg $K\alpha$, R.T.) of sample 13 consisting of PdCl₂(dpm) (9a) adsorbed on γ -alumina.

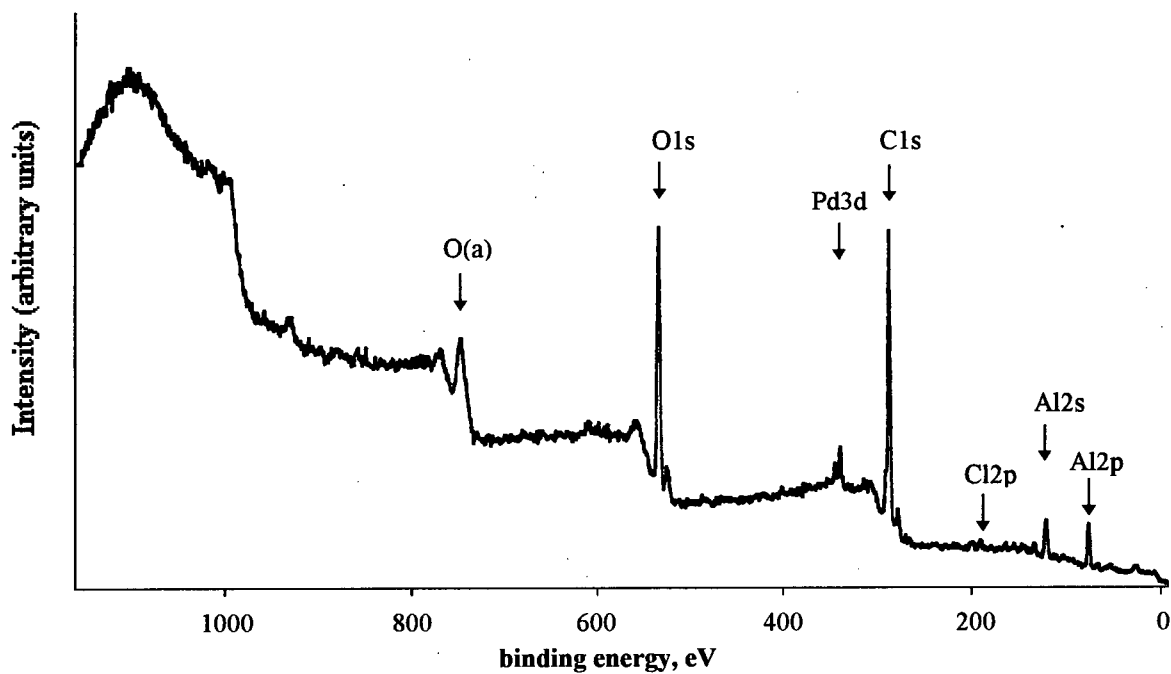


Fig. 6.6. X-ray photoelectron spectra (Mg $K\alpha$, R.T.) showing the Pd 3d photoelectron signals for samples 13, 15, and 16.

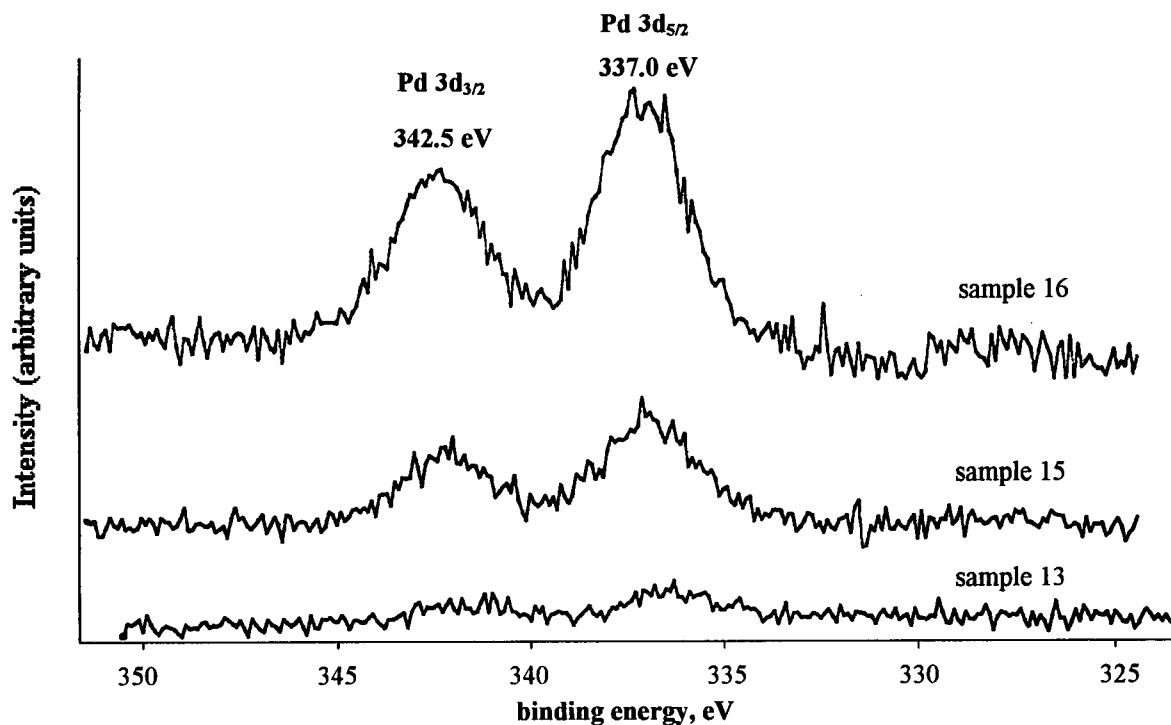


Fig. 6.7. X-ray photoelectron spectra (Mg K α , R.T.) showing the Cl 2p and S 2p photoelectron signals of samples 13, 14, 15, and 16.

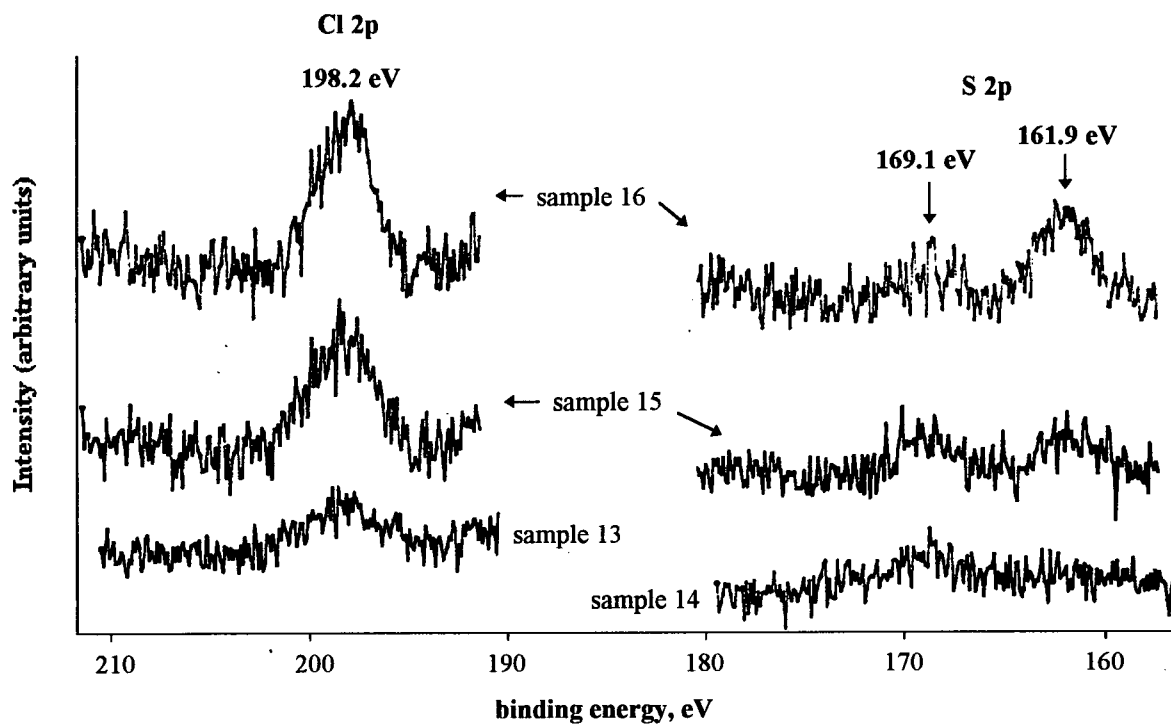
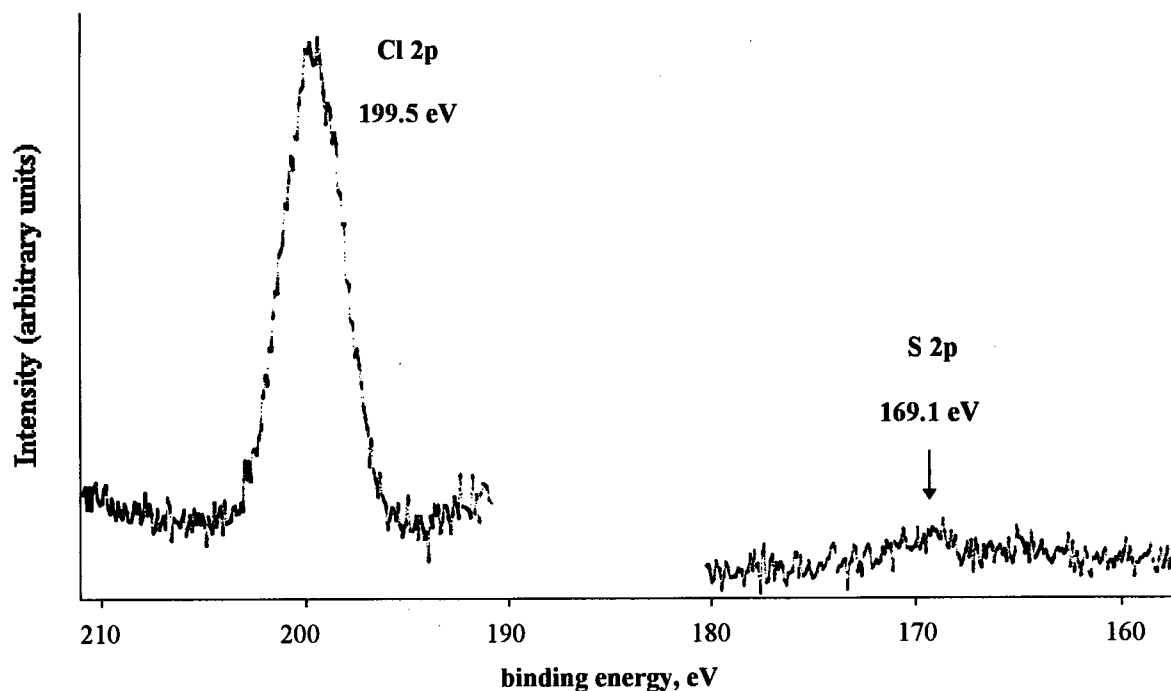


Fig. 6.8. X-ray photoelectron spectra (Mg K α , R.T.) showing the S 2p and Cl 2p photoelectron signals of samples 17 and 18, respectively.



H₂S was added next (~2 h after the introduction of **9a**), the alumina plate immediately turned orange-brown and the solution slowly changed to a final brown colour. The sample was permitted to react for 2 h and then analyzed; undissolved **9a** was no longer seen. The ¹H NMR spectrum reveals the formation of **2a** in >90% yield relative to unreacted **9a** (Fig. 6.2f); trace amounts of H₂S at δ 0.82 were also detected. Surface studies on the alumina plate revealed some findings similar to those for samples 13 and 14. Signals arise, for example, from the photoelectrons of the Pd 3d, Cl 2p, and S 2p subshells (Figs. 6.6 and 6.7); however, a new S 2p signal is seen at 161.9 eV (Fig. 6.7). For sample 16, the order of introducing **9a** and H₂S into the system was reversed (compared to that in sample 15), and addition of H₂S produced no visual changes in the system. When **9a** was added ~2 h later, the colour of the alumina plate immediately turned orange-brown; the solution had a yellow colour and undissolved **9a** (~0.5 mg) was seen. The system was then reacted for 2 h and then analyzed; the solution during the reaction period changed colour to a final brown and undissolved **9a** was no longer seen. NMR and surface analyses gave the same findings as observed for sample 15 (Fig. 6.2f). Samples 17 and 18 were prepared as control samples in which alumina was tested for absorption of S₈ and HCl(g), respectively; yellow and white plates resulted, respectively. The XPS spectrum for sample 17 shows an S 2p signal at 169.1 eV and that of sample 18 a Cl 2p signal at 199.5 eV (Fig. 6.8).

Low temperature NMR analysis of reaction 6.1.2 was performed when H₂S (~1 mole equivalent) was added to a CDCl₃ mixture of **9a** (1.8×10^{-2} M) and γ -alumina (15 mg) held at -42 °C. The solution immediately changed colour from pale yellow to orange-yellow. Analysis at -50 °C 1 h after sample preparation revealed the presence of the starting material **9a** and the product **2a** in ~50% yield; no other species were detected. Re-analysis of the sample after being placed at R.T. for 24 h revealed the presence of only **2a**.

To substantiate and quantify the HX produced in reaction 6.1.2, a series of synthetic-scale experiments were performed in which $\text{PdX}_2(\text{dpm})$ (**9a**, 1.8×10^{-2} M; **9b**, 1.5×10^{-2} M; **9c**, 1.3×10^{-2} M) and H_2S (1.0 M) were reacted at R.T. in 2.5 mL CHCl_3 containing 75 mg finely ground γ -alumina. Addition of H_2S to a rapidly stirred CHCl_3 mixture of **9** and alumina immediately (within seconds) caused a colour change from yellow (chloride or bromide system) or orange (iodide system) to a final brown. The mixture was reacted for ~ 4 h before the alumina was filtered off, washed, and dried. The filtrate and the washings were combined, and the solvents were removed by rotary evaporation with the resulting residue dissolved in CDCl_3 and analyzed using NMR spectroscopy. The ^1H and $^{31}\text{P}\{^1\text{H}\}$ NMR spectra showed the presence of only $\text{Pd}_2\text{X}_2(\mu\text{-S})(\text{dpm})_2$ (**2**); the yields of this product (**2a - c**) were determined to be $\sim 100\%$. The isolated alumina was placed in H_2O and the slurry was titrated with a standardized solution of NaOH (0.010 M). Two blank titrations were also carried out using unused alumina and alumina isolated from a synthetic-scale experiment using **9a** but no H_2S ; both titrations gave similar results (1.1×10^{-5} mol titrated acid). The amounts of titrated HX found were 5.2 , 3.4 , and 3.4×10^{-5} mol for the chloride, bromide, and iodide systems, respectively, all in good agreement with theoretical values within experimental error (4.5 , 3.8 , and 3.4×10^{-5} mol, respectively). The synthetic-scale experiment for the iodide system was repeated twice. In the first re-trial, the isolated alumina (containing HI) was placed in ~ 1 mL CDCl_3 (in an NMR tube fitted with a PTFE J. Young valve) with the resulting mixture placed in the presence of light (laboratory and/or sunlight) for 4 d to allow for possible photodecomposition of HI. During this time, the alumina gradually became yellow but the solvent remained colourless. The mixture was subsequently irradiated using a TLC Hg vapour lamp (18 W), and within 4 h the alumina acquired an orange colour and the solvent a purple tinge; further exposure caused no further changes. UV-vis spectroscopic analysis of the solvent revealed an

absorption band at 512 nm indicating the presence of I_2 ($\sim 1 \times 10^{-7}$ mol) (see Chapter 4, Fig. 4.4). GC and NMR analyses of the head space and solvent, respectively, revealed no detectable H_2 . The orange alumina was filtered out and washed with MeOH which led to elution of an orange substance; the alumina re-acquired a white colour. The orange methanolic eluate was analyzed using UV-vis spectroscopy, and the spectrum shows the presence of two absorption bands at 292 and 360 nm (Fig. 6.9a). These bands were identified as belonging to I_3^- ($n(I^-) = 3 \times n(I_3^-) = 5.4 \times 10^{-6}$ mol); the UV-vis spectrum of NaI_3 (formed by reaction of I_2 with NaI) is shown in Fig. 6.9b. Of interest, the UV-vis spectrum of I_2 in MeOH is shown in Fig. 6.10, and consists of three absorption bands at 292, 360, and 442 nm. The filtered alumina was titrated with NaOH solution to determine the amount of remaining HI; $n(HI) = 2.84 \times 10^{-5}$ mol. The total number of moles of I⁻ (or HI) is therefore 3.38×10^{-5} mol, and this result agrees excellently with the theoretical value of 3.36×10^{-5} mol. In the second re-trial, the isolated alumina was placed in $CHCl_3$ and a solution of I_2 in $CHCl_3$ (2.7×10^{-3} M) was added to determine whether I_2 reacts with the chemisorbed I⁻. During this addition, the alumina changed from white to orange (1.1 mL was added, 2.9×10^{-6} mol I_2); at this stage, the colour of the alumina remained constant and further I_2 addition only caused the solvent to acquire a purple colour (due to unreacted I_2). The alumina was filtered off and washed with $CHCl_3$ before MeOH was used to elute an orange substance which analyzed for I_3^- .

Photodecomposition of HI(57% aq.) was qualitatively studied at R. T. in $CDCl_3$ under laboratory light in the presence of α - or γ -alumina powder; gas chromatography and NMR and UV-vis spectroscopies were used to determine the extent of H_2 and I_2 production, respectively. Four samples were prepared and placed in the presence of light (laboratory and/or sunlight) for periods of time up to 4 d analysis. For the first sample, addition of HI(aq.) ($\sim 2 \mu L$) to $CDCl_3$ (0.5 mL) already containing γ -alumina immediately resulted in a colour change on the alumina from

Fig. 6.9. a) Electronic spectrum (250 to 650 nm) of I_3^- (MeOH) isolated from synthetic-scale studies. b) Electronic spectrum of an authentic sample of I_3^- in MeOH (prepared from $I_2 + NaI$) ($\epsilon_{292} = 2.89 \times 10^4 \text{ M}^{-1} \text{ cm}^{-1}$, $\epsilon_{360} = 1.66 \times 10^4 \text{ M}^{-1} \text{ cm}^{-1}$).

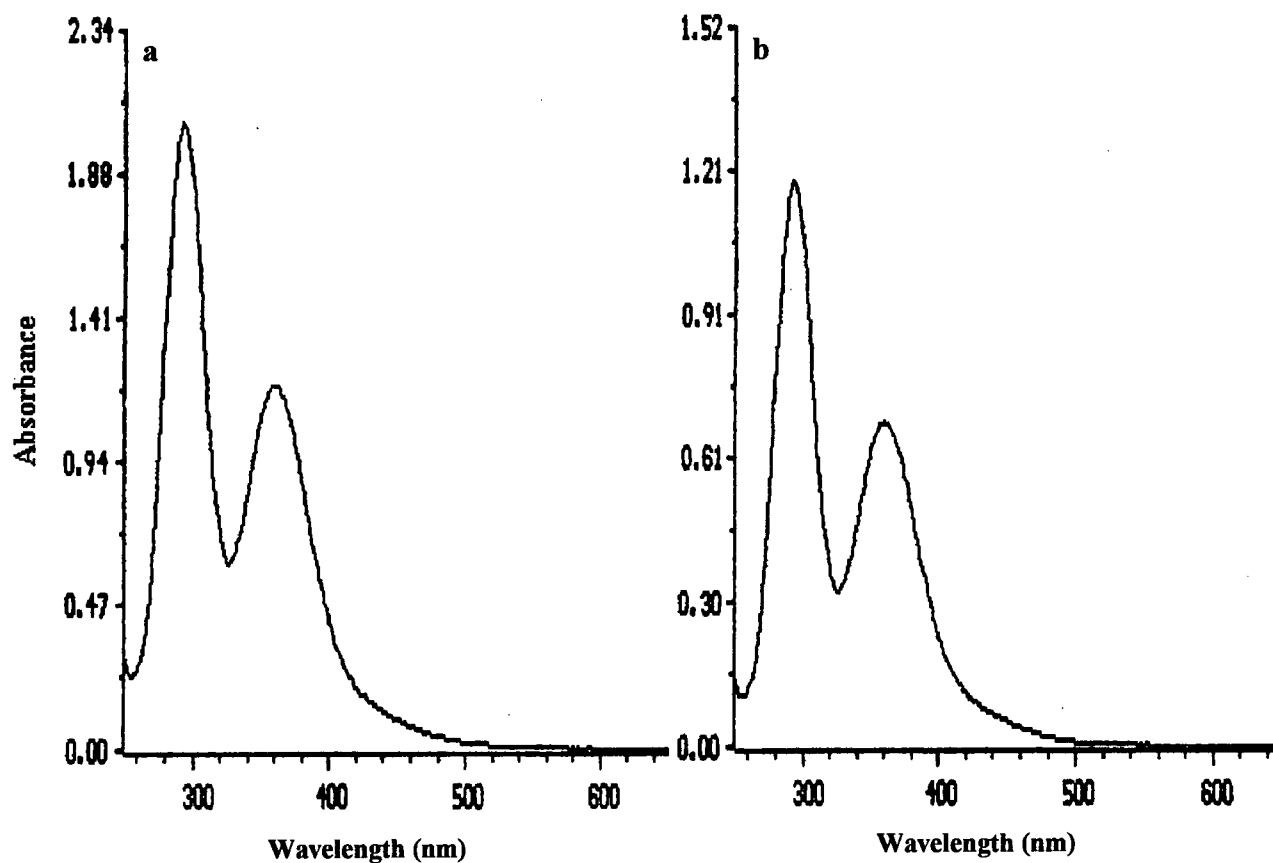


Fig. 6.10. Electronic spectrum (250 to 700 nm) of I_2 in MeOH ($\epsilon_{292} = 2540 \text{ M}^{-1} \text{ cm}^{-1}$, $\epsilon_{360} = 1380 \text{ M}^{-1} \text{ cm}^{-1}$, $\epsilon_{442} = 930 \text{ M}^{-1} \text{ cm}^{-1}$).

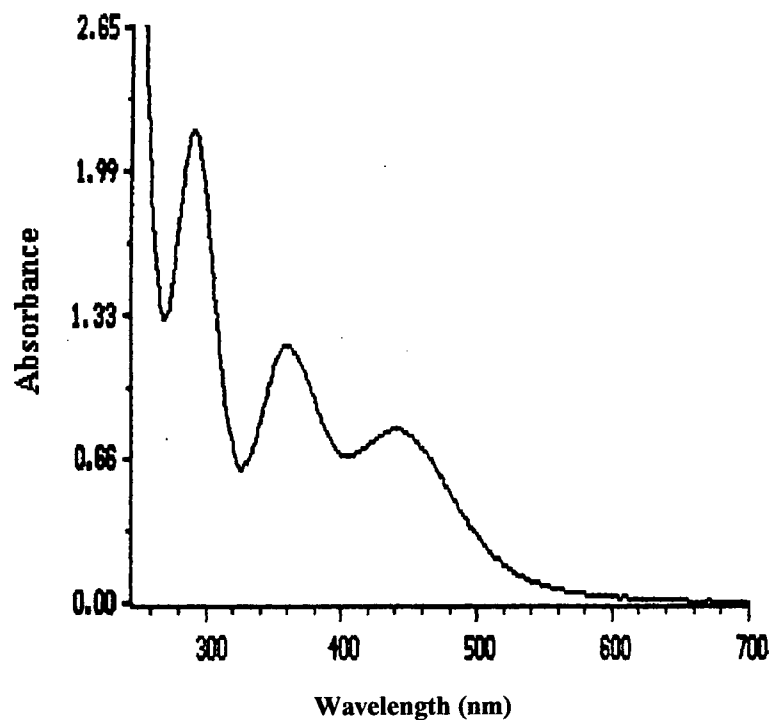
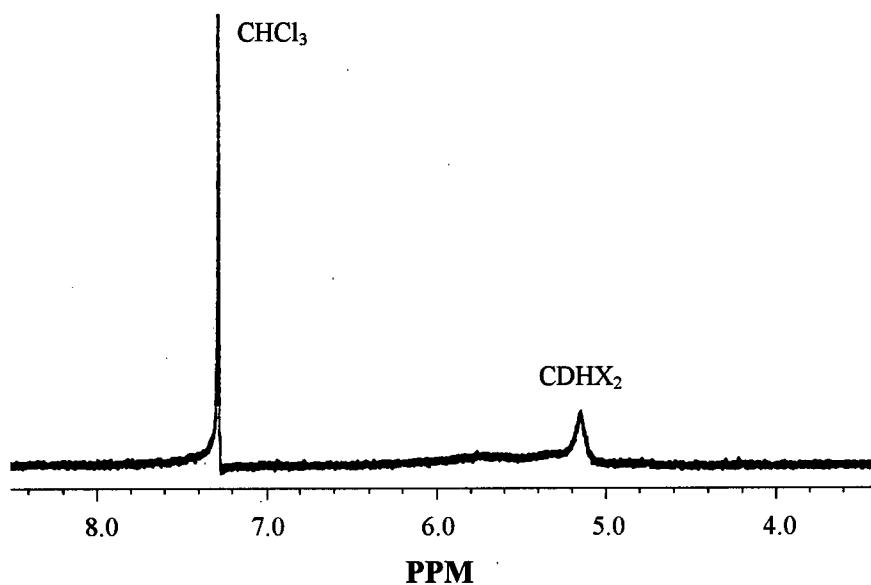


Fig. 6.11. ^1H NMR spectrum (300 MHz) showing the results of the photodecomposition of HI(aq.) ($\sim 2 \mu\text{L}$, 7.58 M) at R.T. in CDCl_3 in the presence of α -alumina (15 mg); X = Cl and/or I.



white to light yellow; the solvent remained colourless. Within minutes, the alumina turned orange-yellow and the solvent became light purple. After 30 min, the alumina was orange and the solvent, a definite purple. The sample was analyzed 24 h after preparation at which time the alumina was still orange-yellow but the solvent now an intense purple; GC analysis revealed no detectable H_2 while UV-vis spectroscopic analysis revealed the presence of I_2 as evidenced by an absorption band at 512 nm. For the second and third samples, HI(aq.) ($\sim 2 \mu\text{L}$) was added to dry γ - or α -alumina powder, respectively, and analyses for H_2 were made (immediately) before CDCl_3 was added; the gas chromatograms again revealed no H_2 peaks. The alumina of both samples immediately turned yellow and remained this colour when CDCl_3 was added. Within minutes, the α -alumina of the third sample turned orange and the solvent purple. In the second sample, however, there were no observable changes until after ~ 2 h when the solvent acquired a light purple tinge and the γ -alumina a yellow-orange. No more observable changes occurred for this sample, and analyses after 24 h revealed the presence of I_2 and still the absence of detectable H_2 . For the third sample, the solvent had an intense purple colour after 24 h and the α -alumina an orange colour. The solvent continued to darken in colour and became black after 4 d. ^1H NMR analysis revealed in addition to the CHCl_3 residual solvent peak at δ 7.24 a broad singlet at δ 5.2 (Fig. 6.11); H_2 was not observed as there was no signal at δ 4.64. GC analysis also revealed no detectable H_2 . The fourth sample was prepared using α -alumina as described for the third except that CDCl_3 was added after 4 d; GC analysis before solvent addition again revealed no detectable H_2 . The resulting intense purple solution was analyzed using NMR and UV-vis spectroscopies, and an absorption band at 512 nm was seen which did not change over time; no H_2 signal was seen in the ^1H NMR spectrum. The solvent remained purple and did not darken as observed for the third sample. The alumina, which acquired a purple-brown colour, was filtered off and washed

with CHCl_3 , eluting the remaining physisorbed I_2 . MeOH was then used to wash the resulting orange-yellow alumina, and an orange-yellow eluate emerged which was analyzed by UV-vis spectroscopy (the alumina turned white). The UV-vis spectrum revealed two absorption bands at 292 and 360 nm indicating the presence of I_3^- (see above). Control samples consisting of I_2 in CDCl_3 over α - or γ -alumina were prepared and were placed under laboratory light for 24 h. There were no observable changes in these systems; the aluminas remained white, and the I_2 512 nm bands constant in intensity. Finally, in blank experiments where samples consisting of CDCl_3 with and without γ -alumina (20 mg) were exposed to light (laboratory, sunlight, or light from a TLC Hg vapour lamp (18 W)) for periods of time up to 4 d, ^1H NMR measurements revealed that no changes occurred in these systems (*i.e.* no H_2 was seen).

6.3 Discussion

Aluminas are commonly employed as chromatographic absorbents, catalysts, and catalyst supports; these uses as well as the methods of preparation and physical properties of these materials have been reviewed.⁵⁻⁸ Reaction 6.1.2 was discovered during the course of this thesis work, the dinucleation process being catalyzed by alumina, and preliminary studies were carried out. Reaction of $\text{PdX}_2(\text{dpm})$ (**9**) with H_2S can take place rapidly to form $\text{Pd}_2\text{X}_2(\mu\text{-S})(\text{dpm})_2$ (**2**) without the need for alumina but a highly polar solvent such as DMSO must be used (see Chapter 5); furthermore, a side-product believed to be $\text{Pd}(\text{SH})_2(\text{dpm})$ also forms. In the present study, **9** does not react with H_2S in CHCl_3 in the absence of alumina (see Chapter 5). Previously in this laboratory, however, it was shown that in the presence of a base (*e.g.* Et_3N), $\text{PdCl}_2(\text{dpm})$ (**9a**) can react with H_2S but the dinuclear product $\text{Pd}_2(\text{SH})_2(\mu\text{-S})(\text{dpm})_2$ forms exclusively.⁹ This same product was also obtained (exclusively) if excess NaSH was used in place of H_2S and Et_3N .⁹ The role of alumina in the present study was ascertained from solution NMR and X-ray photoelectron spectroscopic studies; γ -alumina, commonly employed as laboratory chromatographic absorbents (powder or TLC plate form), was used.

From NMR studies, reaction 6.1.2 appears to proceed rapidly and cleanly with **2** as the only Pd-containing product formed; $\text{Pd}_2(\text{SH})_2(\mu\text{-S})(\text{dpm})_2$ and side-products such as $\text{Pd}(\text{SH})_2(\text{dpm})$ were not observed. The extent of the reaction appears to depend on the surface area of the alumina, and as will be discussed later, the reaction goes to completion quickly (within minutes) when finely ground alumina is used. The free HX product was not detected in solution NMR studies, and indeed, in the free state, HX reacts rapidly with **2** to form **9** and H_2S (see

Chapter 5). The HX chemisorbs on the alumina surface, and titration studies showed quantitative formation of this species (see later).

Reaction of **9** with H₂S probably proceeds via initial activation of H₂S on the alumina surface. From a series of experiments on the chloride system in which emphasis was placed on the order of introducing reactants, when **9a** was added to alumina pre-treated with H₂S, an instant colour change took place in the system (alumina and the solution), and NMR analyses showed the formation of **2a**. Treatment of alumina with a solution of **9a** alone, in contrast, yielded a slow colour change on the alumina but there was no reaction (*i.e.* dinucleation to form, for example, Pd₂Br₂(dpm)₂) as evidenced by NMR measurements. Subsequent addition of H₂S afforded an immediate colour change in the system, and NMR analyses again revealed the formation of **2a**. Worth noting is that alumina that has been pre-treated with H₂S and then removed and exposed to an inert atmosphere of Ar for a few minutes shows no reaction with **9a** (sample 7). As H₂S is adsorbed by alumina (as shown by NMR measurements - sample 2), the interaction may be physical in nature (*i.e.* physisorption) and that subjection to an Ar atmosphere allows desorption to take place.

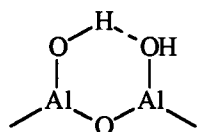
Surface studies were initiated for the chloride system to analyze the alumina in an attempt to determine the nature of the interaction (physisorption vs. chemisorption) of the various species involved in the reaction of **9a** with H₂S. The photoelectron spectrum of the alumina used (powder or TLC plate forms) (Fig. 6.4) compares well with that reported;⁴ the binding energies of the Al and O photoelectrons and the kinetic energies of the O Auger electrons are in excellent agreement with the literature values. Signals arising from the photoelectrons of C and N are also seen; their presence is probably due to adsorption of CO₂¹⁰ and N₂ from the air - the C binding energy also agrees with the literature value (see Fig. 6.4b). The photoelectron spectra of alumina with

adsorbed **9a** (Figs. 6.5 - 6.7) show in addition the photoelectron signals of Pd and Cl and the Pd Auger electron signal; the Pd 3d_{3/2}, Pd 3d_{5/2}, and Cl 2p photoelectron signals are shown in detail in Figs. 6.6 and 6.7, respectively. The Pd 3d_{5/2} energy of 337.0 eV compares to those of Pd(II)X₂(phosphine)₂ complexes (337 - 338 eV),¹¹ while that of Cl (198.2 eV) is in the metal chloride range (197 - 199 eV).¹² These results are consistent with physisorption of **9a**. Although physisorption and facile desorption of H₂S were alluded to above, surface analysis of H₂S-treated alumina (under ultra-high vacuum conditions) revealed the presence of a weak S 2p photoelectron signal at 169.1 eV which corresponds to S in an SO₄²⁻-like environment (Fig. 6.7)¹³ and which was identified in separate studies as deriving from elemental sulfur. A similar weak signal was also seen for alumina treated with elemental sulfur (Fig. 6.8) (note: the S 2p binding energy of free S₈ is approx. 164 eV¹³). Although the origin of the 169.1 eV signal cannot be easily explained (decomposition of H₂S at R.T. to give S₈?), it is noted that alumina is used as a catalyst for the high temperature O₂-oxidation of H₂S to H₂O and S₈ as in the Claus process¹⁴ or the high temperature (500 - 1000 °C) decomposition to H₂ and S₈¹⁵ (note: as evidenced from separate studies, the presence of S₈ does not influence or affect reaction 6.1.2). As S₈ can be eluted off alumina using an appropriate solvent (see Section 4.4, for example), the S₈ interaction is one of physisorption. The weak S 2p photoelectron signal (B.E. = 169.1 eV) is also observed in the spectra of alumina samples after reaction of **9a** with H₂S (Fig. 6.7); however, there is an additional S 2p photoelectron signal at 161.9 eV, which compares with that of S in an S²⁻-like environment (the S 2p binding energy of metal sulfides are in the range 160 - 162 eV),¹³ and is a good indication of the presence of physisorbed **2a** (note: this species can be completely eluted off alumina using MeOH (see Experimental section). The presence of the HCl product in reaction 6.1.2 is not easily ascertained, for example, from the Cl 2p photoelectron signal. As a signal at 199.5 eV can be seen for the

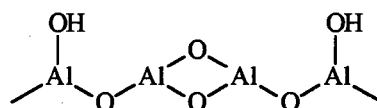
control sample (prepared using a 2.5 mole excess of HCl(g)) (Fig. 6.8), the Cl 2p signal of the HCl product must be part of the broad signal seen at 198.2 eV.

Synthetic-scale studies at R.T. were performed (with X = Cl, Br, and I) using finely ground γ -alumina to substantiate and quantify the HX product in reaction 6.1.2. The alumina was isolated and washed with MeOH which eluted all physisorbed **2**. The chemisorbed HX was then titrated using a standardized NaOH solution, and the amount of acid determined agrees excellently with the theoretical values. This finding along with that of species **2** being recovered in ~100% yields clearly shows that reaction 6.1.2 proceeds quantitatively with respect to species **9**.

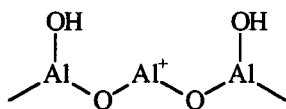
The mechanism of reaction 6.1.2 can only be speculated upon at this point. As mentioned, reaction of **9** with H₂S probably proceeds via initial activation of H₂S on the surface of the alumina. The effect of surface area was clearly demonstrated by comparison of the extent of the reaction using non-ground (10% complete immediately - sample 5) versus finely ground alumina (100% completion of reaction immediately - sample 9, for instance). The surface area of non-ground γ -alumina is typically in the range 100 - 200 m² g⁻¹⁵ and that of finely ground alumina certainly higher (a value could not be found in the literature). The grinding process presumably allows more "active" sites to be exposed for interaction with H₂S. The γ -alumina used here belongs to a group of "transition aluminas" having high surface areas resulting from the calcination of Al(OH)₃ at relatively low temperatures (200 - 600 °C),⁵ when a three-dimensional network of Al-O-Al linkages is formed via the elimination of H₂O. Chromatographic active sites are also created, and these are characterized by four main types⁶ shown below: [note: the surface structure of alumina is not well understood, and the following active site structures are suggestions based on adsorption,⁶ IR,^{6,16} and surface model¹⁷ studies]



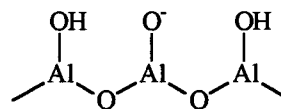
H-bonding



acid-base pair sites

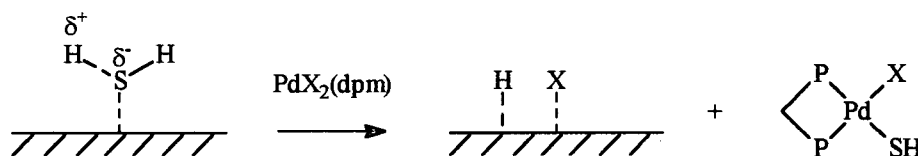


Lewis acidic sites



basic sites

Interaction of H₂S with some or all of these active sites may lead to S-H bond activation that could be followed by nucleophilic substitution of an X⁻ ligand on **9** by SH⁻ to form a reactive species such as PdX(SH)(dpm):

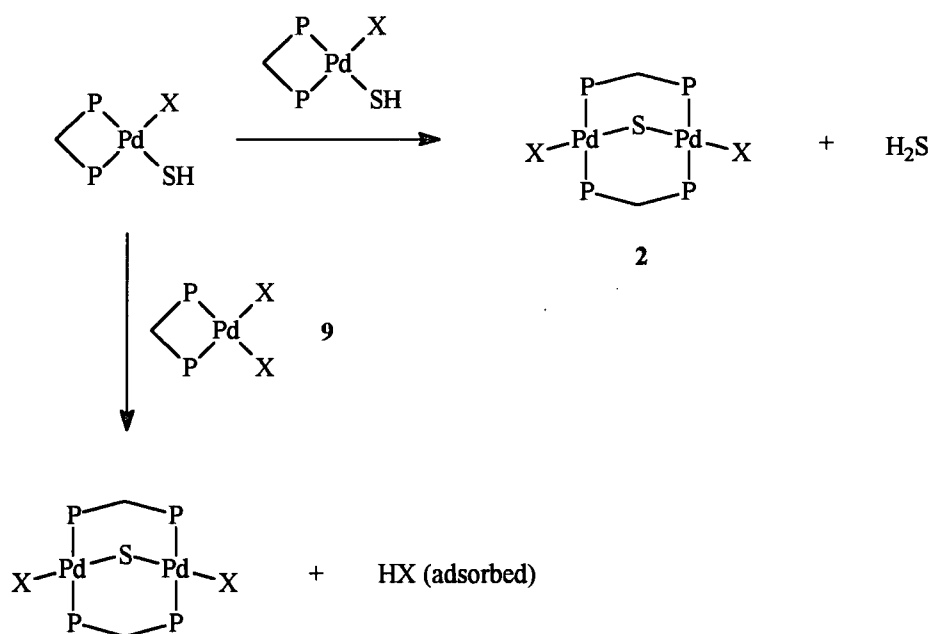


Interaction with active sites is supported by observations that when non-ground alumina pre-dried at a higher temperature (150 vs. 75 °C) was used, reaction 6.1.2 with X = Cl was ~60% complete immediately (vs. 10% - sample 5) (Fig. 6.2d - sample 6). γ -Alumina can have a surface completely covered with a monolayer of H₂O molecules, and drying at high temperatures (>100 °C) permits exposure of more active sites;¹⁸ catalytic activity can depend largely upon the extent to which alumina is dried.¹⁶ Further support for interaction of H₂S with active sites comes from observations that when **9a** was added to non-ground alumina prior to the introduction of H₂S, the dinucleation reaction scarcely proceeded (sample 4); **9a** perhaps interacts with active sites and

blocks access to the H_2S . The reaction, however, proceeded to completion when TLC plates were used and the same experimental conditions employed (**9a** being added first - sample 15). This finding is rationalized by considering the mesh size of the alumina particles of the plate (60) compared to that of the non-ground alumina (av. 200). For the same amount of material used, the lower mesh will have a higher total surface area and more active sites than the higher mesh size alumina, assuming that the density of active sites is the same for the two types of materials (a density value could not be found in the literature).

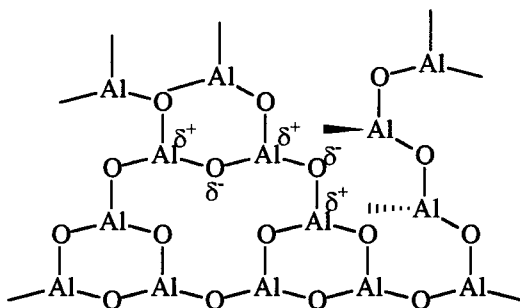
The dinucleation reaction to form $\text{Pd}_2\text{X}_2(\mu\text{-S})(\text{dpm})_2$ (**2**) could be a result of the coupling of $\text{PdX}(\text{SH})(\text{dpm})$ with itself, or with **9** via a deprotonation/protonation process (see Chapter 5):

Scheme



Considering that HX in the free state reacts quickly with **2** (to form **9** and H_2S), the driving force for the dinucleation reaction would be the chemisorption of HX so that the reverse reaction cannot take place.

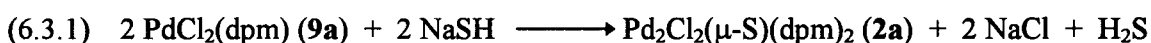
Support for S-H bond activation comes also from the observed reaction of $\text{PdCl}_2(\text{dpm})$ (**9a**) with H_2S using α -alumina (corundum), this giving **2a** as the only Pd product (sample 10). α -Alumina is both chemically inert⁷ and chromatographically inactive;⁶ it is formed from the calcination of $\text{Al}(\text{OH})_3$ or transition aluminas at temperatures ≥ 1100 °C such that water is completely eliminated, resulting in a material with a very low surface area ($\sim 1 \text{ m}^2 \text{ g}^{-1}$).⁶ The complete absence of “active” sites is in keeping with observations that reaction 6.1.2 proceeds very slowly, being $\sim 10\%$ complete after 1 d and $\sim 50\%$ after 3 d (Fig. 6.3). As α -alumina is composed of a three-dimensional network of Al-O-Al linkages shown below,



S-H bond activation probably occurs because of the polarity of the Al-O bond. Of note, adsorption studies of alcohols on γ -alumina have shown that ROH can interact with unsaturated aluminum ions (Lewis acidic sites) with O-H bond activation leading to chemisorption.¹⁹ In the present system, a similar chemisorption process is readily envisaged with H_2S but, considering that reaction 6.1.2 does not proceed when H_2S -pretreated alumina is removed from the system, dried under Ar, and subsequently placed back in the system (with no H_2S present in solution) (see above), this suggests that other types of active sites (for physisorption) may be responsible for S-H bond activation prior to the dinucleation reaction. Moreover, reaction 6.1.2 does not proceed to

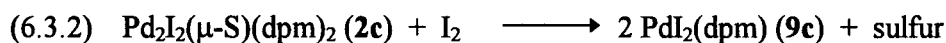
completion when a stoichiometric amount of H₂S is used, and this observation could be interpreted as support for the role of other types of active sites.

Although the proposed reaction intermediate PdX(SH)(dpm) was not observed, for example by NMR studies for the chloride system at -50 °C, its existence is supported by reaction studies of PdCl₂(dpm) (**9a**) with 1 mole equivalent NaSH which show that **2a** forms according to reaction 6.3.1. As noted earlier, previous studies in this laboratory⁹ demonstrated that reaction of **9a** with excess NaSH gives exclusively Pd₂(SH)₂(μ-S)(dpm)₂; nucleophilic substitution of both Cl ligands of **9a** supposedly forms the reactive intermediate, Pd(SH)₂(dpm), which couples to form the product with concomitant elimination of H₂S.



In the present study, reaction of **9a** with 1 mole equivalent NaSH under conditions in which NaSH was slowly added to a solution of **9a** gave **2a** as the only Pd product; Pd₂(SH)₂(μ-S)(dpm)₂ was not formed. It seems reasonable that, under these conditions in which the local concentration of NaSH is kept low, double nucleophilic substitution does not take place and PdCl(SH)(dpm) forms which either reacts with itself or with **9a** (Scheme) (the HCl formed will react with **2a** to give **9a** and H₂S).

Important implications of reaction 6.1.2 are seen with the X = I system; photodecomposition of HI, for instance, can produce H₂ and I₂, the latter then reacting with Pd₂I₂(μ-S)(dpm)₂ (**2c**) to form elemental sulfur and PdI₂(dpm) (**9c**). The catalytic cycle to generate H₂ and 1/8 S₈ from H₂S is then completed via reaction 6.3.2 (see Chapter 4).



Some qualitative studies were carried out to determine the extent of photodecomposition by light (laboratory and/or sunlight) of HI in CDCl₃ in the presence of γ- and α-alumina. Transition

aluminas chemisorb hydrohalic acids,⁶ and this type of interaction may hinder such photodecomposition. Chemisorbed HI on γ -alumina isolated from a synthetic-scale experiment was shown to undergo partial photodecomposition but intense light (TLC Hg vapour lamp (18W)) was needed. The amount of I_2 produced after 4 h was small ($\sim 1 \times 10^{-7}$ mol), however, and no H_2 was detected in NMR and GC analyses; exposure times longer than 4 h had no effect on the system (*i.e.* the I_2 512 nm band intensity remained unchanged and H_2 was still not detected). Interestingly, the alumina itself acquired an orange colour which was determined to be due to physisorbed I_3^- . Elution of this substance using MeOH produced a white alumina that was subsequently titrated using a standardized NaOH solution. This titration showed the presence of much chemisorbed HI remaining; as noted in the Results, all the Γ can be accounted for. Although it is not known how HI is chemisorbed onto alumina or which active sites are responsible for reaction 6.1.2, formation of I_2 probably results from the coupling of photoproduced I atoms, and the formation of I_3^- comes from reaction of I_2 with chemisorbed Γ (as evidenced from separate studies). The latter reaction could be responsible for the partial photodecomposition observed as I_3^- exhibits strong absorption ($\sigma_u^* \rightarrow \sigma_g^*$, $\pi_u^* \rightarrow \sigma_g^*$) in the ultraviolet region (Fig. 6.9b). I_2 formation occurs until sufficient I_3^- forms, this absorbing most or all the light and terminating further photodecomposition. As noted above, titrations studies showed that much chemisorbed HI remains (*i.e.* 2.8×10^{-5} mol, $\sim 85\%$) and the I_3^- formed accounts for the 15% difference. Hence, $\sim 10\%$ of chemisorbed HI was photodecomposed to form I_2 , most of which reacted with Γ to generate I_3^- with a negligible amount appearing in solution. Why H_2 was not observed is not clear (but see below) although the theoretical amount produced (1.7×10^{-6} mol) based on the amount of I_3^- formed should make the H_2 easily detectable, for example by NMR spectroscopy ($\sim 3.4 \times 10^{-3}$ M). 1H NMR analyses in $CDCl_3$ showed no H_2 signal nor any other signals except for that of residual $CHCl_3$. Photodecomposition tests with

HI(57% aq.) on γ -alumina revealed the formation of I_2 but the H_2 product was not detected (e.g. by gas chromatography). Exposure of HI-treated α -alumina in $CDCl_3$ to light resulted in an initially purple solution (the formation of I_2 being evidenced by UV-vis spectroscopy) that gradually darkened to a black colour. NMR analyses revealed a broad signal at δ 5.2 indicative of $CDHX_2$ species ($X = Cl$ and/or I) (Fig. 6.11). It is possible that photochemically produced H atoms react with the solvent to give, for example, HCl and a $CDCl_2\cdot$ radical which could subsequently react with H or I atoms to give species such as $CDHCl_2$ or $CDCl_2I$ (I atoms do not react with $CHCl_3$ or alkanes in general (see Chapter 4)²⁰). As α -alumina is chemically inert, only physisorption of HX can take place (by dipole-dipole interactions), and any H atoms produced in the photolysis probably react with the surrounding solvent species. Exposure of HI-treated α -alumina to light without the presence of solvent also resulted in the formation of I_2 but surprisingly no H_2 was detected; the presence of I_2 was evidenced later by UV-vis spectroscopy when the alumina was subsequently placed in $CDCl_3$ and a purple solution resulted. The colour did not change and the UV-vis spectral characteristics were invariant with time; it is not clear why H_2 was not observed here.

A single catalytic study at R. T. in $CDCl_3$ demonstrated that reaction of **9c** with H_2S (1 atm) in the presence of finely ground γ -alumina proceeded to completion to give **2c** but subsequent exposure to light (laboratory and/or sunlight) for 10 d resulted in decomposition giving unidentifiable products; no H_2 was detected. Although the following illustrates an attractive scheme for the catalytic decomposition of H_2S to give H_2 and elemental sulfur using **9c** and alumina as catalyst and co-catalyst, respectively, more studies need to be carried out to determine the fate of the elusive H_2 and to determine the best set of conditions for catalysis to operate:

6.4 Experimental section

The materials used, synthetic procedures for the ligands and complexes, and instrumentation used for ^1H and $^{31}\text{P}\{^1\text{H}\}$ NMR and UV-vis spectroscopy, gas chromatography, and ESCA (electron spectroscopy for chemical analysis) were described in Chapter 2. Complexes **2a - c** and **9a - c** were synthesized using published methods as outlined in Chapter 2. All experiments were performed under Ar unless otherwise specified. Table 6.1 summarizes the content make-up of each experiment; the alumina powder and plates used were pre-dried at $75\text{ }^\circ\text{C}$ for 24 h. Finely ground alumina was prepared via a manual grinding process using a mortar and pestle.

6.4.1 NMR spectroscopic studies

Expt. 1: Alumina powder (15 mg) was placed in an NMR tube fitted with a PTFE J. Young valve, and the tube was evacuated before CDCl_3 ($\sim 0.7\text{ mL}$) was vacuum transferred in using liquid N_2 .

The system was left at R.T. for 24 h before analysis using NMR spectroscopy.

Expt. 2: As described for Expt. 1. H_2S ($110\text{ }\mu\text{L}$ at STP, 0.0045 mmol) was then vacuum transferred in using liquid N_2 .

Expt. 3: As described for Expt. 1 but $\text{PdCl}_2(\text{dpm})$ (**9a**, 5 mg , 0.0089 mmol) was also used.

Expt. 4: As described for Expt. 3. H_2S ($110\text{ }\mu\text{L}$ at STP, 0.0045 mmol) was vacuum transferred in using liquid N_2 after $\sim 1\text{ h}$.

Expt. 5: Alumina powder (15 mg) and CDCl_3 (0.3 mL) were placed in an NMR tube fitted with a rubber septum. H_2S ($110\text{ }\mu\text{L}$ at STP, 0.0045 mmol) was then injected, and the NMR tube was

briefly shaken to ensure complete mixing. A 0.4 mL solution of **9a** (5 mg, 0.0089 mmol) was injected after ~1 h. The system was permitted to react at R.T. for 24 h before analysis using NMR spectroscopy.

Expt. 6: As described for Expt. 5 except the alumina used was pre-dried at 150 °C instead of 75 °C.

Expt. 7: An alumina plate (1.0 cm x 1.0 cm) and CDCl₃ (1.0 mL) were placed in a Schlenk tube sealed with a rubber septum. H₂S (0.5 mL at STP, 0.021 mmol) was injected, and the system was left at R.T. for ~4 h. The plate was then removed from the solution, dried under a flow of Ar and then placed in a Schlenk tube containing a 1.0 mL CDCl₃ solution of **9a** (5 mg, 0.0089 mmol).

The system was permitted to react at R.T. for 4 h before analysis.

Expt. 8: The alumina (11.5 mg) was scraped off a plate (1.0 cm x 1.0 cm) and placed in a Schlenk tube containing a 1.0 mL CDCl₃ solution of **9a** (5 mg, 0.0089 mmol). H₂S (0.5 mL at STP, 0.021 mmol) was then injected, and the system was permitted to react at R.T. for 4 h before analysis using NMR spectroscopy.

Expt. 9: As described for Expt. 8 except finely ground alumina (15 mg) was used.

Expt. 10: As described for Expt. 8 except α-alumina (corundum, 15 mg) was used. The sample was again analyzed after 72 h.

Expt. 11: **9a** (10 mg, 0.018 mmol) was dissolved in CHCl₃ (10 mL) and a MeOH solution (10 mL) of NaSH (1.0 mg, 0.018 mmol) was added dropwise over a period of 30 min. The solvents of the resulting yellow solution were removed, and the remaining yellow residue was dried *in vacuo*.

CDCl₃ (0.5 mL) was used to dissolve the residue, and the sample was analyzed using ¹H and ³¹P{¹H} NMR spectroscopy.

A single, low temperature NMR study at $-42\text{ }^{\circ}\text{C}$ was carried out in which H_2S (0.25 mL at STP, 0.010 mmol) was injected in a rubber septum-sealed NMR tube containing a 0.5 mL CDCl_3 solution of **9a** (5 mg, 0.0089 mmol) and finely ground alumina (15 mg) in an acetonitrile/liquid N_2 slush-bath. The sample was analyzed at $-50\text{ }^{\circ}\text{C}$ 1 h later using ^1H and $^{31}\text{P}\{^1\text{H}\}$ NMR spectroscopy. The sample was then placed at R.T. for 24 h, and re-analyzed thereafter.

6.4.2 Surface studies

Expt. 12: An alumina plate (1.0 cm x 1.0 cm) and CDCl_3 (1.0 mL) were placed in a Schlenk tube sealed with a rubber septum. The sample was then left at R.T. for ~ 4 h before analysis.

Expt. 13: As described for Expt. 12 but **9a** (5 mg, 0.0089 mmol) was also placed in the Schlenk tube.

Expt. 14: As described for Expt. 12 but H_2S (0.5 mL at STP, 0.021 mmol) was also injected into the Schlenk tube.

Expt. 15: An alumina plate (1.0 cm x 1.0 cm), **9a** (5 mg, 0.0089 mmol), and CDCl_3 (1.0 mL) were placed in a Schlenk tube fitted with a rubber septum. The sample was left at R.T. for ~ 2 h before H_2S (0.5 mL at STP, 0.021 mmol) was injected. The reaction mixture was then left at R.T. for another 2 h before analysis.

Expt. 16: An alumina plate (1.0 cm x 1.0 cm) and CDCl_3 (0.7 mL) were placed in a Schlenk tube fitted with a rubber septum, and H_2S (0.5 mL at STP, 0.021 mmol) was injected. The sample was left at R.T. for ~ 2 h before a 0.3 mL solution of **9a** (5 mg, 0.0089 mmol) was introduced. The reaction mixture was then left at R.T. for another 2 h before analysis.

Expt. 17: An alumina plate (1.0 cm x 1.0 cm), S₈ (12 mg, 0.047 mmol), and CDCl₃ (1.0 mL) were placed in a Schlenk tube, and the system was left at R.T. for ~2 h prior to analysis.

Expt. 18: As described for Expt. 17 but HCl (0.5 mL, 0.021 mmol) was placed (injected) in the Schlenk tube instead of sulfur.

The liquid phases of Expts. 12 - 16 were analyzed using ¹H and ³¹P{¹H} NMR spectroscopy. The alumina plates of all experiments were taken out and dried at R.T. under Ar (few minutes) before they were submitted for surface analyses using ESCA.

6.4.3 Synthetic-scale studies

In a Schlenk tube fitted with a rubber septum were placed 25.0 mg PdX₂(dpm) (**9a**, 0.045 mmol; **9b**, 0.038 mmol; **9c**, 0.034 mmol), 75.0 mg finely ground γ -alumina, and 2.5 mL CHCl₃. The mixture was rapidly stirred and H₂S (5 mL at STP, 0.20 mmol) was injected. The initial yellow (**9a** and **9b**) or orange (**9c**) solution immediately (within seconds) turned brown. The mixture was continuously stirred for ~4 h before being reduced in volume (to ~0.5 mL) with evacuation of the H₂S. CH₂Cl₂ (20 mL) was then added to dissolve all Pd species, and the mixture was filtered to separate out the alumina, which was subsequently washed with CH₂Cl₂ (2 x 10 mL), MeOH (10 mL), and CH₂Cl₂ (10 mL), and then dried *in vacuo*. (Note: MeOH was used to elute all adsorbed Pd species off the alumina; indeed, when this solvent was added, the initially brown-coloured alumina turned white). The washings were combined with the filtrate, and the solvents were removed by rotary evaporation. The resulting residue was then dissolved in CDCl₃ (~0.5 mL) and analyzed using NMR spectroscopy. Yield of Pd₂X₂(μ -S)(dpm)₂: **2a**, 24.0 mg (100%); **2b**, 22.0 mg (98%); **2c**, 21.0 mg (99%). The isolated alumina was placed in an

Erlenmeyer flask, and 10 mL H₂O and a few drops of phenolphthalein indicator were added. The mixture was then titrated with a standardized solution of NaOH (0.010 M).

The above procedure was repeated for the iodide system except the isolated alumina was placed in an NMR tube fitted with a PTFE J. Young valve with CDCl₃ (~0.7 mL) added. The resulting mixture was then placed in the presence of light (laboratory, sunlight, or light from a TLC Hg vapour lamp (18W)) for up to 4 d, and analyzed thereafter for H₂ (using GC chromatography) and I₂ (using UV-vis spectroscopy).

Two blank titrations were performed using unused alumina, and alumina isolated from the above procedure for the chloride system when H₂S was not used.

Possible reactivity of **9a** with S₈ in the presence of γ -alumina was investigated. **9a** (25.0 mg, 0.045 mmol), finely ground alumina (75.0 mg), S₈ (14 mg, 0.45 mmol), and CHCl₃ (2.5 mL) were placed in a Schlenk tube, and the mixture was rapidly stirred for ~4 h. During this period, the initial white alumina gradually turned orange yet the colour of the supernatant was unchanged (yellow). CH₂Cl₂ (20 mL) was then added to dissolve all Pd species, and the mixture was filtered to separate out the alumina, which was subsequently washed with CH₂Cl₂ (2 x 10 mL), MeOH (10 mL), and CH₂Cl₂ (10 mL). The washings were combined with the filtrate, and the solvents were removed by rotary evaporation. The resulting residue was then dissolved in CDCl₃ (~0.5 mL) and analyzed using NMR spectroscopy, which revealed only **9a**.

Possible decomposition of H₂S on γ -alumina was investigated. In a Schlenk tube were placed a γ -alumina plate (1.0 cm x 10.0 cm), CHCl₃ (20 mL), and 1 atm H₂S. The mixture was stirred at R.T. for ~4 h before the plate was taken out and dried in air. The alumina was then scraped off and placed in a glass pasteur pipet. CHCl₃ (~5 mL) was then used to wash the alumina, and the washings were collected and analyzed using UV-vis spectroscopy, which revealed

the presence of elemental sulfur (*e.g.* see Fig. 4.4). A control experiment was performed using alumina isolated from the above procedure when H₂S was not used.

6.4.4 Photodecomposition of HI

Photodecomposition of HI(aq.) was qualitatively studied in CDCl₃ in the presence of γ - and α -alumina powder. Three experiments were performed as follows. In the first experiment, γ -alumina (15 mg) and CDCl₃ (0.5 mL) were placed in an NMR tube, and HI(aq.) (~2 μ L, 0.016 mmol) was added via a glass pasteur pipet. The sample was briefly shaken to ensure complete mixing before being placed at R.T. in the presence of laboratory light for 24 h. Thereafter, the system was analyzed for H₂ (using gas chromatography and NMR spectroscopy) and I₂ (UV-vis spectroscopy). In the second experiment, α - or γ -alumina (15 mg) and HI(aq.) (~2 μ L, 0.016 mmol) were first placed in the NMR tube, and the sample was briefly shaken before it was “immediately” analyzed for H₂. CDCl₃ (0.5 mL) was then added, and the sample was again shaken briefly before being placed at R.T. in the presence of laboratory light for 24 h. Thereafter, the sample was analyzed for H₂ and I₂. In the third experiment, α -alumina (15 mg) and HI(aq.) (~2 μ L, 0.016 mmol) were placed in an NMR tube, and the sample was briefly shaken before being left at R.T. in the presence of light for 4 d. The sample was then analyzed for H₂ before CDCl₃ was added for analysis of I₂.

A control sample consisting of I₂ (0.01 mg, 0.052 μ mol), alumina (15 mg), and CDCl₃ (0.5 mL) was prepared and was left at R.T. for 24 h in the presence of laboratory light.

6.5 References for Chapter 6

1. Lee, C.-L.; Besenyi, G.; James, B.R.; Nelson, D.A.; Lilga, M.A. *J. Chem. Soc., Chem. Commun.* **1985**, 1175.
2. Lee, C.-L.; Yang, Y.P.; Rettig, S.J.; James, B.R.; Nelson, D.A.; Lilga, M.A. *Organometallics* **1986**, *5*, 2220.
3. Wong, T.Y.H.; Barnabas, A.F.; Sallin, D.; James, B.R. *Inorg. Chem.* **1995**, *34*, 2278.
4. Wagner, C.D.; Riggs, W.M.; Davis, L.E.; Moulder, J.F. "Handbook of X-ray Photoelectron Spectroscopy", G.E. Muilenberg (Ed.), Perkin-Elmer Corporation, Physical Electronics Division, Eden Prairie, Minnesota, 1979, p. 43.
5. Snyder, L.R. "Principles of Adsorption Chromatography", Marcel Dekker, New York, 1968, ch. 7, p. 163.
6. Knozinger, H.; Ratnasamy, P. *Catal. Rev.-Sci. Eng.* **1978**, *17*, 31.
7. Oberlander, R.K. "Applied Industrial Catalysis, Vol. 3", B.E. Leach (Ed.), Academic Press, Toronto, 1984, ch. 4, p. 63.
8. Lamb, H.H.; Gates, B.C.; Knozinger, H. *Angew. Chem. Int. Ed. Engl.* **1988**, *27*, 1127.
9. Besenyi, G.; Lee, C.-L.; Gulinski, J.; Rettig, S.J.; James, B.R.; Nelson, D.A.; Lilga, M.A. *Inorg. Chem.* **1987**, *26*, 3622.
10. Parkyns, N.D. *J. Chem. Soc. (A)* **1969**, 410.
11. Ref. 4, p. 110.
12. Ref. 4, p. 58.
13. Ref. 4, p. 56.
14. Sulfur Recovery, "Kirk-Othmer Encyclopedia of Chemical Technology (3rd Ed.), Vol. 22", H.F. Mark, J.J. Mcketta, Jr., D.F. Othmer, John Wiley & Sons, Toronto, 1983, p. 267.
15. Bandermann, F.; Harder, K.B. *Int. J. Hydrogen Energy* **1985**, *10*, 21.
16. Peri, J.B.; Hannan, R.B. *J. Phys. Chem.* **1960**, *64*, 1526.

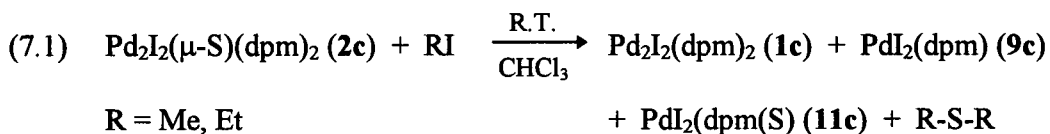
17. Peri, J.B. *J. Phys. Chem.* **1965**, *69*, 220.
18. Peri, J.B. *J. Phys. Chem.* **1965**, *69*, 211.
19. Knozinger, H.; Stubner, B. *J. Phys. Chem.* **1978**, *82*, 1526.
20. See for example: a) Streitwieser, Jr., A.; Heathcock, C.H. "Introduction to Organic Chemistry, 3rd Ed.", Macmillan, New York, 1985, ch. 6. b) Morrison, R.T.; Boyd, R.N. "Organic Chemistry, 3rd Ed.", Allyn and Bacon, Boston, 1973, ch. 3.

CHAPTER 7

Miscellaneous Reactions

7.1 Reaction of Pd₂X₂(μ-S)(dpm)₂ with alkyl halides

While the oxidative addition of halogens to Pd₂X₂(μ-S)(dpm)₂ (**2**) was being studied (see Chapter 4), tests for S-removal were made using alkyl halides; a slow, complex reaction occurs and eq. 7.1 describes the products observed:



In a single *in situ* NMR experiment at R.T., **2c** (10 mg, 0.0079 mmol) was reacted with a 10-fold excess of MeI in CDCl₃ (0.5 mL) in air. ¹H and ³¹P{¹H} NMR analyses after 3 d showed, in addition to unreacted **2c** and MeI, the presence of PdI₂(dpm) (**9c**), Pd₂I₂(dpm)₂ (**1c**), PdI₂(dpm(S)) (**11c**), Me₂SO₂, and Me₂S (Fig. 7.1). Reaction of **2c** (10 mg, 0.0079 mmol) with a 10-fold excess of EtI in CDCl₃ (0.5 mL) under air was slower, and trace amounts of **1c**, **9c**, and **11c** were observed after 5 d (Fig. 7.2); the ¹H NMR signals for the expected Et₂S product are probably buried under those of Et₂I (compare the ¹H NMR signal of Me₂S with that of MeI). In both of these reactions, addition across the Pd-S bond is readily envisaged to account for the **9c** and R₂S products (reaction 7.2).

Fig. 7.1. ^1H (200 MHz) and $^{31}\text{P}\{^1\text{H}\}$ (81 MHz) NMR spectra showing the progress of the reaction in CDCl_3 at R.T. of $\text{Pd}_2\text{I}_2(\mu\text{-S})(\text{dpm})_2$ (**2c**, 1.6×10^{-2} M) with a 10-fold excess of MeI after 3 d; **1c** = $\text{Pd}_2\text{I}_2(\text{dpm})_2$, **9c** = $\text{PdI}_2(\text{dpm})$, **11c** = $\text{PdI}_2(\text{dpm}(\text{S}))$. [The spectra of the various Pd species are discussed in Sections 3.2 (**1c** and **2c**) and 4.2 (**9c** and **11c**).]

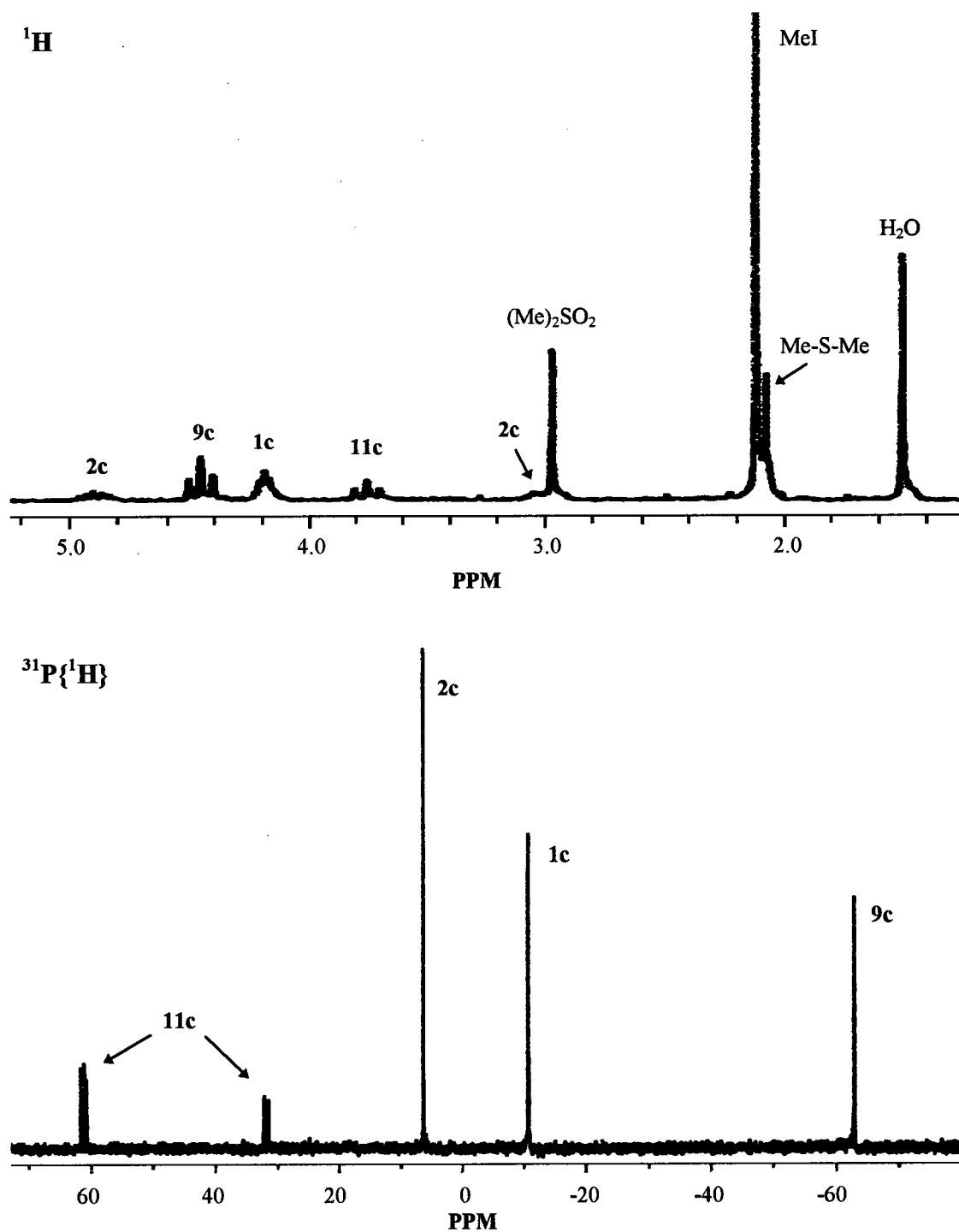
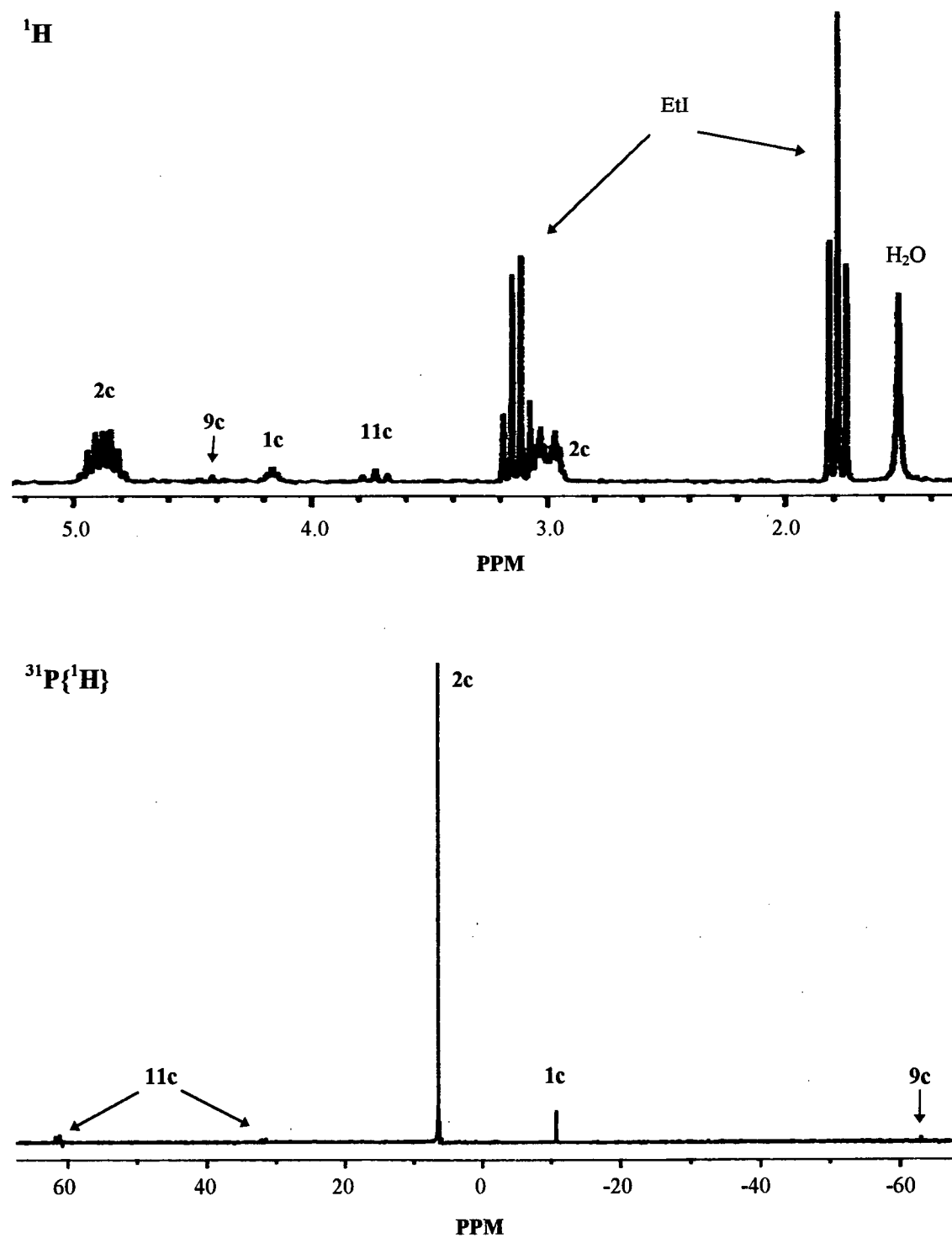
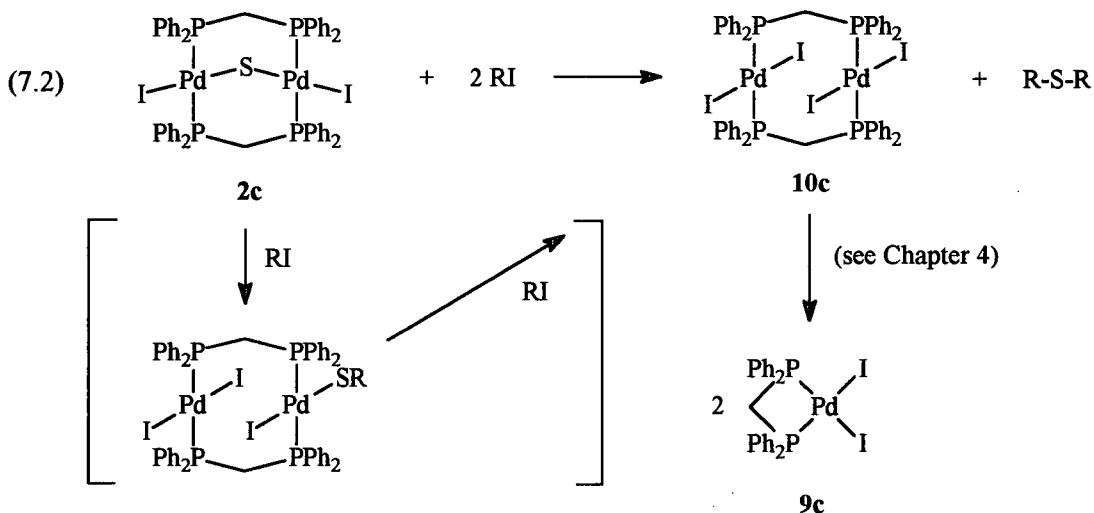
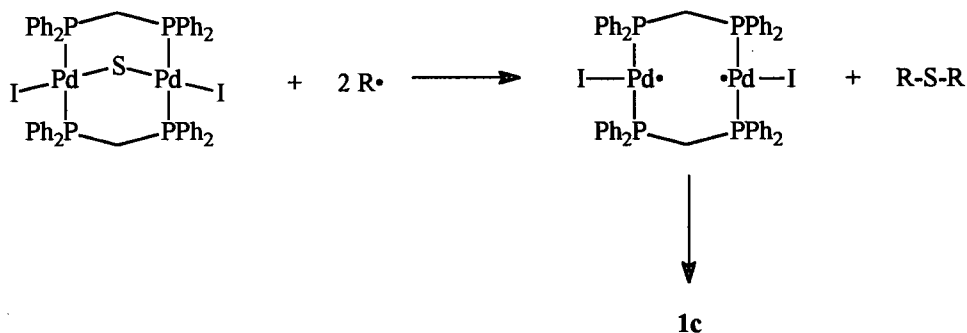


Fig. 7.2. ^1H (200 MHz) and $^{31}\text{P}\{^1\text{H}\}$ (81 MHz) NMR spectra showing the progress of the reaction in CDCl_3 at R.T. of $\text{Pd}_2\text{I}_2(\mu\text{-S})(\text{dpm})_2$ (**2c**, 1.6×10^{-2} M) with a 10-fold excess of EtI after 5 d; **1c** = $\text{Pd}_2\text{I}_2(\text{dpm})_2$, **9c** = $\text{PdI}_2(\text{dpm})$, **11c** = $\text{PdI}_2(\text{dpm}(\text{S}))$.





Abstraction of the bridged S-atom by $\text{R}\cdot$ radicals¹ could lead to establishment of the Pd-Pd bond and formation of R_2S and $\mathbf{1c}$ (reaction 7.3).



The I atoms could form I_2 which would react with $\mathbf{1c}$ or $\mathbf{2c}$ to give $\mathbf{9c}$ (and presumably elemental sulfur) and $\mathbf{11c}$ (from reaction of I_2 with $\mathbf{2c}$, see Chapter 4). In the $\mathbf{2c} + \text{MeI}$ system, the presence of the sulfone[‡] must result from oxidation of Me_2S (reaction 7.1 was carried out under 1 atm air) and, considering that Me_2S does not exhibit reactivity towards O_2 as evidenced from separate

[‡] The presence of Me_2SO_2 was established by comparison of the ^1H NMR signal with that of an authentic sample.

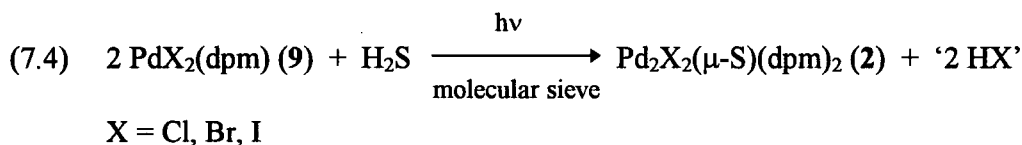
NMR studies,[†] this oxidation is perhaps catalyzed by a Pd species; why an intermediate sulfoxide species is not observed is also not clear. Finally, the difference in reaction rates between the MeI and EtI systems is presumably due to steric reasons.

7.2 Reaction of PdX₂(dpm) (9) with H₂S in the presence of silica gel or aluminosilicate; catalyzed formation of Pd₂X₂(μ-S)(dpm)₂ (2)

The use of alumina in the dinucleation reaction PdX₂(dpm) (9) → Pd₂X₂(μ-S)(dpm)₂ (2) (Chapter 6) led to some studies utilizing other metal oxides, namely silica gel and aluminosilicates (*e.g.* molecular sieves). In a single *in situ* NMR experiment at R. T., reaction of PdCl₂(dpm) (9a, 5 mg, 0.0089 mmol) with 1 mole equivalent H₂S (216 μL at STP) in the presence of silica gel (15 mg) was carried out in CDCl₃ (0.5 mL). ¹H and ³¹P{¹H} NMR analyses immediately after sample preparation revealed, in addition to unreacted 9a and H₂S, the presence of 2a in ~10% yield; there were no further changes in the system. The mechanism of this reaction is probably similar to that when alumina is used (see Chapter 6). The same reaction, when attempted in the presence of molecular sieves (15 mg, type 4A, 8 - 12 mesh, beads, Fisher), proceeded only in the presence of light (18 W TLC Hg vapour lamp) (reaction 7.4). For the chloride system (5 mg, 0.0089 mmol), the reaction was complete after ~2 h, while the bromide (5 mg, 0.0077 mmol) and iodide (5 mg, 0.0067 mmol) systems were only ~10 and ~1% complete, respectively, after 2 h. The HX product, as in the alumina system, is likely chemisorbed on the metal oxide. Interestingly, subsequent exposure of the chloride system to sunlight for ~2 d resulted in the complete disappearance of 2c

[†] Me₂S (250 μL, 3.4 mmol) was dissolved in CDCl₃ (0.5 mL) held in an NMR tube. The sample, prepared under 1 atm air, was analyzed after 10 d using ¹H NMR spectroscopy.

and re-formation of **9c** as evidenced by NMR measurements (whether the S-containing co-product was elemental sulfur or H₂S was not determined).



7.3 Reaction of Pd₂X₂(μ-S)(dpm)₂ (**2**) with CO

Reaction of **2** with CO was briefly explored for the possibility of abstracting the bridged S atom as COS (reaction 7.5):



In a high pressure autoclave, Pd₂Cl₂(μ-S)(dpm)₂ (**2a**, 10 mg, 0.0092 mmol) was dissolved in CDCl₃ (0.5 mL) and subjected to 700 psi CO at R.T. for 24 h before the system was analyzed (the sample in the autoclave was transferred to an NMR tube using a glass pasteur pipet). The ³¹P{¹H} NMR spectrum shows the absence of **2a** and the presence of PdCl₂(dpm) (**9a**), Pd₂Cl₂(dpm)₂ (**1a**), Pd₂Cl₂(μ-CO)(dpm)₂,² PdCl₂(dpm(S)) (**11a**), and an unknown species **X** characterized by a tight AB pattern (Fig. 7.3). Reaction under an atm of CO does not occur for the chloride system but for the iodide system, a slow reaction was observed. In a single *in situ* NMR experiment at R.T., Pd₂I₂(μ-S)(dpm)₂ (**1c**, 10 mg, 0.0079 mmol) was reacted under an atm of CO in CDCl₃ (0.5 mL). NMR analysis after 1 d revealed essentially no reaction, but after 11 d analysis revealed, in addition to unreacted **1c**, the presence of PdI₂(dpm) (**9c**), Pd₂I₂(dpm)₂ (**1c**), Pd₂I₂(μ-CO)(dpm)₂,² PdI₂(dpm(S)) (**11c**), and perhaps two unknown species **Y** and **Z** (Fig. 7.4) (note: the reaction was carried out in the absence of light). Species **Y**, as with species **X**, is characterized by a tight AB

Fig. 7.3. $^{31}\text{P}\{^1\text{H}\}$ NMR spectrum (81 MHz) recorded for the reaction of $\text{Pd}_2\text{Cl}_2(\mu\text{-S})(\text{dpm})_2$ (**2a**) with 700 psi CO at R.T. in CDCl_3 after 24 h; **1a** = $\text{Pd}_2\text{Cl}_2(\text{dpm})_2$, **9a** = $\text{PdCl}_2(\text{dpm})$, **11a** = $\text{PdCl}_2(\text{dpm}(\text{S}))$, **X** = unknown. [The spectra of the various Pd species are discussed in Sections 3.2 (**1a**) and 4.2 (**9a** and **11a**).]

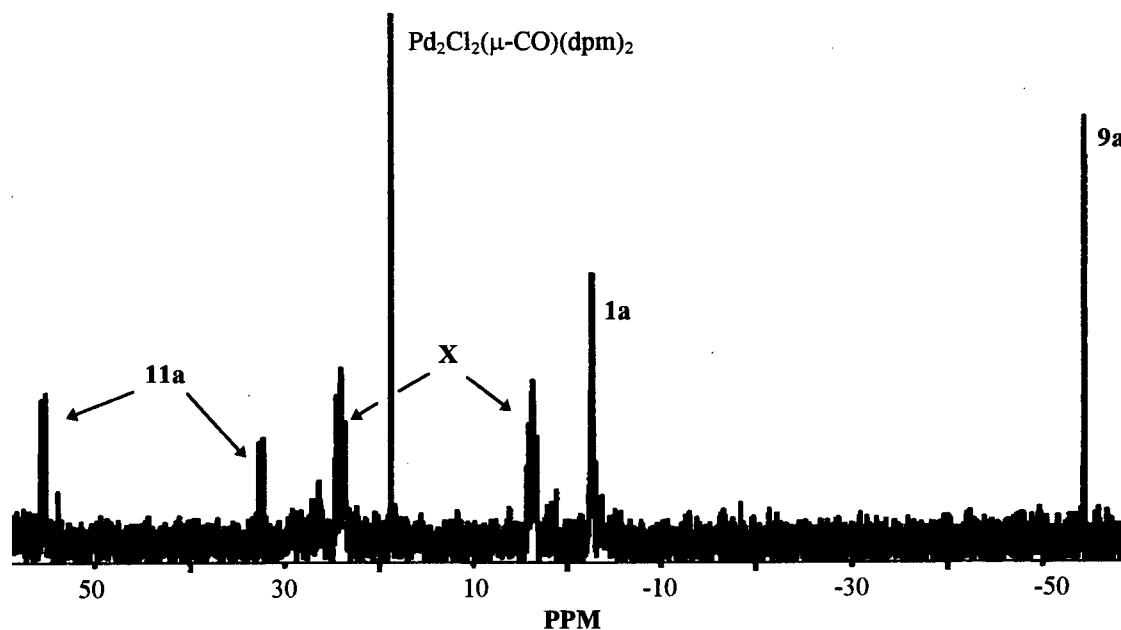
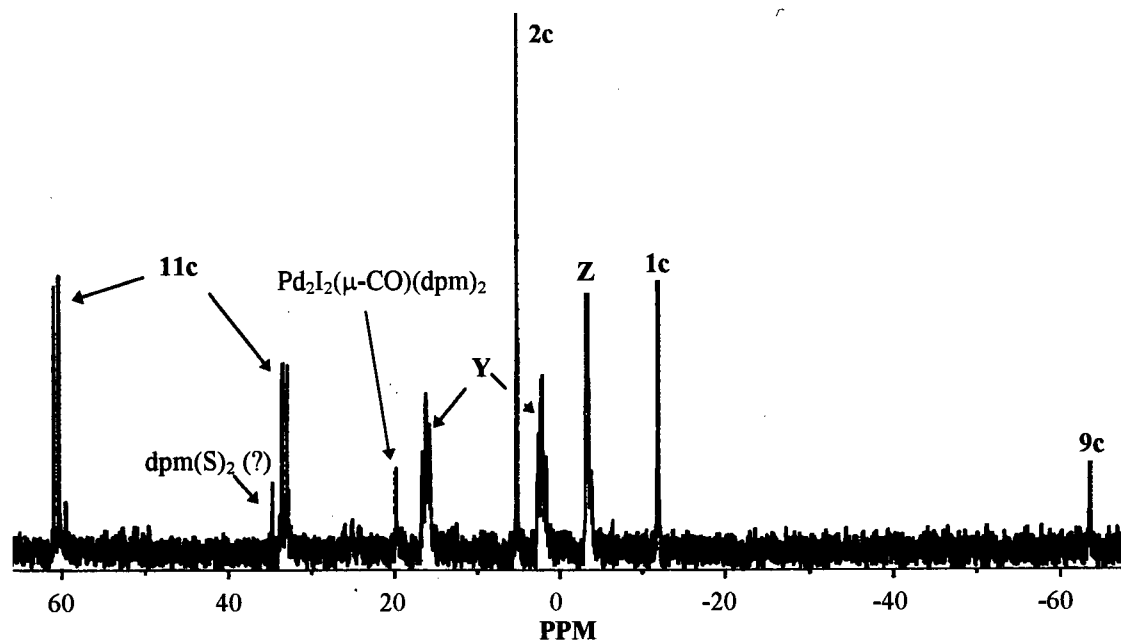
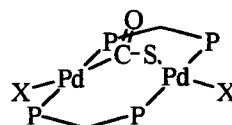
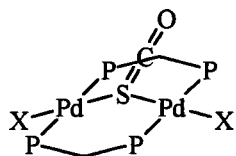


Fig. 7.4. $^{31}\text{P}\{^1\text{H}\}$ NMR spectrum (81 MHz) recorded for the reaction of $\text{Pd}_2\text{I}_2(\mu\text{-S})(\text{dpm})_2$ (**2c**) with 1 atm CO at R.T. in CDCl_3 after 11 d; **1c** = $\text{Pd}_2\text{I}_2(\text{dpm})_2$, **9c** = $\text{PdI}_2(\text{dpm})$, **11c** = $\text{PdI}_2(\text{dpm}(\text{S}))$, **Y**, **Z** = unknown.



pattern in the $^{31}\text{P}\{^1\text{H}\}$ NMR spectrum and species **Z** by a multiplet at δ -3. Species **X** and **Y** could be dinuclear Pd complexes with bridging COS moieties as shown below; dinuclear metal complexes with such bridging COS modes are known.³ Of note, no reaction of **1** (**1a**, 10 mg, 0.0095 mmol; **1c**, 10 mg, 0.0081 mmol) with 1 atm COS in CDCl_3 (~0.5 mL) at R.T. after 5 d was seen as evidenced by NMR measurements.



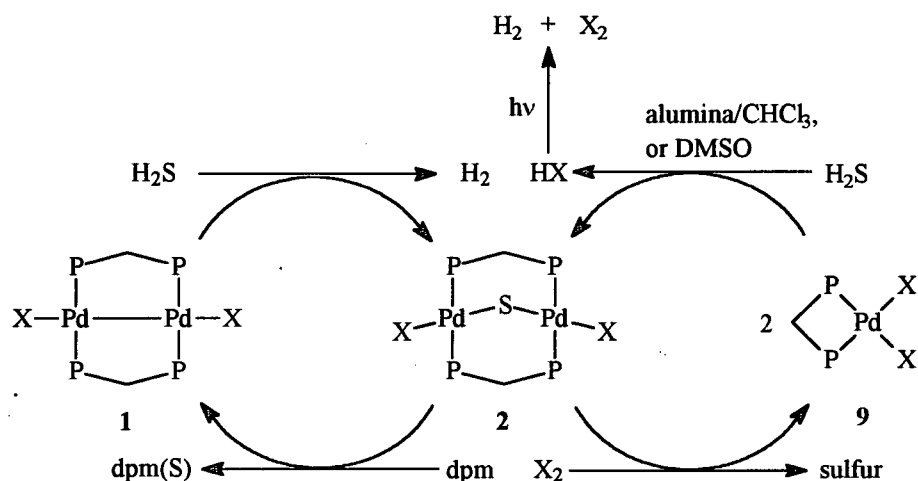
7.4 References for Chapter 7

1. Collman, J.P.; Finke, R.G.; Cawse, J.N.; Brauman, J.I. *J. Am. Chem. Soc.* **1977**, *99*, 2515.
2. a) Benner, L.S.; Balch, A.L. *J. Am. Chem. Soc.* **1978**, *100*, 6099. b) Olmstead, M.M.; Hope, H.; Benner, L.S.; Balch, A.L. *J. Am. Chem. Soc.* **1977**, *99*, 5502. c) Lee, C.-L.; James, B.R.; Nelson, D.A.; Hallen, R.T. *Organomet.* **1984**, *3*, 1360.
3. Pandey, K.K. *Coord. Chem. Rev.* **1995**, *140*, 37.

CHAPTER 8

General Conclusions and Recommendations for Future Studies

In this thesis work, the interaction of H_2S with mono- and dinuclear Pd-dpm complexes was investigated with the main goal being to develop catalytic processes for the generation of H_2 and elemental sulfur from H_2S . Several systems were explored and these are summarized in the following scheme.



Process $1 \rightarrow 2$ was previously studied by others of this laboratory and was shown to proceed via hydrido mercapto intermediates. Kinetic and mechanistic studies were carried out on the re-conversion process $2 \rightarrow 1$ in the present work with the finding that the bridging diphosphine ligands are also involved in the S-abstraction such that the distribution of monosulfide products is close to statistical; no intermediates were observed. The net reaction is shown in eq. 8.1 for which some studies were done on the $\text{X} = \text{Br}$ system substantiating the catalytic nature of **1** and **2**; eq. 8.1 is the first reported homogeneously catalyzed conversion of H_2S to H_2 .



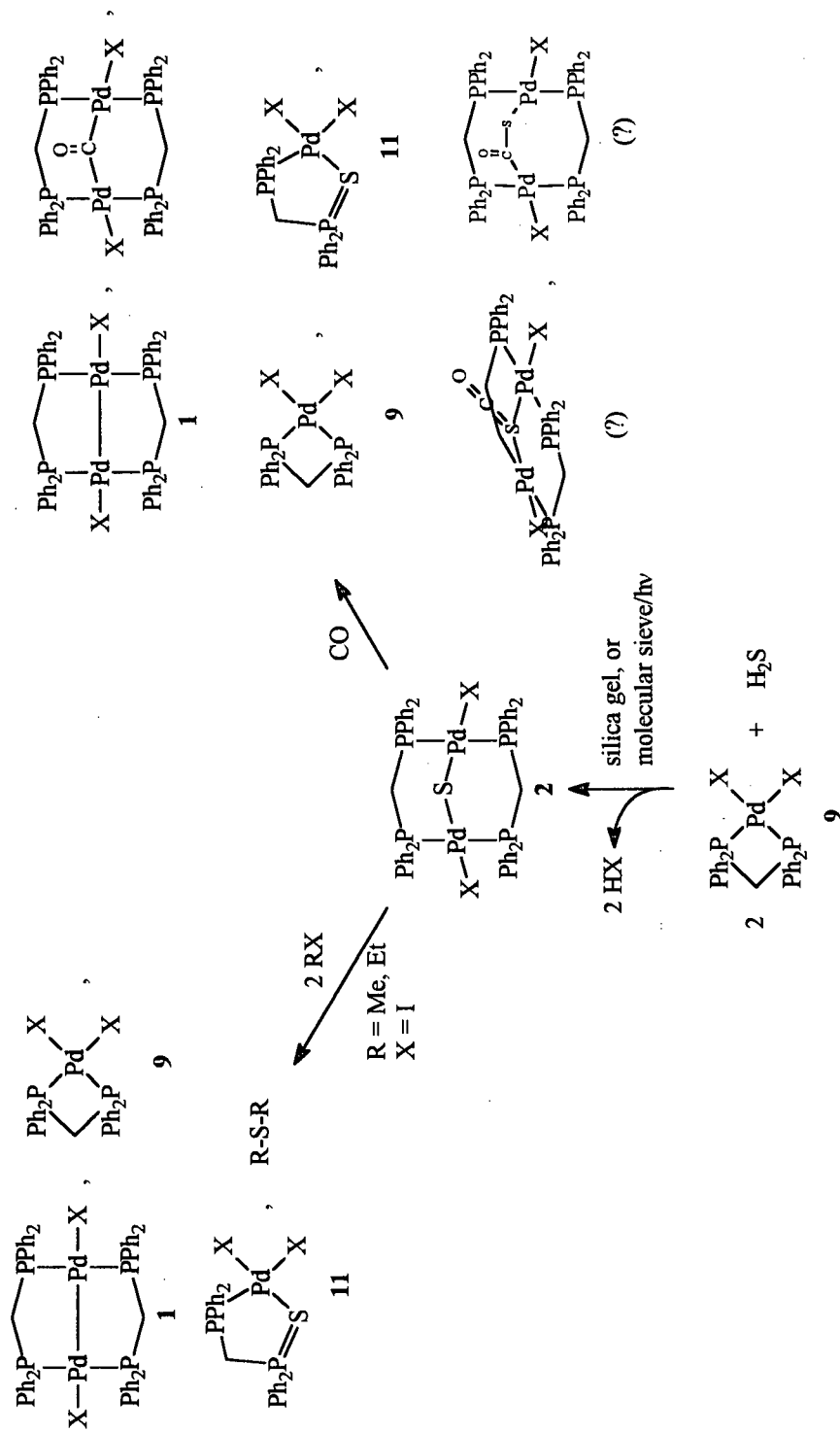
Depending on conditions, a catalytically inactive species with the formulation

$\text{Pd}_2\text{Br}_2(\text{dpm(S)})(\text{dpm})_2$ also forms, its origin and identity not yet unequivocally established. The

poor crystallinity of this species precluded an X-ray crystallographic analysis, and it is suggested that in future studies good crystal growth may be accomplished using low temperature conditions.

The removal of the bridged S atom from **2** by halogens (process **2** → **9**) was discovered, and kinetic and mechanistic studies on the $X = I$ system revealed that the reaction proceeds via oxidative addition thereby generating an intermediate species, $\text{Pd}_2\text{X}_4(\text{dpm})_2$, which undergoes unimolecular decomposition to give **9**. The recovery of sulfur in its elemental form is attractive in terms of possible commercialization of an $\text{H}_2\text{S} \rightarrow \text{H}_2 + 1/8 \text{S}_8$ process. The dinucleation process **9** → **2** was examined in detail in both DMSO and CHCl_3 solvents. In the former solvent, an equilibrium reaction of **9** with H_2S proceeds to form **2** and HX ; however, a side-product thought to be $\text{Pd}(\text{SH})_2(\text{dpm})$ also forms. In CHCl_3 on the other hand, the reaction of **9** with H_2S proceeds completely and cleanly, with alumina necessarily present and functioning as a heterogeneous catalyst for the activation of H_2S prior to the dinucleation process. Ligand substitution to form the intermediate species $\text{PdX}(\text{SH})(\text{dpm})$ is postulated based on reaction studies of **9** with NaSH ; subsequent reaction of this intermediate with itself or **9** to form **2** is proposed. The HX product (chemisorbed on the alumina in the CHCl_3 system) was quantified by titration studies. The overall process **2** → **9** → **2** with $X = I$ constitutes a catalytic cycle as photodecomposition of HI would produce H_2 and the necessary I_2 to continue the cycle; the net reaction would be the photocatalytic decomposition of H_2S to H_2 and elemental sulfur. Some catalytic studies were performed but the generation of H_2 remains to be substantiated; future studies should concentrate on determining the fate of the elusive H_2 .

During the course of this thesis work, some interesting observations, as summarized in Chapter 7 and in the following scheme, were made and these deserve further investigation:



Future studies should concentrate on unraveling further the nature of each of the three reactions shown. For example, a radical process may be involved in the reaction of **2** with RX, and addition of a radical scavenger, *e.g.* TEMPO,[†] would probably yield informative data. In the reaction of **2** with CO, the identity of species thought to be Pd₂X₂(μ-COS)(dpm)₂ should be established as this may be an intermediate en route to formation of **1**; furthermore, the issue of how species **9** and **11** are formed should also be addressed. Finally, in the dinucleation reaction of **9** with H₂S to form **2** using silica gel or molecular sieve/hv, the mechanism may be similar to that when alumina was used (Chapter 6); in future studies, the question of how light is involved in the molecular sieve system should also be answered.

[†] TEMPO = 2,2,6,6-tetramethyl-1-piperidinyloxy, free radical

APPENDIX

Appendix I - Free energy of decomposition of H₂S, ΔG_d

The free energy of decomposition of H₂S, ΔG_d, at a particular temperature is determined from the absolute free energies of H₂, sulfur (S₈(solid, liquid, gas) or S₂(gas)), and H₂S using the following general equation:

$$\Delta G_d(\text{H}_2\text{S}) = [\text{G}(\text{H}_2) + \text{G}(\text{sulfur})] - \text{G}(\text{H}_2\text{S})$$

The G(H₂S), G(H₂), and G(sulfur) values are obtained from thermodynamic data tables found in ref. 1 (Table I.1). The equilibria that exist at certain temperature ranges are as follows:²



The dependence of ΔG_d(H₂S) on temperature is shown in Table I.1 and is illustrated in Fig. I.1.

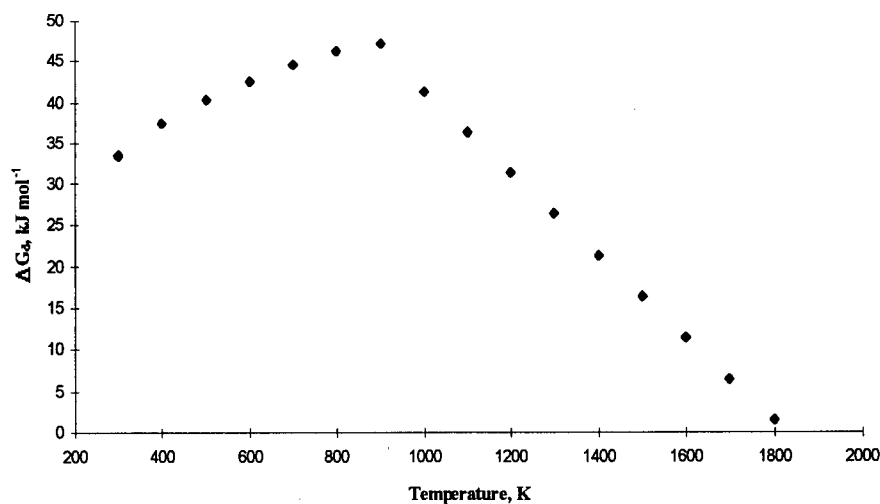


Fig. I.1. Dependence of the free energy of decomposition of H₂S, ΔG_d(H₂S), on temperature in the range 298 to 1800 K.

Table I.1. Absolute free energies values, G , for H_2S , H_2 , $\text{S}_2(\text{g})$, $\text{S}_8(\text{g})$, and $\text{S}_8(\text{s,l})$, and free energy of decomposition for H_2S , $\Delta G_d(\text{H}_2\text{S})$, in the temperature range 298 to 1800 K.

T (K)	$G(\text{H}_2)$ (kcal mol ⁻¹)	$G(\text{S}_2(\text{g}))$ (kcal mol ⁻¹)	$G(\text{S}_8(\text{g}))$ (kcal mol ⁻¹)	$G(\text{S}_8(\text{s, l}))$ (kcal mol ⁻¹)	$G(\text{H}_2\text{S})$ (kcal mol ⁻¹)	$\Delta G_d(\text{H}_2\text{S})$ (kcal mol ⁻¹)	$\Delta G_d(\text{H}_2\text{S})$ (kJ mol ⁻¹)
298	-9.31	14.59	-6.46	-2.28	-19.56	7.98	33.38
300	-9.36	14.49	-6.65	-2.29	-19.65	8.00	33.46
400	-12.59	8.91	-17.53	-3.16	-24.69	8.94	37.40
500	-16.00	3.13	-19.42	-4.33	-29.95	9.63	40.28
600	-19.54	-2.82	-42.14	-5.68	-35.39	10.17	42.56
700	-23.20	-8.91	-55.56	-7.16	-40.98	10.62	44.43
800	-26.96	-15.12	-69.58	-	-46.71	11.05	46.23
900	-30.82	-21.44	-84.14	-	-52.57	11.23	47.00
1000	-34.75	-27.86	-99.18	-	-58.54	9.85	41.23
1100	-38.76	-34.37	-114.65	-	-64.61	8.67	36.28
1200	-42.83	-40.95	-130.51	-	-70.79	7.48	31.30
1300	-46.97	-47.61	-146.73	-	-77.06	6.29	26.31
1400	-51.16	-54.34	-163.28	-	-83.42	5.09	21.31
1500	-55.41	-61.13	-180.14	-	-89.87	3.90	16.31
1600	-59.71	-67.98	-197.29	-	-96.41	2.71	11.33
1700	-64.06	-74.89	-214.72	-	-103.02	1.52	6.37
1800	-68.45	-81.85	-232.40	-	-109.71	0.34	1.42

References

1. Fukuda, K.N.; Dokiya, M.; Kameyama, T.; Kotera, Y. *Ind. Eng. Chem. Fundam.* **1978**, *17*, 243.
2. Barin, I.; Knacke, O. "Thermochemical Properties of Inorganic Substances", Springer-Verlag, Berlin, 1975, pp 316, 317, 325, 648-651.

Appendix II - Kinetic data from the study of the reaction: $\text{Pd}_2\text{X}_2(\mu\text{-S})(\text{dpm})_2$ (2) + dpm

[2] (M)	[dpm] (M)	T (°C)	k_{obs} (s^{-1})
2b, 6.52×10^{-5}	6.52×10^{-3}	20	1.27×10^{-4}
2b, 6.52×10^{-5}	1.30×10^{-2}	20	2.76×10^{-4}
2b, 6.52×10^{-5}	1.96×10^{-2}	20	4.44×10^{-4}
2b, 6.52×10^{-5}	2.61×10^{-2}	20	5.63×10^{-4}
2b, 6.52×10^{-5}	6.52×10^{-3}	25	1.99×10^{-4}
2b, 6.52×10^{-5}	1.30×10^{-2}	25	4.14×10^{-4}
2b, 6.52×10^{-5}	1.96×10^{-2}	25	5.99×10^{-4}
2b, 6.52×10^{-5}	2.61×10^{-2}	25	8.07×10^{-4}
2b, 6.52×10^{-5}	6.52×10^{-3}	30	2.77×10^{-4}
2b, 6.52×10^{-5}	1.30×10^{-2}	30	5.27×10^{-4}
2b, 6.52×10^{-5}	1.96×10^{-2}	30	7.73×10^{-4}
2b, 6.52×10^{-5}	2.61×10^{-2}	30	1.05×10^{-3}
2b, 6.52×10^{-5}	6.52×10^{-3}	35	3.57×10^{-4}
2b, 6.52×10^{-5}	1.30×10^{-2}	35	7.06×10^{-4}
2b, 6.52×10^{-5}	1.96×10^{-2}	35	1.04×10^{-3}
2b, 6.52×10^{-5}	2.61×10^{-2}	35	1.38×10^{-3}
2b, 3.26×10^{-5}	1.96×10^{-2}	25	5.99×10^{-4}
2b, 1.63×10^{-5}	1.96×10^{-2}	25	5.32×10^{-4}
2b, 8.15×10^{-6}	1.96×10^{-2}	25	5.95×10^{-4}
2b, 1.30×10^{-4}	1.96×10^{-2}	25	5.60×10^{-4}
2b, 6.52×10^{-5} , (^{119}Pr) $_4\text{NBr}$, 6.52×10^{-3}	1.92×10^{-2}	25	5.88×10^{-4}
2a, 6.52×10^{-5}	6.52×10^{-3}	30	8.18×10^{-4}
2a, 6.52×10^{-5}	1.30×10^{-2}	30	1.60×10^{-3}
2a, 6.52×10^{-5}	1.96×10^{-2}	30	2.36×10^{-3}
2a, 6.52×10^{-5}	2.61×10^{-2}	30	3.29×10^{-3}
2a, 6.52×10^{-5}	1.96×10^{-2}	20	1.31×10^{-3}
2a, 6.52×10^{-5}	1.96×10^{-2}	25	1.70×10^{-3}
2a, 6.52×10^{-5}	1.96×10^{-2}	25	1.81×10^{-3}
2a, 6.52×10^{-5}	1.96×10^{-2}	35	3.07×10^{-3}
2a, 3.25×10^{-5}	1.96×10^{-2}	30	2.38×10^{-3}
2a, 1.30×10^{-4}	1.96×10^{-2}	30	2.30×10^{-3}
2c, 6.52×10^{-5}	6.52×10^{-3}	25	7.2×10^{-5}

**Appendix III - Computer program to simulate the outcome of the reaction between
Pd₂Br₂(μ-S)(dpm)₂ and n mole equivalent dpm-d₂**

'Program written in qbasic to determine the statistical outcome of the reaction:

' Pd₂(dpm)₂(b-S)Br₂ + n dpm-d₂

'written by Terrance Y. H. Wong, May 31, 1994.

DIM A(5000)

DIM B(5000)

5 CLS

PRINT "TYPE IN NUMBER OF PD₂(DPM)₂(B-S)BR₂ ="; : INPUT PD%

PRINT "TYPE IN NUMBER OF DPM-D₂ ="; : INPUT DPM%

FOR X = 1 TO PD%

 A(X) = 0 'OR 1 FOR PD₂(DPM)₂BR₂

NEXT X

FOR Y = 1 TO DPM%

 B(Y) = 1

NEXT Y

N = 0

DPMS = 0

DPMSD₂ = 0

10 'CLS

LOCATE 22, 1: COLOR 7: PRINT "<ESC> - STOP ",
COLOR 5: PRINT "<SPACE> - CONTINUE Q - QUIT P - PRINT": COLOR 7

DO

RANDOMIZE TIMER

X% = INT(RND * PD%) + 1

Y% = INT(RND * DPM%) + 1

GOSUB LIGEX

11 N = N + 1

LOCATE 3, 1: PRINT "PROCESSING: N = ", N

LOOP UNTIL INKEY\$ = CHR\$(27)

12

LOCATE 22, 1: COLOR 7: PRINT "<ESC> - STOP ",
COLOR 5: PRINT "<SPACE> - CONTINUE Q - QUIT P - PRINT": COLOR 7

DO

RANDOMIZE TIMER

X% = INT(RND * PD%) + 1

Y% = INT(RND * DPM%) + 1

RN = INT(RND * 10) + 1

IF RN <> 1 THEN GOSUB LIGEX: GOTO 14

IF A(X%) = 0 AND B(Y%) = 1 THEN GOSUB REACTION: GOTO 14

IF A(X%) = 0 AND B(Y%) = 0 THEN A(X%) = 1: B(Y%) = 2: DPMS = DPMS + 1: GOTO 14

IF A(X%) = 4 AND B(Y%) = 0 THEN GOSUB REACTION: GOTO 14

IF A(X%) = 4 AND B(Y%) = 1 THEN GOSUB REACTION4: GOTO 14

IF A(X%) = 5 AND B(Y%) = 0 THEN GOSUB REACTION4: GOTO 14

IF A(X%) = 5 AND B(Y%) = 0 THEN A(X%) = 3: B(Y%) = 2: DPMSD2 = DPMSD2 + 1: GOTO 14

14 N = N + 1

LOCATE 3, 1: PRINT "PROCESSING: N = ", N

LOOP UNTIL INKEY\$ = CHR\$(27)

UU = 0 'NO. OF UNREACTED PD2(DPM)2(B-S)BR2

ZZ = 0 'NO. OF UNSUBSTITUTED PD2 SPECIES

ZO = 0 'NO. OF MONOSUBSTITUTED PD2 SPECIES

OO = 0 'NO. OF DISUBSTITUTED PD2 SPECIES

DPM = 0

DPMD2 = 0

FOR X = 1 TO PD%

IF A(X) = 0 THEN UU = UU + 1

IF A(X) = 4 THEN UU = UU + 1

IF A(X) = 5 THEN UU = UU + 1

IF A(X) = 1 THEN ZZ = ZZ + 1

IF A(X) = 2 THEN ZO = ZO + 1

IF A(X) = 3 THEN OO = OO + 1

NEXT X

FOR Y = 1 TO DPM%

IF B(Y) = 0 THEN DPM = DPM + 1

IF B(Y) = 1 THEN DPMD2 = DPMD2 + 1

NEXT Y

PRINT "NO. OF UNREACTED PD2 SPECIES.....=", UU

PRINT "NO. OF UNSUBSTITUTED PD2 SPECIES....=", ZZ

PRINT "NO. OF MONOSUBSTITUTED PD2 SPECIES..=", ZO

PRINT "NO. OF DISUBSTITUTED PD2 SPECIES....=", OO

PRINT "NO. OF DPM.....=", DPM

PRINT "NO. OF DPMD2.....=", DPMD2

PRINT "NO. OF DPMS.....=", DPMS

PRINT "NO. OF DPMSD2.....=", DPMSD2

LOCATE 22, 1: COLOR 5: PRINT "<ESC> - STOP ",

```

COLOR 7: PRINT "<SPACE> - CONTINUE   Q - QUIT   P - PRINT"
15 C$ = INKEY$
IF C$ = " " THEN 12
IF C$ = "Q" THEN 16
IF C$ = "P" THEN GOSUB PRINTSUB
IF C$ = "" THEN 15
GOTO 15

```

```
16 END
```

```

REACTION:
RANDOMIZE TIMER
RN = INT(RND * 3) + 1
IF RN = 1 THEN A(X%) = 1: DPMSD2 = DPMSD2 + 1
IF RN = 2 THEN A(X%) = 2: DPMS = DPMS + 1
IF RN = 3 THEN A(X%) = 2: DPMS = DPMS + 1
B(Y%) = 2
RETURN

```

```

REACTION4:
RANDOMIZE TIMER
RN = INT(RND * 3) + 1
IF RN = 1 THEN A(X%) = 3: DPMS = DPMS + 1
IF RN = 2 THEN A(X%) = 2: DPMSD2 = DPMSD2 + 1
IF RN = 3 THEN A(X%) = 2: DPMSD2 = DPMSD2 + 1
B(Y%) = 2
RETURN

```

```

LIGEX:
IF A(X%) = 0 AND B(Y%) = 1 THEN A(X%) = 4: B(Y%) = 0: GOTO 20
IF A(X%) = 4 AND B(Y%) = 0 THEN GOSUB SUBST3: GOTO 20
IF A(X%) = 4 AND B(Y%) = 1 THEN GOSUB SUBST4: GOTO 20
IF A(X%) = 5 AND B(Y%) = 0 THEN A(X%) = 4: B(Y%) = 1: GOTO 20
IF A(X%) = 1 AND B(Y%) = 1 THEN A(X%) = 2: B(Y%) = 0: GOTO 20
IF A(X%) = 2 AND B(Y%) = 0 THEN GOSUB SUBST1: GOTO 20
IF A(X%) = 2 AND B(Y%) = 1 THEN GOSUB SUBST2: GOTO 20
IF A(X%) = 3 AND B(Y%) = 0 THEN A(X%) = 2: B(Y%) = 1: GOTO 20
20 RETURN

```

```

SUBST1:
RANDOMIZE TIMER
RN = INT(RND * 2) + 1
IF RN = 2 THEN A(X%) = 1: B(Y%) = 1
RETURN

```

```

SUBST2:
RANDOMIZE TIMER
RN = INT(RND * 2) + 1
IF RN = 2 THEN A(X%) = 3: B(Y%) = 0
RETURN

```

```

SUBST3:
RANDOMIZE TIMER

```

```
RN = INT(RND * 2) + 1
IF RN = 2 THEN A(X%) = 0: B(Y%) = 1
RETURN
```

```
SUBST4:
RANDOMIZE TIMER
RN = INT(RND * 2) + 1
IF RN = 2 THEN A(X%) = 5: B(Y%) = 0
RETURN
```

```
PRINTSUB:
LPRINT "NO. OF PD2(DPM)2(B-S)BR2 (INITIAL)..=", PD%
LPRINT "NO. OF DPM-D2 (INITIAL).....=", DPM%
LPRINT "NO. OF PROCESSES.....=", N
LPRINT
LPRINT "NO. OF UNREACTED PD2 SPECIES.....=", UU
LPRINT "NO. OF UNSUBSTITUTED PD2 SPECIES....=", ZZ
LPRINT "NO. OF MONOSUBSTITUTED PD2 SPECIES..=", ZO
LPRINT "NO. OF DISUBSTITUTED PD2 SPECIES....=", OO
LPRINT "NO. OF DPM.....=", DPM
LPRINT "NO. OF DPMD2.....=", DPMD2
LPRINT "NO. OF DPMS.....=", DPMS
LPRINT "NO. OF DPMSD2.....=", DPMSD2
RETURN
```

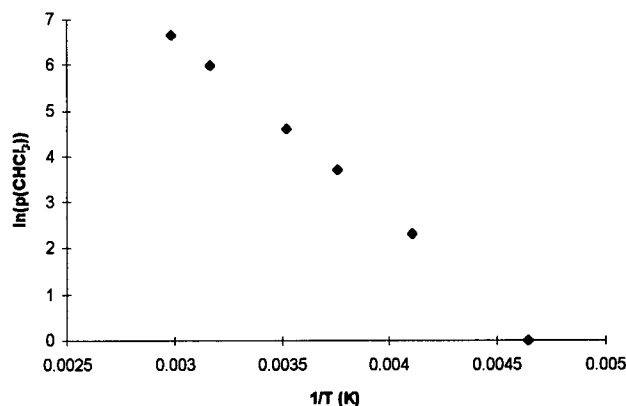
Appendix IV - Determination of the concentration of H₂S in chloroform

The concentration of H₂S in CHCl₃ at R.T. and 1 atm total pressure is determined from knowledge of Henry's constant ($K = 1.3 \text{ M atm}^{-1}$)¹ and vapour pressure data for CHCl₃.² The dependence of vapour pressure of CHCl₃ on temperature is shown in Table IV.1 and is illustrated in Fig. IV.1. At R.T. (295.15 K), the vapour pressure of CHCl₃ is 176 mm Hg or 0.23 atm. Thus, when the total pressure of the system is 1 atm, the partial pressure of H₂S ($p(\text{H}_2\text{S})$) is 0.77 atm. The corresponding concentration of H₂S in CHCl₃ is therefore 1.0 M ($\text{conc.} = K \times p(\text{H}_2\text{S}) = 1.3 \times 0.77$).

Table IV.1. Dependence of the vapour pressure of CHCl₃ on temperature in the range T = 215.15 to 334.45 K

T (K)	p(CHCl ₃) (mm Hg)
215.15	1
243.45	10
266.05	40
283.55	100
315.85	400
334.45	760

Fig. IV.1. Plot of $\ln(p(\text{CHCl}_3))$ versus $1/T$



To determine the volume of H₂S (introduced under STP conditions by injection via syringe) needed for a particular concentration in CHCl₃, knowledge of the volumes of the solution (V_s) and the head space (V_h) above it are also required. The total number of moles of H₂S (n_T) is equal to the number of moles of H₂S in the head space (n_h) plus that in solution (n_s):

$$(IV.1) \quad n_T = n_h + n_s$$

The partial pressure of H₂S (p(H₂S)) is calculated as follows:

$$(IV.2) \quad p(\text{H}_2\text{S}) = n_h RT / V_h$$

Substitution into Henry's equation gives the following:

$$(IV.3) \quad \text{conc.} = Kp(\text{H}_2\text{S}) = n_s / V_s = Kn_h RT / V_h$$

Finally, the volume of H₂S needed is determined by application of the gas law with T = 295.15

K, p = 1 atm, and R = 0.08206 L atm.

$$(IV.4) \quad V = n_T RT / p$$

References

1. Fogg, P.G.T.; Young, C.L. (Eds.) "Solubility data series. Vol. 32" Pergamon Press, Oxford, 1988, p. 279.
2. Handbook for Chemistry and Physics. 56th ed. Chemical Rubber Co., Cleveland, OH. 1979, p. D-191.

Appendix V - Kinetic data from the study of the reaction: $\text{Pd}_2\text{I}_2(\mu\text{-S})(\text{dpm})_2 (2\text{c}) + \text{I}_2$

Kinetic data from conventional UV-vis spectroscopic studies

[2c] (M)	[I ₂] (M)	T (°C)	k _{obs} (s ⁻¹)
9.39 x 10 ⁻⁵	3.76 x 10 ⁻⁴	25	2.34 x 10 ⁻³
9.39 x 10 ⁻⁵	3.76 x 10 ⁻⁴	25	2.35 x 10 ⁻³
9.39 x 10 ⁻⁵	5.63 x 10 ⁻⁴	25	2.27 x 10 ⁻³
9.39 x 10 ⁻⁵	7.51 x 10 ⁻⁴	25	2.18 x 10 ⁻³
9.39 x 10 ⁻⁵	7.51 x 10 ⁻⁴	25	1.97 x 10 ⁻³
9.39 x 10 ⁻⁵	7.51 x 10 ⁻⁴	19	1.31 x 10 ⁻³
9.39 x 10 ⁻⁵	7.51 x 10 ⁻⁴	29.5	4.05 x 10 ⁻³
9.39 x 10 ⁻⁵	7.51 x 10 ⁻⁴	35	7.87 x 10 ⁻³

Kinetic data from stopped-flow spectroscopic studies

[2c] = 9.9 x 10 ⁻⁵ M	T = 19.6 °C	T = 25.0 °C	T = 30.1 °C	T = 35.1 °C
[I ₂]	k _{obs} (s ⁻¹)			
3.9 x 10 ⁻⁴ M	0.06748	0.08922	0.1090	0.1448
	0.06932	0.08865	0.1080	0.1413
	0.06840			
4.9 x 10 ⁻⁴ M	0.08804	0.1115	0.1400	0.1744
	0.09037	0.1140	0.1448	0.1751
	0.08945			
5.9 x 10 ⁻⁴ M	0.1035	0.1335	0.1529	
	0.09888	0.1320	0.1546	
7.9 x 10 ⁻⁴ M	0.1416	0.1913	0.2292	0.2905
	0.1419	0.1904	0.2361	0.3014

T = 19.6 °C	[2c] = 3.3 x 10 ⁻⁵ M	[2c] = 1.6 x 10 ⁻⁵ M
[I ₂]	k _{obs} (s ⁻¹)	k _{obs} (s ⁻¹)
7.9 x 10 ⁻⁴ M	0.1537	0.1763
	0.1530	0.1790

Appendix VI - X-ray crystal structure data for PdI₂(dpm(S))•0.5CH₂Cl₂

Experimental details

A. Crystal data

Empirical formula	C _{25.50} H ₂₃ Cl ₂ P ₂ PdS
Formula weight	819.13
Crystal color, Habit	brown, plate
Crystal dimensions	0.05 x 0.20 x 0.30 mm
Crystal system	monoclinic
Lattice type	primitive
No. of reflections used of unit cell determination (2θ range)	25 (14.1 - 24.7°)
Omega scan peak width at half-height	0.37°
Lattice parameters	a = 9.378(2) Å b = 14.231(3) Å c = 21.049(2) Å β = 91.60(1)° V = 2808.1(9) Å ³
Space group	P2 ₁ /n (#14)
Z value	4
D _{calc}	1.937 g/cm ³
F ₀₀₀	1564
μ(MoKα)	31.57 cm ⁻¹

B. Intensity measurements

Diffractometer	Rigaku AFC6S
Radiation	MoK α ($\lambda = 0.71069 \text{ \AA}$) graphite monochromated
Take-off angle	6.0°
Detector aperture	6.0 mm horizontal 6.0 mm vertical
Crystal to detector distance	285 mm
Temperature	21 °C
Scan type	ω -2 θ
Scan rate	16°/min (in ω) (up to 9 scans)
Scan width	(1.15 + 0.35 tan θ)°
2 θ_{\max}	55°
No. of reflections measured	Total: 7107 Unique: 6709 ($R_{\text{int}} = 0.055$)
Corrections	Lorentz-polarization Absorption (trans. factors: 0.529 - 1.000)

C. Structure solution and refinement

Structure solution	Direct methods (SIR92)
Refinement	Full-matrix least-squares
Function minimized	$\Sigma \omega (F_o - F_c)^2$
Least squares weights	$\frac{1}{\sigma^2(F_o)} = \frac{4F_o^2}{\sigma^2(F_o^2)}$
p-factor	0.000
Anomalous dispersions	All non-hydrogen atoms

No. observations ($I > 3\sigma(I)$)	2465
No. variables	301
Reflection/parameter ratio	8.19
Residuals: R; R_w	0.035; 0.028
Goodness of fit indicator	1.32
Max shift/error in final cycle	0.006
Maximum peak in final diff. map	$0.51 \text{ e}^-/\text{\AA}^3$
Minimum peak in final diff. map	$-0.50 \text{ e}^-/\text{\AA}^3$

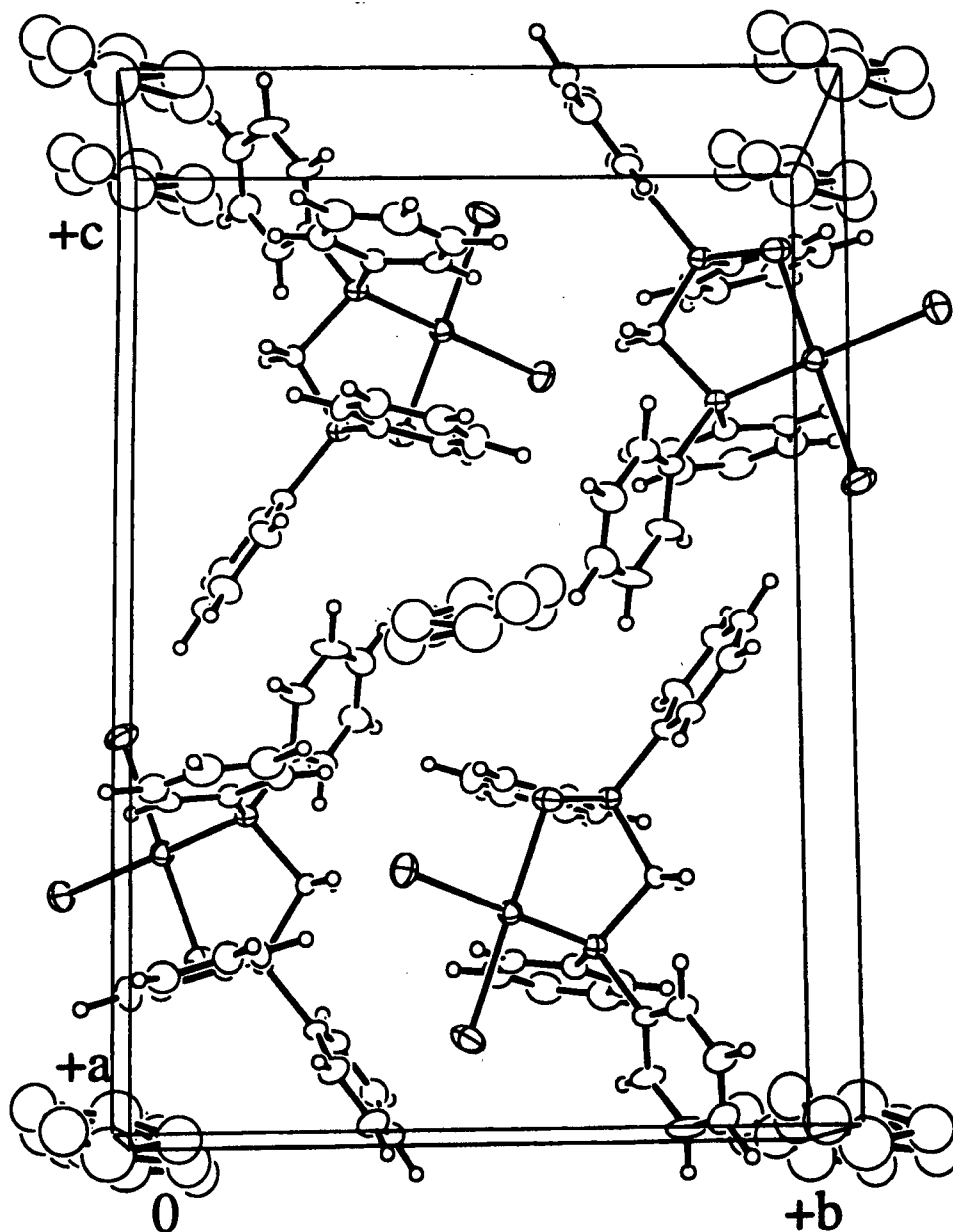
Fig. VI.1. Unit cell of the complex $\text{PdI}_2(\text{dpm}(\text{S})) \cdot 0.5\text{CH}_2\text{Cl}_2$.

Table VI.1. Atomic coordinates of PdI₂(dpm(S))•0.5CH₂Cl₂ (11c).

atom	x	y	z
I(1)	-0.17339(7)	-0.10480(5)	0.25511(3)
I(2)	0.00641(7)	-0.01346(5)	0.40701(3)
Pd(1)	-0.02793(7)	0.04611(5)	0.29079(3)
Cl(1)	0.450(2)	0.4007(9)	0.4752(6)
Cl(2)	0.496(2)	0.413(2)	0.4951(9)
Cl(3)	0.359(2)	0.442(2)	0.498(1)
S(1)	-0.0686(2)	0.1006(2)	0.1874(1)
P(1)	0.1029(2)	0.1717(2)	0.3199(1)
P(2)	0.0895(2)	0.1945(2)	0.1797(1)
C(1)	0.0976(8)	0.2589(5)	0.2541(4)
C(2)	0.0415(8)	0.2393(6)	0.3870(4)
C(3)	-0.0907(9)	0.2843(6)	0.3822(4)
C(4)	-0.1421(9)	0.3337(7)	0.4311(5)
C(5)	-0.066(1)	0.3411(7)	0.4870(5)
C(6)	0.064(1)	0.2963(8)	0.4934(4)
C(7)	0.1176(10)	0.2457(7)	0.4435(4)
C(8)	0.2911(8)	0.1491(6)	0.3320(4)
C(9)	0.3440(9)	0.0598(6)	0.3250(4)
C(10)	0.490(1)	0.0422(7)	0.3313(4)
C(11)	0.5820(10)	0.1147(9)	0.3441(5)
C(12)	0.531(1)	0.2041(8)	0.3529(5)
C(13)	0.3854(9)	0.2225(6)	0.3464(4)
C(14)	0.0496(8)	0.2725(6)	0.1143(4)
C(15)	-0.0881(9)	0.3025(6)	0.1050(4)

Table VI.1. Atomic coordinates of PdI₂(dpm(S))•0.5CH₂Cl₂ (**11c**) (cont.).

atom	x	y	z
C(16)	-0.1245(10)	0.3597(7)	0.0539(5)
C(17)	-0.023(1)	0.3837(7)	0.0104(4)
C(18)	0.116(1)	0.3552(7)	0.0198(5)
C(19)	0.1536(9)	0.2982(7)	0.0716(4)
C(20)	0.2614(8)	0.1411(6)	0.1694(4)
C(21)	0.2693(9)	0.0487(6)	0.1513(4)
C(22)	0.401(1)	0.0070(7)	0.1426(5)
C(23)	0.5237(10)	0.0569(8)	0.1538(4)
C(24)	0.5169(9)	0.1484(7)	0.1709(4)
C(25)	0.3870(9)	0.1916(6)	0.1787(4)
C(26)	0.573(4)	0.503(3)	0.482(2)

Table VI.2. Bond Lengths(Å) in the complex PdI₂(dpm(S))•0.5CH₂Cl₂ (**11c**).

atom	atom	distance	atom	atom	distance
I(1)	Pd(1)	2.6419(9)	I(2)	Pd(1)	2.6006(9)
Pd(1)	S(1)	2.331(2)	Pd(1)	P(1)	2.243(2)
S(1)	P(2)	2.007(3)	P(1)	C(1)	1.860(8)
P(1)	C(2)	1.815(8)	P(1)	C(8)	1.805(8)
P(2)	C(1)	1.814(8)	P(2)	C(14)	1.799(8)
P(2)	C(20)	1.802(8)	C(2)	C(3)	1.40(1)
C(2)	C(7)	1.37(1)	C(3)	C(4)	1.35(1)
C(4)	C(5)	1.36(1)	C(5)	C(6)	1.38(1)
C(6)	C(7)	1.38(1)	C(8)	C(9)	1.37(1)
C(8)	C(13)	1.40(1)	C(9)	C(10)	1.39(1)
C(10)	C(11)	1.37(1)	C(11)	C(12)	1.37(1)
C(12)	C(13)	1.40(1)	C(14)	C(15)	1.370(10)
C(14)	C(19)	1.39(1)	C(15)	C(16)	1.38(1)
C(16)	C(17)	1.38(1)	C(17)	C(18)	1.37(1)
C(18)	C(19)	1.40(1)	C(20)	C(21)	1.37(1)
C(20)	C(25)	1.39(1)	C(21)	C(22)	1.38(1)
C(22)	C(23)	1.37(1)	C(23)	C(24)	1.35(1)
C(24)	C(25)	1.38(1)			

Table VI.3. Bond Angles(°) in the complex PdI₂(dpm(S))•0.5CH₂Cl₂ (**11c**).

atom	atom	atom	angle	atom	atom	atom	angle
I(1)	Pd(1)	I(2)	92.97(3)	I(1)	Pd(1)	S(1)	86.28(6)
I(1)	Pd(1)	P(1)	177.90(7)	I(2)	Pd(1)	S(1)	177.64(6)
I(2)	Pd(1)	P(1)	87.14(6)	S(1)	Pd(1)	P(1)	93.69(8)
Pd(1)	S(1)	P(2)	101.3(1)	Pd(1)	P(1)	C(1)	109.0(3)
Pd(1)	P(1)	C(2)	116.9(3)	Pd(1)	P(1)	C(8)	115.0(3)
C(1)	P(1)	C(2)	102.9(4)	C(1)	P(1)	C(8)	103.3(4)
C(2)	P(1)	C(8)	108.3(4)	S(1)	P(2)	C(1)	106.3(3)
S(1)	P(2)	C(14)	109.6(3)	S(1)	P(2)	C(20)	113.2(3)
C(1)	P(2)	C(14)	110.6(4)	C(1)	P(2)	C(20)	107.5(4)
C(14)	P(2)	C(20)	109.6(4)	P(1)	C(1)	P(2)	107.8(4)
P(1)	C(2)	C(3)	119.1(6)	P(1)	C(2)	C(7)	122.7(7)
C(3)	C(2)	C(7)	118.1(8)	C(2)	C(3)	C(4)	121.3(8)
C(3)	C(4)	C(5)	120.7(9)	C(4)	C(5)	C(6)	119.2(9)
C(5)	C(6)	C(7)	120.5(9)	C(2)	C(7)	C(6)	120.2(9)
P(1)	C(8)	C(9)	120.3(7)	P(1)	C(8)	C(13)	120.5(7)
C(9)	C(8)	C(13)	119.2(7)	C(8)	C(9)	C(10)	120.8(8)
C(9)	C(10)	C(11)	119.8(10)	C(10)	C(11)	C(12)	120.4(9)
C(11)	C(12)	C(13)	120.2(9)	C(8)	C(13)	C(12)	119.6(9)
P(2)	C(14)	C(15)	118.5(6)	P(2)	C(14)	C(19)	121.4(6)
C(15)	C(14)	C(19)	120.0(8)	C(14)	C(15)	C(16)	120.4(8)
C(15)	C(16)	C(17)	120.0(9)	C(16)	C(17)	C(18)	120.0(9)
C(17)	C(18)	C(19)	120.1(9)	C(14)	C(19)	C(18)	119.3(8)
P(2)	C(20)	C(21)	119.5(7)	P(2)	C(20)	C(25)	121.5(7)
C(21)	C(20)	C(25)	118.9(8)	C(20)	C(21)	C(22)	120.2(8)

Table VI.3. Bond Angles(°) in the complex PdI₂(dpm(S))•0.5CH₂Cl₂ (**11c**) (cont.).

atom	atom	atom	angle	atom	atom	atom	angle
C(21)	C(22)	C(23)	120.3(9)	C(22)	C(23)	C(24)	119.9(9)
C(23)	C(24)	C(25)	120.6(9)	C(20)	C(25)	C(24)	120.1(8)

**Appendix VII - Synthesis and characterization of [Pd(dpm(S))₂]Cl₂,
trans-bis- η -P,S-(bis(diphenylphosphino)methane monosulfide)palladium(II) chloride**

Synthesis

Dpm(S) (0.27 g, 0.65 mmol) was dissolved in 5 mL CH₂Cl₂, and a solution of PdCl₂(PhCN)₂ (0.050 g, 0.15 mmol) in 5 mL CH₂Cl₂ was added. The resulting orange-red solution was stirred at R.T. for 1 h before it was reduced in volume to ~5 mL. Et₂O (20 mL) was then added precipitating an orange solid which was filtered off, washed with Et₂O (2 x 10 mL), and dried *in vacuo*; yield: 0.12 g (91%). ¹H NMR (20 °C, DMSO-d₆): δ 7.0 - 8.0 m (40H, Ph), δ 5.66 p.t (4H, CH₂). ³¹P{¹H} NMR (20 °C, DMSO-d₆): δ 49.6, 37.6 (AB pattern, J_{PP} = 23 Hz). A yellow crystal, obtained by diffusion of hexanes (10 mL) into a CH₂Cl₂ (6 mL) solution of 10 mg of the complex, was analyzed using X-ray crystallography.

X-ray Crystal Structure Data

Experimental details

A. Crystal data

Empirical formula	C ₅₂ H ₄₈ Cl ₆ P ₄ PdS ₂
Formula weight	1180.08
Crystal color, Habit	yellow, prism
Crystal dimensions	0.15 x 0.25 x 0.35 mm
Crystal system	triclinic
Lattice type	primitive

No. of reflections used of unit cell determination (2θ range)	25 (27.8 - 32.9°)
Omega scan peak width at half-height	0.36°
Lattice parameters	$a = 11.612(1) \text{ \AA}$ $b = 11.813(1) \text{ \AA}$ $c = 10.3623(7) \text{ \AA}$ $\alpha = 97.898(6)^\circ$ $\beta = 96.011(7)^\circ$ $\gamma = 80.174(8)^\circ$ $V = 1382.4(2) \text{ \AA}^3$
Space group	$P\bar{1}$ (#2)
Z value	1
D_{calc}	1.417 g/cm ³
F_{000}	600
$\mu(\text{MoK}\alpha)$	8.50 cm ⁻¹
B. Intensity measurements	
Diffractometer	Rigaku AFC6S
Radiation	MoK α ($\lambda = 0.71069 \text{ \AA}$) graphite monochromated
Take-off angle	6.0°
Detector aperture	6.0 mm horizontal 6.0 mm vertical
Crystal to detector distance	285 mm
Temperature	21 °C
Scan type	ω - 2θ
Scan rate	32°/min (in ω) (up to 9 scans)

Scan width	$(1.26 + 0.35 \tan \theta)^\circ$
$2\theta_{\max}$	60°
No. of reflections measured	Total: 8441 Unique: 8069 ($R_{\text{int}} = 0.028$)
Corrections	Lorentz-polarization Absorption (trans. factors: 0.967 - 1.000) Decay (6.51% decline)

C. Structure solution and refinement

Structure solution	Direct methods (SIR92)
Refinement	Full-matrix least-squares
Function minimized	$\Sigma \omega (F_o - F_c)^2$
Least squares weights	$\frac{1}{\sigma^2(F_o)} = \frac{4F_o^2}{\sigma^2(F_o^2)}$
p-factor	0.000
Anomalous dispersions	All non-hydrogen atoms
No. observations ($I > 3\sigma(I)$)	4663
No. variables	295
Reflection/parameter ratio	15.81
Residuals: R; R_w	0.036; 0.033
Goodness of fit indicator	1.77
Max shift/error in final cycle	0.0003
Maximum peak in final diff. map	$0.61 \text{ e}/\text{\AA}^3$
Minimum peak in final diff. map	$-0.49 \text{ e}/\text{\AA}^3$

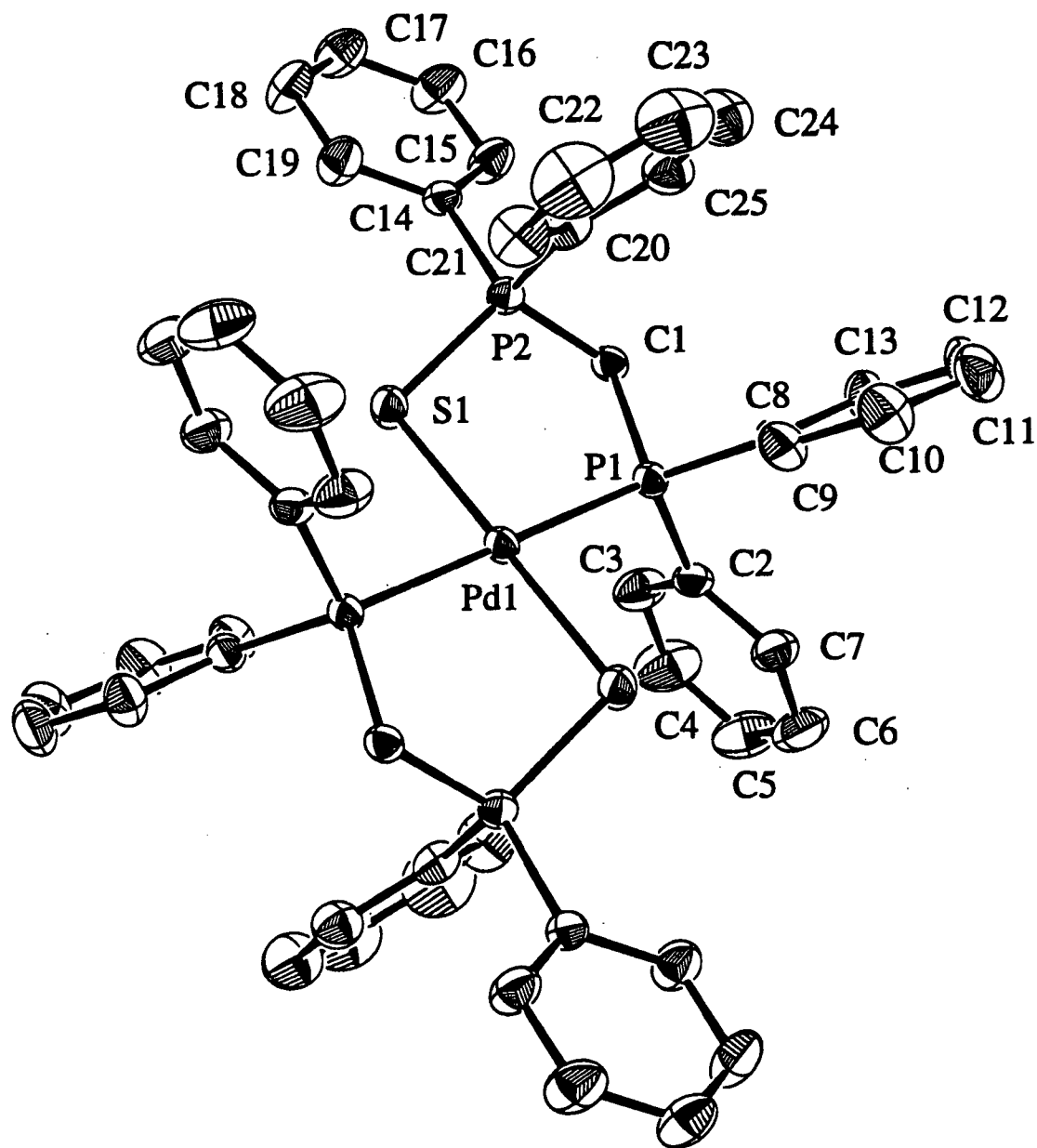
Fig. VII.1. ORTEP drawing of $[\text{Pd}(\text{dpm}(\text{S}))_2]\text{Cl}_2$. Hydrogen atoms are omitted.

Fig. VII.2. Stereoview of $[\text{Pd}(\text{dpm}(\text{S}))_2]\text{Cl}_2$. Hydrogen atoms are omitted.

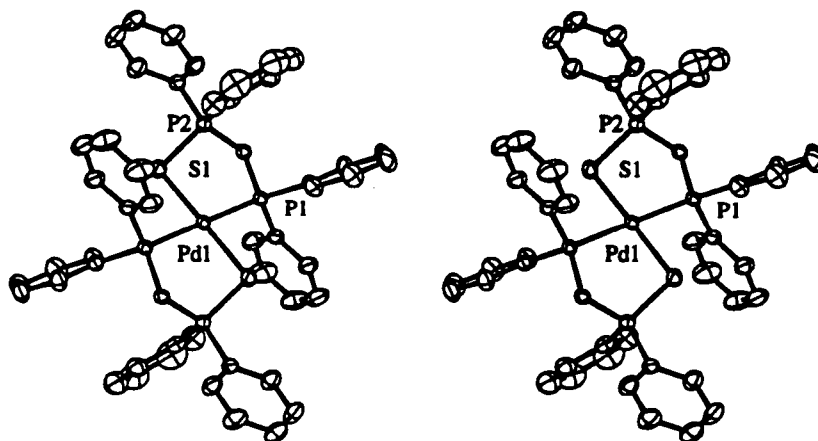


Fig. VII.3. Stereoview of the unit cell of $[\text{Pd}(\text{dpm}(\text{S}))_2]\text{Cl}_2$.

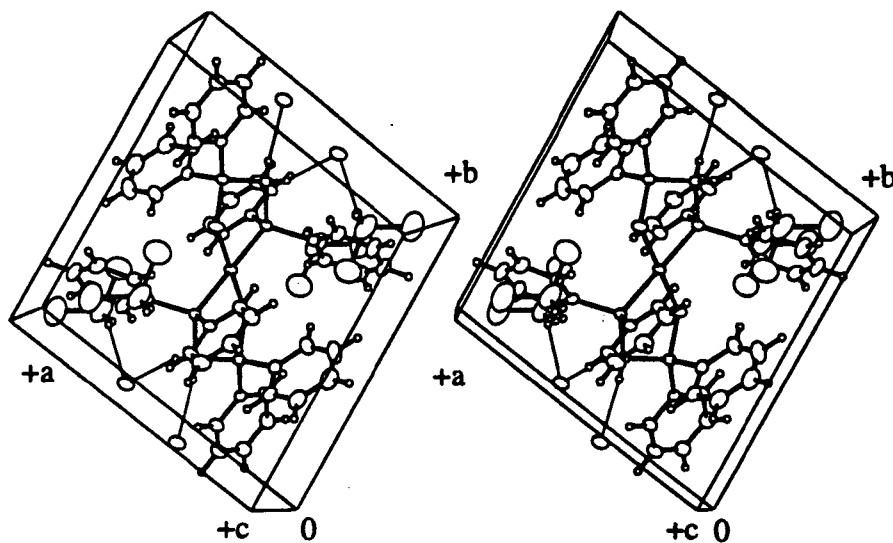


Fig. VII.4. PLUTO drawing showing 1/2 of $[\text{Pd}(\text{dpm}(\text{S}))_2]\text{Cl}_2$ with interactions with a dichloromethane solvate molecule.

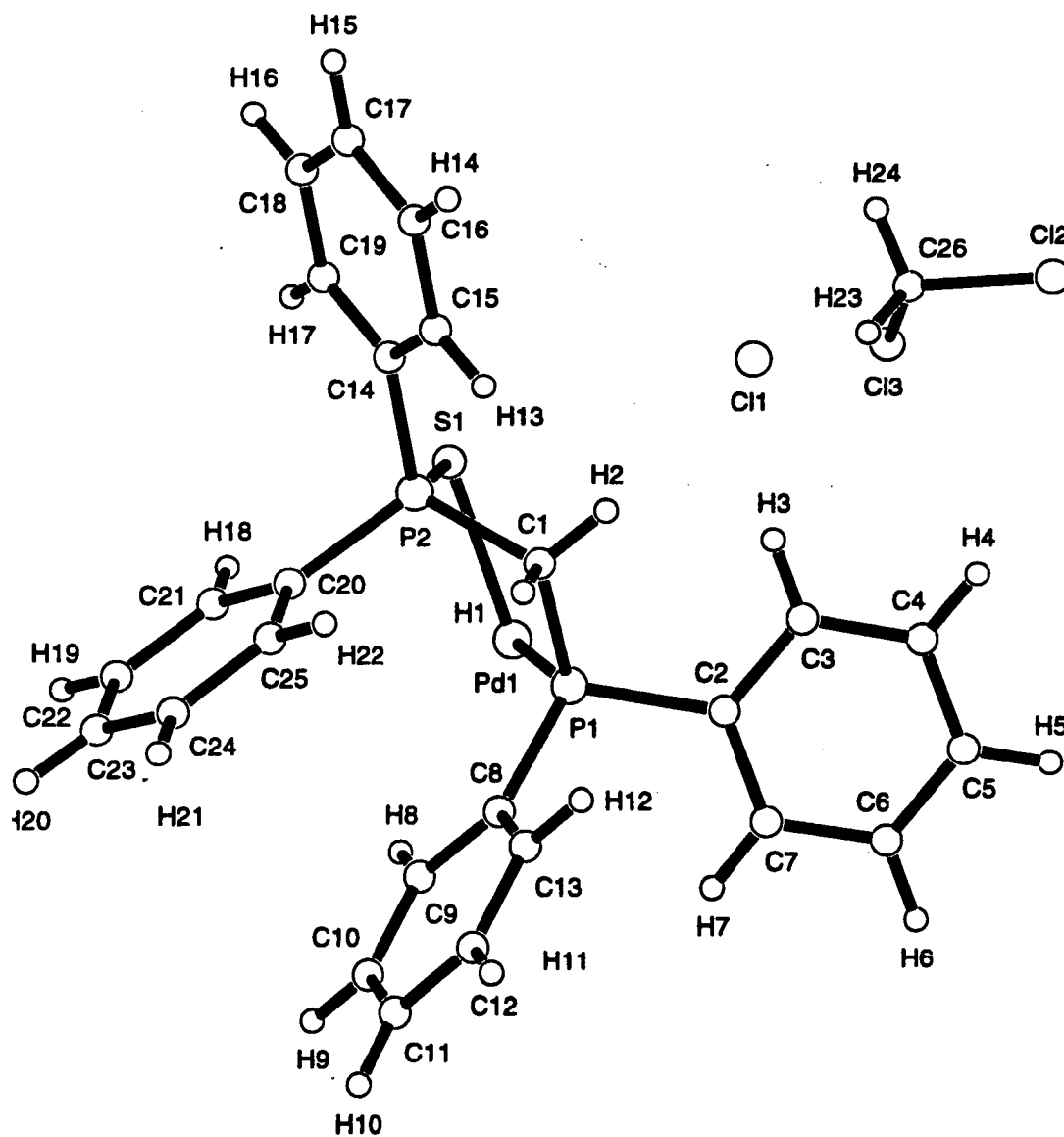


Table VII.1. Atomic coordinates of $[\text{Pd}(\text{dpm}(\text{S}))_2]\text{Cl}_2 \cdot 0.5\text{CH}_2\text{Cl}_2$.

atom	x	y	z
Pd(1)	0.50000	0.50000	0.50000
Cl(1)	0.59790(9)	0.04112(7)	0.70599(8)
Cl(2)	0.8889(2)	0.1085(2)	0.9711(2)
Cl(3)	0.7815(2)	0.3319(2)	0.9288(3)
S(1)	0.37946(8)	0.44301(7)	0.63642(8)
P(1)	0.54085(7)	0.31222(6)	0.39609(7)
P(2)	0.33265(7)	0.30243(6)	0.52318(8)
C(1)	0.4639(3)	0.2152(2)	0.4669(3)
C(2)	0.6963(3)	0.2568(2)	0.4182(3)
C(3)	0.7436(3)	0.2096(3)	0.5308(4)
C(4)	0.8627(4)	0.1750(4)	0.5499(5)
C(5)	0.9352(3)	0.1876(4)	0.4591(5)
C(6)	0.8891(4)	0.2353(4)	0.3476(4)
C(7)	0.7695(3)	0.2701(3)	0.3264(3)
C(8)	0.4989(3)	0.2938(2)	0.2223(3)
C(9)	0.4493(3)	0.3876(3)	0.1569(3)
C(10)	0.4198(4)	0.3717(3)	0.0239(3)
C(11)	0.4397(4)	0.2632(4)	-0.0448(3)
C(12)	0.4867(4)	0.1699(3)	0.0189(3)
C(13)	0.5163(3)	0.1836(3)	0.1520(3)
C(14)	0.2606(3)	0.2274(2)	0.6217(3)
C(15)	0.2830(3)	0.1089(3)	0.6177(4)
C(16)	0.2263(3)	0.0562(3)	0.6973(4)
C(17)	0.1487(3)	0.1189(3)	0.7794(4)

Table VII.1. Atomic coordinates of $[\text{Pd}(\text{dpm}(\text{S}))_2]\text{Cl}_2 \cdot 0.5\text{CH}_2\text{Cl}_2$ (cont.).

atom	x	y	z
C(18)	0.1252(3)	0.2369(3)	0.7831(4)
C(19)	0.1816(3)	0.2911(3)	0.7051(3)
C(20)	0.2360(3)	0.3385(3)	0.3825(3)
C(21)	0.1796(4)	0.4508(3)	0.3751(4)
C(22)	0.1063(5)	0.4757(4)	0.2650(6)
C(23)	0.0912(4)	0.3909(5)	0.1651(5)
C(24)	0.1473(4)	0.2805(4)	0.1710(4)
C(25)	0.2195(3)	0.2530(3)	0.2802(3)
C(26)	0.7631(5)	0.1971(6)	0.9356(6)

Table VII.2. Bond Lengths (Å) in the complex $[\text{Pd}(\text{dpm}(\text{S}))_2]\text{Cl}_2 \cdot 0.5\text{CH}_2\text{Cl}_2$.

atom	atom	distance	atom	atom	distance
Pd(1)	S(1)	2.3256(8)	Pd(1)	P(1)	2.3229(7)
Cl(2)	C(26)	1.684(6)	Cl(3)	C(26)	1.654(7)
S(1)	P(2)	2.017(1)	P(1)	C(1)	1.835(3)
P(1)	C(2)	1.814(3)	P(1)	C(8)	1.809(3)
P(2)	C(1)	1.791(3)	P(2)	C(14)	1.791(3)
P(2)	C(20)	1.797(3)	C(2)	C(3)	1.384(4)
C(2)	C(7)	1.382(4)	C(3)	C(4)	1.375(5)
C(4)	C(5)	1.365(6)	C(5)	C(6)	1.373(6)
C(6)	C(7)	1.383(5)	C(8)	C(9)	1.387(4)
C(8)	C(13)	1.395(4)	C(9)	C(10)	1.380(4)
C(10)	C(11)	1.373(5)	C(11)	C(12)	1.367(5)
C(12)	C(13)	1.379(4)	C(14)	C(15)	1.376(4)
C(14)	C(19)	1.380(4)	C(15)	C(16)	1.377(4)
C(16)	C(17)	1.357(5)	C(17)	C(18)	1.371(5)
C(18)	C(19)	1.374(4)	C(20)	C(21)	1.384(5)
C(20)	C(25)	1.382(4)	C(21)	C(22)	1.384(6)
C(22)	C(23)	1.357(7)	C(23)	C(24)	1.361(6)
C(24)	C(25)	1.379(5)			

Table VII.3. Bond Angles (°) in the complex $[\text{Pd}(\text{dpm}(\text{S}))_2]\text{Cl}_2 \cdot 0.5\text{CH}_2\text{Cl}_2$.

atom	atom	atom	angle	atom	atom	atom	angle
S(1)	Pd(1)	S(1)*	180.0	S(1)	Pd(1)	P(1)	91.21(3)
S(1)	Pd(1)	P(1)*	88.79(3)	P(1)	Pd(1)	P(1)*	180.0
Pd(1)	S(1)	P(2)	99.84(4)	Pd(1)	P(1)	C(1)	110.46(9)
Pd(1)	P(1)	C(2)	110.71(9)	Pd(1)	P(1)	C(8)	115.52(10)
C(1)	P(1)	C(2)	106.8(1)	C(1)	P(1)	C(8)	105.7(1)
C(2)	P(1)	C(8)	107.1(1)	S(1)	P(2)	C(1)	107.48(10)
S(1)	P(2)	C(14)	107.60(10)	S(1)	P(2)	C(20)	112.8(1)
C(1)	P(2)	C(14)	111.6(1)	C(1)	P(2)	C(20)	108.1(1)
C(14)	P(2)	C(20)	109.3(1)	P(1)	C(1)	P(2)	106.1(1)
P(1)	C(2)	C(3)	120.7(2)	P(1)	C(2)	C(7)	119.5(3)
C(3)	C(2)	C(7)	119.6(3)	C(2)	C(3)	C(4)	119.9(3)
C(3)	C(4)	C(5)	120.6(4)	C(4)	C(5)	C(6)	119.9(4)
C(5)	C(6)	C(7)	120.4(4)	C(2)	C(7)	C(6)	119.6(3)
P(1)	C(8)	C(9)	121.2(2)	P(1)	C(8)	C(13)	119.8(2)
C(9)	C(8)	C(13)	119.0(3)	C(8)	C(9)	C(10)	120.2(3)
C(9)	C(10)	C(11)	120.3(3)	C(10)	C(11)	C(12)	120.0(3)
C(11)	C(12)	C(13)	120.6(3)	C(8)	C(13)	C(12)	119.8(3)
P(2)	C(14)	C(15)	121.8(2)	P(2)	C(14)	C(19)	118.7(2)
C(15)	C(14)	C(19)	119.4(3)	C(14)	C(15)	C(16)	119.2(3)
C(15)	C(16)	C(17)	121.4(3)	C(16)	C(17)	C(18)	119.7(3)
C(17)	C(18)	C(19)	119.8(3)	C(14)	C(19)	C(18)	120.5(3)
P(2)	C(20)	C(21)	120.7(3)	P(2)	C(20)	C(25)	119.3(3)
C(21)	C(20)	C(25)	120.0(3)	C(20)	C(21)	C(22)	119.2(4)
C(21)	C(22)	C(23)	120.2(4)	C(22)	C(23)	C(24)	121.0(4)

Table VII.3. Bond Angles (°) in the complex $[\text{Pd}(\text{dpm}(\text{S}))_2]\text{Cl}_2 \cdot 0.5\text{CH}_2\text{Cl}_2$ (cont.).

atom	atom	atom	angle	atom	atom	atom	angle
C(23)	C(24)	C(25)	120.1(4)	C(20)	C(25)	C(24)	119.6(4)
Cl(2)	C(26)	Cl(3)	113.4(3)				

* Symmetry operation: 1-x, 1-y, 1-z.

Table VII.4. C-H...Cl interactions* in the complex [Pd(dpm(S))₂]Cl₂·0.5CH₂Cl₂.

A	H	B	A-H	H...B	A...B	A-H...B
C(1)	H(1)	Cl(1)a	0.98	2.50	3.446(3)	162
C(1)	H(2)	Cl(1)	0.98	2.57	3.505(3)	160
C(3)	H(3)	Cl(1)	0.98	2.75	3.592(4)	144
C(26)	H(23)	Cl(1)	0.98	2.53	3.432(5)	153

* Symmetry operation: (a) 1-x, -y, 1-z.